UNIVERSIDAD AUTÓNOMA DE MADRID

Lead Acid Batteries for Micro Hybrid Electrical Vehicles – influence of different carbon materials and organic expanders on the performance of the negative plates.

Tesis Doctoral / Doctoral Thesis
María Blecua de Pedro

Dirigida por / Directed by
Pilar Ocón Esteban
Jesús Valenciano Martínez

"El placer más noble
es el júbilo de
aprender"

Agradecimientos / Acknowledgement

Sorprendentemente llego al punto en el que tengo que escribir los agradecimientos… y digo bien sorprendentemente, ya que durante esta travesía ha habido muchos momentos en los que pensé que nunca llegaría a escribirlos. Sin embargo, también hubo otros muchos momentos en los que me imaginé haciéndolo, y eso es porque, sin lugar a dudas, hay mucho que agradecer.

Lo primero agradecerle a Pilar Ocón su paciencia y confianza en mí. Sin tu apoyo incondicional y persistencia esto no hubiera sido posible. Lo segundo, agradecerle Paco Trinidad su apoyo, no solo durante mi doctorado, sino durante toda mi etapa en Exide Technologies. Gracias por todas las contribuciones que has hecho al mundo de la batería plomo ácido. En tercer lugar dar las gracias a Jesús Valenciano, otra persona que siempre ha estado ahí apoyándome en lo que he necesitado.

To the doctor Holger Fricke, for giving me the opportunity to work for him in the Exide Technologies R&D department in Germany, and for trusting me in many other issues.

Me gustaría hacer un inciso para agradecer a TODA la comunidad científica los esfuerzos que hacen día a día en sus investigaciones. Sin vuestra ayuda esto tampoco hubiera sido posible.

Mi familia… ¿qué decir? Sin lugar a dudas mi pilar más importante. Desde papá y mamá hasta María pequeña y las últimas adquisiciones (en este caso Quique). De este doctorado sois participes todos, porque ninguno habéis fallado, todos habéis estado ahí para ayudar a vuestra hija o hermana pequeña, cuñada o tía. Gracias. Y gracias en especial a papá, por enseñarnos que las cosas o se hacen bien o no se hacen, y a mamá, por sacar fuerzas siempre de donde parece que no hay.

El turno de las amigas de toda la vida, Esther, Bea, Celia, Miriam, Rocío y Sofía. Con todos los "problemas" que tengo… ¿qué haría si no os tuviera a vosotras para escucharlos? Muchas gracias por vuestra comprensión y vuestra forma de ser.

Amigos de la uni…menudo grupito, y para variar Bea también está aquí… La carrera de química hubiera sido un fracaso sin vosotros.

Amigos de Abiego, nunca leerán estas palabras pero en ellos encuentro muchas veces la paz que necesito. No sé si es más por Abiego o por ellos, lo que está claro es que siempre están en el paisaje.

Y como no unas palabras para la gente que he encontrado en mi vida profesional, pero que han llenado con creces mi vida personal.

INDEX

3

Abstract

As we all know, climate change is one of the world's most pressing challenges. The emission of greenhouse gasses, which includes the emission of carbon dioxide, has increased the global temperatures by around 1°C since pre-industrial times. For the purpose of reducing CO_2 emissions, the European Commission has established CO_2 emissions targets for the European passengers' cars since 1995. Nowadays the CO_2 emissions average for a European passenger car is 119.4g/km, and the target for 2021 is 95g/km. The unfulfillment of this restriction can lead to the payment of fines 5€ to 95€ per gram of CO_2 exceed per car sold.

In order to achieve this target, the automotive industry is continuously developing new ways to reduce the fuel consumption of the car. One of the recent approaches is the implementation of the Start and Stop system as well as the regenerative braking in Internal Combustion Engine cars named Micro Hybrid Electrical Vehicles (HEVs). These two features are carried out by the Lead Acid Battery (LAB) from the car.

For working in a micro HEV the LAB must be able to fulfill several cycles for the good performance of the Start & Stop system. In addition, the battery is recharged by the regenerative braking, which means that the cycles will be performed when the battery is working at 60% – 70% State of Charge (SoC). Conventional LABs are not able to work in these conditions. Therefore, the industry has developed a new fleet of batteries called Enhanced Flooded Batteries (EFBs), which incorporate carbon materials, such as expanded graphite, graphite, carbons blacks, nanocarbon materials, in their negative plates for improving their Specific Surface Area (SSA).

The NAM of the LABs is made of metallic lead mixed with a group of additives called expanders. These expanders increase the porosity of the NAM. When they are not added, the porosity is quite low, and the electrolyte is not able to reach the inner part of the plate. The lead sulfate crystals created during the discharge of the battery cannot be reconverted to lead, and LAB fails. This fact is known as sulfation of the negative plate. The addition of carbon materials lead to the increase of the SSA of the negative plate. This effect depends on the size and concentration of the carbon materials. Nanometer carbon materials with high SSA at concentrations lower than 0.5% in the negative plate, are pushed to the surface of the Negative Active Material (NAM) during the formation process, also known as energetic structure, improving its SSA. When these types of

carbon materials are added at concentrations higher than 0.5% they are incorporated into the bulk of the lead skeleton during the formation process. The same happens for the micrometer carbon materials no matter their concentration; they are always incorporated into the lead skeleton. From the lead skeleton, the carbon materials are able to create a more porous structure which results in a more dynamic electric system, as the electrolyte can reach the inner parts of the negative plate. In addition, when these materials are electrically conductive they improve in a further way the current distribution throughout the negative plate, especially when it is partly sulfated.

The worst disadvantage of using carbon materials in the negative plate of the LAB is that they increase the Hydrogen Evolution Reaction (HER) rate during the overcharge of the battery. This water consumption increase leads to the dry out of the battery, and the resulting failure, as EFB are Valve Regulated Lead Acid (VRLA) batteries that cannot be refilled with water. For this reason, the type of carbon additive, as well as the dosage, must be wisely selected.

Another important additive for the negative plate is the Organic Expanders (OEs) which are active polymers that are able to delay the passivation phenomena, i.e. accumulation of lead sulfate crystals on the surface of the negative plate which leads to the collapse of the pores and the failure of the LAB. Most usual OEs are the sodium lignosulfonates (LS).

During this doctoral thesis, we have worked on the addition of different carbon materials and OEs in the negative plates of LABs on the purpose of achieving longer cycle life, as well as charge acceptance. In addition, the effect of the concentration and type of carbon material was studied in order to find the best LAB performance while maintaining the lowest water consumption. All the experiments were done on 2 V / 1 Ah LAB cells where the negative plate was the limiting component. In this way, the successful additives could be used in the negative plates of EFBs.

The first part of the study was focused on performing all the LABs manufacturing processes in the laboratory: mixing, pasting and curing processes for getting the unformed negative and positive plates. Once all these processes were optimized, 2 V / 1 Ah LAB cells were assembled and formed. The most relevant electrical tests for EFBs, according to the standards *VW75073 2012-07 and RNDS SS 36 11 003 2014-05,* were selected and adapted to the cells. This procedure included the capacity test, Cold Cranking Ability (CCA) test, Initial Charge Acceptance (ICA) test, the negative polarization study and the cycle life at Partial State of Charge (PSoC) test. Furthermore, the negative plates were

analyzed during the whole process with the following techniques: lead sulfate and carbon determination, porosity analyses, Brunauer, Emmett and Teller (BET) SSA, X-Ray diffraction, Scanning Electron Microscopy (SEM) study. The results of this thesis were divided into 4 different batches.

The first carbon materials understudies in batch 1 were 5 carbon materials (C1, C2, C3, C4 and C5) and 2 LS (LS1 and LS2). 6 mixtures were chosen and the negative plates were prepared, as well as the 2 V / 1 Ah cells. Carbon materials from C1 to C4 were micrometer carbon materials, so they were expected to be allocated in the bulk of the lead skeleton. C5 was a nanometer carbon material that was pushed to the surface of the NAM. All these carbon materials were able to improve the charge acceptance of the negative plate; however, C5, which was located at the surface of the NAM, showed the lowest cycle life. In the case of C5 it was also appreciated how this carbon material interacted with the LS impairing its performance. Higher HER rates were found for those carbon materials whose dosage was not well chosen. LS2 showed good performance when it was accompanied by micrometer carbon materials. In the case of LS1, its performance was better when it was accompanied by high conductive carbon materials.

The second type of carbon material understudy in **batch 2** was the graphitized carbon nanofibers produced by the company Grupo Antolin (GANFg). These fibers were chosen because of their high aspect ratio: high aspect ratio, as well as their low electrical resistivity ($1 \cdot 10^{-4}$ Ohm m). They had a diameter between 20 – 80 nm, and a maximum length of 30 μm. In this way, these fibers were thought to be integrated into the lead skeleton, and due to their high aspect ratio, they could for a conductive network inside the lead skeleton if the percolation threshold was reached. The selected LS was LS2 from batch 1, which was called OE1 for this batch and the following. The first step of this batch was the dispersion of the GANFg together with a part of OE1. This process was carried out by GAIKER, a technological center that provided the GANFg dispersions. The dispersions were used to prepare the different mixtures with different GANFg concentrations: S5 – 0.50%, S6 – 0.20% and S7 – 0.10%, all of them accompanied with an OE1 final concentration equal to 0.30 %. As a result, the GANFg did not improve the charge acceptance, as they neither improved the BET SSA of the formed negative plates, but they improved the cycle life of the 2 V / 1 Ah cells. This improvement was noticeable even when GANFg were added at 0.10%, so this concentration was established as the optimum one. Furthermore, the HER rate, and thus the water consumption, did not increase by the addition of GANFg at 0.10%.

For the **batch 3,** we used the optimum GANFg dosage (0.10%) together with a mix of OEs = OE1 + OE2. In this way, we wanted to see if it was possible to improve the charge acceptance of the negative plate by changing the OEs types and concentration. The mix of OEs was also used for dispersing the GANFg. Finally, 5 mixtures were prepared with or without 0.10% of GANFg, and including 0.20% or 0.30% of the OEs mix. The results confirmed the effect of the OEs on the performance of the negative plate: impaired the passivation phenomena while restrainting the charge acceptance processes. The charge acceptance of the plates was not improved by the addition of the OEs mix. However, the cycle life of the 2 V / 1 Ah cells was improved again by the addition of GANFg, and was higher for the mixture that contained 0.30% of OEs mix.

As we failed to improve the charge acceptance of the negative plates by adding the mix of OEs, for **batch 4**, we selected C1 (expanded graphite) and C4 (conductive carbon black) to be added together with GANFg (at 0.10%) to the negative plate. The concentration of the carbon materials was adapted according to the batch 1 results. Therefore, we expected an increase of the charge acceptance and the cycle life while maintaining the water consumption of the cells. The GANFg dispersions were prepared with part of the carbon material, and the rest was added during the mixing process. OE1 at 0.30% was used for all the mixtures. The charge acceptance of the negative plates was not significantly improved by the addition of carbon materials together with GANFg. In the case of the cycle life, a little increase was seen when the carbon materials were added, especially in the addition of C1. The water consumption was increased by the addition of carbon materials. After the results of this batch, we can conclude that the carbon materials must be added in their optimum dosage in order to improve the charge acceptance of the negative plates.

The results of this doctoral thesis led to the conclusion that the most suitable additives for the negative plates of the EFB are carbon materials such as expanded graphite or conductive carbons blacks, although they lead to higher water consumption. The addition of GANFg or combination of them with different carbon materials led to higher cycle life but failed to improve the charge acceptance of the cells which would lead to a bad performance of the LAB during the regenerative braking. Therefore, the future approaches in the EFB research should be focused on finding new additives that restrain the water consumption and add them together with carbons blacks or expanded graphites.

Resumen

Como todos sabemos, el cambio climático es uno de los retos más importantes de nuestra época. La emisión de gases de efecto invernadero, que incluye la emisión de dióxido de carbono, ha provocado la subida de 1°C de la temperatura global antes de la edad industrial. Con el propósito de reducir las emisiones de CO_2 la comisión europea ha marcado objetivos referentes al nivel de emisiones de los coches de pasajeros europeos desde 1995. Hoy en día las emisiones de CO_2 de un coche de pasajeros europeo son 119.4g/km, cuando el objetivo para 2021 es de 95g/km. El incumplimiento de este objetivo puede dar lugar a multas entre 5€ y 95€ por gramo de CO_2 extra emitido por coche vendido.

Para conseguir este objetivo, la industria de la automoción está continuamente desarrollando nuevos formas de reducir el consumo de combustible del vehículo. Una de las recientes iniciativas es la implementación del sistema Start & Stop junto con la parada regenerativa para coches de Ingeniería de Combustión Interna, también llamados Micro Vehículos Híbridos Eléctricos (VHE). Estas dos nuevas implementaciones son alimentadas por la batería de Plomo Ácido del coche.

En el caso de un micro VHE, la batería tiene que ser capaz de realizar los suficientes ciclos de vida para el buen funcionamiento del sistema Start & Stop. Además, la batería es recargada por medio de la parada regenerativa, por lo que los ciclos se realizan cuando el estado de carga de la batería es del 60% – 70%. Las baterías convencionales no están preparadas para trabajar en estas condiciones. Por ello, una nueva flota de baterías llamadas Enhanced Flooded Batteries (EFBs) han entrado en el mercado. Estas baterías incorporan materiales de carbón, como grafitos expandidos, grafito, carbones black, materiales de carbón nanométricos, en la placa negativa para así aumentar el Área de la Superficie Específica (ASE) de la Materia Activa Negativa (MAN).

La placa negativa de la batería está compuesta por plomo metálico mezclado con un grupo de aditivos denominados "expanders". Estos expanders son responsables del incremento de la porosidad de la MAN. Cuando no son adicionados, la porosidad de la MAN es baja, y por ello el electrolito no puede alcanzar la parte interna de la placa. De este modo, los cristales de sulfato de plomo creados durante la descarga de la batería no pueden ser reconvertidos a plomo, y la batería deja de funcionar. Este hecho es conocido como sulfatación de la placa negativa. La adición de materiales de carbono incrementa la ASE de la placa negativa. Este efecto depende del tipo y de la concentración utilizada del

material de carbón. Carbonos nanométricos, con alta ASE, añadidos a concentraciones menores de 0.5% en la placa negativa, son empujados a la superficie de la MAN, o estructura energética, durante el proceso de formación, desde donde aumentan la ASE de dicha estructura. Cuando este tipo de materiales de carbono se añaden en concentraciones más altas del 0.5%, se incorporan en el interior del esqueleto de plomo durante el proceso de formación. Lo mismo ocurre en el caso de los materiales de carbono de tamaño micrométrico, sin tener importancia aquí la concentración a la que se añadan. Desde el esqueleto de plomo los materiales de carbono son capaces de generar una estructura más porosa que acaba siendo un sistema eléctrico más dinámico, ya que el electrolito puede alcanzar las partes más internas de la placa negativa. Además, en el caso de que estos materiales sean conductores, mejoran la distribución de la corriente a lo largo de la placa negativa, especialmente cuando ésta está parcialmente sulfatada.

La peor desventaja de utilizar estos materiales es que aumentan el rendimiento de la Reacción de Evolución de Hidrógeno (REH) durante la carga de batería. Este consumo de agua puede conducir al secado del electrolito, y al correspondiente fallo de la batería, ya que las EFBs son baterías plomo ácido reguladas por válvula que no pueden ser rellenadas con agua. Por esta razón, el tipo y dosis de material de carbón tienen que ser minuciosamente seleccionados.

Otro importante aditivo para la placa negativa son los Expanders Orgánicos (EOs); polímeros activos capaces de retrasar el fenómeno de pasivación, es decir, la acumulación de cristales de sulfato de plomo en la superficie de la placa negativa, lo que conduce a colapso de los poros y al fallo de la batería. Los EOs más utilizados son los lignosulfonatos de sodio (LS).

Durante esta tesis doctoral hemos trabajado en la adición de diferentes materiales de carbono y EOs en la placa negativa de baterías plomo ácido con el objetivo de alcanzar una mayor durabilidad, así como un incremento de la aceptación de carga. El efecto de la concentración y del tipo de carbón ha sido estudiado para encontrar una dosis óptima que mejore las características de la batería sin aumentar el consumo de agua. Todos los experimentos se llevaron a cabo sobre celdas plomo ácido de 2 V / 1 Ah donde la placa negativa era el componente limitante. De esta manera, los mejores aditivos podrían ser utilizados en las placas negativas de las EFBs.

La primera parte del estudio estuvo centrada en la adaptación de todos los procesos de fabricación de baterías plomo ácido en el laboratorio: procesos de mezclado, empastado y curado para conseguir las placas positivas y negativas

curadas y sin formar. Una vez que todos estos procesos fueron optimizados, las celdas de 2 V / 1 Ah fueron montadas y ensayadas. Los test eléctricos más relevantes realizados para EFBs, de acuerdo a los estándares *VW75073 2012-07 y RNDS SS 36 11 003 2014-05,* fueron seleccionados y adaptados a nuestras celdas. Este procedimiento incluyó el test de capacidad, el arranque en frío, la aceptación de carga, el estudio de polarización negativa y el test de ciclos de vida trabajando en un estado parcial de carga. Las placas negativas también fueron analizadas a lo largo de todo el estudio utilizando las siguientes técnicas: determinación de sulfato de plomo y carbón, análisis de porosidad, determinación de la ASE de Brunauer, Emmett y Teller (BET), difracción de rayos X, y Microscopía Electrónica de Barrido. Todos los resultados derivados de esta tesis se dividieron en 4 lotes.

En el **lote 1** se estudiaron 5 tipos de materiales de carbono (C1, C2, C3, C4 y C5) y dos LS (LS1 y LS2). 6 formulaciones fueron seleccionadas y las placas negativas fueron preparadas, junto con las celdas de 2 V / 1 Ah. Los materiales de carbono de C1 a C4 eran carbonos de tamaño micrométrico, por lo que se esperaba que se localizaran en el esqueleto de plomo de la placa negativa. En el caso del carbón C5, éste era un carbón de tamaño nanométrico, el cual se encontraría localizado en la estructura energética de la MAN, al haber sido expulsado hacia la superficie del esqueleto de plomo durante el proceso de carga. Todos estos materiales de carbono mejoraron la aceptación de carga de la placa negativa. Sin embargo, C5, que fue el único carbón localizado en la estructura energética de la MAN, fue el que menos ciclos de vida completó. En el caso del material de carbón C5 se pudo apreciar la interacción entre este material y el LS, lo que resultó en el empeoramiento del funcionamiento de dicho EO. En el caso de los materiales de carbono cuya dosis no fue bien escogida, un incremento del rendimiento de la REH fue apreciado. LS2 mostró un buen comportamiento cuando iba acompañado de materiales de carbono micrométricos. En el caso del LS1, éste mostró un mejor comportamiento cuando fue acompañado de material de carbono micrométrico y altamente conductor.

El segundo tipo de materiales de carbono que estudiamos durante el **lote 2** fueron las nanofibras de carbono grafitizadas comercializadas por el Grupo Antolin (GANFg). Estas fibras fueron elegidas debido a su alta relación de aspecto, y a su baja resistividad eléctrica ($1 \cdot 10^{-4}$ Ohm m). Estas fibras tienen un diámetro entre 20 y 80 nm, y una longitud máxima de 30 μm. De este modo, se encontrarían integradas en el esqueleto de plomo, y debido a su alta relación de aspecto podrían ser capaces de crear una red conductora dentro de dicho esqueleto si el umbral de percolación es alcanzado. El LS seleccionado fue el

LS2 del lote 1, que durante este lote y en adelante se ha denominado OE1. El primer paso fue la dispersión de las GANFg utilizando parte del OE1. Este proceso fue realizado por GAIKER, un centro tecnológico que nos proporcionó las dispersiones de GANFg. Estas dispersiones fueron utilizadas para preparar las siguientes formulaciones con diferente contenido en GANFg: S5 – 0.50%, S6 – 0.20% y S7 – 0.10%, todas ellas acompañadas de OE1 con una concentración final de 0.30%. Las placas negativas sin formar fueron preparadas, al igual que las celdas de 2 V / 1 Ah. Como resultado, GANFg no mejoraron la aceptación de carga, ya que tampoco mejoraron la superficie específica de las placas negativas formadas. Sí mejoraron la durabilidad de las celdas durante los ciclos de vida. Esta mejora fue representativa cuando las GANFg fueron adicionadas al 0.10%, y por ello esta concentración fue elegida como la concentración óptima de GANFg. Además, el rendimiento de la REH, y con ello el consumo de agua, no sé incrementó cuando las GANFg fueron añadidas al 0.10%.

En el caso del **lote 3,** utilizamos la concentración óptima de GANFg (0.10%) junto con una mezcla de EOs = OE1 + OE2. De este modo, nuestro objetivo fue ver si era posible mejorar la aceptación de carga de la placa negativa cambiando el tipo y concentración de EOs. La mezcla de EOs también se utilizó para la dispersión de las GANFg. Finalmente, se prepararon 5 formulaciones con y sin GANFg al 0.10%, e incluyendo la mezcla de EOs al 0.20% y 0.30%. Los resultados confirmaron el efecto de la adición de EOs en la placa negativa: evitan el fenómeno de pasivación mientras que empeoran los procesos de aceptación de carga. La aceptación de carga de las placas negativas no mejoró debido a la adición de la mezcla de EOs. Sin embargo, la durabilidad de las celdas en el test de ciclos de vida mejoró con la adición de las GANFg, y fue mejor para la formulación que contenía la mezcla de EOs al 0.30%.

Debido a que no conseguimos mejorar la aceptación de carga de las placas negativas con la adición de la mezcla de EOs, en el **lote 4** decidimos utilizar como aditivos las GANFg al 0.10% junto con materiales de carbono del lote 1: C1 (grafito expandido) y C4 (carbón black conductivo). La concentración de los materiales de carbono fue elegida acorde a los resultados obtenidos en el lote 1. De este modo los resultados esperados eran un aumento de la aceptación de carga y de los ciclos de vida, mientras se mantenía el consumo de agua. Las dispersiones de GANFg fueron preparadas con parte del material de carbono, y el resto fue adicionado durante el proceso de mezclado. La concentración final de OE1 fue 0.30% para todas las formulaciones. La aceptación de carga de las placas negativas no se incrementó significativamente por la adición de materiales de carbono junto con las nanofibras. En el caso de los ciclos de vida, pudimos

ver un pequeño aumento en el número de ciclos cuando los materiales de carbono fueron añadidos, especialmente en el caso del material de carbón C1. El consumo de agua se incrementó debido a la adición de materiales de carbono. Después de los ensayos correspondientes a este lote, podemos concluir que los materiales de carbono deben ser añadidos en su dosis óptima para mejorar la aceptación de carga de las placas negativas.

Los resultados de esta tesis doctoral nos llevaron a la conclusión de que los aditivos más adecuados para la placa negativa de las EFBs son los materiales de carbono como grafitos expandidos y cabón blacks conductores, aunque éstos conllevan un alto consumo de agua. La adición de GANFg o su combinación con otros materiales de carbono conllevó a un aumento de los ciclos de vda, pero no mejoró la aceptación de carga de las celdas, lo cual conduciría a un comportamiento no apropiado de la batería durante la parada regenerativa. Por todos estos motivos, los siguientes pasos para mejorar las prestaciones de las EFBs deberían estar centrados en la búsqueda de aditivos que disminuyan el consumo de agua, para así poder utilizar al mismo tiempo grafitos expandidos o carbon blacks como aditivos.

List of abbreviations

Micro Hybrid Electrical Vehicles	Micro HEVs
Internal Combustion Engine	ICE
Carbon dioxide	CO_2
Lead Acid Batteries	LABs
Enhanced Flooded Battery	EFB
Starting Lighting Ignition	SLI
Absorptive Glass-Mat	AGM
Valve Regulated Lead Acid	VRLA
State of Charge	SoC
Partial-State of Charge	PSoC
High Rate Partial State of Charge	HRPSoC
Deep of Discharge	DoD
Current for 20 h capacity	I_{20}
20 h capacity	C_{20}
Leady Oxide	LO
Red tetragonal lead oxide	tet-PbO or α-PbO
Yellow orthorhombic lead oxide	ort -PbO or β-PbO
Monobasic lead sulfate	$PbO \cdot PbSO_4$; 1BS
Tribasic lead sulfate	$3PbO \cdot PbSO_4 \cdot H_2O$; 3BS
Tetrabasic lead sulfates	$4PbO \cdot PbSO_4$; 4BS
Lead hydrocarbonate or hydrocerussite	$2PbCO_3 \cdot Pb(OH)_2$
Grupo Antolin Graphitized carbon nanofibers	GANFg
Organic expanders	OEs
Lignosulfonates	LS
Negative Active Material	NAM
Positive Active Material	PAM
Specific Surface Area	SSA
Brunauer-Emmett-Teller	BET
X-Ray Diffraction	XRD
Scanning Electronic Microscopy	SEM
Cold Cranking Ability	CCA
Initial Charge Acceptance	ICA
Cyclic Voltammetry	CV
Hydrogen Evolution Reaction	HER
Apparent hydrogen overpotential	$\eta_{app, H2}$
Open Circuit Potential	OCP; E_{OCP}

1. Introduction

1.1. Micro Hybrid Electrical Vehicles (HEVs) and Lead Acid Batteries (LABs)

1.1.1. European passenger car emissions study

According to the Organisation for Economic Co-operation and Development (OECD) Glossary of Statistical Terms, "a passenger car is a road motor vehicle, other than a motorcycle, intended for the carriage of passengers and designed to seat no more than nine persons (including the driver). The term "passenger car" therefore covers microcars (need no permit to be driven), taxis and hired passenger cars, provided that they have fewer than ten seats. This category may also include pick-ups" [1]. Nowadays millions of European citizens use this type of car every day for transporting themselves to several places (work, university, schools, nurseries, leisure travels…). The exact number of passenger cars per European citizen older than 18 years old in 2017 (including the following countries: Austria, Belgium, Croatia, Cyprus, Czechia, Denmark, Estonia, Finland, France, Germany, Hungary, Ireland, Latvia, Lithuania, Malta, Norway, Poland, Portugal, Slovenia, Spain, Sweden, Switzerland, and United Kingdom) is 48 [2]. This calculation assumes that every European citizen older than 18 years old has got a driving license. In this way, each person older than 18 years old in Europe can drive 48 cars at the same time. This amount is higher (around 60 cars) for Czechia, Estonia, Malta, and Slovenia, and lower (around 35 cars) for Croatia, Denmark, Ireland, and Latvia. Using passenger cars every day seems to be the main transporting method use by European citizens.

These passenger cars implement a motor engine responsible for their movement. Depending on the type of fuel that feeds the motors, cars can be classified in three main groups: Petroleum products or Gasoline, Diesel and Alternative Energy. On the one hand, the first two groups are conventionally petroleum-based fuels which use an Internal Combustion Engine (ICE). The third group, Alternative Energy or Alternative fuels, includes electricity, Liquefied Petroleum Gas (LPG), Natural Gas Liquids (NGL), Compressed Natural Gas (CNG), alcohols, mixtures of alcohols with other fuels, hydrogen, biofuels (such as biodiesel), etc. [2], although, LPG, NGL, and CNG use also ICE technology [3]. **Figure 1** shows the passenger cars motor engine distribution in Europe for 2017. As can be seen, the largest extent of the European automotive business is based on conventionally petroleum-based fuels, basically the 97% versus 3% corresponding to the alternative fuels.
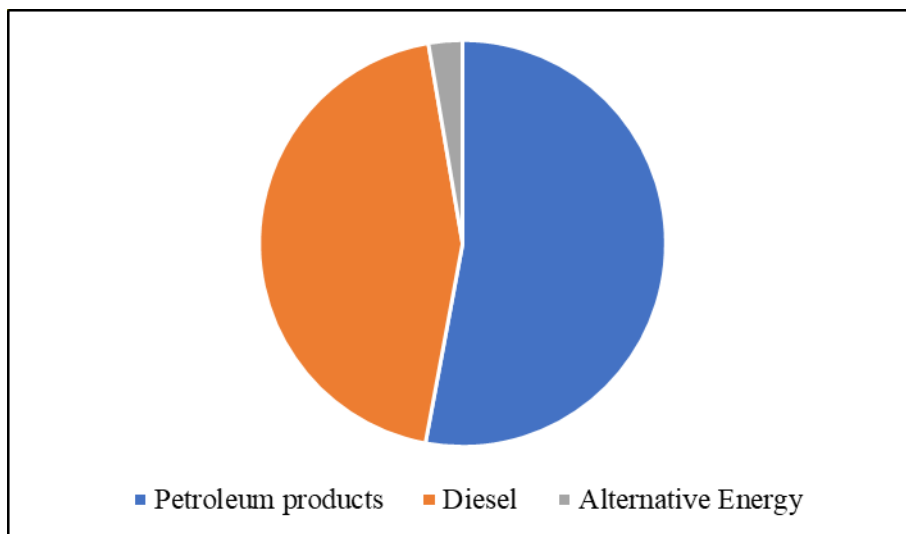
Figure 1. European passenger cars distribution for 2017. Petroleum products or Gasoline (53%), Diesel (44%) and Alternative Energy or Fuels (3%). Based on the following countries: Austria, Belgium, Croatia, Cyprus, Czechia, Denmark, Estonia, Finland, France, Germany, Hungary, Ireland, Latvia, Lithuania, Malta, Norway, Poland, Portugal, Slovenia, Spain, Sweden, Switzerland, and United Kingdom [2].

The main chemical reaction for the ICE is the combustion of fuel and air in a closed chamber. The products of this reaction are high-temperature and high-pressure gases, that exert a force on some component of the engine, converting the chemical energy into mechanical energy. Diesel is normally used for Compression Ignition (CI) engines, whereas gasoline is used for Spark Ignition (SI) engines [4]. One of the main problems related to these conventionally petroleum-based fuels is the impact of both of them on the environment. The combustion of gasoline and diesel is not complete, resulting in the emission of different gasses through the exhaust pipe, such as carbon dioxide (CO_2), carbon monoxide (CO), hydrocarbons (HC), nitrogen oxides (NO_X) and particle matter ($PM_{2.5}$ and PM_{10}) [5,6] These gasses increase the Greenhouse Gases (GHG) emissions and air pollution [3], being the CO_2 emissions the most important due to their implication in the climate change [6,7]. In order to regulate the CO_2 emissions from passenger cars, these emissions are measured during the vehicle certification test, based on the New European Driving Cycle (NEDC) [5]. It is important to understand the link between the CO_2 emissions and fuel consumption. Those are magnitudes directly proportional: less fuel consumption

involves less CO_2 emissions. Keeping this concept in mind, any action that improves the efficiency of the ICE will reduce the CO_2 emissions.

A summary regarding the CO_2 emissions regulatory actions by the European Commission (EC) is below:

- 1970: an introduction of the NEDC together with test protocol for measuring pollutant emissions.
- The early 1980s: CO_2 emissions measurements were added to the European mandatory vehicle certification process. No limit emissions were defined.
- 1995: EC sat a fleet average CO_2 emissions target of 120 g/km for 2005.
- 1999: due to discussions with the vehicle manufacturers a new target of 140 g/km for 2008 was proposed as a voluntary auto industry commitment.
- 2009: Automotive industry did not fulfill the target. New target from the European regulation: fleet average mass-dependent CO_2 emissions target of 130 g/km for 2015 (EU Regulation 443/2009). An additional 10g reduction was expected to be gained due to supplementary actions not measured in the test.
- 2014: CO_2 emissions target of 95 g/km for 2021 (EU Regulation 333/2014).

The breach of this target can lead to fines from 5€ to 95€ per gram of CO_2 exceed per car sold [5].

Figure 2 shows the evolution from 2000 to 2017 of the average of European new passenger cars CO_2 emissions for European countries. Since 2000 the automotive industry has made many efforts to reduce the CO_2 emissions, indeed there has been a reduction of 31% since 2000. However, the emissions level has been the same in 2016 and 2017. If we come back to **Figure 1**, in 2017 most of the passenger cars implement ICE technology (97% exactly). In order to reduce the CO_2 emissions using this type of technology, fuel consumption must be reduced. Keeping the same values of CO_2 emissions in 2016 and 2017 insinuates that there are not more options to reduce fuel consumption, rather the ICE technology in the automotive industry has peaked regarding this issue. Nowadays European new passenger cars are far away to reach the CO_2 emissions target for 2021. The current value of CO_2 emissions is 119.4g/km (from **Figure 2**), and 118.5g/km for EU (27 countries) [2], versus the target for 2021: 95g/km. These figures are not very encouraging for the ICE technologies, which must change and even be combined with new technologies in order to reach the 2021 target.
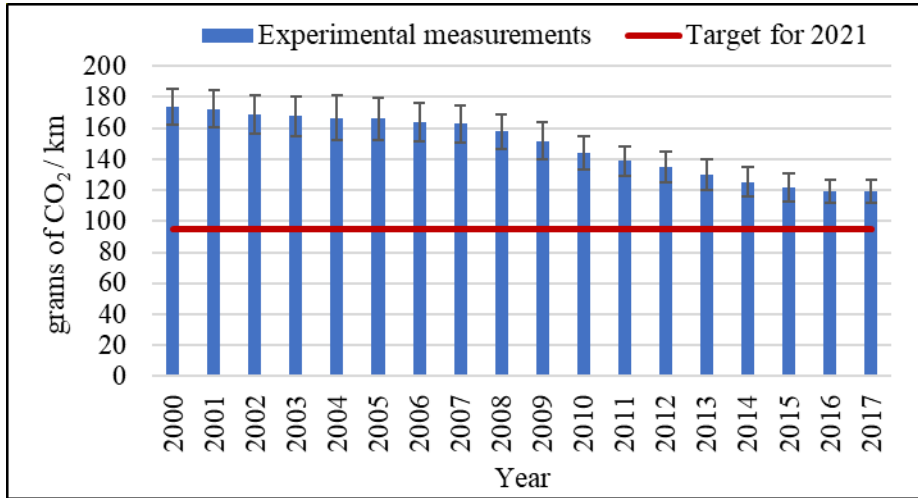
Figure 2. Average of the CO_2 emissions by the European new passenger cars from 2000 to 2017. Based on the following countries: Austria, Belgium, Croatia, Cyprus, Czechia, Denmark, Estonia, Finland, France, Germany, Hungary, Ireland, Latvia, Lithuania, Malta, Poland, Portugal, Slovenia, Spain, Sweden, and United Kingdom. Norway and Switzerland do not provide this info to Eurostat [2].

1.1.2. How can we reduce CO_2 emissions?

The Electrical Vehicle (EV) could be the ideal solution for reducing the CO_2 emissions, as it is powered just by electrical energy. However, EV is still expensive enough to be not affordable for a large extend of the population. Therefore, it is necessary to look for solutions regarding the passenger cars that implement ICE technology or conventional vehicles. In order to reduce fuel consumption in conventional vehicles, the vehicle characteristics and sub-systems that directly impact on this magnitude are listed below:

- Mass and road loads: vehicle mass, aerodynamic resistance, rolling resistance and tires.
- Auxiliary systems: air conditioning (A/C; cooling), heating (electric heating or A/C), steering assist systems and other electrical consumers and auxiliaries (headlights, windscreen wipers, heated seats).
- Friction and lubricants.
- Maintenance and aging: tire maintenance and pressure and other factors (wheel misalignment, suspension system maintenance and air filter clogging.

- Environmental and traffic conditions: weather conditions, altitude, road, road grade, road roughness and texture, and traffic conditions and congestion.
- Driver and user related factors: driving, aggressive driving, driving mode, four-wheel drive, eco-driving, Advanced Driver Aid Systems (ADAS) [5].

Working on the efficiency of these characteristics and sub-systems will bring benefits in terms of fuel consumption and reduction of CO_2 emissions too. I.e. reducing the vehicle mass, while maintaining the materials' resistance, would involve a reduction on the necessary power to accelerate the vehicle during acceleration phases, as well as the rolling resistance, and thus fuel consumption.

In the former section (1.1.1) the passenger cars were classified into three main groups depending on the type of fuel: Petroleum products or Gasoline, Diesel, and Alternative Energy or Fuels. The technologies used by each group can be combined, giving rise to Hybrid Electric Vehicles (HEVs). In the past, this strategy was used with the aim of breaking the petrol dependency of the vehicles [8]. Nevertheless, HEV consumes less conventionally petroleum-based fuels, so produces less CO_2 emissions. The term hybrid means "a thing made by combining two different elements", therefore different levels of hybridization are known, and the current HEVs are divided in micro, mild, full, and Plug-in Hybrid Electric Vehicle (PHEV) [9]. Before getting into details related to the types of HEVs, let's explain some new technologies arising from the necessity of fuel consumption reduction:

- Start & Stop system: this system shuts down the ICE when the vehicle stops, and switches on the ICE when the driver releases the brake pedal. In this way, the vehicle does not waste fuel during the breaks, hence the CO_2 emissions are also reduced. This system can reduce a high amount of emissions in the cities, where the traffic conditions and congestions are more severe.
- Integrated Starter Generator (ISG): this generator acts as an electric motor that can start in a soundless way the ICE. In addition, it can also replace the alternator, supplying the vehicle with the necessary energy for the electrical consumers (lights, A/C etc.). The main functions of the ISG are the start & stop system, electricity generation and the power assistance [10].
- Regenerative braking: during the braking of the vehicle, the kinetic energy can be converted into electrical energy for recharging the battery. This

energy conversion is made by the generator. The capacity of the battery restricts the power generated by the motor during the regenerative braking. With this system a higher energy utilization is achieved, and a longer life of the batteries, and consequently vehicle operation, is expected [11].

Table 1 shows the categorization of the HEVs, as well as some characteristics of them, including the EV too [9,11]. There are five types of HEVs, those ones that combine the ICE with an electric motor. Theoretically, the Micro Hybrid vehicle cannot be considered a HEV, as it does not combine these two engines. However due to implementing the Start and Stop system and the regenerative braking, this type of vehicle contributes to reduce the CO_2 emissions, and improves fuel consumption, therefore we will categorize it as a HEV. Some examples of this type of vehicle are BMW 1 and 3 series, Fiat 500, SMART car, Peugeot Citroen C3, Ford Focus and Transit, and Mercedes-Benz A-class. The Mild and Strong (or Full) HEVs differ from the Micro HEV because of their ability to assist the driving force using the energy stored in the battery from the regenerative braking. Moreover, the strong HEV due to its higher battery capacity and the implementation of an electric motor is also able to travel a short distance with the assistance of the electrical motor. Some Mild HEVs that are currently on the market are BMW 7 Series Active Hybrid, Buick La Crosse with eAssist, Chevrolet Malibu w/ eAssist, Honda Civic and Insight Hybrid, and the Mercedes-Benz S400 Blue Hybrid. In the case of Strong HEVs we have the Chevrolet Tahoe Hybrid, Toyota Prius and Camry Hybrid, Ford C-Max, Honda CR-Z, and Kia Optima Hybrid. PHEVs I and II comprise a battery with higher capacity that provides enough power to travel during medium distances, and they can be charged from external sources (through a plug). Both types store in the battery the kinetic energy from the regenerative braking, but in the case of the type II, which is equipped with an auxiliary power unit, this energy cannot be used to assist the driving force. Chevy Volt, Ford C-Max Energi and Fusion Energi, Fisker Karma, Porsche Panamera S E-Hybrid, and Toyota Prius Plug-in are PHEVs that can be found on the road. EVs are not equipped with an ICE, so they need high capacity batteries, and also a good operation of the regenerative braking that can determine the autonomy of these vehicles. Mitsubishi i-MIEV, Chevrolet Volt EV, Chevrolet Spark EV, Ford Focus Electric, Tesla Model S, BMW i3, Mercedes-Benz B-Class, and Nissan LEAF are examples of EVs that are in the top eight electric cars by CarMax [12]. **Table 1** also shows the fuel

economy improvement. As is expected, higher hybridization leads to higher fuel consumption and CO_2 emissions reductions.

1.1.3. Role of the LABs in the HEVs – Enhanced Flooded Battery (EFB)

Let's focus now in the role of the LABs in the vehicle. Since the early times, the LABs in the vehicles have been known as Starting Lighting Ignition (SLI) because of the main function of them: powering the starting motor, the lighting and the ignition system of the vehicle. However, nowadays the LABs are powering more electrical features such as power seats, power operated tailgate, power sliding doors, fuel-operated parking heaters etc. These features are also running when the engine is off, being powered only by the energy from the LABs. In addition, the Start & Stop system and the regenerative braking are also maintained by the LAB. In the case of the Start & Stop system, the battery must be able to start the engine several times. At the same time, the battery must be easily recharged by the alternator, in order to store enough energy to restart the engine many times.

For the regenerative braking the battery must be able to accept all the electrical energy supplied by the generator during the braking. All these features cannot be powered by a SLI, so the modern cars need more advanced LABs. Furthermore, the LAB helps the vehicle operation when the engine is working at low efficiency. This could happen after a recuperation event, for example, in congestions when the engine is restarted several times (engine standby) the battery is partly suppling the electrical features of the vehicle, even when the engine is on. Consequently, the battery usage is highly dependent on the drive cycle, customer behavior (drive style) and ambient conditions (cabin comfort and visibility tend to inhibit Stop & Start in cold, hot or moist conditions). These factors determine the types and frequency of the discharge and charge cycles of the battery. Furthermore, the voltage for discharging and discharging the battery affect to its life time. Therefore, a Battery Monitoring Sensor (BMS), in combination with an Electrical Energy Management (EEM) strategy are implemented in the modern cars. These two systems control the charging voltage of the battery, preventing over- or undercharging, and maintaining a proper State of Charge (SoC) of the battery. Moreover, the temperature is also monitored, adapting the charging voltage to the battery temperature. This will ensure the starting ability of the battery.

Table 1. Characteristics of HEVs (Micro, Mild, and Strong), PHEV (type I and II), and EV too [9,11].

Types of Vehicles \ Characteristics	Micro HEV	HEV		PHEV		EV
		Mild HEV	Strong HEV	I	II (with an Auxiliary Power Unit)	
ICE	Yes	Yes	Yes	Yes	Yes	No
Fuel tank	Yes	Yes	Yes	Yes	Yes	No
Electrical motor	No	No	Yes	Yes	Yes	Yes
Start & Stop / ISG	Yes	Yes	Yes	Yes	No	No
Battery capacity	Small	Small	Medium	Medium	Large	Large
Cruising distance as EV	Not applicable		short	Medium	Medium	Long
Amount of energy stored during the regenerative braking	Small	Small	Medium	Large	Large	Large
Driving force assistance by motor	Not possible	Low	Medium	High	Not applicable	
Fuel economy improvement	3% to 10%	15% to 20%	20% to 30%	Up to 100%		100%

Knowing the reasons because of the SLI batteries must be replaced by more advanced LABs, we can conclude that new LABs must be able to be easily recharged, due to all the energy that they will accept from the alternator and the regenerative braking. If they are easily recharged, the SoC of the battery will be high, and in those conditions the battery must be able to restart the engine several times, due to the Start & Stop system. Focusing on these demands, the new batteries must have high rechargeability and life time working at high SoC. In order to fulfill these requirements, LABs manufacturers have developed new technologies: Enhanced Flooded Batteries (EFB) or Absorptive Glass-Mat (AGM) batteries. EFB and AGM batteries show higher throughput capability than SLI batteries, which is needed for the operation of the Start & Stop system and the regenerative braking. The main difference between AGM batteries and EFB is the higher deeper cycling capability of the first ones, and thus, a higher price. EFB are more suitable for Start & Stop cars, whereas AGM batteries are more appropriated for commercial vehicles or premium cars [13].

As a summary, the high restrictions from the EC to reduce the CO_2 emissions and improve fuel consumption in the passenger cars have led the car manufacturers to develop HEVs that implement new technologies, such as Start & Stop system and regenerative braking. Some of these HEVs also use an electric motor. When Start & Stop system and regenerative braking are implemented, the conventional SLI battery does not have enough throughput capability to power these features. For this reason, new batteries have emerged for the Start & Stop passenger cars: EFB.

1.2. LABs History

1.2.1. The first LAB

At the beginning of the XIX century may Scientifics devoted their lives to the invention and enhancement of various chemical power sources. As the greatest Detchko Pavlov (September 9th, 1930 – August 25th, 2017. Bulgaria) explained in his book "Lead-Acid Batteries: Science and Technology": *one invention does not come from one inventor* [8]. Many researchers are always working on the same research line, although just a few of them are normally the ones named inventors. Something similar happened with the LAB, whose birth certificate is related to the lecture presented by the scientific Gaston Planté (April 22nd, 1834 – May 21st,

1889. France), 'Nouvelle pile secondaire d'une grande puissance' before the French Academy of Sciences in Paris, on March 26th, 1860 [14].

However, it was a German Medical officer, Dr. Wilhelm Josef Sinsteden (May 6th, 1803 – November 12th, 1891. Germany) the one who gave us the first idea about how the LAB works in 1854 [15]. This officer worked on an electrochemical cell where both electrodes were lead plates, and whose electrolyte was a solution of sulfuric acid. This cell was able to deliver electricity, exactly this homemade accumulator showed an energy density lower than 0.1 W h kg^{-1} at the 15 min discharge duration [15,16]. What happened when this cell was recharged? This fact is explained in **Figure 3. A;** once the cell was charged, different electrochemical reactions occurred on the positive and negative electrode. On the positive electrode, oxidation processes were carried out: oxidation of Pb^0 to PbO_2 and of H_2O (from the electrolyte) to O_2 (g). In this way, the positive electrode surface turned into a bronze color because of the PbO_2 production. At the same electrode, Dr. Sinsteden observed gas evolution explained by the O_2 production. In the case of the negative electrode, the current was used for reducing the H_2O (from the electrolyte) to H_2 (g), and therefore gas evolution was also observed at this electrode. Once the current direction was reversed, the positive electrode acted as the cathode reducing the PbO_2 to $PbSO_4$, and the negative electrode acted as the anode, oxidizing the Pb^0 to $PbSO_4$ (see **Figure 3. B**). These reactions are the current reactions that happen during the discharge of a LAB. At this point, Dr. Sinsteden measured the energy density of the homemade accumulator, and thus discovered the mechanism of a potential secondary battery, the LAB.

Figure 3. C shows the current charge reactions for the LAB, where the positive electrode acts as the anode (oxidation of $PbSO_4$ to PbO_2) and the negative electrode as the cathode (reduction of $PbSO_4$ to Pb^0).
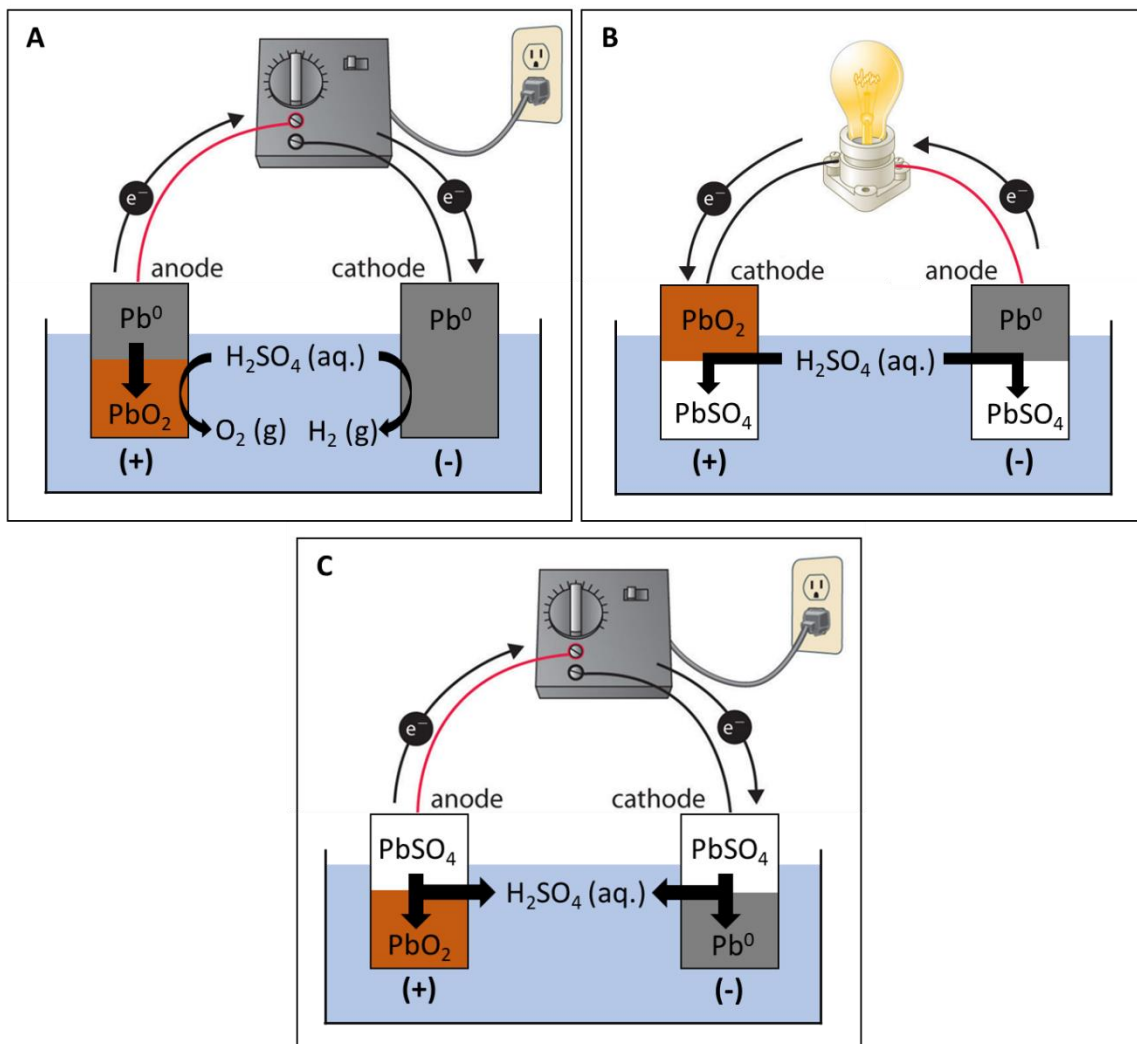
Figure 3. Homemade electrochemical cell. (+) Positive electrode. (-) Negative electrode. **A.** Charge of the cell initially made of two lead electrodes submerged in an aqueous solution of sulfuric acid (electrolyte). Gas evolution was observed on both electrodes. **B.** Discharge of the cell. Same reactions as occur in the current LAB. **C.** Recharge of the cell. Same reactions as occur in the current LAB.

In 1859 G. Planté developed more deeply this idea, and worked on a similar electrochemical cell type, using identical electrodes made of silver, lead, tin, copper, gold, platinum or aluminum submerged in a solution of sulfuric acid. This time the electrodes or plates were separated by a rubber sheet. The polarization of these cells depended on the type of metal used as electrodes, and

all of them delivered energy once the current was reversed, acting as generators. Lead plates showed the highest secondary current, and thus the highest energy delivery, as well as the highest voltage [17]. Finally, on March 26th, 1860 G. Planté was able to present before the French Academy of Sciences in Paris a LAB made of 9 cells connected in parallel (**Figure 4**), giving room to the birth certificate of the LAB, as was mentioned previously [14]. The positive and negative plates were lead sheets separated by a rubber sheet and rolled. One lead strip was connected to the positive plate and another one to the negative plate, forming which are nowadays known as the positive and the negative terminals, respectively. Finally, the cell was filled with diluted sulfuric acid. The negative terminals of three cells were connected in series, at the same for the positive terminals. This happened for three groups of three cells each. Finally, these three groups were connected in parallel. The resulting battery had one positive and one negative terminal, as it is shown in **Figure 4**. When the battery was connected to a generator, reactions from **Figure 3** happened, and the battery delivered energy. This was the birth of the oldest rechargeable battery.
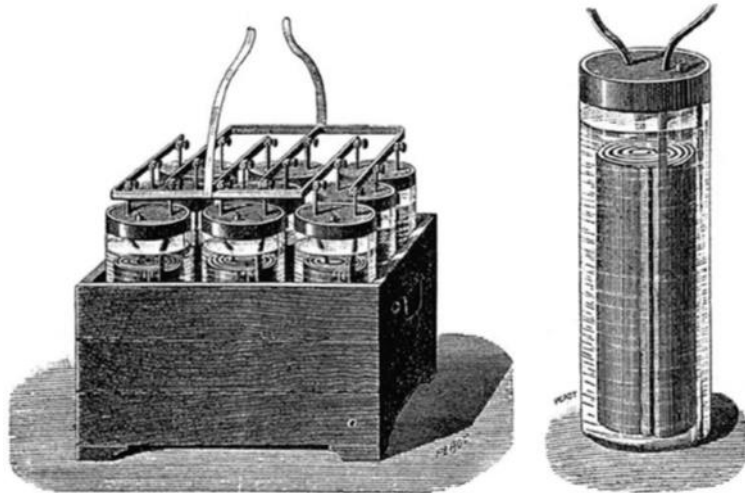
Figure 4. The first rechargeable LAB comprising a series of nine cells.

1.2.2.First technological development and applications of LABs

At the beginning LABs were known as Planté LABs, honoring his inventor. LABs started to be useful and easy to charge once the first electric generators were invented. For example, in 1869 Zénobe Gramme built the first direct

current dynamo machine whose energy was stored in a LAB. In 1873 Bréquet Company was the unique company that manufactured dynamo machines as well as LABs, implementing a system of generation and store of electricity at once. As a handicap, electricity was not essential for human life at that point. All of this was changed in 1879 when Thomas Edison (in EEUU) and Joseph Swan (in England) invented the incandescent lamp, bringing the electricity to everywhere homes as well as increasing the necessity of energy storage. Therefore, LAB demand increased, and the manufacturing technology needed to be updated rapidly in order to maintain a main position in the market. For this purpose, the first technological development occurred since late1870s:

- 1881:
  - The invention of the Positive and Negative Active Material (PAM and NAM) by Camille Fauré. The lead plates were coated by a mix of lead oxide, sulfuric acid and water, and then converted to Pb, in the case of the negative electrode, and to PbO_2 in the case of the positive electrode, once the battery was recharged. This action increased the specific energy of the battery to 8 $Whkg^{-1}$ at a discharge rate of 10 h.
  - Replacement of the lead sheet for a lead grid by Ernest Volckmr.
  - Introduction of a lead antimony alloy for the grids by Scudamore Sellon.
- 1882:
  - The first idea about the tubular plates by S.C. Curie [8].
  - Double sulfate theory: explanation about the electrochemical reactions that occur in the LAB by Gladstone and Tribe [18].
- 1883: Deep study on the charge and discharge reactions by Hermann Aron that explains the correlation between the sulfuric acid density and the discharge time [19].

According to this first technological development, new applications of the LAB were born:

- 1881: LAB was used in a three-wheeled electric automobile by Gustave Trouvé. The maximum speed was 12 kmh^{-1}.
- 1886: LAB was used for propelling the first submarine in France.
- 1899: a cigar-shaped electric car was powered by LAB and reached 109 kmh^{-1}. It was driven by Camille Jenatzy.

- 1882: a system of dynamos and LABs was installed in Paris for the distribution of electricity for lighting.
- 1883: The Imperial Palace of Vienna was lighted by stationary and portable equipment of LAB supplied by G. Planté.

In addition, LABs were rapidly adopted by different telecommunications systems, such as Morse electric telegraph and the telephone. At this point, the LAB completed the first technological development and became one of the most important energy storage and generator system [8].

1.2.3. Second technological development and applications of LABs

The second stage of technological development of LABs brought several changes related to the material as well as the processes involved in their manufacture. One of the most important, if not the most, component of LABs is the lead oxide, which is used for producing both, PAM and NAM. After the introduction of these active materials by Camille Fauré (1881), the necessity for improving the lead oxide production efficiency came. The first method for producing lead oxide involved the oxidation of molten lead in a reverberatory furnace with air flow and water steam, which lasted 30 hours. Moreover, the resulting lead oxide was not fine enough and it has to be milled. In order to reduce the processing time, in 1898 George Barton patented a new method where small droplets of molten lead were oxidized by a humidified air steam in a pot. Furthermore, the lead oxide particles were classified by size: the big ones were taken back to the pot to be more oxidized and the fine ones were taken out of the pot and collected in a silo. Another method patented by G. Shimadzu in 1926, was the use of lead balls in a ball-mill: the lead balls tumble against each other's generating heat due to the friction of the balls. This heat is hot enough to oxidize the lead balls surface, which becomes lead oxide powder that is removed from the surface and evacuated from the ball by air flow at a certain speed. The coarse particles are thrown again in the ball to be reprocessed, and the fine particles are collected in silos. By 1926, thanks to these two methods, the lead oxide production time had been drastically reduced which resulted in a big improvement in the LAB manufacture.

During the twentieth century many new materials arose and were implemented in the LAB, as well as new manufacturing processes. Such as the following:

- The ebonite used for the battery container was replaced by Polypropylene (PP) and Polyethylene (PE) copolymer or by Acrylonitrile Butadiene Styrene (ABS).
- Wooden separators, used for separate the negative and positive plates, were replaced by Polymerizing Vinyl Chloride (PVC), PE, PP or AGM separators.
- The first lead alloy used for the lead grid contained 11% of Sb, commonly known as "hard lead". New additives were used in the lead alloys such us Sn, As, Ca and Ag, and the antimony content was reduced.
- The first grids were made by gravity casting, where the molten lead falls down into a grid mold by gravity. New methods for processing the lead grids were developed: die-cast, continuous casting, punching, expansion technology…

Also, along the twentieth century many problems with the performance of LABs arose mainly linked to the lack of knowledge of the chemistry of many processes. Such as:

- The Premature Capacity Loss (PCL) discovered when the antimony was eliminated from the positive grid alloy. The reason of this effect was the formation of a PbO layer on the positive grid with high ohmic resistance that prevented the charge and discharge reactions at the positive electrode.
- Research on the basic lead sulfate pastes: once the lead oxide is mixed with sulfuric acid and water, as was introduced by Camille Fauré in 1881, basic lead sulfate pastes are processed, which will give room to the PAM and NAM. These pastes are comprised by different basic lead sulfates which will determine the performance of the LAB. For example, when tetrabasic lead sulfates ($4PbO \cdot PbSO_4$; 4BS) are used in the PAM the cycle life of the battery will improve.
- The active materials are made of two different structures: the skeleton, a grid that gives support to the energetic structure.
- How to improve the utilization coefficient of the NAM. Once the discharge starts at the negative plate the lead is converted to lead sulfate that passivates the plate and prevents the discharge. For this reason, the NAM must be like a lead spongy where the electrolyte has no limitation to access. In order to achieve this challenge, a group of substances called expanders must be added to the NAM [8].

As a summary, LABs mechanism was found by Dr. Sinsteden in 1854, however it was G. Planté the one that introduced to the world the first LAB in 1859. This finding had a great impact on the society, that started using this technology for storing the energy from a dynamo at the very first time, but soon the LABs were lightening the streets of Paris or the Imperial Palace of Vienna. This technology has continued growing up and developing, and nowadays LABs are still essential for the human life.

1.3. Secondary batteries and comparison to LABs

While LABs were developing, other technologies were arising too. During this section we will talk about basic concepts regarding the secondary batteries, the types of secondary in the current market and a comparison between LABs and those ones.

1.3.1.Basic concepts about secondary batteries

The term battery refers to a device that carries chemical energy that can be converted into electric energy whenever it is needed. There are two types of batteries: primary or disposable, and secondary or rechargeable. The primary batteries are just able to deliver energy, and after used them, they are disposed. In the case of the secondary batteries, these can be recharged and used again. The secondary batteries are energy storage systems that are completely integrated into our daily life, e.g. we use them in our smartphones, laptops, medical devices etc.

The main components of a secondary battery are the positive electrodes, the negative electrodes, keeping apart by separators (made of porous material), and this assembly is submerged in an electrolyte. The electrodes of the same type, positive or negative, are connected to the current collectors using a conductive compound (normally a metal like lead, copper…) resulting in the negative or positive terminal. The positive and the negative electrodes form a redox system: when the battery is being discharged, the positive electrode is being reduced (cathode), and the negative electrode is being oxidized (anode). The reverse reactions occur during the charge of the battery, the positive electrode is being oxidized (anode), and the negative electrode is being reduced (cathode). The redox reaction that occurs during the discharge must be spontaneous.

The main characteristics of a secondary battery are the following:

- Open Circuit Voltage (OCV): the OCV of a battery comes from the internal redox reactions that occur inside it during the discharge of the battery.

$$OCV_{battery}(V) = E_{cathode} - E_{anode} = E_{positive\ electrode} - E_{negative\ electrode}$$

- Capacity: the capacity is the time that a battery can maintain a constant discharge current. It is expressed in Ah. For example, a battery that can deliver 200 A during 20 h has a capacity of 400 Ah.

$$C_t = I_t*t; \text{ in this case: } C_{20} = I_{20}*20\ h = 200\ A*20\ h = 400\ Ah.$$

This type of capacity would be called C_{20}, and the discharging current I_{20}. The capacity is directly related to the amount of energy that a battery is able to deliver. Depending on the application of the battery, the capacity is given at a time or another: C_5, C_{10}, C_{20}... It is important to define which type of capacity is provided.

- SoC: percentage of the charge stored in the battery. When the battery is fully charged the SoC is equal to 100%. If the battery has a C_{20} equal to 400 Ah, and it is discharged for 20 h at 20 A (I_{20}) the SoC would turn to 0%.

$$SoC = ((C_{20} - t * I_{20}) / C_{20}) *100$$
$$SoC = ((400\ Ah - 20\ h * 20\ A) / 400\ Ah) * 100 = 0\%$$

If it is discharged for 10 h at 20 A (I_{20}) the SoC would turn to 50%.
$$SoC = ((400\ Ah - 10\ h * 20\ A) / 400\ Ah) * 100 = ((400\ Ah - 200\ Ah) / 400\ Ah) * 100 = 50\%$$

- Deep of Discharge (DoD): is defined as the percentage of discharged Ah. If the battery has a C_{20} equal to 400 Ah, and it is discharged for 10 h at 20 A (I_{20}) the DoD is:

$$DoD = 100\% - SoC_{after\ discharge} = 100\% - ((C_{20} - t * I_{20}) / C_{20}) * 100 = 100\% - 50\% = 50\%$$

- Power capacity or energy: is defined as the energy stored in a battery. It is expressed in Wh, and it comes from multiplying the voltage by the current provided from a battery during a period of time.

$$\text{Power capacity (Wh)} = V \text{ (V)} * I \text{ (A)} * t \text{ (h)}$$

- Specific energy: is defined as the energy stored in a battery per unit of mass and it is expressed in $Whkg^{-1}$. It comes from divided the power capacity by the mass of the battery in kg.

- Energy efficiency (ε): the overall efficiency of a battery comes from the efficiency during the discharge process and the efficiency from the charge process. Energy efficiency during the discharge ($\varepsilon_{Discharge}$) is defined as the energy delivered (E_{out}) by the battery during the discharge divided by the energy stored (E_{stored}). Energy efficiency during the charge (ε_{Charge}) is defined as the energy stored (E_{stored}) divided by the energy provided to the battery for the recharge (E_{in}).

  Energy efficiency (ε) = $\varepsilon_{Discharge} * \varepsilon_{Charge} = (E_{out}/E_{stored}) * (E_{stored}/E_{in}) = E_{out}/E_{in}$

1.3.2. Types of secondary batteries technologies

As secondary batteries are defined as chemical storage systems, each type of battery follows a type of chemistry. In this section the main battery chemistries will be explained:

- Lead Acid Battery
  - Discovery: 1860.
  - Electrochemical reactions during discharge:
    Anode: Pb (s) + H_2SO_4 (aq) $\Rightarrow$ $PbSO_4$ (s) + $2H^+$ + $2e^-$ / $\mathbf{E^0 = -1.69\ V}$
    Cathode: PbO_2 (s) + H_2SO_4 (aq) + $2H^+$ + $2e-$ $\Rightarrow$ $PbSO_4$ (s) + $2H_2O$ (l) /
    $\mathbf{E^0 = 0.36\ V}$
    Total: Pb (s) + PbO_2 (s) + H_2SO_4 (aq) $\Rightarrow$ $2PbSO_4$ (s) + $2H_2O$ (l) /
    $\mathbf{E^0 = 2.05\ V}$
  - Anode composition: lead grid covered by spongy lead.
  - Cathode composition: lead grid covered by a lead dioxide paste.
  - Electrodes configuration: typically, planar.
  - Electrolyte: diluted sulfuric acid or sulfuric acid gel.
  - Separator: sheet made of porous material or of a non-conductive glass mat.
  - Current collectors' composition: lead for the anode and the cathode.

- Advantages: inexpensive, lead is always in solid state and not losing during the battery performance.
- Disadvantage: lead is very heavy -> low power density.
- Applications: power accumulator for stationary applications, Uninterrupted Power Systems (UPS), Start & Stop batteries [20].

- NiCd Battery
- Discovery: end of the 19th century.
- Electrochemical reactions during discharge:

  Anode: $Cd + 2OH^-$ (aq) $\Rightarrow$ Cd(OH)2 (s) + 2e− / $\mathbf{E^0 = \text{-0.40 V}}$

  Cathode: $2NiO(OH) + 2H_2O$ (l) + 2e− $\Rightarrow$ $2Ni(OH)_2$ (s) + 2OH− (aq) / $\mathbf{E^0 = 0.80 \text{ V}}$

  Total: $Cd + 2NiO(OH) + 2H_2O$ (l) $\Rightarrow$ $2Ni(OH)_2$ (s) + $Cd(OH)_2$ (s) / $\mathbf{E^0 = 1.20 \text{ V}}$

- Anode composition: Cadmium.
- Cathode composition: Nickel (III) oxide-hydroxide.
- Electrodes configuration: typically, planar. Can be shaped as a jelly-roll design to make up cylindrical cells.
- Electrolyte: potassium hydroxide, KOH, either as a liquid or as a gel.
- Separator: sheet made by non-woven material.
- Current collectors' composition: Cadmium for the anode. For the cathode a metal covered by Nickel (III) oxide-hydroxide is used.
- Advantages: energy density twice of the lead acid battery.
- Disadvantage: low energy density, expensive, and cadmium represents hazards to biological systems.
- Applications: first battery technology put into portable electronics (laptops, cellular telephones...) [20].

- Nickel Metal Hydride (NiMeH) Batteries
- Discovery: 1990.
- Electrochemical reactions during discharge:

  Anode: MeH (s) + OH^- (aq) $\Rightarrow$ Me (s) + $2H_2O$ + 1e− / $\mathbf{E^0 = \text{-0.80 V}}$

  Cathode: $2NiO(OH) + 2H_2O$ (l) + 2e− $\Rightarrow$ $2Ni(OH)_2$ (s) + 2OH− (aq) / $\mathbf{E^0 = 0.80 \text{ V}}$

  Total: $Cd + 2NiO(OH) + 2H_2O$ (l) $\Rightarrow$ $2Ni(OH)_2$ (s) + $Cd(OH)_2$ (s) /

$E^0 = 1.60$ V

- Anode composition: hydrogen adsorbed on a metal surface (Me). The intermetallic AB_5 compounds are the most used, where A is a rare-earth mixture of lanthanum, cerium, neodymium, praseodymium, and B is nickel, cobalt, manganese, or aluminium.
- Cathode composition: Nickel (III) oxide-hydroxide.
- Electrodes configuration: typically, planar. Can be shaped as a jelly-roll design to make up cylindrical cells.
- Electrolyte: potassium hydroxide, KOH, typically as aqueous gel.
- Separator: sheet made by non-woven material.
- Current collectors' composition: metal alloy for the anode. For the cathode a metal covered by Nickel (III) oxide-hydroxide is used.
- Advantages: well known, high energy density.
- Disadvantage: special charging software needed due to the charge memory effect (the battery needs to be completely discharged to not losing capacity).
- Applications: portable electrodes for almost a decade, late 1990s to around 2005. Competitor of Li-Ion battery in HEVs [20].

- Zeolite Battery Research Africa (ZEBRA) Batteries
- Discovery: during the Second World War (1939 – 1945).
- Electrochemical reactions during discharge:
  Anode: Na (l) $\Rightarrow$ Na$^+$ (l) + 1e$^-$ / $E^0 = $ **-2.71 V**
  Cathode: $NiCl_2$ (l) + Na$^+$ (l) + 2e− $\Rightarrow$ $NaCl_2$ (l) + Ni / $E^0 = $ **-0.24 V**
  Total: Na (l) + $NiCl_2$ $\Rightarrow$ $NaCl_2$ (l) + Ni / $E^0 = $ **2.47 V**
- Working temperature: 245°C.
- Anode composition: liquid sodium.
- Cathode composition: porous structure of nickel (Ni) and salt (NaCl) which is impregnated with $NaAlCl_4$, a 50/50 mixture of NaCl and $AlCl_3$.
- Electrodes configuration: prismatic batteries where the cathode is in the center.
- Electrolyte: molten sodium tetrachloroaluminate ($NaAlCl_4$).
- Separator: β''-Al_2O_3-ceramic which is conductive for Na$^+$ ions. It separates the sodium liquid and the $NaAlCl_4$.
- Current collectors' composition: carbon submerged in the liquid cathode mixture.

- Advantages: higher energy density than NiCd and NiMeH batteries.
- Disadvantage: the battery must be kept warm when it is not being used, more expensive than Li-Ion batteries.
- Applications: high working temperatures; large-scale stationary energy storage, possibly in combination with distributed heating systems [20,21].

- Li-Ion Batteries
- Lithium Metal batteries: these batteries were the precursor of the Li Ion batteries. They power devices such as calculators, watches, car key fobs etc. However these batteries are not rechargeale, so they evoluted to the Li Ion battery.
- Discovery: 1985, the $LiCoO_2$ (LCO) battery was reported and patented.
- Electrochemical reactions during discharge for LCO:
  Anode: $Li_xC \Rightarrow C + xLi$ (diss) $+ xe^-$ / $\mathbf{E^0 = \text{-}3.04\ V}$
  Cathode: $Li_{(1-x)}CoO_2$ (s) $+ xLi^+$ (diss) $+ 1e^- \Rightarrow LiCoO_2$ (s) /
  $\mathbf{E^0 = 1.00 - 1.30\ V}$
  Total: $Li_{(1-x)}CoO_2$ (s) $+ Li_xC$ (s) $\Rightarrow LiCoO_2$ (s) / $\mathbf{E^0 = 4.00 - 4.30\ V}$
- Anode composition: carbon-based active anode material (~ 90 μm). However, several newer batteries also use silicon-based or titania-based anode material. When the battery is fully charged the Li atoms are located inside the carbon structure; the ratio is normally LiC_6.
- Cathode composition: LCO active electrode material (~ 110 μm) is home to the Li^+ ions when the battery is being discharged. LCO formula is $Li_{(1-x)}CoO_2$, an x is limited to 0.55. Li^+ ions must be always present in the cathode structure, otherwise the crystalline structure is lost and the battery cannot work anymore. Normally a very large family of transition metal oxides can be used as cathode, using the lighter metals with partially filled d-orbitals, such as $LiMn_2O_4$ (LMO), NMC $LiNi\frac{1}{2}Mn\frac{1}{2}CoO4$ (NMC), $LiFePO_4$ (LFP).
- Electrodes configuration: sheets of the active electrode materials on both sides of the current collectors.
- Electrolyte: lithium salts solved in organic solvent such as ethyl carbonate and dimethyl carbonate (50%/50%).
- Separator: porous material around 20 μm thick, either organic, polymeric, or like fiber glass.

- Current collectors' composition: anode current collector of copper ($\sim$ 30 μm), and cathode aluminum current collector ($\sim$ 30 μm).
- Advantages: broad range of cathode chemistries for making the battery less expensive, and improving the power and energy density.
- Disadvantage: aggressive fire when temperature increases significantly above 100°C due to thermal runaway. SoC equal to 80% at the end of the battery life, at that point batteries degrade very quickly, and several different safety issues arise much more frequently.
- Applications: portable electronics, EVs, home battery by Tesla… [20].

- Redox Flow Batteries
  - Discovery: emerging technology.
  - Working principle: two different liquid electrolytes of metallic salts located in the positive and in the negative tanks, are pumped through the battery reactor. The battery reactor consists of a positive electrode, positive solution tank, ionic exchange membrane, negative solution tank and negative electrode. The salts contained in the positive solution are oxidized and the resultant electrons are used for reducing the salts contained in the negative solution. There are different types of redox flow batteries, depending on the transition metals used in them. One of the most important is the vanadium redox battery (VRB). Organic redox flow batteries are also under development.
  - Electrochemical reactions during discharge for the (VRB):

    Anode: V^{2+} (aq) $\Rightarrow V^{3+}$ (aq) + $1e^-$ / $\mathbf{E^0}$ **= -0.26 V**

    Cathode: VO_2^+ (aq) + $2H^+$ + $1e^- \Rightarrow VO^{2+}$ (aq) + H_2O / $\mathbf{E^0}$ **= 1.00 V**

    Total: V^{2+} (aq) + VO_2^+ (aq) + $2H^+ \Rightarrow V^{3+}$ (aq) + VO^{2+} (aq) + H_2O /

    $\mathbf{E^0}$ **= 1.26 V**
  - Positive solution: V (V) and V (IV) supported in a sulfuric acid solution.
  - Negative solution: V (III) and V (II) supported in a sulfuric acid solution.
  - Electrodes composition: graphite bipolar plates where the redox reactions take place.
  - Separator between the positive and the negative solutions: ionic exchange polymer membrane.
  - Advantages: The reactor size and design define the power (kW) capacity and the storage tanks define energy (kWh) capacity of flow cell batteries.

Reasonably high volumetric energy density (3 – 30 WhL^{-1}) and low self-discharge rates.

- Disadvantage: low mass-specific energy content, which correspondingly would be 1–20 Wh kg^{-1}.
- Applications: stationary use in centralized energy storage systems, in less urban areas, large-scale energy storage systems….

Other type of flow batteries are the concentration flow batteries, where Electrodialysis (ED) can be used to build up concentration differences between the two solutions [20].

1.3.3. LABs vs other technologies

In order to compare the different batteries technologies **Table 2** shows the capacity factors of the main ones described in the above section. It is also included in this table the time framework. Some relevant factors are the specific energy and the power of a battery, as it really matters when we are talking about portable applications. Specific energy and power values over the time show the interest of the scientific community to increase in a higher degree the specific energy, instead of the power of the batteries. Higher specific energy batteries are needed for portable batteries, where high power is not necessary. The most competitive batteries in terms of cycle life are the LAB and Li-ion battery. Li-ion, due to being a newer and more sophisticated technology, is able to perform the highest number of cycles, far away from LAB. Energy efficiency has been improved through the years according to the improvement of the energy density: new geometries that pack more active material in the same space, making the active material more available, reducing the ohmic resistance of the battery, and thus, increasing the energy efficiency. Wide temperature ranges are related to high battery capacities, as the ohmic resistance of the battery is relatively low in the whole range. The electrochemical reactions take place even at extreme conditions. The SoC window is linked to the ageing factor of the different batteries. When the battery is working out of this window, ageing problems come. In the case of Li-ion batteries, just 70% of the energy is available, and special systems are required for monitoring the SoC window during its performance.

Table 2. Battery capacity metric ranges for the main technologies.

Capacity factor	Lead Acid	NiCd	NiMeH	ZEBRA	Li-ion
Specific energy / $Whkg^{-1}$	20–40	40–60	50–70	100–150	150–250
Power / Wkg^{-1}	5–200	10–150	10–100	150–250	100–500
Cycles / 1000	1–5	1–3	1–3	1–2	1–20
Energy Efficiency / %	60–90	80	80	90	90–98
T-range / °C	−10 / 50	−20 / 45	−20 / 45	90 / 250	−20 / 50
OCV / V	2.05	1.20	1.60	2.60	3.00–4.00
SoC window / %	0–100	0–100	0–100	-	20–90
Time framework	1940 – currently	1992 – 2002	1998 – 2005	1995 – 2009	2005 – currently

Figure 5 shows the Ragone plot that allows us to compare very different storage devices systems.
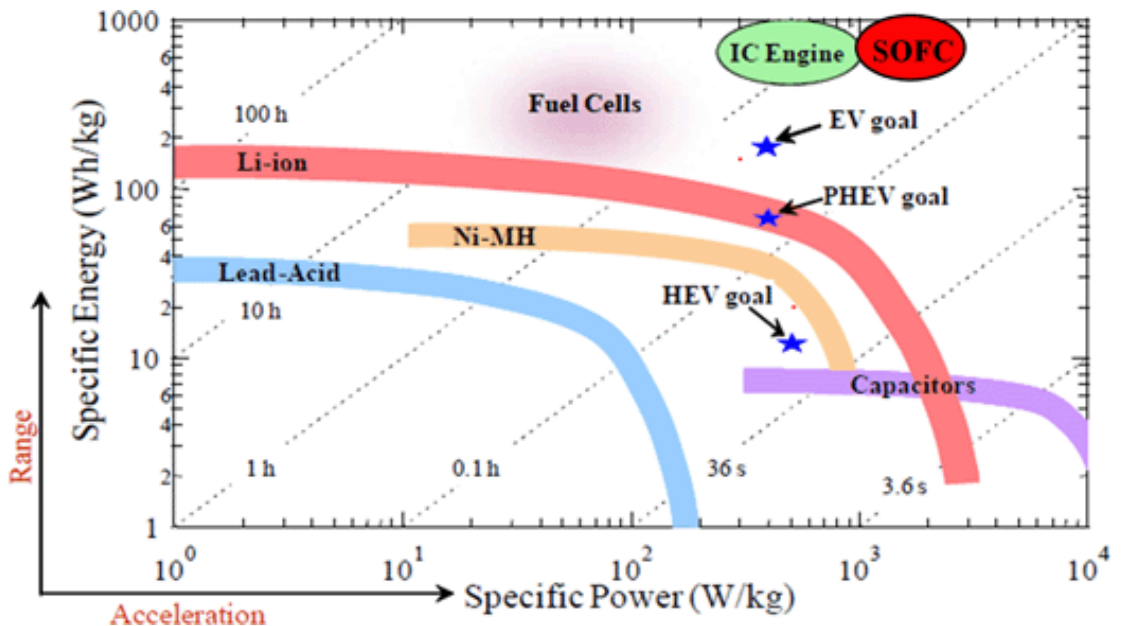
Figure 5. Ragone plot. SOFC: Solid Oxide Fuel cells [22].

1.4. Types of LABs and applications

As it was mentioned above, LABs have been used since 1881, and they still have an important role as a secondary power source. Why? How has this old technology survived to all the developments of the last years? We have been working for more than 120 year on this technology: researching on the chemical manufacturing processes, as well as on understanding the chemistry of the battery performance. All this research has brought an improvement on the battery performance, and a reduction of the processing time, together with the achievement of a robust, reliable and cheap technology. Because of these three attributes, the LAB has survived to all these last years of continuous technological development. In addition, 99% of the used lead is recycled at the different recycling centers, which shows the environmental responsibility of the LAB companies.

There are many classifications of LABs depending on the different selection criteria, such as type of plates, alloys, maintenance, electrolyte status, power or applications. **Table 3** shows a summary of all of them.

Table 3. Classification of LABs.

Type of LAB	Voltage	Type of positive plate	Electrolyte status	Maintenance	Power	Application	
SLI	6 V – 12 V	Flat	Liquid	Yes	300 Wh – 1.5 kWh	Conventional LAB used for passenger cars	Automotive
EFB	12 V	Flat	Liquid	No		For micro-hybrid vehicles with Stop & Start	
VRLA AGM	6 V – 12 V	Flat	Absorbed in the AGM separator	No		For micro-hybrid vehicles with Stop & Start	
Spiral cells VRLA AGM	6 V – 12 V	Flat	Absorbed in the AGM separator	No		High power and deep cycle for special vehicles and construction machines	
VRLA gel	6 V – 12 V	Flat or tubular	Gel	No		Very deep cycle board net batteries in vehicles	
Stationary batteries – Network Power	2 V	Tubular	Liquid	Yes	5 kWh - 50 MWh	Use as backup power supply, i.e., to generate and store electric energy for use, on request, by telecommunication systems, electric utility centers, computer systems...	Industrial
			Gel	No			
Traction batteries – Motive Power	2 V	Tubular	Liquid	Yes	3 kWh - 300 kWh	Used to power in-house transport vehicles: fork-lift trucks, electric cars, mining equipment, etc.	
			Gel	No			
Special purpose	2 V	Tubular	Liquid	Yes	-	For use in aircraft, submarines, special military equipment.	-
			Gel	No			

As is indicated in **Table 3**, the LABs can be also classified by the type of <u>maintenance</u>:

- <u>No maintenance-free or flooded batteries</u>: the electrolyte of these batteries is diluted sulfuric acid that becomes more concentrated due to the loss of water during the battery performance. For this reason, these batteries have a plug for topping up the battery with water. The grid of these battery plates can be made by high Sb content lead alloys, as Sb involves high-water consumption, but for this type of battery that is not a matter of importance.
- <u>Maintenance-free batteries</u>: on the contrary to the above group, these batteries cannot be refilled with water, so all the compounds that involve an increase in the water consumption must be eliminated. For example, in the case of the positive plates, the alloy can contain low Sb content, or Sb can be completely replaced by calcium and tin. In the case of the negative plates, the preferable alloy is PbCa. In order to lose the lowest amount of water, instead of having a plug, these batteries have a valve where the water can be recovered, and are called Valve Regulated Lead Acid (VRLA) batteries. The electrolyte of these batteries can be in the form of liquid or in the form of a gel. The gel is a semisolid structure made by mixing sulfuric acid, silica and water.

Two main categories of <u>applications</u> are differentiated in **Table 3**, for the application of LABs, Automotive, for the batteries used by different vehicles, and Industrial, for the batteries used in another type of business, such as network or motive power. Submarine batteries and other types are not classified.

Nevertheless, there is only one battery that must catch our attention in this study, the EFB, the one that the Micro HEV implements. It is important to notice here that the term EFB does not refer to a new design or technology. EFB could be understood as an advanced SLI battery, in fact the similarity of these two batteries design has made possible to increase the performance of the EFB with a low cost in production, as the same production machinery is used for both batteries, EFB and SLI [23].

1.5. Manufacturing processes and LABs components

1.5.1.   Grids production → Plate grids

Figure 6 shows an example of a flat plate grid. Plate grids are plates made with lead alloys with a square / rectangular geometry. As can be seen in the figure, the center of the plate has network geometry of horizontal and vertical wires (current collectors), surrounded by the frame. At the upper part of the frame, there is the lug that will be connected to the strap. The central part could also be named as pasting area, and will be the location of the paste.
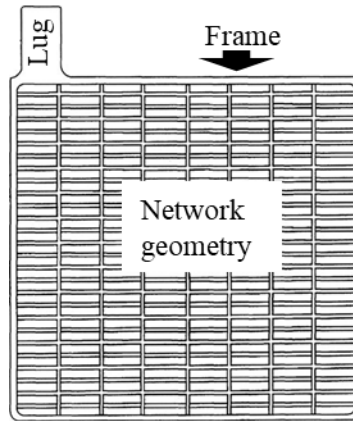
Figure 6. Example of a flat plate grid.

Functions of the plate grids:
- Mechanical support for the paste, or active material, of positive and negative plates.
- Current conductor: the current reaches the lug and then it must be homogenously distributed through the plate grid.
- Direct contact between the current and the active material. This contact is denominated Corrosion Layer (CL).

Key characteristics of the plate grids:
- Grid geometry must be adapted for reducing the ohmic resistance of the grid, and made possible a homogeneous current distribution. Different geometries are chosen depending on the LAB application.
- Plate grids must be hard enough for maintain the shape during the manufacturing process, as well as during the battery life.
- As the lug is the current input way, and must be welded to the strap, a good weldability of the grid is needed.
- The alloy composition is also important for reducing the ohmic resistance, and for improving the formation of the CL. The final plate grid must show a high electrical conductivity.

Main plate grid designs:
- Flat: this type of design is showed in **Figure 6**. The network geometry can be changed, but the final plate will be flat, and the overall thickness will be the same as the frame thickness. Flat design is used for positive and negative plates.
- Tubular: **Figure 7** shows an example of a tubular grid plate together with the gauntlet and the PE bottom bar (other types of materials can be also used). This type of grid is made of spines, lead tubes that will be the current collectors of the grid. The active material is in direct contact to the spines, while it is retained by the gauntlets. The bottom part is closed

with the bottom bar. This type of design is used for the industrial batteries, where a high number of cycles at high DoD is required.
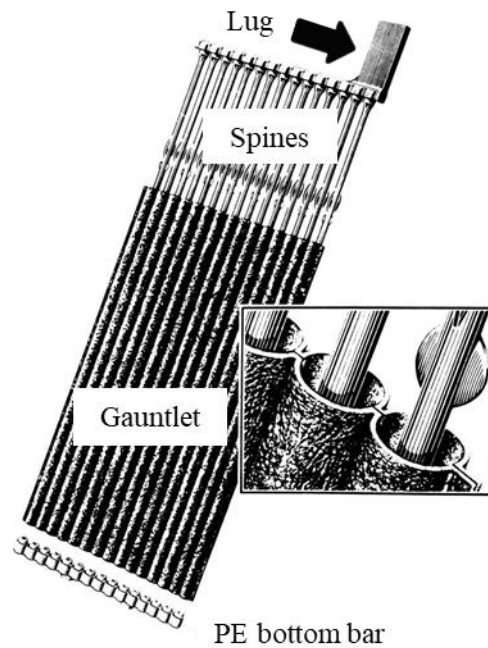
Figure 7. Tubular design plate grid. PE bottom bar and gauntlet included.

Manufacturing technologies:

- Grid/spines casting: plate grids are casted by gravity or pressure, using molds at a certain temperature depending on the type of lead alloy. This technology is mainly used for the industrial batteries.

- Continuous production grid plate process: for SLI batteries, the continuous production for grids has been developed in order to increase the productivity. Below are listed the main technologies:

- Continuous expanded grid production process. A rolled metal sheet cast form lead alloy is slit and then expand. Finally a lower thickness sheet with diamonds geometry is obtained.

- Continuous punched grid production process. A rolled metal sheet with the same thickness of the final grid is punched for getting the desired structure.

- Continuous drum-casting process for grid production (Concast process). The lead alloy ingots are poured into a casting shoe where they are melted. The casting shoe is directly connected to a rotating drum which rolls the final grid sheet.

Historically, antimony was the main alloying additive due to providing good mechanical properties to the grid. However, it also increased the water consumption of the battery. Because of this it had to be partially replaced for other additives such as As and/or Sn (mechanical properties), Sn, Se, S, and/or Cu (casting properties), Ag (anti-corrosion properties) and Sn and/or Bi (electrochemical properties).

1.5.2. Lead ingots oxidation → Leady oxide (LO) powder

One of the main components of the LAB is the LO used for the PAM and the NAM. LO comes from the oxidation of lead ingots, and it is defined as a mixture of Pb^0 and lead oxide (PbO). Depending on the Pb^0 concentration, the LO is considered less or more oxidized. The PbO has two polymorphs:

- Red tetragonal lead oxide (tet-PbO) or α-PbO. Also called litharge.
- Yellow orthorhombic lead oxide (ort -PbO) or β-PbO. Also called massicot.

The polymorph stable at low temperature and low oxygen pressures is the tetragonal one (α-PbO). Tet-PbO, the polymorph preferred by the LAB industry, converts to ort-PbO at temperatures higher than 489°C.

Both polymorphs have a well-defined layered structure. As was said before, the LO comes from the oxidation of the lead. This reaction occurs at room temperature when the medium is humid. In this case, the outer surface of the lead reacts with the oxygen from the atmosphere and forms PbO at the Pb/air interface. Once the first layer of surface has been produced, the oxygen diffuses through the PbO layer via a vacancy mechanism, reaching the lead surface and producing more PbO at the Pb/PbO interface [24]. This reaction is exothermic.

At the end of XIX century the two methods for the LO production were developed, and are the ones that are used in the current LAB industry. The final oxidation of the LO is between 20 and 30 wt%. The LO particles can be considered a round lead particle covered by PbO layers.

-       Barton pot method: in this method the molten lead at 450°C is pumped in large reaction pot equipment. This equipment comprises a rotating paddle that agitates the lead, forming drops of molten lead. At the same time a stream of humidified air enters into the reaction pot (470°C). At this moment the humidified air oxidizes the drops of molten lead, reaction that is catalyzed by the water, producing grains of LO (dust). The particles are carried to a classifier, where coarse particles are selected and taken back to the pot for further oxidation. The reaction pot temperature must be kept at temperatures lower than 487°C for getting only tet-PbO particles. However, this temperature is difficult to maintain

due to the hot generated by the oxidation reaction itself. Because of this, higher temperatures are reached in some areas of the pot, and a 15% of the final LO is made of ort-PbO. The final degree of oxidation of the LO is between 70% - 80%,

- Ball mill method: this method was first invented by Shimadzu in Japan in 1924. Despite of the several changes, the principle of the method remains intact. At first step the lead ingots are melted and converted to lead cylinders or balls. These lead balls are fed into a large steel drum. The drum starts rotating and the lead balls start rubbing each other and the lead ball surface is oxidized to lead oxide. At the same time, air flow is entering in the drum through two ways: the lead balls feeder and several vents located at the drum case. This air flow provides oxygen for the oxidation reaction and sweeps along the LO particles. Due to the oxidation reaction generates heat, as well has the rubbing of the lead balls, the temperature inside the drum is maintained at 90°C - 100°C by two methods: cold air flows and water spraying. The LO particles are carried to a separator that sends the coarse particles to the drum again for further oxidation. Due to the low temperature reached in the drum, the lead oxide polymorph obtained with this method tet-PbO. The final oxidation degree of the LO is 20% - 35%.

The main properties of the LO measured for controlling its quality are the following:
- Sulfuric acid absorption (mg of H_2SO_4 / mg LO): the amount of sulfuric acid absorbed on the LO particles is related to the particle size and thus, the specific surface of the LO. It is important to maintain the correct particle size for the reaction between the LO and the sulfuric acid that will take place during the mixing process.
- Lead concentration (%) is measured in order to control the thermal oxidation process of the lead. In addition, this parameter is critical for having a certain amount of lead in the unformed plates.

1.5.3. Mixing → Positive and negative paste

During the mixing process the compounds that will comprise the PAM and NAM are mixing altogether for getting the negative and positive paste. For getting both pastes, the main compounds that have to be mixed are LO, sulfuric acid and water. Afterwards, the positive and negative pastes contain different additives that are thought to improve the battery performance.
At first place, the LO is mixed with water. The PbO from the LO reacts with the water:
$$PbO + H_2O \rightarrow Pb(OH)_2 \text{ (R. 1)}$$
At the same time the lead is reacting with the water and the oxygen from the air:
$$Pb + H_2O + 1/2O_2 \rightarrow Pb(OH)_2 \rightarrow PbO + H_2O \text{ (R. 2)}$$
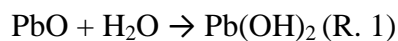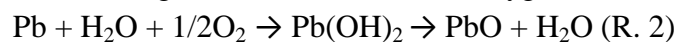
This reaction is catalyzed by the water, as $Pb(OH)_2$ is formed as intermediate product.

Not all the PbO and Pb particles react. So the final composition of the paste after water addition is LO, lead particles and $Pb(OH)_2$.

When the sulfuric acid is added the following reactions can take place:

$$PbO + H_2O \rightarrow Pb(OH)_2 \text{ (R. 1)}$$
$$Pb + H_2O + 1/2O_2 \rightarrow Pb(OH)_2 \rightarrow PbO + H_2O \text{ (R. 2)}$$
$$PbO + H_2SO_4 \rightarrow PbSO_4 + 2H_2O \text{ (R. 3)}$$
$$Pb(OH)_2 + H_2SO_4 \rightarrow PbSO_4 + 2H_2O \text{ (R. 4)}$$
$$Pb(OH)_2 + PbSO_4 \rightarrow PbO \cdot PbSO_4 + H_2O \text{ (R. 5)}$$
$$5PbO + H_2SO_4 \rightarrow 4PbO \cdot PbSO_4 + H_2O \text{ (R. 6)}$$
$$2PbO + H_2SO_4 \rightarrow PbO \cdot PbSO_4 + H_2O \text{ (R. 7)}$$
$$4PbO + H_2SO_4 \rightarrow 3PbO \cdot PbSO_4 \cdot H_2O \text{ (R. 8)}$$
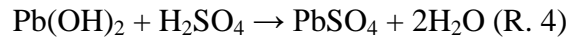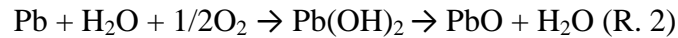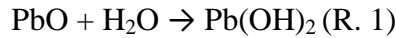
Reactions (R. 1) and (R. 2) still take place during this step because more water is being added as part of the sulfuric acid. At this moment the basic lead sulfates appear: monobasic lead sulfate ($PbO \cdot PbSO_4$; 1BS), tribasic lead sulfate ($3PbO \cdot PbSO_4 \cdot H_2O$; 3BS) and 4BS. The existence of these compounds in the paste depends on the acid sulfuric and water concentration in the paste, mixing time, and the temperature inside the mixer. **Figure 8** shows the dependence between the acid concentration and the paste composition. As can be seen in the figure, just 3BS (at all acid concentrations) and 1BS (at acid concentrations higher than 8%) are present in the paste. In contrast, 4BS does not appear in the figure. The reason for this is that the nucleation of 4BS depends strongly on temperature, and is only obtain at temperatures between 65°C and 80°C, and after a long mixing time. These temperatures are not reached in the mixer unless it is heated. However, 3BS crystals formation can be completed within 10 min of mixing. In addition 3BS particles and agglomerates possess the adequate size and structure. For these reasons 3BS pastes are the preferred by the LAB industry.
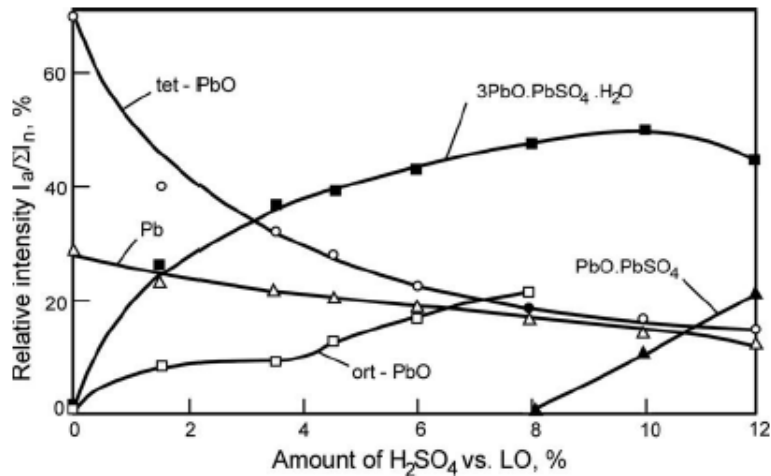
Figure 8. Dependence of relative intensity of the characteristic diffraction lines for the different crystal phases in the paste on the H_2SO_4/ LO ratio [8].

The preparation of positive and negative pastes, which is named as mixing process, is very similar for both pastes, negative and positive.

- Mixing of dry components.
- Addition of water.
- Mixing step.
- Addition of sulfuric acid. Standard acid density equal to 1.40 g cm^{-3}.
- Mixing step until the paste reaches a temperature equal to 40°C.
- Density and penetration measurements.

During the acid addition the paste reaches high temperatures due to the different exothermic reactions that are taken place. However, mixers are equipped with cooling system for maintaining the temperature of the paste at safe and steady temperatures, not above 50°C, as the transformation from 3BS to 4BS occurs at that temperature.

The addition of the additives can be done in two ways:

- Additives are mixed together with the LO, in the first step.
- Additives are mixed with the water and then added to the LO.

Depending on the type of paste the recipe can change, especially the additives. LO, red lead, water and sulfuric acid are considered main components of the paste. The rest of compounds added to the paste are considered additives. **Table 4** shows the main components of the different pastes.

Table 4. Components for pastes used for flat positive and negative plates, and tubular positive plates. Density window for the different pastes [8].

Component / parameter	Flat negative plates	Flat positive plates	Tubular positive plates
LO	X	X	X
Red lead		X	X
Polymer fibers	X	X	
Expanders	X		
Density / g cm^{-3}	4.10 - 4.50	3.90 - 4.40	3.40 - 4.50

Red lead can be used in the positive plates. This compound is also known as minimum, the molecular formula is Pb_3O_4, it is made by one molecule of PbO_2 and two molecules of PbO. When it reacts with the sulfuric acid, one molecule of PbO_2 and two molecules of $PbSO_4$ are formed. In this way the PAM becomes more conductive and the formation process is facilitated. Normally it is added to the tubular plates that are used for the industrial LAB. The concentration of red lead recommended is 2/3 of the total paste amount. This compound can be added to the flat positive plates, but it is not normally added.

Polymer fibers are added for improving the consistency of the pastes, as well as for reducing the scrap during the pasting process. The amount of these fibers in the paste is very low, around 0.3 wt. % related to the LO mass.

The expanders are just used for the negative paste, and are comprised by three components: carbon materials, organic expanders (OEs) and barium sulfate. The carbon materials, such as graphite, expanded graphite, carbon black, flake graphite etc. are used for improving the porosity of the negative plate as well as the conductivity. When they are added the NAM is spongier, and allows the penetration of the acid in the inner areas of the negative plate. In addition as these carbon materials are conductive they increase the overall conductivity of the plate. OEs are added as surface active polymers that avoid the sulfation of the negative plate. In this way they delay reduce the formation of a layer of lead sulfate during the discharge, and improve the utilization of the active material. The most famous OEs are the sodium lignosulfonates (LS) that are derivatives from the lignin. The third component, the barium sulfate, is a nucleating agent for the lead sulfate, providing many nucleuses for the lead sulfate growth and avoiding the formation of big lead sulfate particles. A standard expander formulation for the negative plate in the LAB industry would be 0.3 wt. % of carbon material, 0.2 – 0.3 wt. % of LS and 0.8 – 1.0 wt. % of barium sulfate. The weighted percentage is always related to the LO mass [8].

The main brands specialized in the mixer production are EIRICH, in Germany [25] and Oxmaster, in USA.
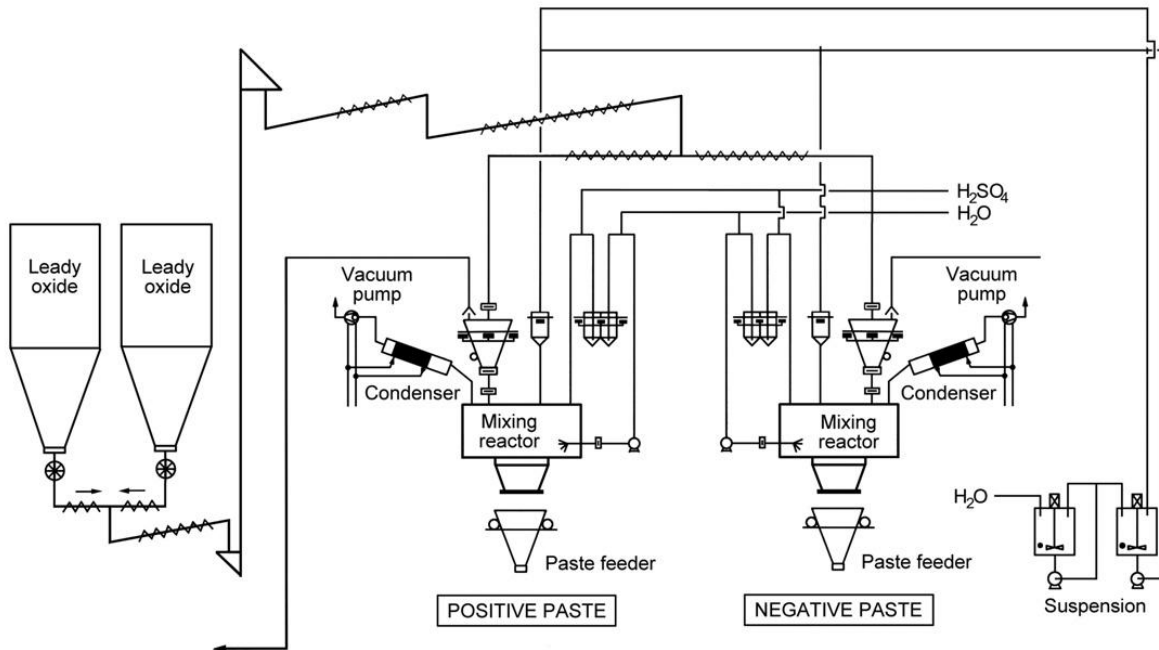
Figure 9. Block scheme of paste preparation equipment [26].

Figure 9 shows the block scheme of the equipment for paste preparation. Nowadays it is possible to control the processing time, temperature, agitation speed and pressures inside the mixing reactor.

1.5.4. Pasting → Positive and negative unformed plates

Flat positive and negative plates

During the pasting process the paste is spread into the grid to conform the final pasted plate. For this process, when the paste is ready (density, temperature and penetration parameters are correct) it is transferred to the paste feeder (see **Figure 9**). **Figure 10** shows the schematic of a belt-type pasting line machine. The paste feeder is a cone on top of the pasting line, and the paste is arriving to this cone by batches. Then the paste is poured in the hopper of the pasting line. The lines are equipped with a sensor for ordering to pour more paste to the hopper when this is at the limit level. In this way the hopper is never empty. Inside the hopper screws are mixing the paste continuously in order to have the same paste consistency in the whole hopper. The grid is put at the bottom part of the hopper, and the paste is pushed and spread into the grid. The thickness between the belt (transport line) and the hopper is adjusted in order to have a certain plate thickness. Then the pasted plates are transported through a paste pressing and levelling device system, in order to ensure the

same plate thickness for all the plates. This device can be a calender roller that forces the paste to be completely integrated into the grid, improving the adherence between the paste and the grid.

For transportation plates, both surfaces of the plates must covered by a "pasting paper". The face of the plate located next to the belt has the pasting paper on this side form the beginning of the process. The other face is covered by the pasting paper after the paste is poured into the grid. The pasting paper function is to prevent the plates to stick to each other's when they are collected in piles after the pasting process.
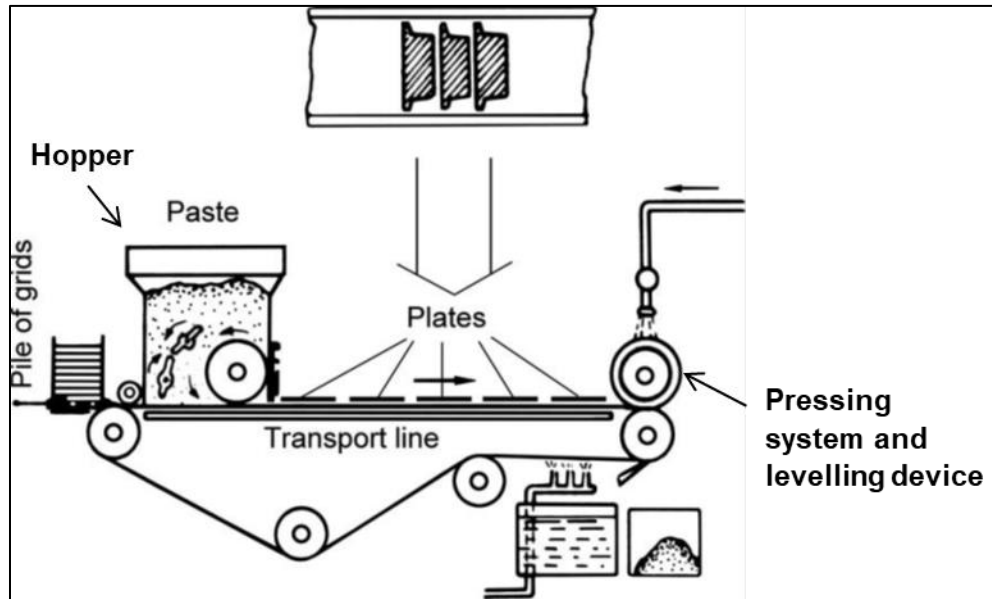
Figure 10. Block scheme of pasting line for flat plates [8].

After the pressing system and levelling device the plates are transported through the Flash Drying Oven (FDO). During this way the pates are dried until the active materials reaches the right temperature (40 - 45°C) and moisture (9.5%). The final moisture of the plates is important for the efficiency of the curing process. The plates are stacked on pallets until they are introduced into the curing chambers.

MAC Engineering and Equipment Company (USA) is the main company specialized in pasting lines [27].

Positive tubular plates

In the case of the tubular plates, the paste is poured into the gauntlets through a filling pipe, in special lines called wet filling lines. The working procedure is as follows:
- The paste is introduced into the hopper.

- The filling pipes are introduced into the gauntlet, surrounding the spines until they reach the top part of the positive grid.
- The paste is pushed through the filling pipes while they are moving out of the plate.
- The speed of the pump and of the filling pipes movement can be controlled for reaching the target paste weight.
- The bottom bar is fixed at the end of the plate.

HADI Maschinenbau Company (Austria) is the main company specialized in wet filling lines [28].

1.5.5.   Curing → Positive and negative cured plates

The curing process of the plates is the next step after the plates are pasted. For the curing process the plates are introduced in the curing chamber. Flat plates are stored in piles of plates on pallets, and tubular plates can be stored in piles or in racks, where they are hanging allowing a better air flow.

The curing process is divided by two steps:

1.   Curing process: during this process the paste inside the plates must maintain moisture equal to 5%. The chamber is sat at a certain temperature and relative humidity in order to maintain the moisture plate. In addition, the way of pilling the plates is important for allowing the same air flow for all the plates.
The targets of this process are:
- The <u>formation of the skeleton of the active material</u> inside the cured plates. This structure, also called skeleton, must be porous in order to allow the electrolyte to reach all the particles of the plate. The porous structure is achieved by the dissolution of small particles that are joined afterwards to big particles for forming big crystals. These big crystals are interconnected in order to form this porous structure. In the case of the 3BS pastes, the skeleton is made of 3BS, $PbSO_4$ and PbO particles interconnected. These processes occur during the stage 1 of the curing process.
- The <u>reduction of the free lead content</u> in the active material. This lead comes from the LO that was added during the mixing process. Part of the lead inside the LO has remained unoxidized, and has to be oxidized during the curing process. This step is important because the free lead will not take part in the afterwards electrochemical reactions, as it will not be part of the skeleton of the unformed active material. Because of that, this lead has to be oxidized to PbO which will join to the porous structure. The oxidation reaction occurs via two mechanisms, chemical an electrochemical.
  - Chemical reactions [8]:
$$Pb + H_2O + \tfrac{1}{2}O_2 \rightarrow Pb(OH)_2 \rightarrow PbO + H_2O \text{ (R. 2)}$$

52

Another reaction occurs to the oxygen before reacting with the Pb. In reaction (R. 2) the break of the covalent bound in the oxygen molecule is not explained, so oxygen is reduced to oxygen peroxide (R. 9) using the electrons from the Pb oxidation (R. 2).

$$O_2 + 2e^- + 2H^+ \rightarrow H_2O_2 \, / \, k_9 \text{ (R. 9)}$$
$$H_2O_2 + 2e^- + 2H^+ \rightarrow 2H_2O \, / \, k_{10} \text{ (R. 10)}$$

- Electrochemical reactions [29]:
$$\text{Anodic reaction: } Pb \rightarrow Pb^{2+} + 2e^- \text{ (R. 11)}$$
$$\text{Cathodic reaction: } 2H_2O + 2e^- \rightarrow H_2 + 2OH^- \text{ (R. 12)}$$
$$\text{Electrochemical reaction: } 2H_2O + Pb \rightarrow H_2 + Pb(OH)_2 \text{ (R. 13)}$$
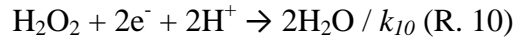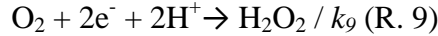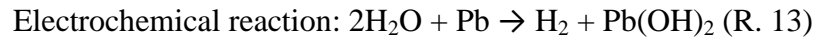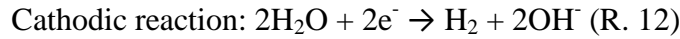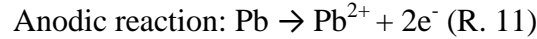
As a summary, water is a catalyst in both mechanisms, chemical and electrochemical, so it has to be maintained in order to oxidize the free lead inside the active material.

The best results in terms of lead oxidation rate are obtained at relative humidity levels between 55 and 86%, and at 50°C [8]. These processes occur during the stage 2 of the curing process.

- The <u>formation of the CL</u> between the active material and the grid surface. The CL is a PbO layer that allows the current flow from the grid to the active material. The CL is formed at the Pb (grid)/PbO (active material) interface. The lead is oxidized and an oxygen vacancy (O^{2+}_v) is formed in the PbO lattice (R. 14). The following reactions occur:

$$Pb \rightarrow PbO^{2+}_v + 2e^- \text{ (R. 14)}$$
$$PbO^{2+}_v + 2e^- + H_2O \rightarrow PbO + H_2 \text{ (R. 15)}$$
$$PbO^{2+}_v + 2e^- + \tfrac{1}{2} O_2 \rightarrow PbO \text{ (R. 16)}$$
$$PbO + H_2O \rightarrow Pb(OH)_2 \text{ (R. 1)}$$
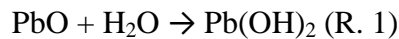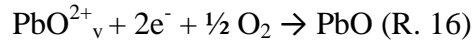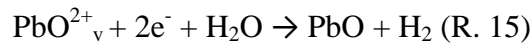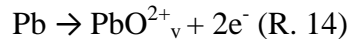
Finally the PbO layer grows up and thus the corrosion layer. In this case, the water is also a catalyst of the reaction, so again the relative humidity inside the chamber should be maintained for the formation of the CL. These processes occur during the stage 2 of the curing process.

2.   Drying process: during the drying process the temperature of the chamber is increased and the relative humidity is decreased. In this way the air flow is able to heat the active material, and evaporate the water inside it. The water escapes from the active material leaving the pores that will lead to the porous unformed plates.

Figure 11 shows different drawings related to the state of the lead particles in the mixer, in the paste, and after the 1st and the 2nd steps of the drying process. During the 1st step (**Figure 11. (c)**) of the drying process the water less bounded to the particles, i.e. capillary

53

water, is evaporated. During the 2nd step (**Figure 11. (d)**) the water from the thin films and the water that surrounds the particles (wedge water) is evaporated. Finally we have the active porous mass.
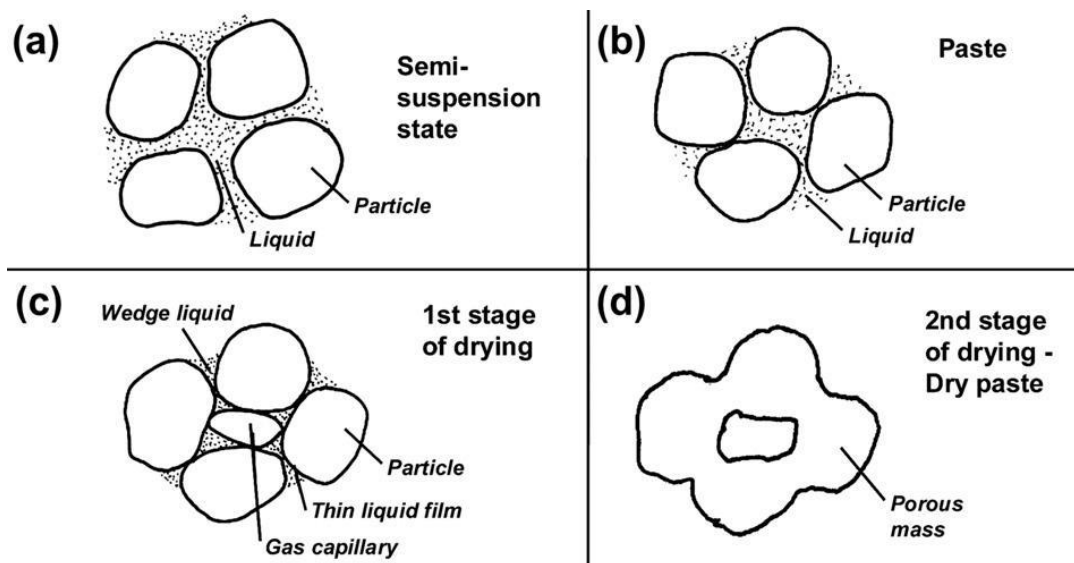
Figure 11. Particle/liquid system during the mixing process (**a**), in the paste (**b**), during the 1st (**c**) and the 2nd (**d**) steps of the drying process [8].

Table 5 shows the conditions of each process for flat plates made with 3BS paste used in SLI batteries.

Table 5. Curing and drying process for flat plates done with 3BS paste. Process conditions [8].

Process	Stage	Purpose	Conditions			Time / h
			Paste	Chamber		
			Moisture / %	Relative humidity / %	Temperature / °C	
Curing	1	Porous skeleton formation	9.0 – 10.0	95	45	12
	2	CL and oxidation of free lead	6.0 – 7.0	60	50	12
Drying	1 & 2	Drying of the mass	<0.2	≈1.0	60	12

The final parameters that are measured in the plates in order to evaluate the efficiency of the curing process are the free lead content and the mass moisture. In the case of 3BS flat plates used for SLI batteries the framework values are indicated in **Table 6**.

Table 6. Curing process. Control parameters.

Flat plate type	Free lead content / %	Mass moisture / %
Positive	<3.0	<0.2
Negative	<5.0	<0.2

1.5.6.   Battery assembly → Dry battery

The unformed negative and positive plates are the main components of the plate group, together with the separator. The unformed positive and negative plates are alternately stacked. Between plates of different polarity a separator sheet is put. The final amount of unformed negative and positive plates depends on the battery design. In some cases, the already formed plates are used for the assembly.

The separator is made of polymers, such as polyethylene (PE) or polypropylene (PP) and, in some battery types, of Absorptive Glass Mat (AGM). The separators must be permeable in order to allow the ions flow through them. They must show a high porosity, and a low electrical resistivity for not increasing the internal resistance of the battery. In addition, they must be resistant to the attack of sulfuric acid, oxygen and hydrogen. The separator must cover the whole surface of the plates, in order to avoid the contact between plates of different polarity, and thus short-circuits and the failure of the battery. In some cases the separator is a sheet, or it is an envelope covering both faces, as well as the bottom part of one of the plates. In other cases the bottom part is not covered, and the separator just surrounds the surface of the plates, like a sleeve. The separators also include some ribs located at the side of the positive plate, which make more space for the reaction at the positive plate. The envelope or sleeve can be surrounding the positive or the negative plates; it will depend on the battery design.

In the case of the AGM separators, their design is just a sheet. This material comprise up to 85% borosilicate glass microfibers (hydrophilic; length = 1 – 2 mm) and 15% polymer fibers (hydrophobic) that provide mechanical strength. They also need to be porous, permeable to ions, and resistant to the different attacks (sulfuric acid, oxygen and hydrogen). These separators are used for AGM LAB, where the electrolyte is impregnated in the AGM separators, so this type of separators has also the role of providing electrolyte to the chemical reactions. The compression of the plate group must be high for favoring the acid flow. In addition, the AGM separator is able to reduce the oxygen consumption, by the Closed Oxygen Cycle (COC). The polymer fibers, because of their hydrophobicity create gas channels. When oxygen evolved from the positive plate, during the charge, it can cross through the gas channels to the negative plates, where it is reduced. This system is known as COC [8].

Some separators manufacturers are ENTEK [30], DARAMIC [31], Microporous [32] or Hollingsworth & Vosen [33].

Once the plate group is prepared the positive plate's lugs or straps (see the lug in **Figure 6**) are casted to each other using a lead alloy. The same for the negative plates lugs. As a result, the positive and the negative bridges are casted (**Figure 12. a, b, c**).

This casting process is done according to Cast on Strap (COS) technology. Once the positive and the negative bridges have been casted, the whole assembly (plate group plus the bridges) is known as element (**Figure 12. a, b, c**). The elements are introduced in the container (**Figure 12. d).** Each element can provide a nominal voltage of 2 V, so depending on the final voltage of the battery several elements are casted in parallel: positive bridge of one element will be casted to the negative bridge of the next element, and the contrary for the other polarity bridge **(Figure 12. e**). The elements are connected through the "through" **(Figure 12. f**).

For example, for a 12 V batteries 6 elements are needed, and each one will be located in each cubicle of the container showed in **Figure 12. d**. The elements are casted to the next element through the "through". Exterior elements will contain the positive and the negative pillars (**Figure 12. a, c**), which will be the positive and negative terminals of the battery.

The containers are made of PP, or other plastic materials such as Acrylonitrile Butadiene Styrene (ABS). The main role of the container is to contain each plate group in its corresponding cubicle, as well as the acid inside each cubicle. The container material must be acid resistant and electrically insulating.

The next process is the junction of the lid to the container to give room to the dry battery (**Figure 12. g**). This junction can be done using a thermowelding process, as well as mechanically or using any type of glue for pasting the lid to the container. Each option should ensure the tightness of the battery, i.e. when air at high pressure is introduced in the covered battery no air leakages must be observed. Normally, for transportation batteries a thermowelding process is carried out.
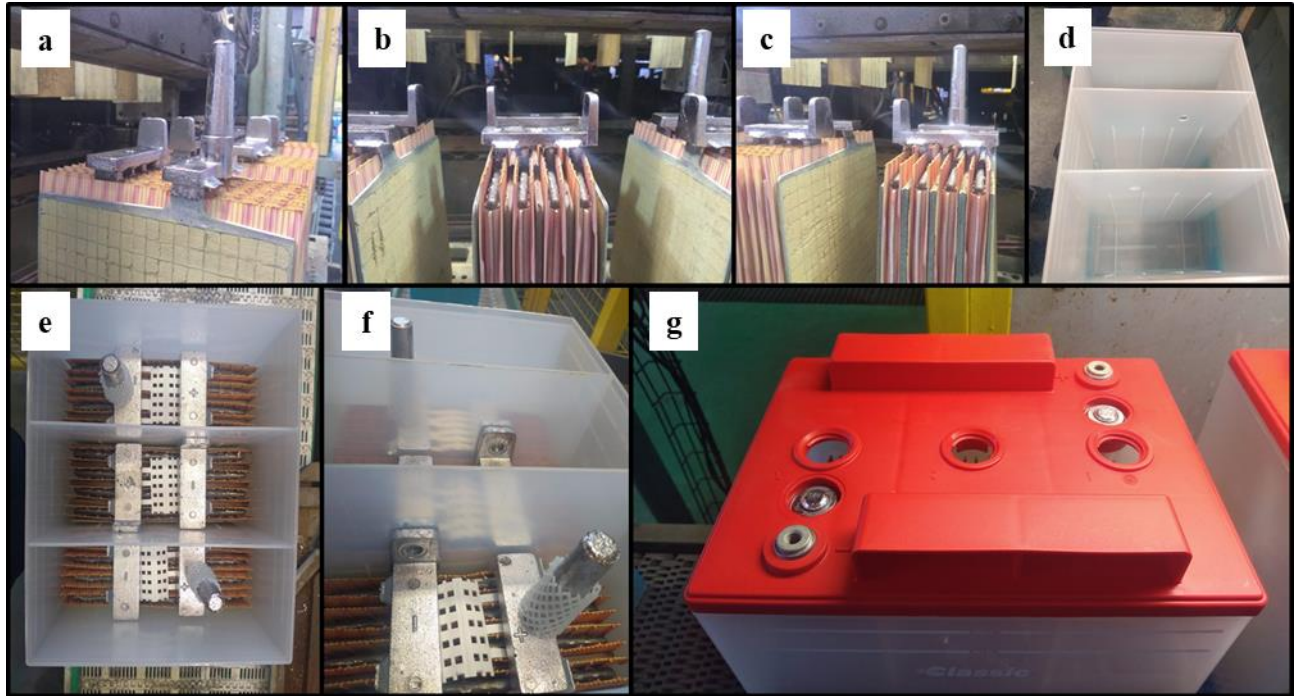
Figure 12. Battery assembly. a, b, c. Three elements after the COS process. **d.** Battery container with three cubicles for the three elements. **e.** Each element is located in each cubicle. **f.** Connection of the elements through the "through". **g.** Final dry battery.

The final product is the dry battery (**Figure 12. g**).

1.5.7. Acid filling → Wet battery

The dry battery is filled with the electrolyte which could be one of the following:

- <u>Solution of sulfuric acid:</u> this is the type of electrolyte used for most of the batteries. The acid density, and thus the concentration of the acid, is defined by the final acid density of the battery. When the dry charged contains unformed plates, the filling acid density must be lower than the final acid density of the battery, as the unformed plates are made of basic lead sulfates. The $-SO_4^{2-}$ groups contained in the plates will be transferred to the electrolyte after the charging process, so they have to be taken into account. In the case of a dry battery containing formed plates, the filling acid density is the same as the final acid density of the battery. Apart of the density of the acid, another important characteristic of the acid is its purity:

- Multi-valent ions (Fe^{2+}/Fe^{3+}, Cu^+/Cu^{2+}, Cu^{3+}/Cu^{5+}, etc.) accelerate the self-discharge of the battery by acting as redox couples at the positive and negative plates.
- Noble metals catalyst the Hydrogen Evolution Reaction (HER) in the negative plate, and thus, the water consumption.

- ClO_3^-, ClO_4^-, $2NO_3^-$ are oxidant components that form soluble salts at low H_2SO_4 concentrations and damage the active material [8].

All these impurities must be avoided in the sulfuric acid solutions used as electrolytes.

The chosen density depends on the amount of $-SO_4^{2-}$ groups needed for the electrochemical reactions. The density of the acid also influence in the specific conductivity of the electrolyte, and thus the internal resistance of the battery. The normal acid density window for LAB is 1.10 g cm^{-3} - 1.28 g cm^{-3} (T = 25°C). In the case of batteries used for transportation applications, SLI, the acid density used is 1.28 g cm^{-3} (T = 25°C).

In addition the acid density is directly linked to the open circuit voltage of the battery by the following equation:

$$\Delta E = \rho + 0.845$$

ρ is the electrolyte density at 25°C. This formula applies when the battery is in a steady state, and a LAB fully charged has a ΔE equal to 2.15 V per element [8].

- Gel electrolytes: the gel is made of sulfuric acid solution mixed with silica (SiO_2). When these components are mixed together the SiO_2 particles react forming a 3-dimensional branched structure through the liquid. At the beginning of the mixing, the gel viscosity is low. This process is known as gelling. After the gelling process, the viscosity of the gel increased and it remains fixed, which is the final state of the gel inside the battery. The 3-dimensional branched structure is maintained in the gel during the battery operation and allows the flow of the liquids (sulfuric acid and water), which is necessary for the electrochemical reactions. In addition, gas channels are created inside the gel, which facilitates the COC. The sulfuric acid solution used for the gel production must fulfill the same characteristics as the one used directly for filling the LABs. And as well as was mentioned before, the concentration or density of this sulfuric acid is also chosen as function of the amount of $-SO_4^{2-}$ groups needed for the electrochemical reactions.

Filling process

The filling process depends on the type of electrolyte and battery. For flooded batteries, the battery is filled by gravity with the sulfuric acid. In the case of the AGM batteries, as the sulfuric acid has to be impregnated in the AGM separator, a vacuum system is used. The same happens for the gel electrolyte, the gel is introduced in the battery with a vacuum system, as because of the high viscosity of the gel the filling by gravity is not facilitated.

Once the electrolyte has been introduced into the battery, the soaking process starts, and the sulfuric acid reacts with the active material of the unformed negative and positive plates. The reaction between the lead oxide and basic lead sulfates of the unformed plates with the sulfuric acid is exothermic, and because of that the battery should be maintained at

temperatures lower than 50°C. The soaking process lasts from 1 to 2 hours. If this time is extended the plates are covered by a passive layer of $PbSO_4$ that increases the internal resistance of the battery and hampers the charge of the battery.

In the case of the dry battery that contains formed negative and positive plates, once the dry battery is filled the sulfuric acid penetrated in the pores of the active material, but the active material does not react with the sulfuric acid.

1.5.8.   Formation → Final battery

Once we have the wet battery, the unformed positive and negative plates must be formed. On this purpose a formation program consisting in several charges and discharges is done according to the final capacity of the battery. One formation program example is the one showed below for a transportation flooded LAB of 70 Ah (**Table 7**).

Table 7. Formation program for a transportation flooded LAB of 70 Ah.

Nominal capacity / Ah			70
Step	**Current / A**	**Time / h**	**Capacity / Ah**
Charge	22.4	13.0	291.20
Discharge	-8.4	4.7	-39.48
Charge	16.8	3.0	50.40
Charge	18.2	6.3	114.66
Discharge	-16.8	2.5	-42.00
Charge	16.8	3.2	53.76
Charge	8.4	4.2	35.28
Sum		36.9	463.82

The battery must be kept at temperatures lower than 50°C during the whole process.

We are going to explain here the formation of unformed negative and positive plates made with 3BS pastes, as these pastes are the preferred for the transportation LABs.

-        Formation of unformed positive plates made with 3BS paste

The formation of the positive plates occurs in two stages.

- Stage 1: lead oxide and 3BS are oxidized to mainly α-PbO_2, and small amounts of β-PbO_2. At the same time, these compounds, lead oxide and 3BS, reacts wth the sulfuric acid forming $PbSO_4$. The final amount of $PbSO_4$ depends on the density of the filling acid. The potentials during charge as well as at open circuit increase.
- Stage 2: $PbSO_4$ formed during the soaking process and the first stage is oxidized to α-PbO_2. The potentials during charge as well as at open circuit increase.
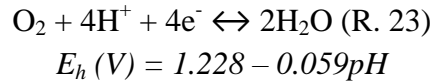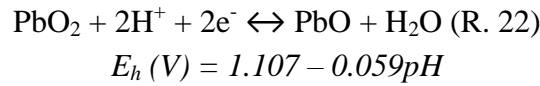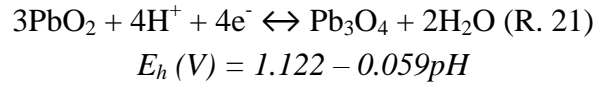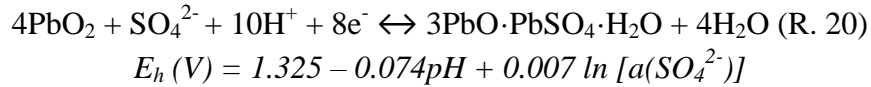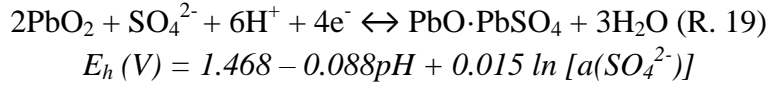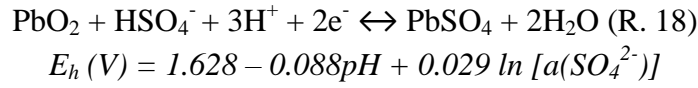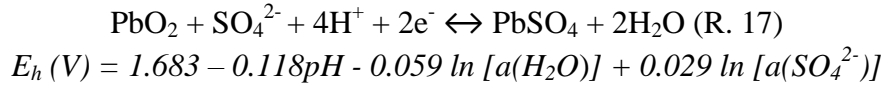
$$PbO_2 + SO_4{}^{2-} + 4H^+ + 2e^- \leftrightarrow PbSO_4 + 2H_2O \text{ (R. 17)}$$
$$E_h \text{ (V)} = 1.683 - 0.118pH - 0.059 \ln [a(H_2O)] + 0.029 \ln [a(SO_4{}^{2-})]$$

$$PbO_2 + HSO_4{}^- + 3H^+ + 2e^- \leftrightarrow PbSO_4 + 2H_2O \text{ (R. 18)}$$
$$E_h \text{ (V)} = 1.628 - 0.088pH + 0.029 \ln [a(SO_4{}^{2-})]$$

$$2PbO_2 + SO_4{}^{2-} + 6H^+ + 4e^- \leftrightarrow PbO \cdot PbSO_4 + 3H_2O \text{ (R. 19)}$$
$$E_h \text{ (V)} = 1.468 - 0.088pH + 0.015 \ln [a(SO_4{}^{2-})]$$

$$4PbO_2 + SO_4{}^{2-} + 10H^+ + 8e^- \leftrightarrow 3PbO \cdot PbSO_4 \cdot H_2O + 4H_2O \text{ (R. 20)}$$
$$E_h \text{ (V)} = 1.325 - 0.074pH + 0.007 \ln [a(SO_4{}^{2-})]$$

$$3PbO_2 + 4H^+ + 4e^- \leftrightarrow Pb_3O_4 + 2H_2O \text{ (R. 21)}$$
$$E_h \text{ (V)} = 1.122 - 0.059pH$$

$$PbO_2 + 2H^+ + 2e^- \leftrightarrow PbO + H_2O \text{ (R. 22)}$$
$$E_h \text{ (V)} = 1.107 - 0.059pH$$

$$O_2 + 4H^+ + 4e^- \leftrightarrow 2H_2O \text{ (R. 23)}$$
$$E_h \text{ (V)} = 1.228 - 0.059pH$$

-     Formation of unformed negative plates made with 3BS paste

The formation of the negative plates occurs in two stages too.

- Stage 1: lead oxide and 3BS are reduced to Pb. At the same time, these compounds, lead oxide and 3BS, reacts wth the sulfuric acid forming $PbSO_4$. The formation of $PbSO_4$ predominates. The H_2SO_4 concentration in the bulk of the electrolyte is reduced, and the battery voltage decreases as these redox systems have lower potentials.
- Stage 2: $PbSO_4$ formed during the soaking process and the first stage is are reduced to Pb. The battery voltage increases as these redox systems have higher potential.

$$PbO + 2H^+ + 2e^- \leftrightarrow Pb + H_2O \text{ (R. 24)}$$
$$E_h \text{ (V)} = 0.248 - 0.059pH$$

$$3PbO \cdot PbSO_4 \cdot H_2O + 8H^+ + 8e^- \leftrightarrow 4Pb + H_2SO_4 + 4H_2O \text{ (R. 25)}$$
$$E_h \text{ (V)} = 0.030 - 0.044pH - 0.007 \ln [a(SO_4{}^{2-})]$$

$$PbO \cdot PbSO_4 + 4H^+ + 4e^- \leftrightarrow 2Pb + H_2SO_4 + H_2O \text{ (R. 26)}$$
$$E_h \text{ (V)} = -0.013 - 0.029pH - 0.015 \ln [a(SO_4{}^{2-})]$$

$$PbSO_4 + 2H^+ + 2e^- \leftrightarrow Pb + H_2SO_4 \text{ (R. 27)}$$
$$E_h \text{ (V)} = -0.356 - 0.029pH - 0.029 \ln [a(SO_4^{2-})]$$

$$PbSO_4 + 2H^+ + 2e^- \leftrightarrow Pb + HSO_4^- + H^+ \text{ (R. 28)}$$
$$E_h \text{ (V)} = -0.302 - 0.029pH - 0.029 \ln [a(SO_4^{2-})]$$

$$2H^+ + 2e^- \leftrightarrow H_2 \text{ (R. 29)}$$
$$E_h \text{ (V)} = -0.059pH - 0.029 \ln [P(H_2)]$$
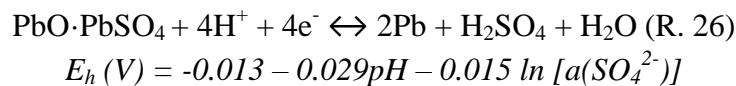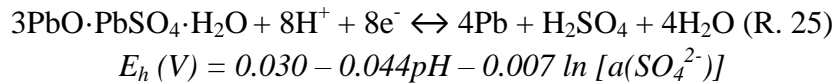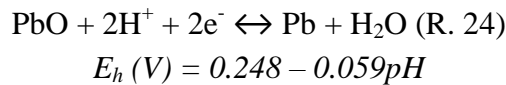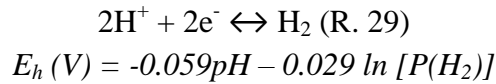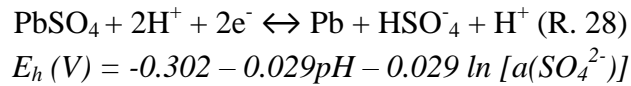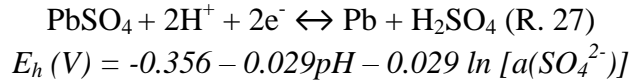
Figure 13 shows an example of an Exide EFB, as well as its different compounds.

Figure 13. 12 V EXIDE Start-Stop EFB of 70 Ah. Flat positive plate covered by the pasting paper and surrounding by the separator. Flat negative plate covered by the pasting paper. Plate group [34].

1.6. Electrochemical reactions during battery operation

Charge and discharge reactions

These are the main electrochemical reactions that occur at the negative and the positive plates, and are the responsible for providing the power of the LAB.

- Negative plate:

Discharge reaction – oxidation: $Pb + SO_4^{2-} \rightarrow PbSO_4 + 2e^- \text{ (R. 30)}$

Charge reaction – reduction: $PbSO_4 + 2e^- \rightarrow Pb + SO_4^{2-} \text{ (R. 30)}$
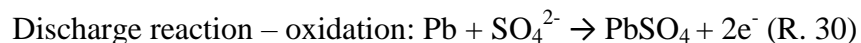
Equilibrium potential: $E_{Pb/PbSO4}(V) = -0.385 – 0.029 \ln [a(SO_4^{2-})]$

- Positive plate:

Discharge reaction – reduction: $PbO_2 + SO_4^{2-} + 4H^+ + 2e^- \rightarrow PbSO_4 + 2H_2O$ (R. 17)

Charge reaction – oxidation: $PbSO_4 + 2H_2O \rightarrow PbO_2 + SO_4^{2-} + 4H^+ + 2e^-$ (R. 17)
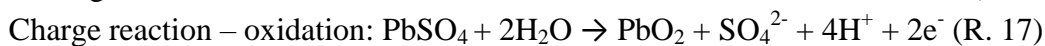
Equilibrium potential: $E_{PbO2/PbSO4}(V) = 1.683 – 0.118pH - 0.059 \ln [a(H_2O)] + 0.029 \ln [a(SO_4^{2-})]$

- Overall reaction:

Discharge reaction: $Pb + PbO_2 + 2H_2SO_4 \rightarrow 2PbSO_4 + 2H_2O$ (R. 31)

Charge reaction: $2PbSO_4 + 2H_2O \rightarrow Pb + PbO_2 + 2H_2SO_4$ (R. 31)
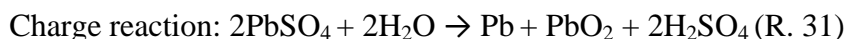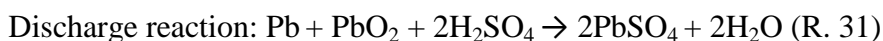
Equilibrium potential: $\Delta E = E_{PbO2/PbSO4} - E_{Pb/PbSO4}$

$\Delta E (V) = 2.041 – 0.118pH – 0.059 \ln [a(H_2O)/a(SO_4^{2-})]$

The equilibrium potential of the overall reaction (R. 31) is equivalent to the electromotive force of the LAB. It depends on the activity of the sulfate ions and water, as well as to the pH. This related to the consumption of water, sulfate ions and protons during the overall charge and discharge reactions. The battery should maintain a constant voltage during its operation in order to provide the right power to the installation. A LAB is considered fully discharged when ΔE reaches a value between 1.70 – 1.80 V.

Secondary reactions

- HER at the negative plate while charging the battery:
$$2H^+ + 2e^- \leftrightarrow H_2 \text{ (R. 29)}$$
$$E_{H2/H+} (V) = -0.059pH – 0.029 \ln [P(H_2)]$$
The difference between the $E_{Pb/PbSO4}$ and $E_{H2/H+}$ electrodes is about 0.30 V. So the predominant reaction at the negative plate is the ones related to the $Pb/PbSO_4$ system.

- Oxygen Evolution Reaction (OER) at the negative plate while charging the battery:
$$O_2 + 4H^+ + 4e^- \leftrightarrow 2H_2O \text{ (R. 23)}$$
$$E_{H2O/O2} (V) = 1.228 – 0.059pH$$
The difference between the $E_{PbSO4/PbO2}$ and $E_{H2O/O2}$ electrodes is about 0.50 V. So the predominant reaction at the positive plate is the one related to the PbO_2/Pb system.
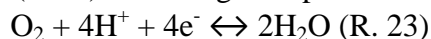
- Self-discharge reactions while storing the battery:

Negative plate: $Pb + H_2SO_4 \rightarrow PbSO_4 + H_2$ (R. 32)

Positive plate: $PbO_2 + H_2SO_4 \rightarrow PbSO_4 + H_2O + \frac{1}{2}O_2$ (R. 33)
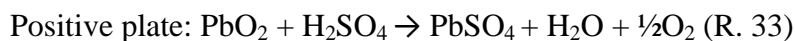
The self-discharge processes occur at the negative and the positive plates at the same time while the battery is stored. Reduction and oxidation reactions occur at the same time at the same electrode. At the negative plate Pb is oxidized to $PbSO_4$, while protons are reduced to H_2. At the positive plate PbO_2 is reduced to $PbSO_4$, while oxygen is oxidized to O_2. The final result is the water consumption and the sulfation of the plates.

1.7. Special additives for the negative plates

As was mentioned in **section 1.5.3**, the negative paste includes a group of additives named expanders: carbon materials, OEs and barium sulfate. The expanders are able to improve the performance of the negative plates by making the lead surface spongier, i.e. increasing the active surface of the negative plate, and delaying the passivation phenomena produced by the formation of a thick $PbSO_4$ layer during the discharge of the battery. In this section the properties as well as the beneficial effects of carbon materials and OEs are explained.

1.7.1. Carbon materials

- Properties of the carbon materials

The two main allotropes of carbon are:

1. **Diamond**: formed by sp^3 hybridized carbon atoms. This material is characterized by high hardness and high electronically resistivity. It is an insulator material.
2. **Graphite**: formed by sp^2 hybridized carbon atoms organized in hexagonal structures collected in layers, pilled in the direction of the c-axis. This material is characterized by its low hardness and low electronically resistivity. It is a semi-conductor material.

Table 8 shows the main physical properties of both allotropes, together with the lead.

<div align="center">Table 8. Physical properties of diamond, graphite and lead.</div>

Property	Diamond	Graphite	Lead
Crystal structure	Cubic	Hexagonal	Cubic
Orbital hybridization	sp^3	sp^2	-
Covalent radius / pm*	77	73	-
Density / g cm^{-3}	3.515	2.267	11.34
Mohs hardness	10	≈ 1	1.5
Heat capacity / J mol^{-1} K^{-1}	6.155	8.517	26.5
Thermal conductivity / W m^{-1} K^{-1}	≈ 2200	≈ 150	35.3
Resistivity / Ω m	$\approx 10^{12}$	$\approx 3 \cdot 10^{-7}$ (c-axis) $\approx 4 \cdot 10^{-6}$ (a-axis)	$2.08 \cdot 10^{-7}$

<div align="center">*pm: picometres. 100 pm = 1 angstrom.</div>

Structures made of combinations of sp^3 and sp^2 hybridized carbon atoms give rise to other forms of carbon materials: activated carbons, carbons blacks, carbon fibers, glassy carbon, carbon aerogels or sp^3/sp^2 combinations. These carbon materials show properties between diamond (insulator) and graphite materials (semi-conductor). In the case of sp^3/sp^2 combinations, a higher amount of sp^3 carbon atoms causes the appearance of "non-graphitic" domains that reduce the conductivity; this can be solved by a thermal treatment at 200 – 400°C that forces the migration from sp^2 to sp^3. A domain formed by clusters of sp^2 hybridized carbon atoms is considered a "graphitic-domain". Depending on the degree of clustering the carbon form would be more or less conductive.

The electrochemical behavior of the graphite strongly depends on its amphoteric character (it is able to act as an oxidant or as a reductant) and its layered structure. These two properties are responsible for the rich intercalation chemistry of the graphite: due to the low bods between the graphitic layers, several compounds can be allocated between the layers (such as lithium or sulfuric acid) resulting in an increase of the conductivity of the final compound. These compounds are called expanded graphites, which show higher surfaces areas than the graphite, due to the expansion of the interlayer distance, as well as higher conductivities.

On the one hand, activated carbons are amorphous materials comprised by aromatic sheets. These sheets are broken creating different pores. Heteroatoms present in the activated carbon determine the acid character and the ion-exchange properties of the material. The aromatic sheets result in a poor electrical conductivity of these materials. On the other hand, carbons blacks are also amorphous materials are made of clusters of graphitic-domains interconnected to form agglomerates. In this way the electrical conductivity scale would be expanded graphite > graphite > carbon black > activated carbon.

- Effect of the carbon materials in the negative plate of the LAB

The properties of the carbon material that affect to the performance of the negative plate are listed by Patrick T. Moseley et al. [35]:

- The presence of metal contaminants in the metal surface.
- Surface functional groups.
- Hydrogen evolution overpotential.
- Electronic conductivity.
- Capacitance.
- The size of any pores in the carbon.
- The affinity of the carbon for lead.
- Interaction with the organic component of the expander mix.
- Wettability by the aqueous electrolyte solution.

- Specific Surface Area (SSA).

Carbon materials addition affect to different properties of the negative plates:

- Capacitance during charge

When the LAB is charged the carbon material, due to its high amount of pores, is able to act as capacitive buffer. It has been discovered that the double-layer capacitance exhibits a linear correlation with the external surface area of the carbon that is added to the negative plate [36]. This capacitive effect also depends on the functional groups located at the surface of the carbon material. This capacitive effect provided by the carbon materials is predominant on the Faradaic reaction (lead sulfate reduction) when the battery is working at High Rate Partial State of Charge (HRPSoC) regimes; the battery is charged with a high current during a lapse. It has been also reported that the carbon material capacitive effect is also extended to the HER [37].

- Extension of the conducting surface area of the negative plate

This could be one of the most important properties influenced by the carbon materials. It has been demonstrated that the electrochemical reactions in the negative plate can occur on the lead surface as well as on the carbon material surface. So, the behavior of the carbon material during charge – discharge reactions could proceed via two mechanisms:

a) Charge and discharge of the double layer. For short duration reactions.
b) Faradaic process or electrochemical reactions: reduction of $PbSO_4$ during charge, and oxidation of Pb during discharge [38].

Figure 14 shows a schematic view of the electrochemical reactions that can take place on the carbon material surface (EAC) and on the lead surface.
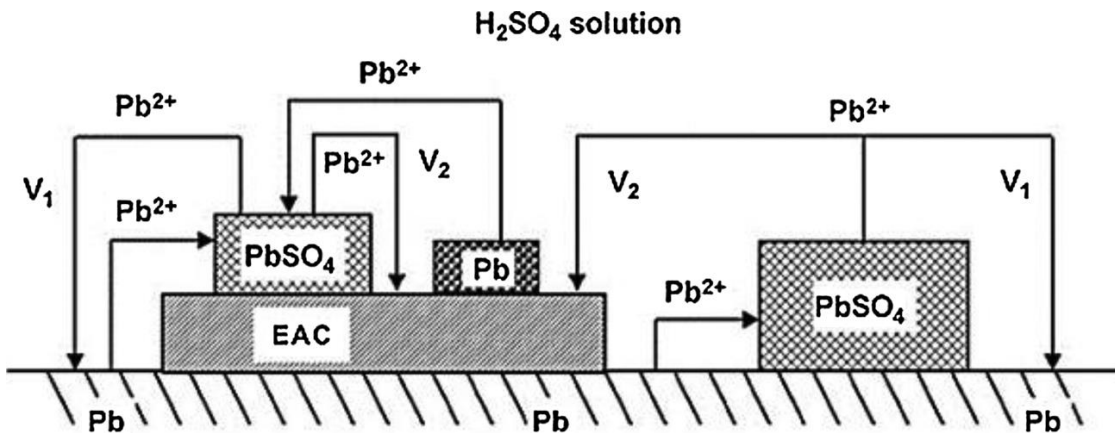
Figure 14. Electrochemical reactions on the negative plates of LAB containing Electrochemically Active Carbon (EAC) [39].

Carbon materials can act as a steric hindrance in the negative plate by obstructing the formation of big lead sulfate crystals. In this way the size of the crystals is controlled, and the surface area of the electrode is maintained [40,41]. This effect has been linked to high particle size carbon materials, considering that low particle size carbon materials can be buried by the lead sulfate crystals becoming useless for the charge discharge reactions [42]. Other carbon materials that are able to reduce the pores diameter of the lead-carbon electrode provoke the lack of SO_4^{2-} inside the pores, and the rise of the pH due to the high proton concentration. In these conditions, α-PbO is formed [43].

As the addition of carbon materials increases the porosity of the negative plate, the sulfuric acid irrigation is also increased. In addition, the pores of the carbon material can act as an electro-osmotic pump. This effect depends on the specific surface of the carbon material as well as on the functional groups presented on its surface (affinity to aqueous solutions). When the carbon material acts as an electro-osmotic pump, the distribution of the electrolyte inside the negative plate is improved, as well as the formation of lead sulfate throughout. This results in a better active mass utilization for the negative plate [42,44].

- • Considerations before adding carbon materials to the negative plate

One of the effects that must be taken into consideration before adding carbon to the negative plate is the effect of this addition during the paste mixing. Carbon materials, due to their high specific surface, are able to absorb big amounts of water on their surface. For this reason it is important to modify the paste recipe in order to get the final paste properties needed for the manufacturing process of the negative plates.

Another consideration is the effect of the carbon materials addition on the HER. Carbon materials are able to increase the surface area of the negative plate, and this not only means a higher surface for the capacitive effect and for the $Pb/PbSO_4$ system reactions, the HER can also take place on the carbon surface during charging the negative plate [45].

HER proceeds at the carbon or lead surface in two steps (**Figure 15**):

a) Adsorption of the H^+_{ad} on the surface and reduction to H_{ad} through **Volmer** mechanism. The H_{ad} atom remains adsorbed on the surface.

b) **Tafel** mechanism: desorption of two H_{ad} and evolution of H_2.
   Heyrosvsky mechanism: desorption of one H_{ad} that reacts with one H^+ from the solution plus $1e^-$ to form H_2.
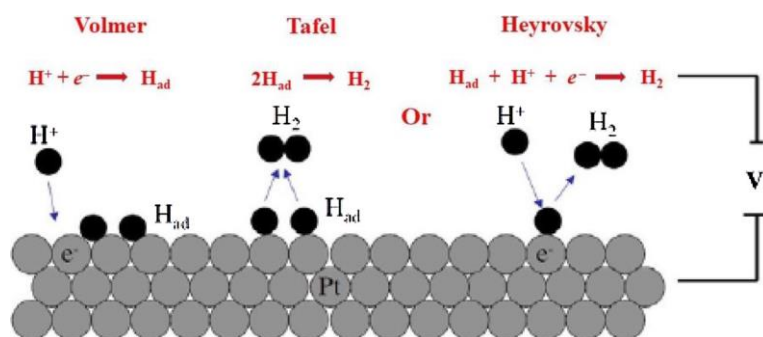
Figure 15. Alternative mechanisms proposed for HER [46].

HER rate is increased by several factors: higher charging potential, higher surface area (HER rate correlates directly with the external surface area of the negative plate [36]) and the presence of certain impurities.

When carbon is added, the only way to maintain in a safe degree the HER, and thus the water consumption of the LAB, is to adjust the carbon material dosage. Carbon materials reach their best performance at a peak concentration that depends on the carbon material properties. The best performances, including maintain the HER rate at a safe degree, have been reached for dosages between 0.5 wt. % and 2.0 wt. % [47].

It is important to notice the important role of the carbon purity. Carbon materials go through many manufacturing processes that can imply the presence of metallic impurities. The resource used for produce these carbon materials can also contains several impurities. These impurities rise the HER rate, and are a contaminant and a danger for the negative plate of the LAB.

1.7.2. Organic expanders (OEs)

The term "Organic Expander" refers more frequently to the LS used in the manufacturing process of the negative plate. The use of these compounds was discovered during the Second World War, when the wooden separators were replaced by synthetic materials separators. At that moment the negative plate capacity during cycling at low temperatures decreased abruptly. This effect was related to the absence of lignosulfonic acids in the NAM. So these lignosulfonic acids became essential to the negative plate performance. From that moment many LS, humic acids and tanning agents have been tested in order to find the right organic expander.

LS or sulfonated lignin are water-soluble anionic polyelectrolyte polymers. They are byproducts from the production of wood pulp using sulfite pulping [48]. When LS are added to the NAM they are adsorbed on the lead surface.

Lignin comprises different types of structures made with a similar chemical composition. The presence of different functional groups in their structure lead s to the formation of

micro pores. When lignin is added to the NAM, a layer of polyelectrolyte is formed where these micro pores are present. In other words, the lignin forms a three dimensional netlike layer which is colloid like [49]. The ions can be transferred through these micro pores, which are located at several places on the negative plate surface. This distribution results in the isolation of the active sites where $PbSO_4$ can be formed during the discharge. In this way small $PbSO_4$ crystals are formed during the discharge and no $PbSO_4$ passivation layer is formed, thus the capacity of the negative plate increases.

It is clear from the above mechanism that the lignin layer induces the creation of isolated $PbSO_4$ crystals, but it also delays the transfer of the Pb^{2+} ions from the lead surface to the lignin – electrolyte interface through the lignin micro pores [50]. In this way the crystal size is controlled and the discharge is extended. However, the same mechanism is followed during the charge of the negative plate: Pb^{2+} located at the lignin surface as $PbSO_4$ crystals must travel to the lead layer (inner part of the negative plate) to be reduced. This migration is delayed by the lignin layer, as happens during the discharge, and because of that the charge acceptance of the negative plates is impeded. The same happens for the HER: the lignin layer impedes the migration of the H^+ protons from the electrolyte to the lead surface, reducing the HER rate. So a better performance of the OE during the discharge involves a lower charge acceptance of the negative plate.

The performance of the OE depends on its following properties:

- Molecular weight: High Molecular Weight (HMW) lignins form a stable and flexible polyelectrolyte layer, while Low Molecular Weight (LMW) lignins tends to dissociate or to form micelles.
- Chemical structure: OEs contain a big variety of functional groups such as methoxyl, phenolic, carboxylic, ketonic, carbinol etc. Many scientists [51–54] have been focused on the correlation between the functional groups and the performance of the OE. However, this correlation is very difficult to establish, as the structure of the OE also has a big influence on its performance. Phenolic [53], aldehyde and SO3H groups, quinones and their derivate [52] and groups of the pyrocatechol type [54] exert a beneficial effect on the performance of the OE. A study carried out by the company Borregaard LignoTech [53,54] concludes that carboxylic and phenolic groups increased the cycle life of the SLI batteries, while decreased the charge acceptance and accelerate the self-discharge of the battery.
- Chemical stability: OEs are attacked by the H_2 and O_2 generated when the battery is being overcharged. In this way the OE is disintegrated when it is attacked by these compounds, and it is more rapidly disintegrated when the attacking agent is the oxygen.
- Working temperature: during operation the battery must be kept at temperatures around 40°C, otherwise the OE is disintegrated.

1.7.3. Interaction of the carbon materials and OEs with the NAM

From time ago many carbon materials and LSs or OEs have been used in the manufacturing process of the negative plate. For understanding the effect of these additives on the negative plates is important to differentiate between the two main structures present in the NAM: the lead or NAM skeleton and the energetic structure of the NAM. The NAM skeleton is referred to as the main lead structure present in the NAM. This structure is formed in the first stage of the formation of the negative plate when PbO and 3BS are being reduced to lead. The lead skeleton is directly connected to the plate grid and is responsible for conducting the current from the plate grid to the energetic surface. It also gives mechanical support to the energetic surface. The energetic structure of the NAM is made of all the lead particles that are deposited on the NAM skeleton during the second stage of formation when lead sulfate particles are reduced to lead. It is responsible for the SSA of the NAM. Both structures are involved in the chemical reactions (Pb $\leftrightarrow$ PbSO$_4$), however, the capacity of the negative plate strongly depends on the energetic surface, as just 15% of the lead skeleton is oxidized during this discharge [8]. So, where will the carbon materials and the LS be located in the NAM?

On the one hand, the LS has an influence on both structures: lead skeleton and energetic structure. However, LS has a greater effect on the nature of the energetic structure, as it will be finally located on the surface of the NAM. This active polymer prevents the formation of PbSO$_4$ layer on the lead NAM surface (passivation phenomena). In this way, the addition of LS improves the capacity of the negative plates and also helps in the cycle life of the negative plate. It is important to notice that this polymer is degraded along with the battery operation.

On the other hand, carbon materials are also added to the NAM, but their interaction with the NAM skeleton and energetic structure is more complicated. Firstly, carbon materials show some characteristics that make them suitable to be added to the NAM: they are steady during battery operation, electrochemically active and they have an affinity to lead. In addition, these materials show high SSAs and high conductivity. These properties are responsible for increasing the conductivity of the NAM, especially when the negative plate is discharged. In these conditions, most of the negative plate is made of PbSO$_4$ which is an insulator, and carbon particles are able to conduct the current during the recharge and carry on the sulfate reduction on their surface. The high surface of the carbon materials is responsible for increasing the SSA of the NAM, converting the lead into a more spongy structure where more nucleation sites for the PbSO$_4$ reduction can be found. This advantage can turn also in a non-beneficial situation, as the protons from the electrolyte can be also absorbed on the carbon surface, and get reduced, increasing the HER, and thus the water consumption. In addition, carbon materials interact also with the OE (in this case LS). The

OE can be adsorbed on the high SSA carbon material surface, preventing its beneficial effect.

As was proposed by Pavlov [47], depending on the particle size of these materials and its concentration, and if they have enough affinity for the lead, they can be incorporated in the NAM in different ways:

a) Into the bulk of the lead skeleton branches → carbon particles size higher than the cross-section of the lead skeleton branches (micrometers = high particle size) or carbon particles size lower than the cross-section of the lead skeleton branches (nanometers = low particle size) but at concentrations higher than 0.5.wt%.
b) On the lead surface → carbon particles size lower than the cross-section of the lead skeleton branches (nanometers) but at concentrations lower than 0.5.wt%.

During the formation of the lead skeleton, the reduction of PbO or 3BS to Pb is carried out, and the lead branches are created. In the presence of high particle size carbon materials, the reduction of these compounds can also happen at the carbon surface. This means that these particles act as lead nuclei. Finally, the high size carbon materials are completely covered by lead, and become part of the bulk of the lead skeleton, making a more conductive structure. In the case of carbon materials with low particle size, the particles are further separated in finer grains due to the pasting process. In this way, their size doesn't let them act as lead nuclei and they are pushed to the lead surface. In the surface they are able to increase the SSA of the NAM, making the lead spongier and reactant, and also contributing to increasing the conductivity of the NAM. However, when the concentration of this material is higher, the concentration of these particles throughout the negative plate is quite high, and finally, the particles end forming part of the lead skeleton as well the energetic structure.

The final target of adding carbon materials in the negative plates, especially in the EFB, is to increase the charge acceptance of battery, which is very important for the batteries when they have to accept the energy from the regenerative braking. Another important target is the increase of the battery life during the HRPSoC cycles. These cycles simulate the operation of the battery during the Start & Stop mode when the battery is working at high PSoC. In these conditions, a good charge acceptance is required as well as good Cold Cranking Ability (CCA) performance. How do the carbon materials increase the charge acceptance and the cycle life? Easy, as was explained before the carbon materials can act as lead nuclei reducing the sulfation of the negative plate. When the battery is operating, the negative plate is oxidized (Pb → $PbSO_4$) and reduced ($PbSO_4$ → Pb). This reaction is not 100% reversible: some $PbSO_4$ crystals remain oxidized acting as nuclei for the formation of more $PbSO_4$ crystals in the future discharges. $PbSO_4$ is an insulator, i.e. an obstacle for the current. When the $PbSO_4$ crystals are becoming bigger a passivation layer of $PbSO_4$ will be formed, impeding the current to reach the Pb particles and continue with the discharge of

the plate. This means the battery failure. When carbon materials are present they are able to increase the overall conductivity of the NAM, making the current distribution more homogeneous throughout the negative plate. So firstly, the current can reach more $PbSO_4$ crystals and reduces them, and secondly, this reaction can happen in two surfaces: the lead surface and the carbon surface. The $PbSO_4$ reduction rate increases, leading to smaller $PbSO_4$ crystals that have a higher solubility in the sulfuric acid and easier to reduce. No passivation layer is formed and the LAB can continue operating.

1.8. EFB: state of the art of the use of carbon materials as additives for the negative plates

As in the **section 1.2.3** we already focused on the latest developments of LAB we are going to focus now on the carbon materials that have been added to the negative plate of the LAB along history.

EFBs are the emerged solution for fulfilling the high restrictions from the EC to reduce the CO_2 emissions and improve fuel consumption in the passenger cars. HEVs implement new technologies, such as Start & Stop system and regenerative braking. Some of these HEVs also use an electric motor. EFB has enough throughput capability to power for the Start & Stop system and regenerative braking implemented in these types of passenger cars. These batteries are able to work in these conditions thanks to the addition of carbon materials in their negative plates. These carbon materials, as explained in **section 1.7.1**, are able to reduce the sulfation of the negative plates and in this way extend the battery life working at HRPSoC (working conditions for the Start & Stop system). In addition, carbon materials increase the charge acceptance of the negative plates, leading to an efficient regenerative braking.

Carbon materials have been used as additives for the negative plates for more than 20 years. Two stages can be differentiated:

1. First introduction of carbon black in the negative plates by Nakamura et al. [55] where it was discovered that an increase in the carbon black concentration led to a prevention of the accumulated lead sulfate, and therefore an increase in the cycle life of VRLA batteries.
2. After the above finding, more specialized carbon materials have come, such as activated carbons, graphite, expanded graphite, conductive carbons blacks, hybrid carbons, carbon nanomaterials, nanostructured materials made of lead and carbon etc.

Here we are going to list a sort of carbon materials that have been studied by different scientists, and the improvement that they have brought to the negative plate performance:

- CSIRO laboratories in Australia have demonstrated that **carbon black** at concentrations from 0.2 to 2.0 wt. % in the negative plates of VRLA batteries increased the conductivity by some five orders of magnitude [56].
- Low concentrations of **graphite** (1 wt. %) [40] and mixtures of **flake graphite and carbon black** [57] enhanced the cycle life of the LABs at Partial-State of Charge (PSoC). However, flake graphite with low surface area did not improve cycle life at PSoC [58].
- Differences between **carbon black and graphite** as additives for the negative plate have been studied by P.T. Moseley. This study showed better performance on HEV duty by those cells which contained graphite at 2.0 wt.% [59].
- Studies based on the addition of **expanded graphite** showed that the optimum concentration of this carbon material was 1.50 wt.%, which made possible to double the PSoC life of the battery by increasing charge acceptance [60].
- Studies based on the utilization of **carbons blacks with different order degrees** showed that the batteries with highly ordered carbons blacks increases the lifetime of the corresponding battery by up to a factor of two [61].
- Addition of **graphite combined with titanium dioxide** showed an improvement in the cycle life of LABs due to the hindrance of the crystal growth of lead sulfate deposited in the electrode pores [62].
- **New materials called Pb@C** [63], made by high adhesion of Pb to carbon, were able to restraint hydrogen evolution while improving performance of the battery.
- **Discrete Carbon Nanotubes (dCNTs)** have been used as an additive for NAM added at 0.16 wt. % (related to the LO mass). They enhanced charge acceptance, but hampered the capacity and the cold cracking performance; furthermore, a proper dispersion of this additive was completely necessary for a good performance [64].
- **dCNTs** have been also added in both, PAM and NAM; these experiments resulted in an increase in cycle life by 60% (HRPSoC), and water consumption of the battery [65].
- **Multi Wall Carbon Nano Tubes (MWCNTs)** have also been tested as NAM additive for SLI flooded lead acid battery. They were able to double the cycle life of real batteries [66].
- **Three-dimensional reduced graphene oxide (3DRGO)** has been employed as NAM additive. Results showed a high porosity of those 3DRGO's NAM, which implied a decrease on the size of the $PbSO_4$ crystals, and a prolonged cycle life of the LABs working in HRPSoC conditions [67].
- Nanostructured materials, such as **MWCNTs or graphene**, have been also tested by S. Logeshkumar and R. Manoharan [68]; these materials were incorporated into the lead skeleton and underwent the creation of bead shape $PbSO_4$ crystals with small size, making easier their conversion into lead and prolonged PSoC cycle life.
- **Lead-doped mesopore-dominated porous carbon (Pb@MC)** composite in a Pb^{2+} containing H_2SO_4 electrolyte was used for conducting electrochemical experiments.

The main finding was that it was possible to reduce the lead crystal size to the atomic scale. These nanolead particles could effectively inhibit the hydrogen evolution, contribute the pseudo capacitance and enhance the reversible reaction of $Pb/PbSO_4$, resulting in a longer cycle performance of lead-carbon batteries [69].

Although it has been already commented, all these carbon materials increased the HER rate, and thus the water consumption. This fact must be taken into consideration, as EFBs are no maintenance batteries and they cannot be refilled with water. For this reason the carbon material dosage must be wisely selected. In addition carbon materials can contain different metal impurities that catalyze the HER [70], so high purity of the carbon material is required if we want to use it as additive for the negative plates of EFBs.

As can be seen there are three main groups of carbon materials that can be used as additives for the negative plate:

1. Micrometer carbon materials including graphites, expanded graphites, and carbons blacks. These porous materials increase the SSA of the negative plate, and thus the charge acceptance. In addition they also improve the cycle life of the batteries but they increase in a high degree the water consumption.
2. Nanostructured carbon materials including nano fibers and nanotubes, discrete or multiwall. The addition of these nanostructured materials prolongs the cycle life of the LAB. However their addition doesn't increase the water consumption, as a small dosage is needed for achieving the beneficial effects in the cycle life.
3. Nanocomposites where nanolead particles are deposited on porous carbon materials. These types of carbon materials are able to improve the charge acceptance as well as the HRPSoC life of LAB, while retrainting the water consumption, but they are still under development. The needed dosage for getting beneficial effects is aroubd 1%.

Nowadays many batteries, that incorportate carbon materials in the negative plate, are sold by the main companies. Exide Technologies was the first company that introduced in the market the EFB in 2008. This company is currently selling a new fleet of batteries under the name Carboon Boost 2.0 [34]. Yuasa EFB design includes special Carbon additives which improves high charge acceptance [71].

It is important to mention here the UltraBattery developed by CSIRO Energy Technology in Australia. Despite of this battery is not considered an EFB, this battery combine an asymmetric super-capacitor and a lead–acid battery in single unit cells [72]. The components of this battery are: conventional LAB positive plate made by PbO_2, separator, and a negative plate made by two plates: a carbon sheet and a conventional LAB negative plate made of lead. In this way, the carbon sheet acts a super capacitor, improving the short term and thus non faradaic, charges and discharges reactions. The conventional negative

plate is used for the electrochemical or faradaic reactions that take place during the long term charges and discharges. This technology is able to reach higher cycle life than NiMH batteries, bringing the opportunity of using this type of battery in the Micro and Mild HEV at a lower cost [72].

2. Aim of the study and methodology

2.1. Main target and project management of the doctoral thesis within the SPECTRA project

It was clear from the introduction that EFBs are one of the solutions for the reduction of the CO_2 emissions from the passenger's cars to the atmosphere, as they are able to reduce the fuel consumption. The failure mode of these batteries while they are working at HRPSoC is related to the accumulation of lead sulfates on the negative plates, which is also called "passivation phenomena". Carbon materials and OEs are known as suppresser of the passivation phenomena. For all these reasons the final purpose of this study was to evaluate the influence of different carbon materials and OEs on the performance of the negative plates of EFBs.

It is important to specify here that this doctoral thesis was part of the SPECTRA project: Smart Personal CO2-free transport in the city. This project was an R&D consortium in which 8 companies and 10 research technological centers participate.

Exide Technologies, a LAB multinational company with more than 130 years of experience in this field, was in was responsible for the improvement of Recharge Infrastructures through the use of EFBs. Under this target, Exide Technologies collaborated with the following companies and research centers:

- Grupo Antolin [73] one of the largest players in the car interiors market internationally and number 1 worldwide supplier of headliner substrates, as well as advance carbon materials, located in Burgos (Spain). The main target of Grupo Antolin was to supply its graphitized Carbon Nanofibers called GANFg that would be used as additive for the negative plates of EFB for improving their performance. In addition, Grupo Antolin was also supporting the team with their expertise.
- GAIKER [74] technological center located in Bilbao (Spain). This center was in charge of dispersing the GANFg using different OEs, as well as characterized the final dispersions. In this way GANFg would be suitable to be used in the negative plates of EFBs.
- Universidad Autónoma de Madrid (UAM), and more specifically its Department of Applied Physical Chemistry [75] located in Madrid (Spain), as research center was in charge of carried out the electrochemical experiments, in Exide Technologies and UAM facilities. This work was done by the PhD student, as part of her doctoral thesis.

Within this project, the UAM had to fulfill the following tasks:

- **T2.3.3.** Research on paste-based electrodes with carbon nano-fibers and / or synthetic materials derived from graphite.
- **T2.3.4.** Research in materials and electrodes of lead with coal.

Therefore, the specific targets of the doctoral thesis were linked to these tasks.

In order to carry out this main target, the following general targets were proposed:

T.1. Optimization of the method.

This part included the optimization of the following processes at the electrochemical laboratory:

- Mixing process: preparation of 1 kg LO positive and negative pastes using a laboratory machine. Laboratory density measurement equipment was also sat up.
- Pasting process: pasting of 1 Ah lead grids manually and compressing them using a calender roller.
- Curing process: an oven was adjusted to work as a curing chamber. On this purpose a water bath was introduced for generating the required relative humidity. Then the process was optimized for the 1 Ah plates.
- Assembly of the 2 V / 1 Ah cells: the cells were comprised by two positive plates and one negative plate. In this way the plate under study was the negative, as it was the limiting one.
- ARBIN equipment set up: potentiostat/galvanostat equipment was purchased and the electrical tests were adapted and created for the 2 V / 1 Ah cells. The performed electrical tests were: formation of the cells, capacity, CCA, Initial Charge Acceptance (ICA), negative polarization study and PSoC cycling tests. The tests were prepared according to the standards *VW75073 2012-07 and RNDS SS 36 11 003 2014-05*.
- Metrohm Autolab PGSTAT204 potentiostat/galvanostat and BOOSTER10A was also used for performing Cyclic Voltammetry (CV) tests.
- Physicochemical analyses: different analyses were carried out on the NAM depending on the step of the study we were working on. We analyzed the lead and sulfate content, porosity, and Brunauer-Emmett-Teller (BET) SSA. We also used the X-Ray Diffraction (XRD) and Scanning Electronic Microscopy (SEM) techniques.
- A procedure was created in order to follow the same steps for all the batches.

T.2. Preliminary study working with different carbon materials in the negative plates currently used in the LAB industry.

This study was done for corroborating the good performance of the negative plates when they included these carbon materials in the NAM. Some of these materials have been used in real batteries. We used five types of carbon materials (C1 – C5): 2 expanded

graphites, 1 hybrid carbon made of graphite and carbon black, and 2 conductive carbons blacks. Two OEs were also used: LS1 and LS2.

T.3. Use of graphitized carbon nanofibers from the company Grupo Antolin (GANFg) in the negative plates of LABs.

This commercial nano carbon material was called GANFg. These fibers needed to be dispersed previously to be added in the NAM. GANFg were dispersed by the technological center GAIKER using OE1 (same as LS2) as an active polymer. GAIKER also characterized the dispersions. **The final aim of this target was to know the optimum concentration of GANFg that could lead to the highest cycle life.** On this purpose, three GANFg concentrations were used: 0.10, 0.20 and 0.50 wt. % (related to the mass of LO).

T.4. Use of GANFg at the optimum concentration dispersed with a mix of OEs in the negative plates of LABs.

The optimum concentration of GANFg in NAM (found in the former target) was dispersed with a mix of OEs (OE1 + OE2). Both OEs were added at the same concentration in the mix. In addition two OEs mix concentrations were used for checking the effect of reducing OEs dosage in NAM. **The final aim of this target was to increase the charge acceptance of the negative plates by using a mix of OEs at different concentrations. In addition the highest cycle life of the cells should be maintained.**

T.5. Use of GANFg at the optimum concentration and expanded graphite or carbon black dispersed with OE1 in the negative plates of LABs.

The optimum concentration of GANFg in NAM (found in the former target) was dispersed with OE1, and with expanded graphite (C1 from T.2) and carbon black (C4 from T.1). **The final aim of this target was to increase the charge acceptance of the negative plates by adding carbon materials apart of the GANFg at the optimum concentration. In addition the highest cycle life of the cells should be maintained.**

T.6. Publication of at least three articles in scientific journals based on targets 2 to 5.

T.7. Doctoral research internship. Duration of at least 3 months.

T.8. Writing of the doctoral thesis.

Table 9 summarizes the management of the whole PhD studies according to the mentioned targets.

Table 9. PhD Project - Gantt chart.

Year	2015			2016				2017				2018				2019			
Quarter	**2**	**3**	**4**	**1**	**2**	**3**	**4**	**1**	**2**	**3**	**4**	**1**	**2**	**3**	**4**	**1**	**2**	**3**	**4**
Targets	Master degree studies			PhD studies															
T1	█	█	█																
T2		█	█	█	█														
T3			█	█	█	█													
T4						█	█	█	█	█									
T5								█	█	█	█								
T6						█	█	█	█	█	█		█	█	█				
T7											*	█	█						
T8																█	█	█	█

*Since December 2017.

As can be seen in the table, during the master degree part T1 was completed. During the master degree the PhD student was working at Exide Technologies R&D center located in Azuqueca de Henares (Spain) as an intern. During that time the optimization of the method was carried out.

The PhD student completed the Doctoral research internship in the R&D center of Exide Technologies R&D center located in Büdingen (Germany) since December 2017 to May 2018. The report *Loss on Ignition – How to check the purity level of a carbon material. Optimization of the method*. (annex IV) shows part of the work developed by the student during this time. Then she continued working there as an R&D Engineer.

3. Experimental part

3.1. Materials

3.1.1. Chemical compounds

- LO: from a ball-mill process; oxidation degree equal to 72%.
- Sulfuric acid (H_2SO_4): density 1.40 g cc^{-1} for the mixing process and 1.28 g cc^{-1} as electrolyte.
- Ultra-pure water.
- Polyacrylonitrile fiber (PAC) fiber used as NAM and PAM additive. Length = 1.6mm, coarseness = 2.1 dtex.
- Barium sulfate ($BaSO_4$) used as NAM additive. Purity of 99% and maximum moisture of 0.3%.
- OEs used as NAM additives:
- LS1 [76] – Sodium Lignosulfonate 1: selectively modified lignin-based additive.
- LS2 [76] or OE1 [77] - Sodium Lignosulfonate 2: highly modified lignin-based additive.
- OE2 [77] – Lomar D: highly polymerized naphthalene sulfonate supplied as a sodium salt.
- Carbon materials used as NAM additives:
- C1 – Expanded graphite 1.
- C2 – Expanded graphite 2.
- C3 - Conductive carbon black and graphite.
- C4 – Conductive carbon black 1.
- C5 – Conductive carbon black 2 – this carbon was previously dispersed by the supplier with LS2 (also called OE1). The final composition was: 83% Carbon black + 17% LS2.
- GANFg – Graphitized carbon nanofibers from Grupo Antolin [78].

3.1.2. Lead grid for positive and negative plates

The lead alloy used for the grids was Pb Sn 0.80% obtained by a continuous casting process. The final thickness of the grid was 0.90 mm. The dimensions are shown in **Figure 16**:

- a: 20.36 mm.
- b: 50.00 mm.
- c: 13.00 mm.
- d: 148.00 mm.
- Pasting area of 26 pellets. Surface = a*b = 1018 mm^2 = 10.18 cm^2.
- Pellet surface = (a/2)*(b/13) = 10.18 mm*3.85 mm = 39.19 mm^2 = 0.39 cm^2 / pellet.
- Lug. Surface = d*c = 1924 mm^2 = 19.24 cm^2.
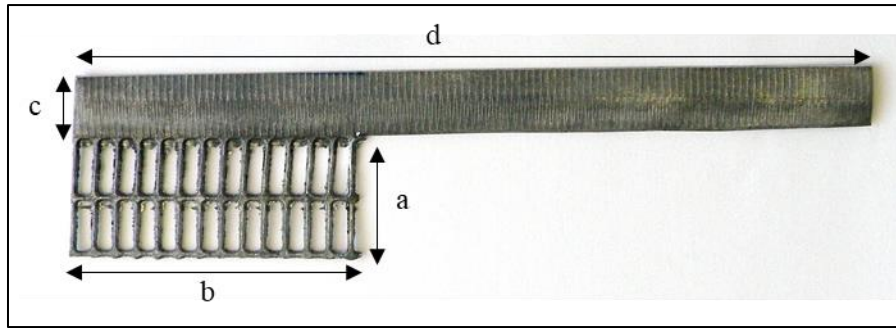
Figure 16. Lead grid used for the positive and the negative plates.

3.1.3. AGM Separator and pasting paper

Figure 17. b shows the AGM sheets used as pasting paper and separator during the pasting and the cell assembly processes. They were obtained from an AGM roll (**Figure 17**. a) from Bernard Dumas (France).
- Material: non-woven fabric made with microfiber glass and plastic fiber
- Composition: glass fiber (86%) and polyester fiber (14%).
- Thickness: 0.37 mm measured under a pressure of 10 kPa.
- Surface: a*b (**Figure 17**. **b**) = 60 mm*30 mm = 1800 mm^2 = 18 cm^2.
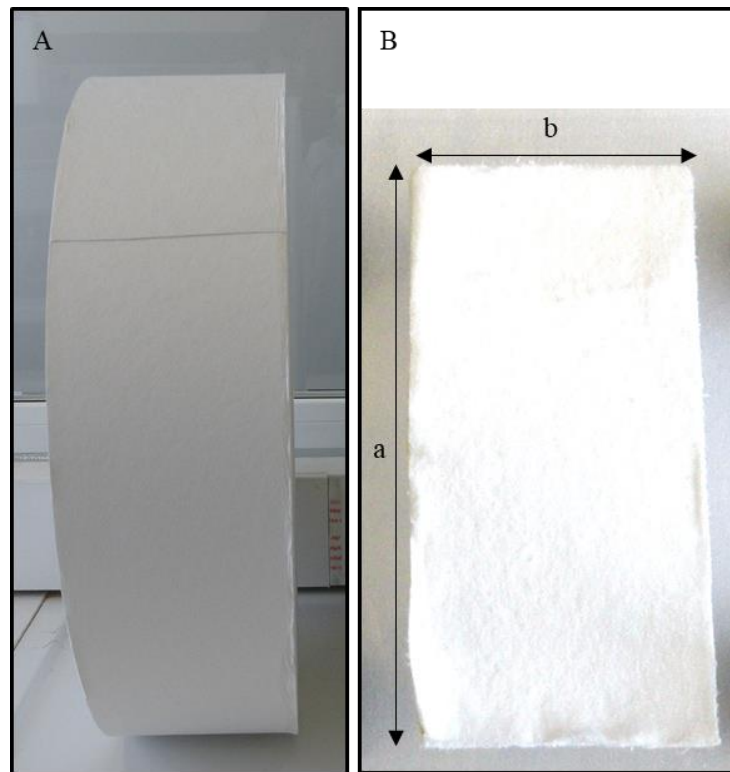
Figure 17. AGM sheets: used as pasting paper and separator.

3.1.4. Materials for the cell assembly

- Sn60Pb38Cu2 solder wire (ISO EN 9453; Ø: 0.7 mm) for welding the positive lugs
(**Figure 18. A**).
- Methacrylate sheets for containing the plates. Thickness of 5 mm (**Figure 18. B**).
- PVC screws, nuts and washer for compressing the methacrylate sheets (**Figure 18. C**).
- Parafilm M from Sigma-Aldrich for covering the cell (**Figure 18. D**).
- A 500mL autoclavable beaker made of chemical-resistant polypropylene was used as cell
container (**Figure 18. E**).
- Adhesive tape (commercial) for attaching the parafilm to the beaker.
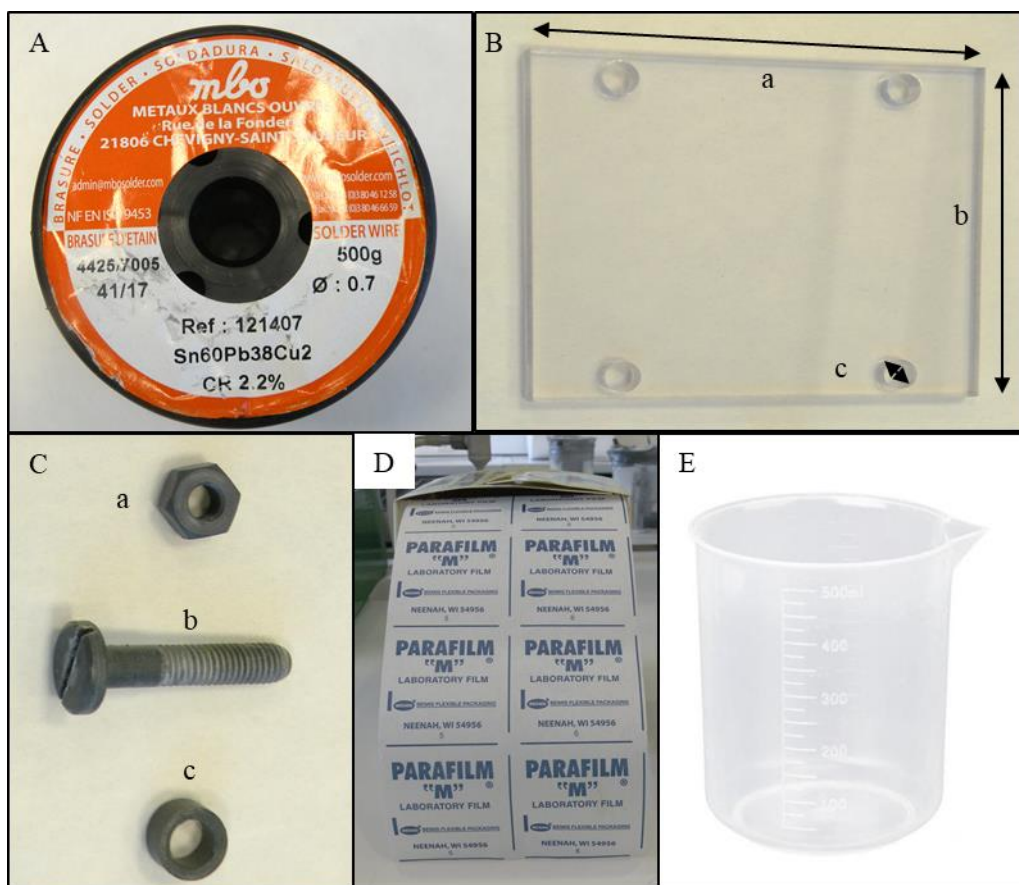
Figure 18. Materials for the cell assembly. A. Sn60Pb38Cu2 – solder wire. **B.** Methacrylate sheet:
a = 80 mm. b = 70 mm. c = 6.5 mm. **C.** PVC nut (a), screw (b) and washer (c). **D.** Parafilm M. **E.**
500 mL beaker.

3.2. Equipment

At GAIKER facilities

3.2.1. DISPERMAT CN 10 from VMA-GETZMANN GMBH

DISPERMAT CN 10 (**Figure 19**) is a dispersion equipment that was used to prepare the GANFg dispersions in GAIKER facilities. Its characteristics are listed in **Table 10**.

Table 10. Dissolver DISPERMAT® CN10 characteristics.

DISPERMAT® type	Power / kW	Speed / rpm	Torque / N m	Product volume / L
Dissolver DISPERMAT® CN10	1.1	0 – 11000	1.8	0.25 – 10

Figure 19. A. DISPERMAT ® CN 10 from VMA-GETZMANN GMBH. B. 1 and 2: Dissolver disc Ø = 40 mm. C. 1 and 2: Bead mill APS accessory.

Figure 19 shows the two accessories that have been used for preparing the dispersions:

- Dissolver disk made of hard chrome (**Figure 19. B),** diameter of 40 mm. This device can be used for disperse 1 L of total volume.
- Bead mill Air Pressure System (APS) 250 (**Figure 19. C**). 100 mL can be dispersed in a total volume of 250 mL. The disks have a diameter of 35.5 mm. Ceramic balls made of yttrium with a diameter of 0.6 – 0.8 mm are used for milling.

3.2.2. SEM coupled by X-ray detector (SEM-EDX)

SEM coupled by X-ray detector (SEM-EDX) for analyzing the surface of different samples, including dispersions and powder samples. This instrument was from ZEISS (model EVO50). The microscope is equipped with an X-ray detector for qualitative and quantitative analysis of the chemical elements on a spot, area or the whole image.

3.2.3. Brookhaven

Brookhaven (model ZETA PALS 90PLUS). The technique Dynamic Light Scattering (DLS) can be performed with this equipment. The liquid sample is beamed with IR light. The light goes across the whole sample height. Two detectors detect light transmission and backscattering. Different light profiles as a function of the sample height are obtained. In this way we can know the particle size of the particles inside the dispersion. The equipment can measure sizes from 3 nm to 3 μm. In addition, with this equipment, the Zeta Potential (ZP) can be also measured. ZP is the required potential for traversing the ionic layer that surrounds the particles inside the dispersion; it provides information about the dispersion stability.

3.2.4. Mastersizer

MATERSIZER equipment for determining the particle size. The equipment can measure sizes from 100 nm to 1000 μm in solution. The equipment was from MALVERN (model 2000 equipped with an accessory HYDRO 2000SM).

At EXIDE TECHNOLOGIES facilities

3.2.5. Weighing scale

Materials, plates and density cup were weighed on the weighing scale SARTORIUS BP8100 from year 1995 (**Figure 20**). It has a capacity of 8,100 g and a readability of 0.1 g.
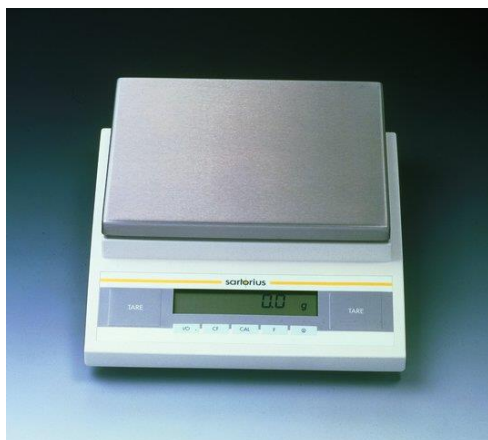
Figure 20. Weighing scale SARTORIUS BP8100.

3.2.6. Mixer and paste density measurement tools

The kitchen machine Kenwood Chef Titanium was used as a mixer. A glass bowl was used together with a plastic bowl tool for stirring, both materials were acid resistant (**Figure 21. A**). This mixer can run at 8 different speeds. In addition, a decanter with a water valve was used for adding the acid into the glass bowl (**Figure 21. B**).
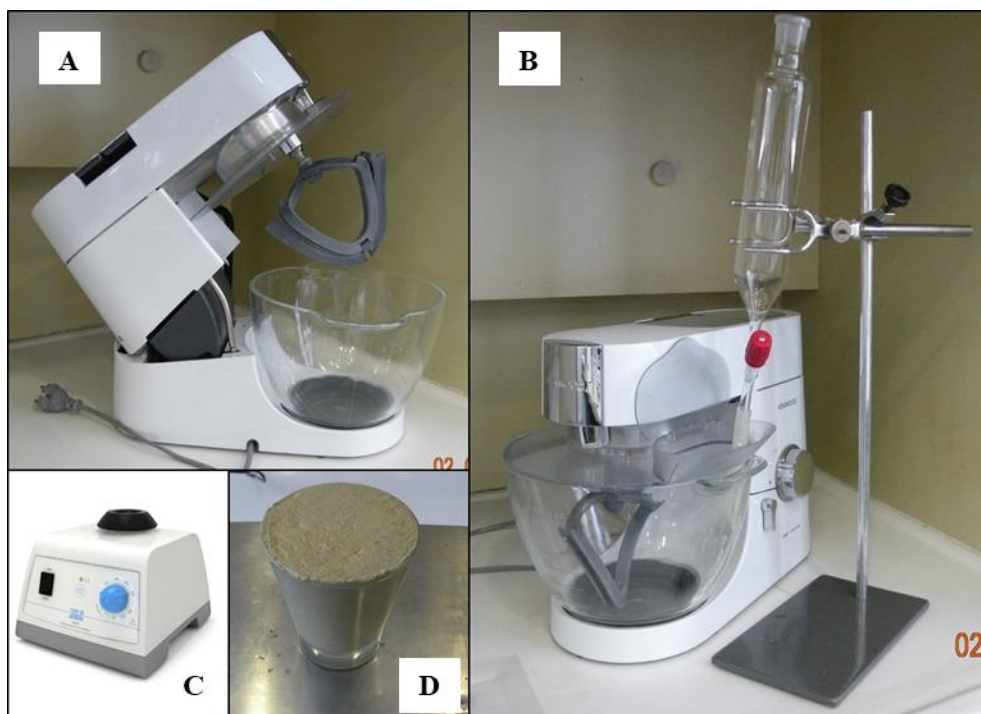
Figure 21. Mixing equipment. A. Mixer. **B.** Mixer together with the acid decanter. **C.** Vortex ZX3 from VELP® SCIENTIFICA. **D.** Full density cup.

For measuring the paste density, a Vortex ZX3 from VELP® SCIENTIFICA together with a universal platform (**Figure 21. C)**, was used for agitating and homogenizing the paste inside the calibrated glass, denominated density cup, of 86.97 cm^3 and 110.32 g (**Figure 21. D**).

3.2.7. Calender roller

The pasted plates were compressed by a calender roller showed in **Figure 22**.

Figure 22. Calender roller.

3.2.8. Curing chamber

The pasted plates were cured in a curing chamber showed in **Figure 23**. This chamber was originally a climate chamber with the following accessories:

- Water bath.
- Heating resistance inside the water bath.
- Relative humidity controller.
- Contactor.
- Ventilator.
- Vault made of a plastic sheet.

Figure 23. Laboratory curing chamber.

<u>Operation procedure</u>:

The climate chamber itself maintains the target temperature inside the chamber. The heating resistance and the relative humidity controller are connected to a contactor. When the relative humidity is lower than the target the contactor switches on the heating resistance. In the reverse case, the contactor switches off the heating resistance. The ventilator is located close to the water bath for spreading out the steam throughout the entire chamber.

3.2.9. Thermostatic water bath

Thermostatic water baths (**Figure 24**) were used for maintaining the cell temperature during the electrical tests. The temperatures most frequently used were 27 ± 2 ⁰C and 40 ± 2 ⁰C. A heating resistance was used for heating the water, connected to a contactor and to a temperature controller. The baths were connected directly to the tap water pipe and were refilled once the water level was lower than the target. The water was cover by empty plastic balls for maintaining the temperature, especially for the electrical tests at 40 ± 2 ⁰C.
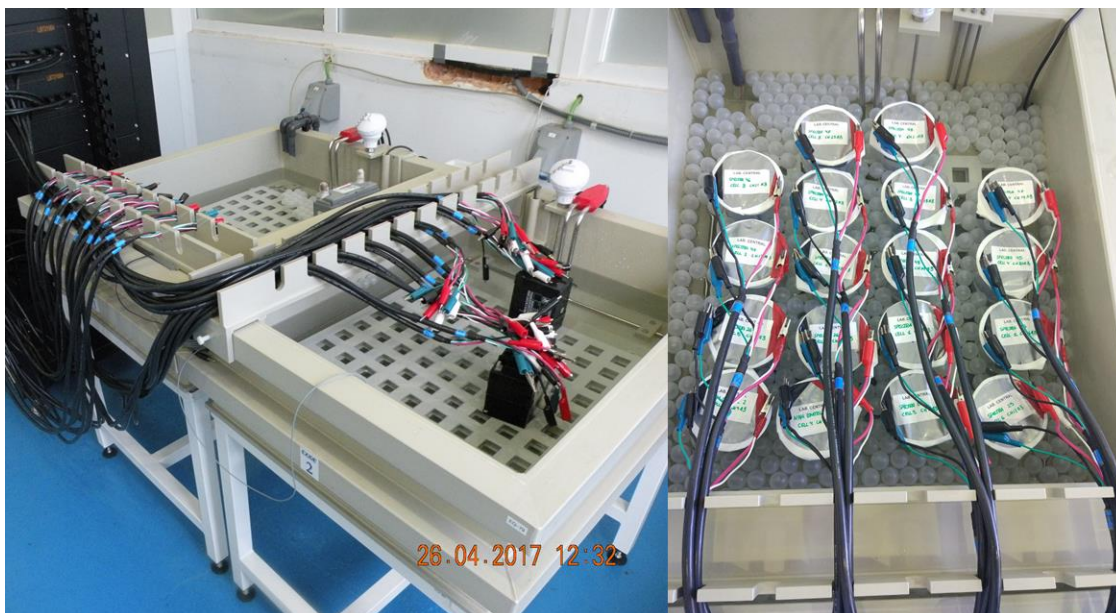
Figure 24. Thermostatic water baths.

3.2.10. ARBIN Potentiostat/Galvanostat Testing Stations

For performing the formation of the cells and the different electrical tests, different ARBIN Potentiostat /Galvanostat Testing Stations were used. Their main characteristics are listed in **Table 11**:

Table 11. Characteristics of the ARBIN Potentiostat / Galvanostat testing stations used during the cell formation and electrical tests.

Model	Number of channels	Max. Voltage / V	Max. Current / A	Current range			Voltage range / V	Software version
				High / A	Medium / mA	Low / mA		
BT2543	16	5	7	± 5	± 100	± 1	0 - 5	MITS Pro 4.3
BT-G-501	16	5	11	± 5	± 100	± 1	0 - 5	
LBT	32	5	18	± 10	± 500	± 20	0 - 5	MITS Pro 7.0

These stations are made by multiple independent channels fine-tuned for testing batteries. MITS Pro and Data Watcher software for writing test schedules, monitoring real-time data, and reviewing and plotting test results. Each station has a different number of multiple independent channels; each channel functions independently which allows running multiple experiments simultaneously. The same programs can be used in the three stations. For proper operation, the room temperature must be between 0 to 35 ºC, but the channels can

stand at higher and lower temperatures (experiments temperatures from -18 ⁰C to 40 ⁰C). **Figure 25** shows BT2543 and BT-G-501 Arbin stations.
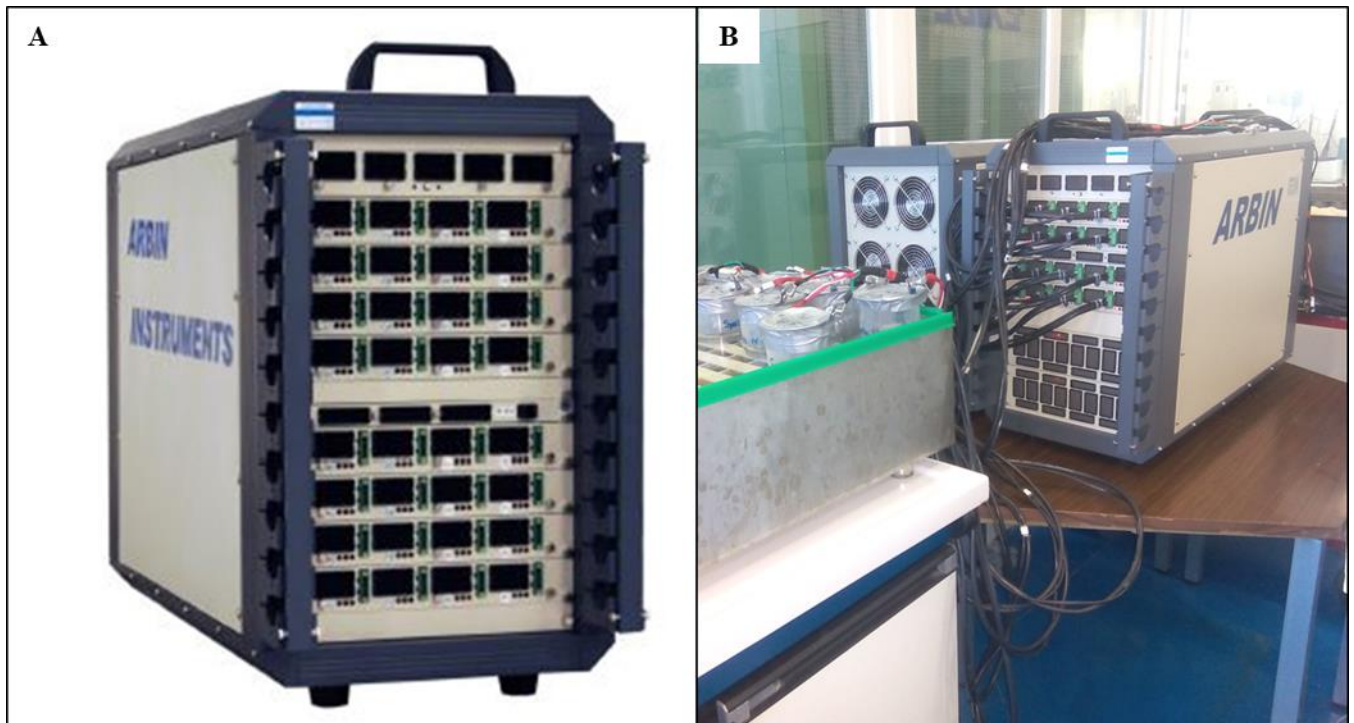
Figure 25. A. BT2543 Arbin station from Arbin website. **B.** BT2543 and BT-G-501 Arbin stations at the laboratory.

3.2.11. Battery TESTER 3554 (HIOKI)

The internal resistance of the cells was measured with a battery portable tester 3554 from HIOKI shows in **Figure 26**. The electrical resistance range is from 3 mΩ (resolution 1 $\mu\Omega$) to 3 Ω (resolution 1 mΩ). It also measured the voltage of the cell, working from $\pm$ 6 V to $\pm$ 60 V (resolution: 1 mV).

Figure 26. Battery TESTER 3554 (HIOKI).

3.2.12. Climate chamber

As climate chamber we used a SELECTA freezer model FRIGEDORM-REG (**Figure 27**). The freezer operation limits went from 0 ⁰C to -30 ⁰C.

Figure 27. SELECTA freezer model FRIGEDORM-REG.

At UNIVERSIDAD AUTÓNOMA DE MADRID facilities

3.2.13. Metrohm Autolab PGSTAT204 potentiostat/galvanostat and BOOSTER10A

For performing the CV on the 2 V / 1 Ah cells a Metrohm Autolab PGSTAT204 potentiostat/galvanostat combined with a 10 Amp Current Booster (BOOSTER10A) was used. This equipment was able to deliver a maximum current of 10 A in combination with the BOOSTER10A, and to work in a voltage range from -10 V to 10 V. The 2 V / 1 Ah cells were used as three-electrodes cells in order to work with this system [79].

3.3. GANFg dispersions preparation

Mother GANFg dispersions were prepared at GAIKER facilities using the Dissolver DISPERMAT® CN10. The different steps following to make the dispersions are listed in **Table 12**.

Table 12. Preparation of GANFg dispersions. Dispersion steps were done with the equipment Dissolver DISPERMAT® CN10.

Step	Hard chrome dissolver disk diameter / mm	Auxiliary equipment	Ceramic balls dimeter / mm	Total volume / L	Time / min	Speed / rpm	Speed / m s^{-1}
1 - Wet	40			1.00	20	4500	9.42
2 - Grinding	35	Bead mill APS 250	0.6 - 0.8	0.25	30	3300	6.00
3 - High shear	40			1.00	20	8170	17.30
4 - Dilution	40			1.00	15	3300	6.00

We differentiated two types of dispersions:

- Dispersions made of GANFg and OEs. For preparing these dispersions, mother dispersion was prepared in advance. The composition of the mother dispersion was the following:

Water (100 g) + OE (7.5 g) + GANFg (12.5 g).

The final amount of OEs was constant, and when two different OEs were used the composition was the following:

Water (100 g) + OE 1 (3.75 g) + OE 2 (3.75 g) + GANFg (12.5 g).

The mother dispersion was made following steps 1, 2 and 3 from **Table 12**. For preparing the diluted and final dispersions, a certain amount of mother dispersion was diluted in water following step 4 (**Table 12).** The final dispersions always had 100 g of water and the other components at a certain concentration.

- Dispersion made of GANFg, carbon materials and OE:

The carbon materials used for these dispersions were listed in section 3.1.1, C1 (graphite) and C4 (carbon black). For preparing these dispersions the mother dispersion was not necessary, as the final carbon material amount was enough for proper operation of the equipment (Dissolver DISPERMAT® CN10). So step 4 from **Table 12** was not performed. The composition of the dispersions was the following:

Water (100 g) + OE1 (0.6 g) + Carbon material (3.0 g) + GANFg (1.0 g).

The same amount of carbon materials was used for both types, C1 (graphite) or C4 (carbon black). The dispersion was made following steps 1, 2 and 3 from **Table 12**. In the case of

the dispersion prepared with C4, special steps were followed at the beginning of the dispersion:

- Part of the water was used for suspending the C4 and stirring for a few minutes.
- Addition of the OE1 and stirring for a few minutes.
- Addition of the rest of the water and continue stirring.
- Addition of the GANFg and start step 1 from **Table 12** followed by steps 2 and 3.

NEGATIVE MIXTURES

Table 13. Batches 1, 2, 3 and 4: negative mixtures composition. LS2 was the same as OE1.

Mixture		Dispersion / g					Components added during the mixing process / g								
Batch	Name	H₂O	GANFg	LS2/OE1	OE2	Carbon	LO	H₂O	H₂SO₄*	PAC Fiber	BaSO₄	LS1	LS2/OE1	OE2	Carbon
1	1						1000	136.2	54.0	2.2	10.0		3.0		C1 15.0
	2							126.2				3.5			C1 15.0
	3							126.2				3.5			C2 15.0
	4							131.2					3.0		C3 18.0
	5							141.2					3.0		C4 8.0
	6							126.2					2.7		C5 1.8#
2	NAM Control						1000	116.2	54.0	2.2	10		3.0		
	S5	100	5.0	3.0				15.0					0.0		
	S6	100	2.0	1.2				15.0					1.8		
	S7	100	1.0	0.6				12.0					2.4		
3	Blank						1000	147.0	46.0	2.2	10.0		3.0	-	
	S25B							135.0					1.5	1.5	
	S25	100	1.0	0.3	0.3			35.0					1.2	1.2	
	S26B							137.0					1.0	1.0	
	S26	100	1.0	0.3	0.3			27.0					0.7	0.7	
4	S44B						1000	35.0	46.0	2.2	10.0		2.4		
	S39	100	1.0	0.6		C4 3.0		35.0							C4 2.0
	S40					C1 3.0		35.0							C1 7.0

*Acid density equal to 1.4 g cm⁻³. #1.8 g of C5 = 1.5 g pure C5 + 0.30 g LS2.

POSITIVE MIXTURE

The same mixture was used in the positive plates for all the batches.

Table 14. Positive mixture composition.

Mixture		Components added during the mixing process / g			
Batches	Name	PbO	H₂O	H₂SO₄ (1.4 g cm⁻³)	PAC Fiber
1 - 4	PAM STD	1000	150.0	40.0	2.2

3.5. Mixing process for the PASTES

Table 15 summarizes the steps followed to perform the mixing process using our lab mixer (section 3.2.6).

Table 15. Mixing process steps.

	Step	Time / min	Speed
0	Addition of dry components	-	0
1	Mixing of the dry components	3	Minimum
2	Addition of water or GANFg dispersion	1	0
3	Wet mixing	5	From 0 to 3
4	Acid addition while mixing	10	1
5	Acid mixing	10	1 - 1.5
6	Control step – Paste density measurements	-	0

Amounts of the different compounds are listed in **Table 13.**

0 - Addition of dry components

NEGATIVE PASTES (Figure 28. A – D)
- LO powder.
- PAC fiber.
- Barium sulfate.
- OEs.
- Carbon materials.

POSITIVE PASTES
- LO powder.
- PAC fiber.

<u>1 - Mixing of the dry components</u> **(Figure 28. E)**

<u>2 - Addition of water or GANFg dispersion</u> **(Figure 28. F)**

NEGATIVE PASTES
- Mixtures without GANFg dispersion: 116 mL of water were added at this step.
- Mixtures with GANFg dispersion: The dispersion was firstly stirred in order to homogenize it. After that, it was added to the dry components. An extra amount of water was added depending on the paste conditions.

POSITIVE PASTES
150 mL of water were added at this step.

<u>3 - Acid addition while mixing</u> **(Figure 28. G)**. The acid was added dropwise in order to cover the whole time of this step. The acid used for the mixing process had a density of 1.4 g cm^{-3}.

<u>4 - Acid mixing</u> for 10 min in order to homogenize the paste.

- At this step, mixtures with carbon materials added as dry components were to dry, the speed was increased to 8 (maximum), and additional water had to be added.

Final aspect of a negative paste is showed in **Figure 28. H.**

• <u>Control step – Paste density measurements</u>:

After step 5 the paste density was measured following the below procedure:

- The density cup (**Figure 21. D**) was overfilled with paste.
- The cup was agitated and homogenized using the VORTEX equipment (**Figure 21. C**).
- The paste was leveled to the top of the density cup.
- The density cup was weighed using the weighing scale (**Figure 20**).
- The density of the paste (ρ_{paste}) was calculated as follows:

$$\rho_{\text{paste}} \, (\text{g cm}^{-3}) = (m_{\text{filled density cup}} - m_{\text{empty density cup}}) \, / \, V_{\text{density cup}}$$

$m_{\text{empty density cup}} = 110.32$ g
$V_{\text{density cup}} = 86.97 \text{ cm}^3$
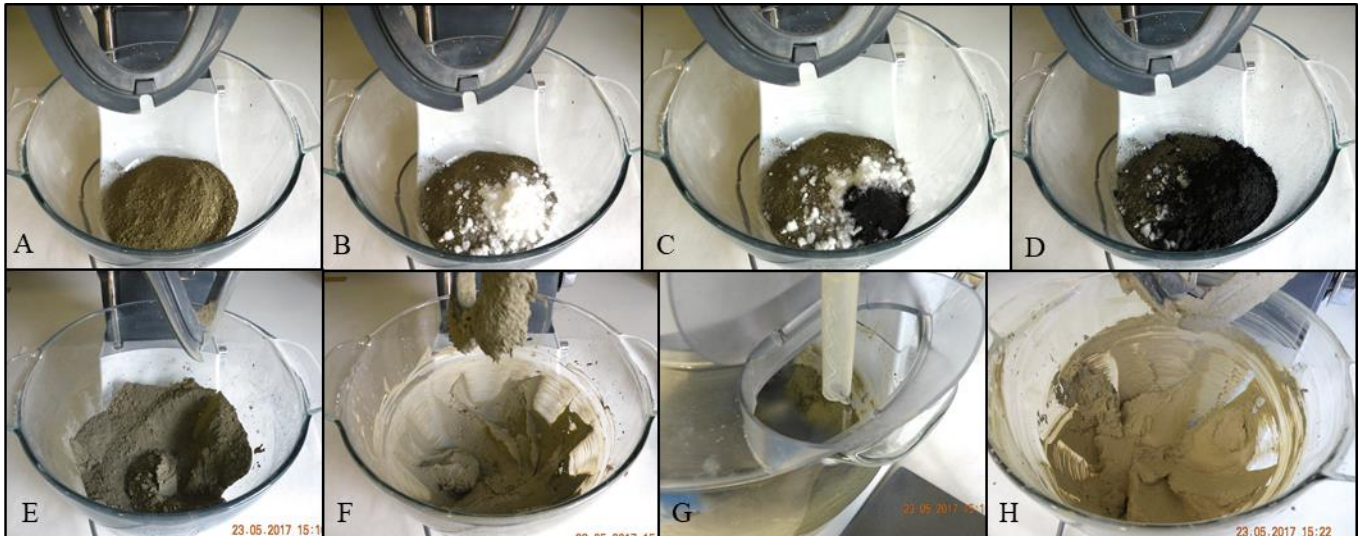
Figure 28. Mixing process for a negative paste. A. LO addition. **B.** PAC fibers and BaSO$_4$ addition. **C.** OE addition. **D.** Carbon material addition. **E.** Paste after mixing. **F.** Paste after water addition and mixing. **G.** Acid addition. **H.** Final paste.

3.6. Pasting process

The same pasting process was used for both plates, positive and negative. After making the pastes, a certain amount of paste (8 g) was coated on the Pb-Sn (0.80%) grid (**Figure 16**) pasting area (10.18 cm^2) using a spatula. **Figure 29. A** shows the pasted grid covered by an AGM sheet (**Figure 17**) underneath. Then, the pasted grid was covered at both sides by two sheets of AGM (**Figure 29. B**). Since this moment the pasted grid was called plate, in this case, unformed and uncured plate. The calender roller (**Figure 22**) was used for compressing the paste and achieving a constant thickness of 1.70 mm throughout the whole plate (**Figure 29. C**). The final plate is showed in **Figure 29. D**. According to the grams of paste, this plate was able to release 1 Ah, so the plate is known as 1 Ah plate.
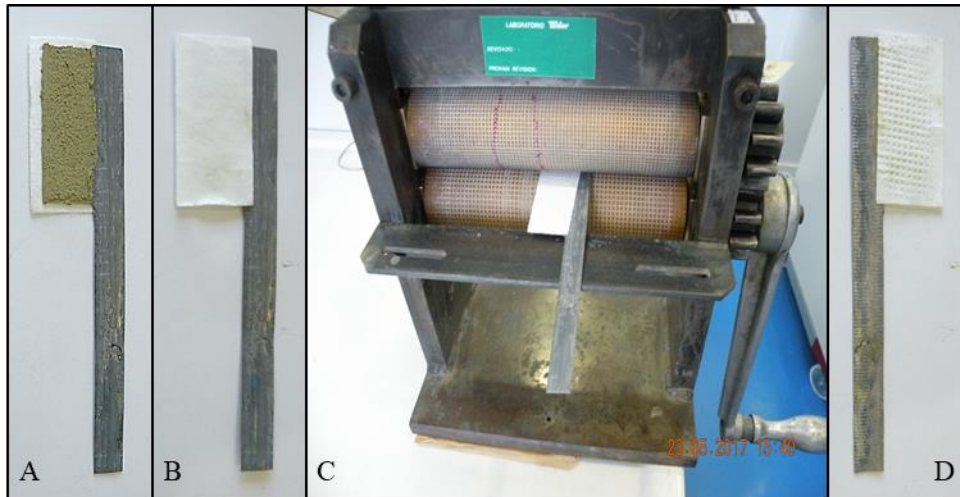
Figure 29. Pasting process. A. Pasted grid covered underneath by an AGM sheet. **B.** Pasted grid covered by the two AGM sheets. **C.** Compression process using a calender roller. **D.** Final unformed and uncured plate.

3.7.Curing and drying processes

The curing and drying process was performed in our laboratory curing chamber (**Figure 23**). Two types of curing processes were performed during the experiments:

- BATCHES 1 & 2:

• Negative plates:
1. Curing stage 1: 24 hours at 55 °C and 85% of relative humidity.
2. Curing stage 2: 24 hours at 30 °C and 100% of relative humidity.
3. Drying stage: plates were dried at room temperature.

• Positive plates:
1. Curing stage 1: 24 hours at 60 °C and 85% of relative humidity.
2. Curing stage 2: 24 hours at 30 °C and 100% of relative humidity.
3. Drying stage: plates were dried at room temperature.

- BATCHES 3 & 4:

• Negative plates:
1. Curing stage: 22 hours at 55 °C and 85% of relative humidity.
4. Drying stage: 2 hours at 70 °C and 15% of relative humidity.

• Positive plates:

1. Curing stage: 22 hours at 60 °C and 85% of relative humidity.

5. Drying stage: 2 hours at 70 °C and 15% of relative humidity.

Figure 30 shows the cured or also called unformed, negative and positive plates. The white color on the surface of the plates comes from removing the AGM sheets for taking the picture.
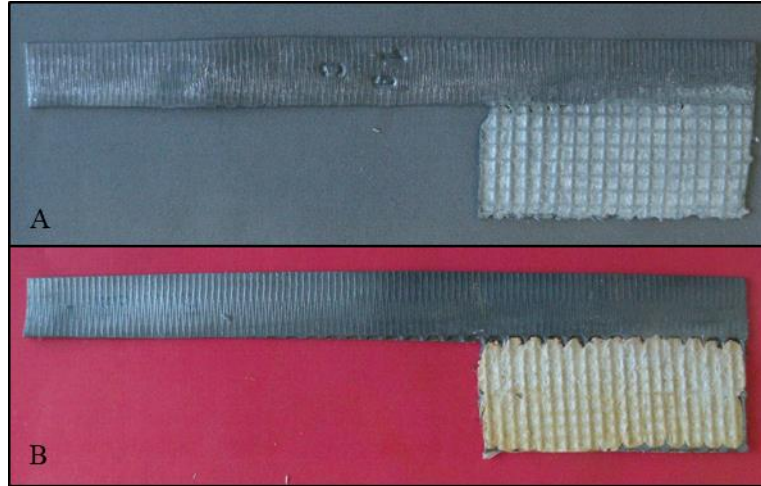
Figure 30. Unformed negative (**A**) and positive (**B**) plates without the AGM sheets.

3.8. Cell assembly

All the materials for the cell assembly were described in **section 3.1.4**, and **Figure 31** and **Figure 32** show the whole process.

2 V / 1 Ah small lead acid cells were prepared following the below procedure:

A. Methacrylate sheet 1 + PVC screws and washers + 2 AGM sheets. PVC washers are used in order to maintain the thickness and compression of the plate group (**Figure 31. A**).
B. A + unformed positive plate 1 (**Figure 31. B**).
C. B + 2 AGM sheets (**Figure 31. C**).
D. C + unformed negative plate (**Figure 31. D**).
E. D + 2 AGM sheets (**Figure 31. E**).
F. E + unformed positive plate 2 (**Figure 31. F**).
G. F + 2 AGM sheets (**Figure 31. G**).
H. Assembly: G + Methacrylate sheet 2 + PVC washers already adjusted. This adjustment was done for maintaining maintain the thickness and compression of the plate group (**Figure 31. H**). The final thickness of the plate group was 6 mm, the same thickness as the PVC washer. Final compression of the AGM sheets was 35%.
I. The two positive lugs were welded together using the solder wire (**Figure 31. I**).

As a note, this assembly had a total of 8 AGM sheets: each unformed plate was surrounded by two AGM sheets, as it was explained in the pasting process section 3.6. So, 6 AGM sheets were used for the unformed plates. 2 AGM sheets were located at the sides of the plate group in order to increase the acid impregnation: the acid was able to impregnate the whole sheet when this one was in contact with it.
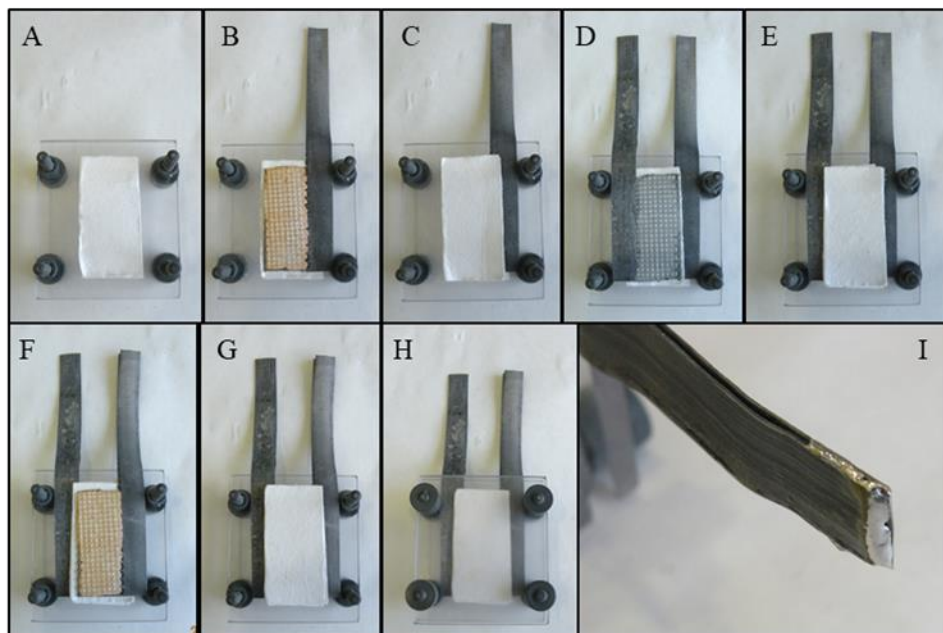
Figure 31. Cell assembly 1. A. Methacrylate sheet 1 + PVC screws and washers + 2 AGM sheets. **B.** A + positive plate 1. **C.** B + 2 AGM sheets. **D.** C + negative plate 1. **E.** D + 2 AGM sheets. **F.** E + positive plate 2. **G.** F + 2 AGM sheets. **H.** G + methacrylate sheet 2 adjusted with the PVC nuts: assembly. **I.** Welded positive lugs.

Once the assembly was prepared, the 2 V / 1 Ah lead acid cell was finalized following the below procedure:

A. The assembly was introduced in a 500 mL beaker (**Figure 32. A**).

B. The beaker was topped up to 250 mL with H_2SO_4 (1.28 g cm^{-3}), which will be the electrolyte of the cell (**Figure 32. B**).

C. Parafilm M and commercial adhesive tape was used for making the cover of the cell (**Figure 32. C**).

D. The positive and negative terminals were stood out in order to make them accessible (**Figure 32. D**).

E. The final cell was connected to the circuit (**Figure 32. E**).
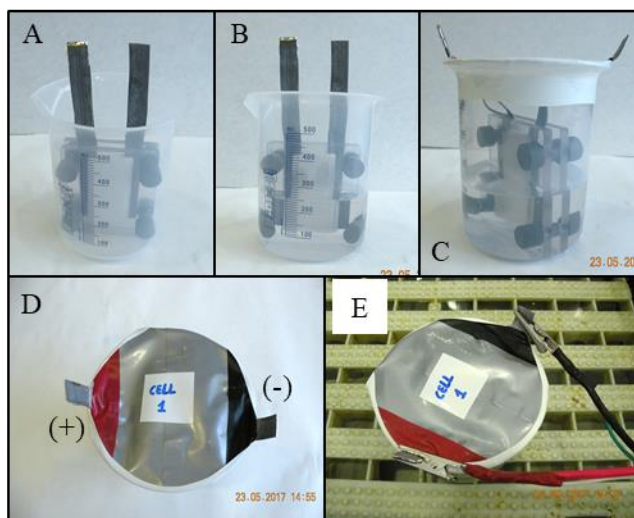
Figure 32. Cell assembly 2. A. Final structure in 500 mL beaker. **B.** A + H$_2$SO$_4$ (1.28 g cm^{-3}) until 250 mL. **C.** B + Parafilm M and commercial adhesive tape. **D.** 2 V / 1 Ah cell: (+) positive terminal – (-) negative terminal. **E.** 2 V / 1 Ah cell connected to the circuits.

3.9. Electrochemical techniques

The electrochemical techniques consist on the application of an electrical current or potential to the cell or battery. The electrical response, also in the shape of potential or current is measured and analyzed. In this way we can get information of the electrical behavior of different cells depending on the materials it contains in the anode or cathede as well in the electrolyte. These techniques are carried out using a potentiostat / galvanostat. For example if we want to study materials contained in the anode, this will be connected as working electrode. The cathode will be connected as counter electrode, and the reference potential will be the cell potential. In the case of working on a three-electrode cell we would need a reference electrode which only has the role of measuring the potential of the working electrode.

Along this study three types of electrochemical techniques have been used:

- **Chronoamperometry:** the potential of the working electrode is fixed at a constant value and the resulting current from faradaic processes occurring at the electrode (caused by the potential step) is monitored as a function of time. This type of technique is used for measuring the charge acceptance of the cells, as well as during the charges at constant voltage. The current at the working electrode is plotted versus the applied potential.
- **Chronopotentiometry**: the current of the working electrode is fixed at a constant value and the resulting potential from faradaic processes occurring at the electrode (caused by the potential step) is monitored as a function of time. This type of technique is used for the discharges of the cell, e.g. capacity, CCA and cycle life tests. The potential at the working electrode is plotted versus the applied current.

101

- **Cyclic Voltammetry**: the working electrode potential is ramped linearly versus time. Two potential limits are set: the initial potential and final potential of the chronoamperometry. When the final potential is reached the working electrode's potential is ramped in the opposite direction to return to the initial potential. These cycles of ramps in potential can be repeated as many times as needed. The current at the working electrode is plotted versus the applied potential to give rise to the Voltammogram. CV is used for sidying many variety of redox processes, to determine the stability of reaction products, the presence of intermediates in redox reactions, electron transfer kinetics, and the reversibility of a reaction.

3.10. Cell formation process

Once the cell was assembled, it was placed at the thermostatic water bath (**Figure 24**), and connected to the BT2543 Arbin station (**Figure 25**) for 4 h at 40 °C, this time is known as soaking time. The whole formation process was performed at 40 °C. After the soaking time, a set of fixed current was applied to the cell:

A. Current ramp: from 0 A to 0.32 A in 15 min.
B. Charge 1: 0.32 A for 13 h.
C. Discharge 1: -0.12 A for 4.7 h.
D. Charge 2: 0.24 A for 3.0 h.
E. Charge 3: 0.16 A for 6.3 h.
F. Discharge 2: -0.24 A for 2.5 h.
G. Charge 4: 0.24 A for 3.2 h.
H. Charge 5: 0.12 A for 4.2 h.

Total time: 37.16 h. Current and voltage data of this process is showed in **Figure 33**.
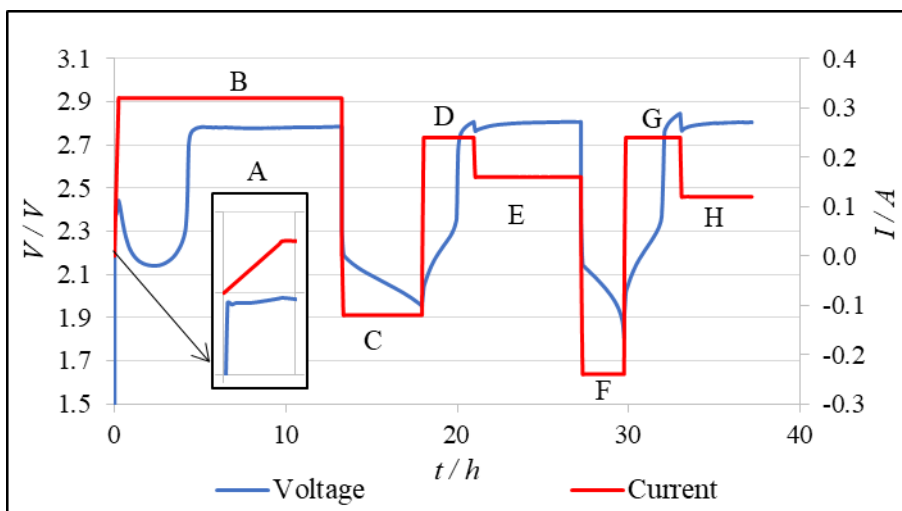
Figure 33. Cell formation process at 40 °C.

After the formation, the electrical resistance of the cells was measured with the battery tester HIOKI 3554 (**Figure 26**).

3.11. Electrical tests

3.11.1. Recharge of the cells

This test was based on the norm *VW75073 2012-07 Section 5.2.1*.
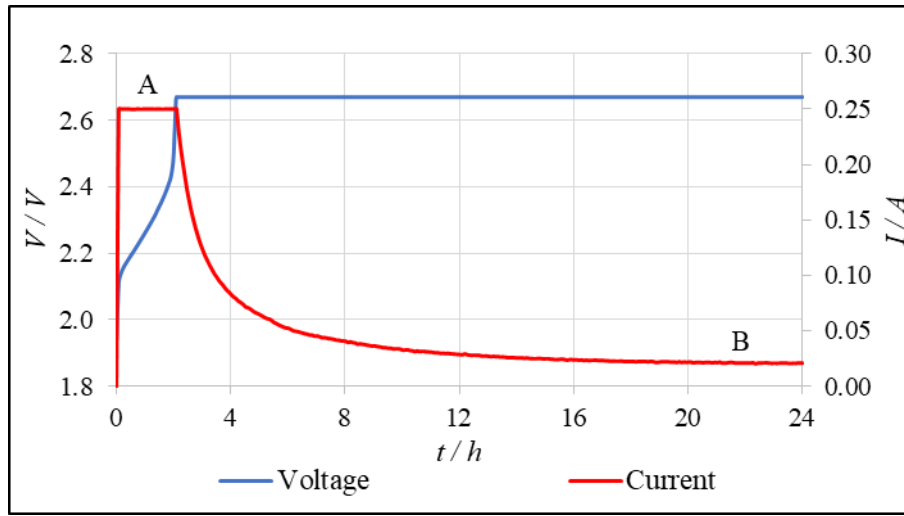
Figure 34. Recharge of the cells for 24 h.

After the capacity test, the CCA test and, in some cases, the cycles at PSoC, the cells had to be recharged following the below procedure:

A. Charge at 0.25 A until reaching 2.67 V.
B. Hold a voltage of 2.67 V until reaching a total test time of 16 h for CCA test and cycles at PSoC, or 24 h for capacity test.

The cell was placed at the thermostatic water bath (**Figure 24**) at 27 ± 2 °C. **Figure 34** shows the current and voltage data of a 24 h recharge. As can be seen in the figure, at the end of the step B the current is constant. At that time the float currents are measured.

3.11.2. Capacity test

This test was based on the norm *VW75073 2012-07 Section 7.1*. The fully charged cell was placed at the thermostatic water bath (**Figure 24**) at 27 ± 2 °C. The capacity at 20 h was determined by discharging the cells at I_{20} equal to -0.05 A (C_{20} / 20 h = 1 Ah / 20 h). The cutoff was 1.75 V. Time, current and voltage values were recorded during the whole test.

Special attention was taken for the duration of the discharge in order to calculate the real capacity of the cell.

3.11.3. Cold-cranking ability test

This test was based on the norm *VW75073 2012-07 Section 7.2*. The fully charged cell was placed at the climate chamber (**Figure 27**) at -18 ± 2 °C for 24 h prior to the test. Before the test, the electrical resistance of the cells at -18 ± 2 °C was measured with the battery tester HIOKI 3554 (**Figure 26**). The CCA was determined by discharging the cells at 5C current equal to -5 A (C_{20} * 5 = 1 Ah * 5). The cutoff was 1.00 V. Time, current and voltage values were recorded during the whole test. Special attention was taken for the duration of the discharge.

3.11.4. Initial Charge Acceptance (ICA) test types 1 and 2

This test was based on the norm *RNDS SS 36 11 003 2014-05 Section 5.2.7*. The fully charged cell was placed at the thermostatic water bath (**Figure 24**) at 27 ± 2 °C. The cell was discharged at -0.05 A for 2 h, in order to reduce the SoC of the cell from 100% to 90%. Then the cell was resting for 72 h (**ICA test type 1**) or 24 h (**ICA test type 2**). After this resting period the cell was charged at a constant voltage of 2.42 V for 60 s. **Figure 35** shows the values during this charging step. Time, current and voltage values were recorded during the whole test. Special attention was taken for the current of the cell at 5 s.
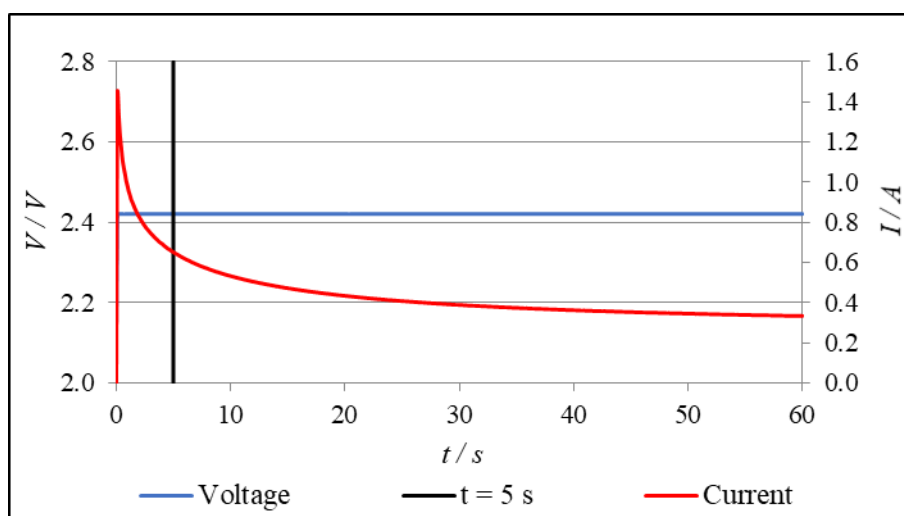
Figure 35. ICA test. Charging step.

3.11.5. Negative polarization study

The fully charged cell was placed at the thermostatic water bath (**Figure 24**) at 27 ± 2 °C. During the negative polarization study, a set of fix current (8 in total: from A to H) were

applied to the fully charged cell during a certain period of time. Time, current and voltage values were recorded during the whole test. The negative plate active surface considered was equal to 20.36 cm^2 (pasting area multiplied by 2; 2*10.18 cm^2). Current (I), current density (j) and time values for each charging step (i) are described in **Table 16**.

Table 16. Parameters for the negative polarization test.

Charging step (i)	I / A	j / mA cm^{-2}	t / min
A	200	9.824	50
B	100	4.912	20
C	40	1.965	20
D	20	0.982	20
E	10	0.491	20
F	4	0.196	15
G	2	0.098	10
H	1	0.049	10

At the beginning of the test, when no current was passing through the cell (I = 0, so j = 0), the potential of the negative plate (negative terminal) was measured using an Ag/AgCl reference electrode with a lugging capillary. This potential was called Open Circuit Potential (OCP; E_{OCP}). After each charging step, when the cell voltage was steady, the same measurement (E_i) was taken. Apparent overpotential (η_{app}) in each step was calculated as: $\eta_{app} = E_i - E_{OCP}$. Apparent hydrogen overpotential ($\eta_{app,\ H2}$) was sat at step D, when the current density was equal to 1 mA cm^{-2}, and it was calculated as following: $\eta_{app,\ H2} = E_{j\ =\ 1\ mA\ cm-2} - E_{OCP}$. **Figure 36** shows the cell voltage values, as well as the applied currents for this test.
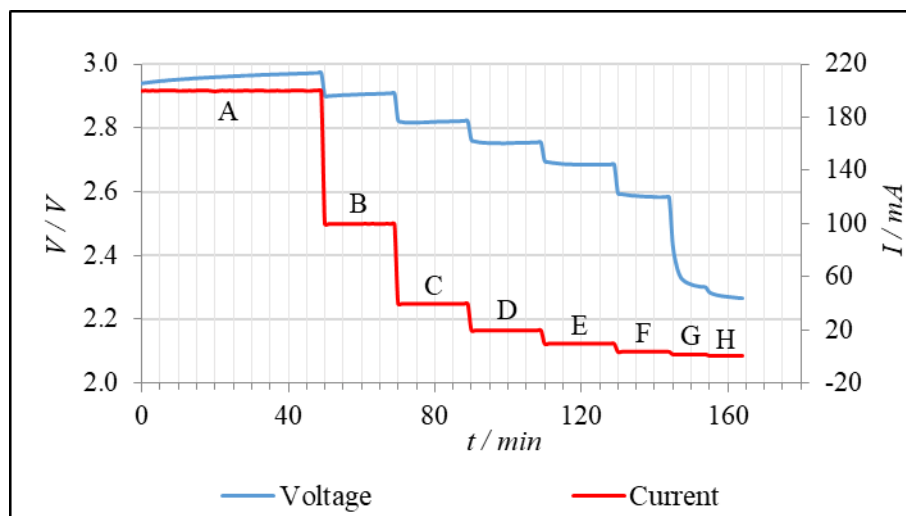
Figure 36. Negative polarization study: cell voltage and current data.

3.11.6. Cycles at PSoC types 1 and 2

The fully charged cell was placed at the thermostatic water bath (**Figure 24**) at 27 ± 2 °C. This test was based on the norm *VW75073 2012-07 Section 7.7*. The main difference between the cycles at PSoC types 1 and 2 was the initial SoC of the cell:

- Type 1: the cell was fully charged at the beginning of the test; SoC = 100%.
- Type 2: the cell was half charged at the beginning of the test; SoC = 50%. In order to achieve this SoC the fully charged cell was discharged at -0.20 A ($4*I_{20}$) for 2.5 h at the beginning of the test.

Besides this difference, the cycle test was the same for both types:

- Step 1: Charge of the cell at 0.35 A ($7*I_{20}$) for 40 min with a maximum voltage of 2.40 ± 0.05 V.
- Step 2: Discharge of the cell at -0.35 A ($7*I_{20}$) for 30 min.

This charge-discharge cycling was performed until the cell reached a voltage lower than 1.66 V during the discharge. Voltage, current, SoC and time values during the PSoC cycles types 1 and 2 are showed in **Figure 37** and **Figure 38** respectively.
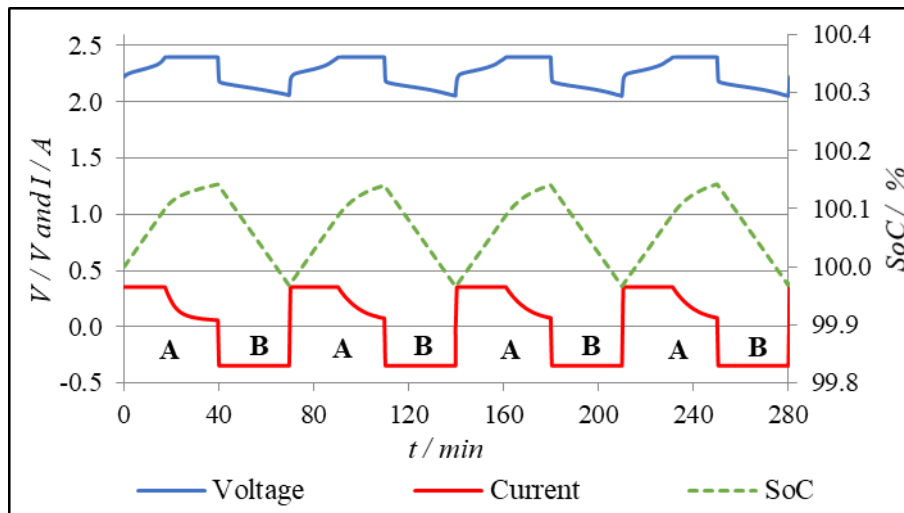
Figure 37. Cycles at PSoC type 1. Initial SoC = 100%. **Step A:** charge step. **Step B:** discharge step.
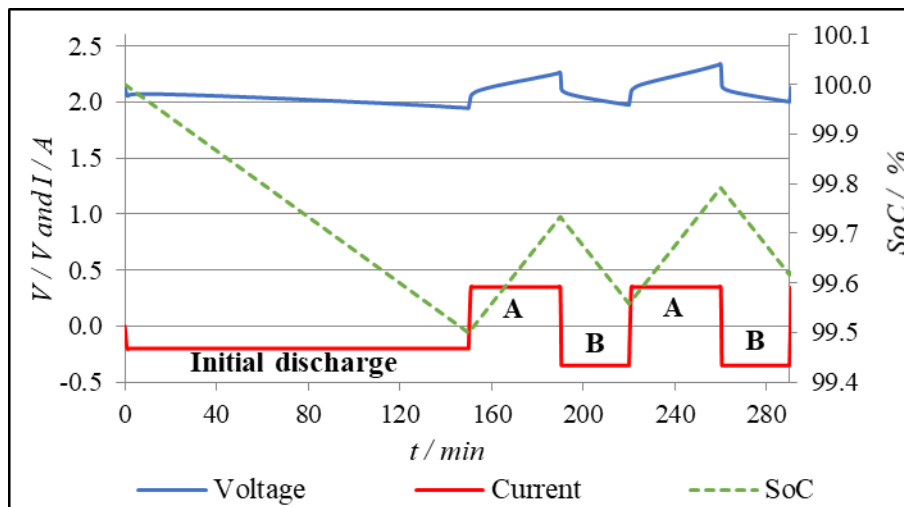
Figure 38. Cycles at PSoC type 2. Initial SoC = 100%. SoC after initial discharge = 50%. **Step A:** charge step. **Step B:** discharge step.

3.12. Cyclic Voltammetry (CV)

The CV was performed using a Metrohm Autolab PGSTAT204 potentiostat/galvanostat combined with a 10 Amp Current Booster (BOOSTER10A) (section **3.2.13.**).
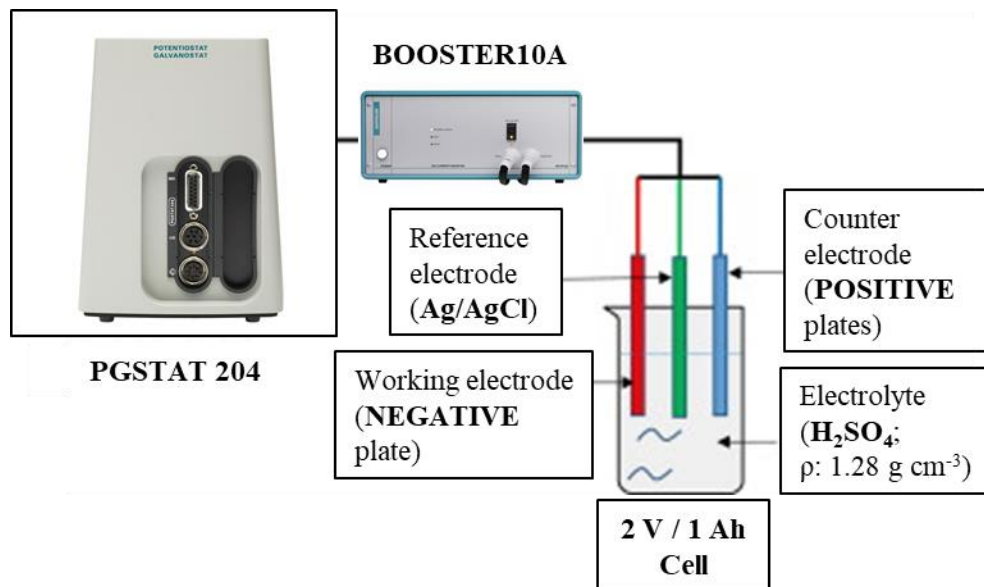
Figure 39. System for performing the CVs. PGSTAT 204 potentiostat/galvanostat connected to BOOSTER10A, and the latest connected to the three-electrode cell.

The 2V / 1Ah cells were turned to a three-electrode cell system. In addition, the plate group was completely covered by acid in order to ensure that the whole plate was submerged in acid. The system is explained in **Figure 39**, where the diagram of a three-electrode cell is showed: an Ag/AgCl electrode as reference electrode used with Lugging capillary, two

positive plates (positive terminal of the cell) as counter electrode and the negative plate (negative terminal of the cell) as working electrode.

The test parameters for the CV were as following:
- Scan rate: 5.00 mV s^{-1}.
- Voltage range: 1.50 V to 0.50 V.
- Number of cycles: 300.

The reactions that occur during one cycle are explained in **Figure 40.**
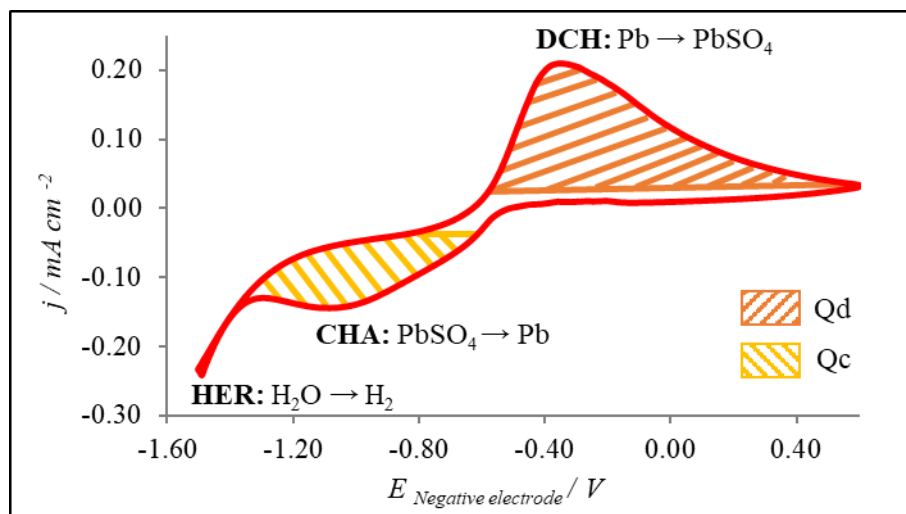
Figure 40. Voltammogram from the three-electrode cell. **E:** Negative electrode potential vs Ag/AgCl reference electrode. Reactions occurred are included in the graphic. **DCH:** discharge reaction. **CHA:** charge reaction. **HER:** Hydrogen Evolution Reaction. **Qd:** charge stored during discharge. Unit: C. **Qc:** charge stored during charge. Unit: C.

The area under the discharge (Qd) and charge (Qc) was calculated using the program OriginPro 8.

3.13. Physicochemical analyses

3.13.1. Sample preparation

Several analyses were done on the unformed plates (after curing process), the formed plates (after the formation process) and the cycled plates (after the cycles at PSoC cycles). In the case of the unformed plates, the pasting paper was removed from the plates, and the remaining pasting paper on the surface of the plate was removed using a tissue. However, when the plates came from the 2 V / 1 Ah cells, i.e. the formed and cycled plates, a treatment was needed before the sample gathering. The plates were taken out from the cell, and wash with water until the pH of the water was equal to 7 (neutral). This step was done for removing the acid from the plates' surface.

After washing, the plates were dried in a climate chamber:

- Positive plates: dried in a climate chamber at 110 ⁰C for a minimum time of 2 h.
- Negative plates: dried in a vacuum climate chamber at 100 ⁰C for a minimum time of 1 h.

The plates were finally taking out from the climate chamber once the weight was constant, in order to ensure the complete dryness of them. It is important to notice here that the formed or cycled negative plates cannot be in direct contact with the air, they must be always submerged in water, after they are removed from the cell. When the negative plates are in contact with the air an oxidation process occurs, the Pb reacts with the oxygen from the air and oxidized to PbO. This problem would turn in a falsification of the measurement, as we wouldn't be analyzing the sample as it really was in the 2 V / 1 Ah cell. Because of this, the formed or cycled negative plates were dried in a vacuum climate chamber. With the formed or cycled positive plates, this problem does not occur, as these plates are made of PbO_2 which cannot be further oxidized.

Once the plates were washed and dried, the active material can be removed from the plate. At this step, the active material was removed pellet by pellet from the grid (**Figure 16**).

3.13.2. Lead sulfate and carbon determination in NAM and PAM

The lead sulfate and carbon content of the unformed, formed and cycled negative and positive plates was analyzed during the whole study. For carrying out these analyses, the pellets of active material were milled using a Tube Mill control from IKA [80], and filtered to 0.25 mm size.

Figure 41. ELTRA CS800. Carbon and sulfur analyzer.

The lead sulfate and carbon content was determined using a ELTRA CS-800 analyzer (**Figure 41**) [81].

The operation principle of this equipment is based on the Infrared (IR) radiation absorbed by the SO_2 and CO_2 gases coming from the combustion with pure oxygen of the active material. The scientific principle is the Lambert-Beer law. The working procedure is as following:

- The active material sample is weighed on a ceramic crucible.
- Catalyzers for improving the combustion are also added.
- The sample is melted in an induction furnace while a flow of compressed air (4 - 6 bar/ 60 – 90 psi) oxygen 99.5% pure (2 - 4 bar /30 - 60 psi) is passing.
- As a result of this combustion the sulfur and carbon from the active material are converted to SO_2, and $CO + CO_2$, respectively. These are called combustion gasses.
- The combustion gases pass through a dust filter and a moisture absorber for purification.
- The SO_2 from the combustion gases is excited in two IR cells fixed at different IR wavelengths specially selected from the SO_2 IR spectrum. Then, the SO_2 from the combustion gases is able to absorb part of the IR radiation and emits the remaining, which is detected and quantified.
- Once the SO_2 has been detected, the combustion gases are further oxidized, and the SO_2 and CO turns to SO_3 and CO_2 respectively. The final composition of the combustion gases is SO_3 and CO_2.
- The combustion gasses pass through the cellulose wool, where the SO_3 gets trapped. The final composition of the combustion gases is CO_2.
- Finally, the CO_2 from the combustion gases is excited in two IR cells fixed at different IR wavelengths specially selected from the CO_2 IR spectrum. Then, the CO_2 from the combustion gases is able to absorb part of the IR radiation and emits the remaining, which is detected and quantified.

Table 17. Lead sulfate and carbon analyses. Sample and catalyzers weights.

Type of analyses	Sample / mg	Catalyzers / mg	
		Tungsten	Tin
Lead sulfate determination	300 - 500	1600 -1800	500
Carbon determination	400 - 500		

Once we know the SO_2 and CO_2 concentrations in the combustion gasses, we can calculate the lead sulfate and carbon concentration of the sample. **Table 17** shows the amount of sample and catalyzers need for each analyses, carbon or lead sulfate determination.

3.13.3. Porosity analysis

The porosity analysis consists on obligating a liquid, in this case mercury, to penetrate into the pores of a material when a certain pressure is applied. This pressure is inversely proportional to the pore diameter, i.e. with a higher pore diameter a lower pressure is needed as the liquid has more available space for penetrating into the material. According to Washburn [82]:

$$d = (-4 \cdot \gamma \cdot \cos\theta) / P$$

d: pore diameter
γ: Surface tension of the interface mercury-air. $\gamma = 485.6$ mN m^{-1}.
θ: contact angle between mercury and the material. $\theta \approx 140^{\circ}$.
P: intrusion pressure of mercury.

In our case, the porosity of the negative unformed plates was analyzed, in order to know how the different additives affect to the NAM structure. The sample was prepared following **section 0**.

For carrying out this analysis a Micromeritics porosimeter Autopore III 9405 (**Figure 42**) was used, and the working procedure was as following:

-The active material sample is introduced in the sampler. Sample weight between 4 g and 6 g.
-The sampler is filled with mercury.
-The mercury is introduced into the pores of the sample by applying an intrusion pressure. This step is repeated several times, until all the pores are filled by mercury. Then, the analysis is over.
-Once the intrusion pressure is constant, the amount of mercury filled inside the sample is recorded, and the intrusion pressure can be increased for the next step.

Pressures and mercury volumes are recorded by the equipment. Following Wahsburn equation, the pore diameter can be calculated for each step. At the end of the analysis, the equipment

Figure 42. Micromeritics porosimeter Autopore III 9405.

delivers a graphic where represents the intrusion pressure (y axe) and the pore size (x axe), together with the median pore diameter, bulk density and porosity data.

3.13.4. Brunauer-Emmett-Teller (BET) SSA determination

The BET SSA determination was used to analyze the active surface area of the unformed and negative plates, and see how this property was affected by the additives. As a summary, the active surface area gives us an idea about the amount of active material that is going to be in direct contact with the electrolyte. The SSA is defined as the number of square meters that would be occupied by a material if all its pores would be projected to the surface. For calculating the SSA the in porous materials most commonly method is the one invented in 1938 by Stephen Brunauer, Paul Hugh Emmett, and Edward Teller (BET) [83] based on the absorption of gases on multimolecular layers. The principle of this method is to cover the first monolayer of the porous materials with molecules of a certain gas. In this way, knowing the volume of gas absorbed on the first monolayer, we can calculate the surface that these molecules occupy, and the SSA of the porous material.

The BET SSA measurements were done with the Micromeritics Flow Sorb II 2300 (**Figure 43**), which has the capability of reporting adsorption and desorption isotherms. The applicability of this equipment is from 0.1 m² to 280 m², and the reproducibility is better than 0.5%. The working procedure was as following:

- The sample is prepared according to **section 0**. After getting the active material pellets, these are cut in small pieces (width around 1 mm).
- 8 g of sample is loaded in the test tube.
- The sample is exposed to flowing N_2/He at room temperature, to purge any air or water in the sample or in the tube. The whole tube and all the pores of the sample are filled with the gases N_2/He.
- After degassing, the sample is ready for analysis.
- A Thermal Conductivity Detector (TCD) is used to measure the thermal conductivity at the start of the experiment.
- Since the sample will not adsorb nitrogen at room temperature, the sample tube is immersed in a Dewar flask of liquid nitrogen (LN_2) at 77 K.
- The sample almost immediately begins to adsorb nitrogen onto the surface. As the nitrogen molecules begin to be adsorbed on the surface, the thermal conductivity also changes.
- After the maximum amount of N_2 is adsorbed, the Dewar is removed to investigate the desorption of the sample.
- The amount of nitrogen consumed is then calculated and used to determine the surface area of the sample in m^2 g^{-1}, based on the weight of the sample loaded in the instrument.

Figure 43. Micromeritics Flow Sorb II 2300.

3.13.5. Powder XRD polycrystalline analysis

The XRD is based on the behavior of the crystalline phases when XR beams go through them, which was developed by Lawrence Bragg and his father William Henry Bragg.

We can see in **Figure 44** the behavior of a crystalline solid when it is traversed by 2 XR beams. These two XR beams (1 and 2) with identical wavelength (λ) and phase (depending on the incident angle; θ) approach a crystalline solid and are scattered off two different atoms (A and B) within it. These two atoms belong to the same family of planes inside the crystalline structure of our solid, and are separated by the interplanar spacing (d). Once the scattered beams reach the detector, the lower beam (2') traverses an extra length of $2d\sin\theta$, in comparison with beam 1'. This leads to Bragg's law which describes the condition on θ for the constructive interference to be at its strongest:

$$n \cdot \lambda = 2 \cdot d \cdot \sin \theta$$

where n is a positive integer and λ is the wavelength of the incident wave.
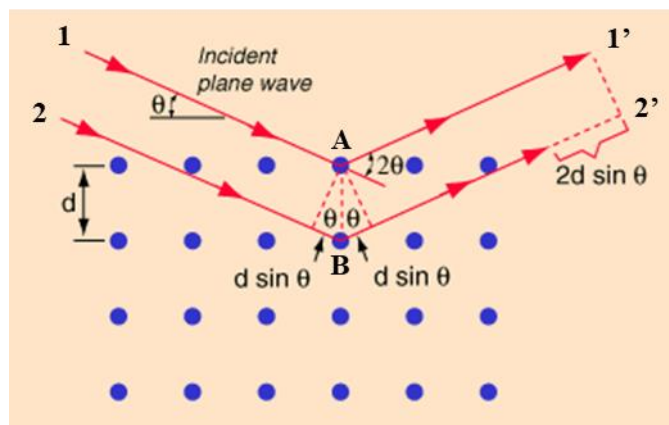
Figure 44. Bragg's law explanation.

In our case, this technique was used for studying the crystalline phase composition of the formed and cycled negative plates; the powder XRD polycrystalline analysis was used. On this purpose, the samples prepared following **section 0**. For carrying out these analyses, the pellets of active material were milled using a Tube Mill control from IKA [80], and filtered using a sieve of 0.25 mm pore size. The equipment used was the Powder X-ray Diffractometer (Siemens D5000) or the PANalytical X'Pert Pro (XRD5) diffractometer using Cu-K α radiation. A scan range of theta / 2 theta was done from 5º to 90º, with a scan rate of 0.0167º s^{-1}. The resultant diffractograms were analyzed.

3.13.6. Scanning Electron Microscope (SEM) analysis

In order to study the morphology and particle size of the active material from the formed or cycled negative plates, the SEM analysis was carried out. SEM analysis consists of the interaction between the sample surface and a focused electron beam of high energy. These electrons generate a variety of signals at the surface of the sample. All these signals are collected and captured in a 2 Dimensions image where the morphology of the surface can be analyzed. The SEM Hitachi S-3000N was used for generating the SEM images. This equipment has a resolution of 3 nm at 25 kV, a voltage range from 0.3 kV to 30 kV, and a detector from ESED.

The samples were prepared following **section 0**. After that, the pellets were split into two pieces in order to study the transversal cut of the sample, and thus the internal structure of the active material. Due to the surface of the sample must be conductive to interact with the electrons, the sample surface was covered by a thin layer of gold / chrome (~10 nm) using a Quórum equipment (Q150T-S) and a sputtering technique before the SEM analysis. The normal magnifications of the images were 3.0x and 6.0x.

4.Results and discussion

4.1. Research on the use of different carbon materials and LS as additives for the negative plates of LABs for Micro HEV

4.1.1. Aim of the study

Due to the importance of both types of additives, LS and carbon materials, in the performance of the negative plate in the EFB, our first study, named Batch 1, was related to the use of 5 different types of carbon materials and 2 types of LS in the negative plate. In this way, it was possible to check the well operation of the whole method: from making the pastes to testing the cells. All the results were summarized in the article called: "Influences of carbon materials and LS in the NAM of lead-acid batteries for microhybrid vehicles" [76]. The article can be also found in **ANEX i.**

4.1.2. Additives and negative mixtures characteristics

The materials used during these experiments were summarized in **section 3.1.1.** Two LS: LS1 and LS2; and five types of carbon materials: C1, C2, C3, C4 and C5.

Data from the properties of the LS and the carbon materials can be found in **Table 18**.

Table 18. **Batch 1.** Characteristics of the carbon materials and LSs added to NAM.

Carbon material	SSA / $m^2\,g^{-1}$	Particle size D_{50} / µm	Conductivity
C1	18	28.0	Excellent
C2	25	11.6	Outstanding
C3	125	14.4	High
C4	120 – 180	11.0	Low
C5	1,300 – 1,550	< 1.0	Low
Lignosulfonate		**Degree of sulfonation***	
LS1		1.4	
LS2		0.9	

*Number of sulfonic acid groups per 1000 unit weight lignin.

The main difference between the LS was the sulfonation degree (number of sulfonic acid groups per 1000 unit weight lignin). LS1 is supposed to behave in a better way at higher temperatures. In the case of the carbon materials, we used several types of carbons: C1 and C2 were expanded graphites; C3 was a hybrid carbon with the properties of a conductive carbon black and graphite; C4 and C5 were conductive carbons blacks. All of them had different SSAs and particle sizes, as well as different conductivity. The expanded graphites (C1 and C2) showed the highest conductivities (C1 higher than C2), followed by the hybrid carbon (C3), and by the two carbons blacks (C4 and C5). Regarding the particle size, from C1 to C4 had a micrometrical particle size. In contrast, C5 had a particle size inside the

nanoscale. For this reason, C1, C2, C3 and C4 had a SSA from 18 to 180 $m^2\ g^{-1}$, and C5 a SSA around 1425 $m^2\ g^{-1}$. The final composition of the mixtures was:

- **Mixture 1**: C1 (1.50 wt. %) + LS2 (0.30 wt. %).
- **Mixture 2**: C1 (1.50 wt. %) + LS1 (0.35 wt. %).
- **Mixture 3**: C2 (1.50 wt. %) + LS1 (0.35 wt. %).
- **Mixture 4**: C3 (1.80 wt. %) + LS2 (0.30 wt. %).
- **Mixture 5**: C4 (0.80 wt. %) + LS2 (0.30 wt. %).
- **Mixture 6**: C5 (0.15 wt. %) + LS2 (0.30 wt. %).

Knowing the final concentration and the particle size of the carbon materials it was expected from C1, C2, C3 and C4 to be found incorporated into the bulk of the NAM skeleton. However, C5 due to its nanometric particle size was expected to be located on the lead surface.

Table 19. Batch 1. Mixtures composition.

Mixture		Components added during the mixing process / g								
Batch	**Name**	**LO**	**H$_2$O**	**H$_2$SO$_4$ (1.4 g cm^{-3})**	**PAC Fiber**	**BaSO$_4$**	**LS1**	**LS2**	**Carbon material**	
1	**1**	1000	136.2	54.0	2.2	10.0		3.0	C1	15.0
	2		126.2				3.5		C1	15.0
	3		126.2				3.5		C2	15.0
	4		131.2					3.0	C3	18.0
	5		141.2					3.0	C4	8.0
	6		126.2					2.7	C5	1.8*

*1.8 g of C5 = 1.5 g pure C5 + 0.3 g LS2.

The negative pastes were prepared according to **section 3.5**, and the final amount of each component is showed in **Table 19**. After the preparation of the pastes, the negative plates were pasted (**section 3.6**) and cured (**section 3.7**). The positive plates were also prepared according to the same sections. However, as these positive plates were prepared according a standard procedure, and were not under study, their properties are not shown in this work.

4.1.3. Unformed negative plates characteristics

The BET SSA of the unformed negative plates was analyzed (**section 3.13.4**), and can be found in **Table 20**.
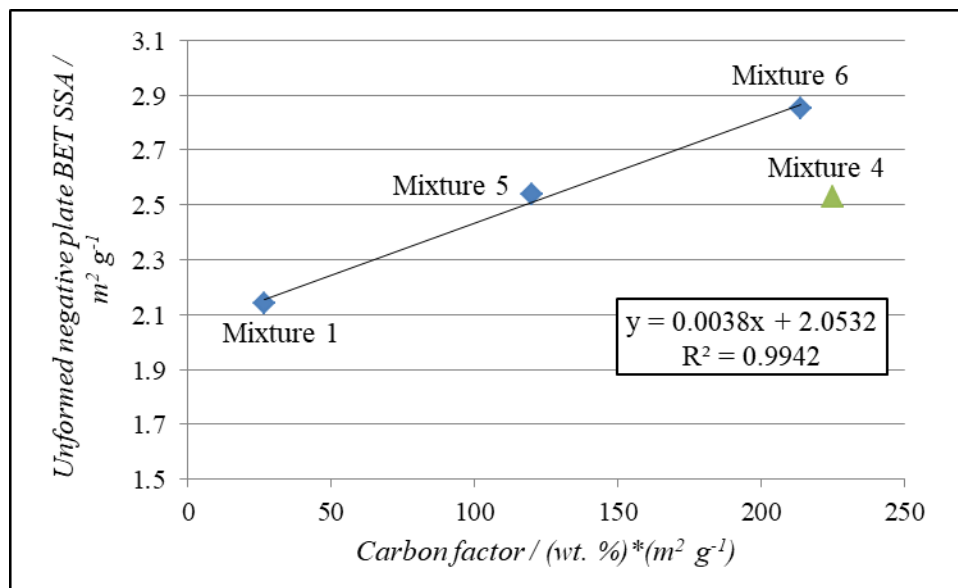
Table 20. Batch 1. BET SSA of the unformed negative plates.

Mixture	1	2	3	4	5	6
BET SSA / m^2 g^{-1}	2.14	2.71	2.36	2.53	2.54	2.85

This parameter depends on the type and concentration of LS and carbon material, both of them. The data showed us that LS1 mixtures have higher BET SSA than LS2 mixtures. Out of this batch of experiments, we prepared a mixture 7 with C1 (1.50%) and LS1 (0.30%). The BET SSA of the unformed negative plates made with mixture 7 was equal to 2.10 g m^{-2}. This value was very similar to mixture 1's value (2.12 g m^{-2}) and quite lower than mixture 2's value (2.71 g m^{-2}). These facts mean two arguments: sulfonation degree of the LS does not affect to the BET SSA of the unformed negative plates, but this value is highly affected by the LS concentration (an increase of 0.05% in LS concentration brought an increase of 0.61 g m^{-2} the BET SSA of the unformed negative plates). A higher LS concentration can improve the mixing process, making the paste more homogeneous and better distributed. This could lead to a more porous structure, as the porosity of the negative plates comes from the water molecules that have left the negative plated during the curing process. Better distribution of these water molecules would lead to a more porous structure, which was the case of LS1 mixtures. It is important to notice here that the porosity can be related to the BET SSA of the negative plates. More porous material would lead to a higher BET SSA. The highest BET SSA was found for mixture 6, and the lowest for mixture 1. Both mixtures contained the same LS at the same concentration (LS2 at 0.30 wt. %). Mixture 6 contained C5, the carbon material with the highest SSA, and the one that was expected to be located at the surface of the lead, in the energetic structure. In contrast, the lowest BET SSA was found for mixture 1, which contained C1, the carbon material with the lowest BET SSA (18 m^2 g^{-1}), and expected to be incorporated in the bulk of the lead skeleton. In an attempt for knowing the relation between the SSA of the carbon material and its concentration in NAM with the BET SSA of the unformed negative plates, a carbon factor (BET SSA of the carbon material*concentration of the carbon material in NAM) was calculated for the mixtures that contained LS2 at 0.30 wt. %. The BET SSA of the unformed negative plates was represented as a function of the carbon factor, for mixtures 1, 4, 5 and 6.

The graphic (**Figure 45**) showed a linear dependence for mixtures 1, 5 and 6. This relation can help us to suspect that the concentration of mixture 4 was not appropriated. Indeed, if we follow this dependence (regression line), and believe that at a limiting concentration of a carbon material the BET SSA does not increase anymore, for C3 maximum concentration would be 0.84 wt. %. This means that the BET SSA would remain at 2.53 m^2 g^{-1} even if the carbon material concentration higher than 0.84 wt. %. Furthermore, Doctor Detchko Pavlov et al. [39] proved that some graphites and carbons blacks reach a peak concentration: above

this concentration the BET SSA of the NAM does not increase, which would support our theory regarding the concentration of C3 in mixture 4.

Figure 45. Batch 1. Graphical representation of the carbon factor as a function of the BET SSA of the unformed negative plates for mixtures 1, 4, 5 and 6. The linear regression equation for mixtures 1, 5 and 6.

4.1.4.Internal resistance, capacity and CCA of the cells

After analyzing the unformed negative plates the cells were assembled (**section 3.8**) and formed (section 3.9). The first test done on them was the capacity test (**section 3.11.2**).

Results are shown in **Table 21**. This test was repeated twice, and it is better to focus on the results of the second capacity, as the cell capacity is increased due to the recharged of the cell after the first capacity. In the second capacity, no significant differences were found among the different mixtures. The capacity of the negative plate strongly depends on the nature of the organic expander and concentration. In this case, most of the samples contained the same LS, so this result was expected.

Table 21. Batch 1. Internal resistance of the cells after formation, results for the capacity tests and for the CCA test.

Mixture	Internal resistance / mΩ	Capacity tests	
		First Capacity / Ah	Second Capacity / Ah
1	11.55	0.79 ± 0.05	0.83 ± 0.06
2	14.85	0.79 ± 0.07	0.85 ± 0.04
3	15.25	0.81 ± 0.02	0.89 ± 0.02
4	13.82	0.75 ± 0.02	0.84 ± 0.02
5	12.32	0.79 ± 0.01	0.87 ± 0.01
6	13.30	0.78 ± 0.00	0.80 ± 0.02

During the CCA test (**section 3.11.3**) we expected to have better results for the mixtures containing LS2, due to the higher sulfonation degree of this one. However, we found the opposite results (**Figure 46**). These results could be linked to higher internal resistance of these mixtures (results in **Table 21**). For the rest of the mixtures, contained LS2 at the same concentration, the lowest SSA carbon material, C1, showed the best results. LS can be adsorbed on the carbon material. Higher SSA carbon materials would adsorb more amounts of LS, and prevent the LS role: suppress the formation of the $PbSO_4$ layer. In this way, it was logical to find the lowest discharge duration for the mixture 6 which contained the highest SSA carbon material (C5).
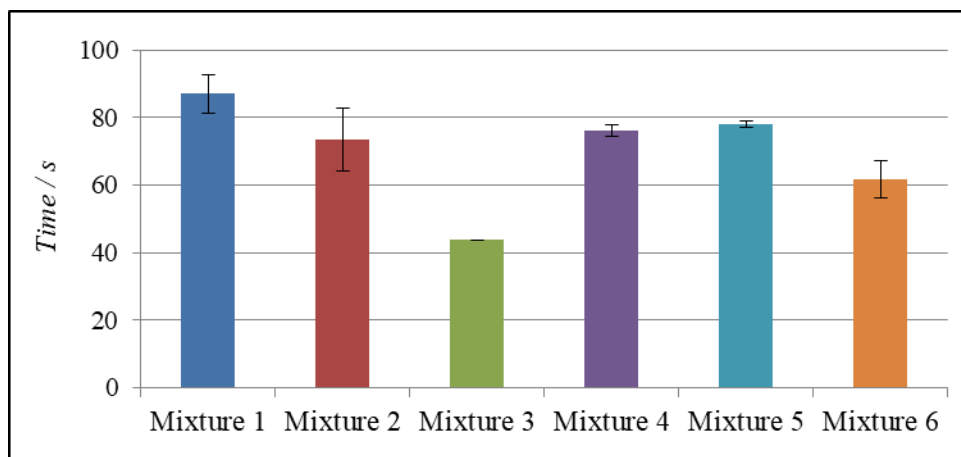

Figure 46. Batch 1. Results for the CCA test: time taken by the cell to reach 1 V during the discharge at 5 A and -18°C. Error bars related to the standard deviation of the measurements.

4.1.5. ICA test

The charge acceptance test (**section 3.11.4 type 1**) revealed that those mixtures with higher amount of LS, mixtures 2 and 3, showed a lower charge acceptance (**Figure 47**). This was linked to the fact that the charge Pb^{2+} reduction depends on the Pb^{2+} migration, which is impeded by the LS layer. Higher amount of LS led to thicker LS layers, and more hindrance of the Pb^{2+} migration, and therefore a lower Pb^{2+} reduction rate. For this reason, the charge acceptance of mixtures 2 and 3 was lower. For the LS2 mixtures, we found higher values for the charge acceptance but no differences among the mixtures. C1, C3 and C4 were supposed to be incorporated into the bulk of the NAM skeleton, increasing the conductivity of this one, and the Pb^{2+} reduction rate.

In the case of C5, its high charge acceptance, even at lower concentrations, was linked to the double-layer capacitance exhibited by this carbon, as the double-layer capacitance exhibits a linear correlation with the external surface area of the carbon that is added to the negative plate [36].
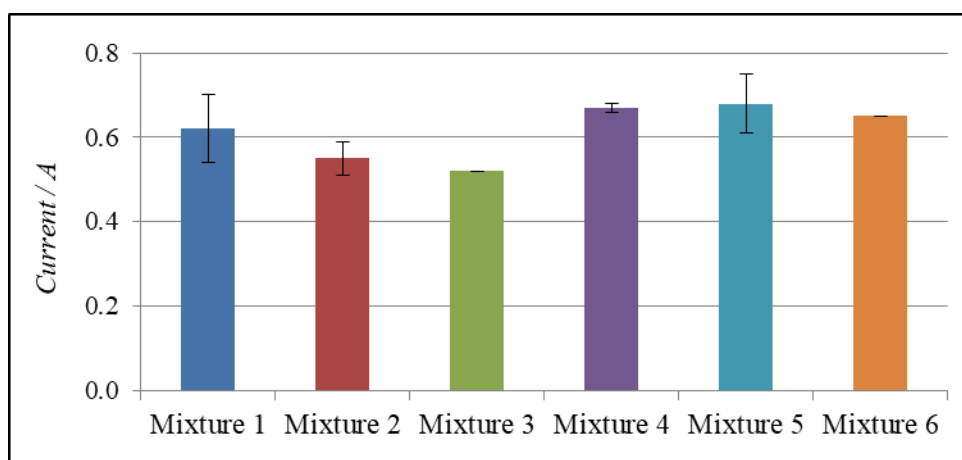
Figure 47. Batch 1. Results from ICA test. Current passing through the cell when it was charged at constant voltage (2.42 V). The data was taken at the 5th second. Error bars related to the standard deviation of the measurements.

4.1.6. Negative polarization test

During the negative polarization study, we evaluated the HER rate of the cells (**section 3.11.5**). The HER rate is directly proportional to the water consumption of the battery. Nowadays most of the batteries for the automotive industry are no maintenance batteries. This means that the battery is completely sealed, so it cannot be refilled with water. If a battery of this type has high water consumption, two things will happen: acid level will decrease and part of the plates will not be used for the energy conversion, and the acid concentration will increase. At high acid concentrations, the solubility of the lead sulfate crystals will decrease leading to an increase of the sulfation process rate, reducing the

capacity of the negative plates. For this reason, it is important to maintain the HER rate at a safe level. In the negative polarization study, different charges at constant current were applied to the cell, which was fully charged at the beginning of the test. When the cell was being charged, the current provided to the cell could be spent in two reactions:

$$PbSO_4 + H^+ + 2e^- \leftrightarrow Pb + HSO_4^- \text{ (R. 28)}$$

$$2H^+ + 2e^- \leftrightarrow H_2 \uparrow \text{(R. 29)}$$
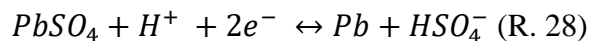
Reaction (R. 28) is related to the charge reaction of the negative plate. Even when the cell is fully charged some $PbSO_4$ can remain in the negative plate and being reduce. Reaction (R. 29) is HER. Protons from the electrolyte can be reduced on the lead surface, and the hydrogen is evolved, which is known as gassing. At low pH values, HER potential shows more positive values than the $Pb/PbSO_4$ potential. This means that HER reaction should prevail above $PbSO_4$ reduction reaction. However, the high overpotential of HER on lead reduces the rate of this reaction. Hydrogen overpotential (η_{H2}) during the negative polarization of a lead electrode in H_2SO_4 solution can be calculated as:

$$\eta_{H2} = E_i - E_0$$

Where, E_i is related to the potential of the electrode during the polarization test, and E_0 is equal to the equilibrium potential of the lead electrode in the H_2SO_4 solution.

According to Tafel, the hydrogen overpotential (η_{H2}) can be also calculated as a function of the current passing through the electrode during the polarization study:

$$\eta_{H2} = a + b \cdot \log (i_C)$$

In this way, η_{H2} is dependent on the constant a, which is directly linked to the nature of the surface where the reaction takes place. And b is known as the Tafel slope, which depends on the mechanism of the HER.

As a summary, higher η_{H2} indicates a lower HER rate due to the nature of the electrode and the mechanism of HER.

During our negative polarization studies (**section 3.11.5**) we applied different charges at constant currents to fully charged cells and measured the potential of the negative plate using a reference electrode (Ag/AgCl). Results are reported in **Figure 48**.
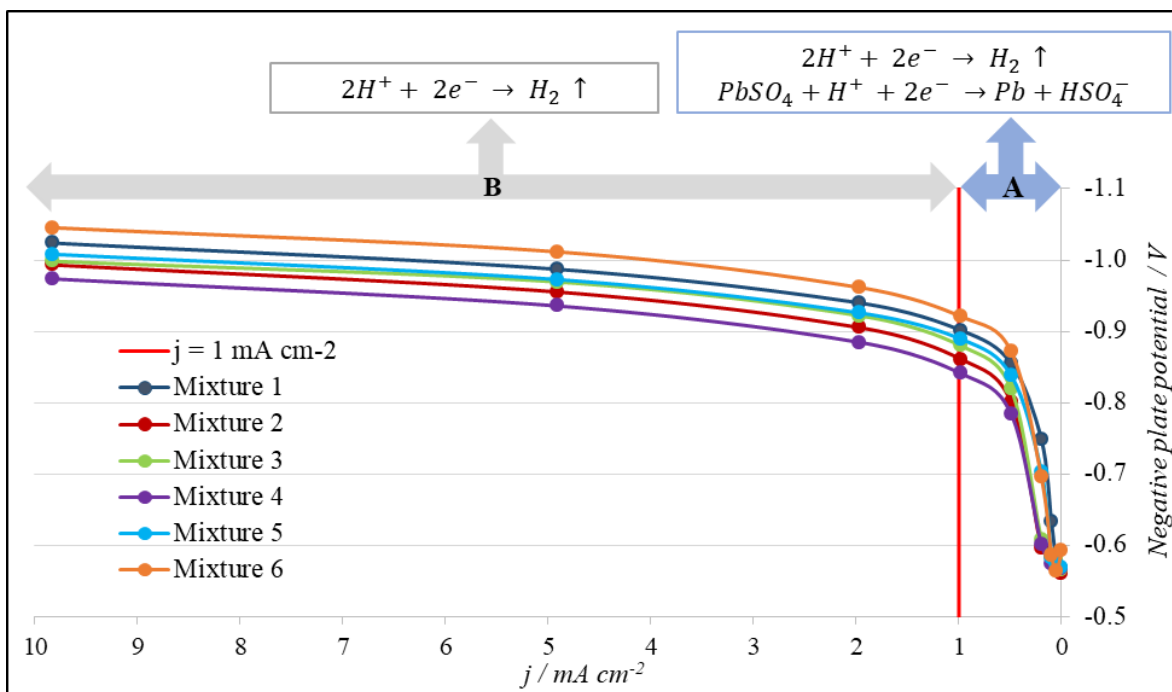
Figure 48. Batch 1. Negative polarization curves for mixtures 1 to 6. The negative plate potential was measured vs Ag/AgCl reference electrode.
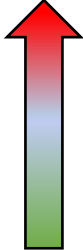
Focusing on the relation between the potential and the current density we can differentiate two zones in the graph:

- **Zone A:** when the cell was charged at current densities lower than 1 mA cm^{-2}, there was not a linear relationship between the potential and the current density. This indicated that two reactions were taken place at the same time, and at a similar rate: lead sulfate reduction (R. 28) and HER (R. 29)**.** These two reactions were competing for the current. Despite starting the test with a full charge cell, there were always some lead sulfate particles present in the negative plate which were susceptible to be reduced.

- **Zone B:** when the cell was charged at current densities higher than 1 mA cm^{-2}, there was a linear relationship between the potential and the current density. This indicated that there was a predominant reaction taking place at these current densities. In this case, as the percentage of lead sulfate in the negative plate was low, the predominant reaction at the negative plate was the HER (R. 29)**.** So we can assume that at current densities higher than 1 mA cm^{-2} the HER starts, and had the predominance at higher current densities as well.

Based on these statements, and in an attempt to quantify the rate of the HER, we established that the overpotential of the negative plate at j = 1 mA cm^{-2} can be directly related to the HER rate. The $\eta_{app, H2}$ for all the mixtures was calculated. Values are shown in **Table 22**.

Table 22. Batch 1. $\eta_{app,\,H2}$ for mixtures 1 to 6. Values are ordered from the lowest to the highest $\eta_{app,\,H2}$ (absolute value). Water consumption degree is also showed.

| Mixture	$\eta_{app\,H2}$ / V	Water consumption degree	
4	-0.274		Highest
2	-0.300		
3	-0.314		
5	-0.321		
6	-0.328		
1	-0.334		Lowest

Higher values of the $\eta_{app,\,H2}$ were related to a less ratio for HER, and lower water consumption of the cell. Mixture 4 showed the lowest $\eta_{app,\,H2}$, thereby the highest water consumption. This makes sense, according to the inappropriate carbon dosage, as was seen in the relation between the BET SSA of the unformed negative plates and the carbon factor of the mixtures. Carbon materials, as conductive particles, are able to catalyze the HER, i.e. protons are reduced on their surface. This problem is present when any kind of carbon material is added, and because of that it is necessary to add the right amount of carbon material that improves the LAB performance, but also keep at a safe degree the water consumption. After mixture 4, mixtures 2 and 3 (containing LS1) showed the lowest $\eta_{app,\,H2}$. Indicating that, the addition of LS1 increased water consumption. The rest of the samples that contained LS2, showed higher $\eta_{app,\,H2}$, being mixture 1 the one that showed the highest value. C1 and C4 were thought to be integrated inside the NAM skeleton. The results for mixtures 1 (C1) and 5 (C4) showed that when both carbon materials are integrated into the NAM skeleton, those with higher SSA catalyzed in a higher rate the HER. According to this argument, is logical that mixture 6 despite containing a low amount of C5 (0.15 wt. %), showed higher water consumption than mixture 1 that contained 1.50 wt. % of C1 (10 times more). On the one hand, C5 was carbon black with very high SSA, which made it more susceptible to catalyze the HER. On the other hand, C5 was thought to be located at the energetic structure of the NAM, i.e. in direct contact with the electrolyte. In this way protons had fewer restrictions to reach this carbon material and to be reduced on its surface.

4.1.7. Cycles at PSoC type 1

Afterwards, the PSoC cycles type 1 (**section 3.11.6**) were performed. The results are showed in **Figure 49.**
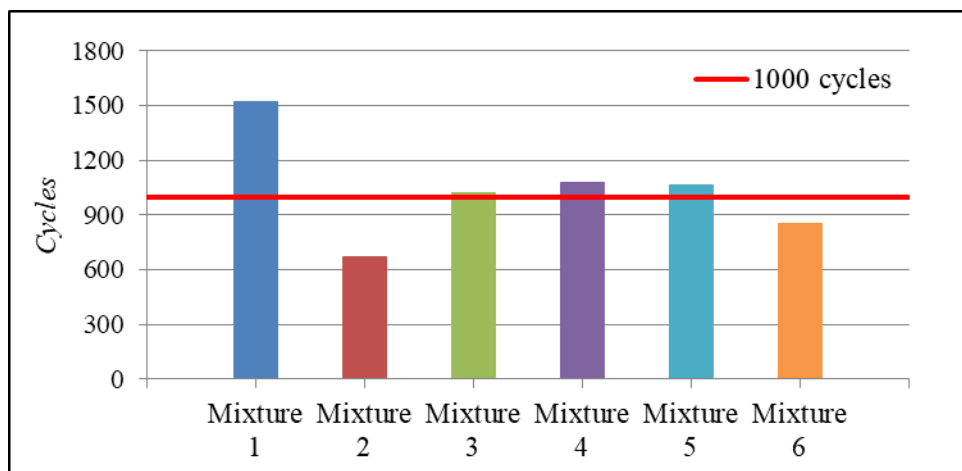
Figure 49. Batch 1. Results for the PSoC cycles type 1. Results: 1525 (1), 673 (2), 1020 (3), 1080 (4), 1065 (5), 857 (6).

The worst results were for the mixtures 2 and 6 that did not reach the 1000 cycles. For the LS1 mixtures, mixture 2 performed a lower number of cycles than mixture 3. The test was stopped at 1000 cycles for mixture 3, although the performance was good. These mixtures showed similar results in all the tests, despite the CCA test, where mixture 2 behaved better. It is thought that better performance of the organic expander during the discharge means a worse performance during the recharge. For mixture 2, the combination of LS1 and C1 lead to a good CCA performance but a bad cycle life. In addition, C2 contained in mixture 3 was more conductive than C1 (from mixture 2). This higher conductivity helped to improve the cycle life, as it made easier the recharge of the negative plate during cycles: when the lead sulfate content is high in the negative plate, the carbon material plays a key role as it can conduct the current and increase the Pb^{2+} reduction rate. Mixture 1 shows the best result (1525 cycles) indicating a good combination of LS2 and C1. In addition, it revealed that the incorporation of C1 in the NAM skeleton increased the cycle life, by improving the Pb^{2+} reduction rate, resulting in the formation of low size $PbSO_4$ crystals with high solubility. Furthermore mixtures 4 and 5 also fulfilled more than 1000 cycles. In the case of mixture 4 (1080 cycles), a better result was expected, due to the good results obtained for mixture 4 during the CCA and the charge acceptance test. As was explained before, C3 in mixture 4 was overloaded. Several studies showed that carbon materials such as activated carbons, carbons blacks and flake graphite have an optimum dosage for providing beneficial effects on the HRPSoC cycle life of LABs. When this dosage is exceeded the HRPSoC cycle life drops [39]. As C3 was a mixture of graphite and carbon black, it could so also this behavior, and because of being added at higher dosages than needed, it did not increase the PSoC cycle life as good as expected. Mixture 5 did not show the best result, but fulfilled the 1000 cycles, and could be a good candidate at that dosage as an additive for the negative plates of LAB. Finally, mixture 6 did not reach more than 850 cycles. Clearly, the contribution of C5 to the performance of the negative plates was not

good enough. It was mentioned before that the LS can be adsorbed on the carbon surface. In the case of C5 this was the carbon with the highest BET SSA, so part of the LS could have been adsorbed on their surface, impeding the prevention of the passivation layer, resulting in a bad performance during the cycle life test. In addition, this carbon material was thought to be located at the energetic structure of NAM due to its low particle size and low concentration in NAM. When lead sulfate covers these particles during the discharge a passivation phenomenon occurs: no more electrolytes reach these carbon particles and big lead sulfate crystals are created on the surface, impeding the beneficial effect of these types of carbon materials. As all the mixtures that contained the carbon material integrated in the lead skeleton showed better results than the one that contained the carbon material on the energetic structure of NAM (mixture 6) we can conclude that the integration of the carbon material in the lead skeleton led to an improvement in the PSoC cycle life of the cells.

It is important to take into consideration here that not all the carbon materials that are located inside the NAM skeleton improve the cycle life in the same way. Carbon materials can improve the cycle life in two ways:

I)   Improving the electrical conductivity of the NAM skeleton, and thus the electrochemical reactions. This behavior is expected for high conductive active materials.

II)   Acting as electro-osmotic pumps inside the NAM skeleton: the pores of the carbon materials are filled or emptied by H^+ and SO_4^{2-} ions during charge and discharge reactions.

After this explanation, C1 and C2 would increase the NAM skeleton conductivity, while C4 would increase the electro-osmotic pump effect. In the case of C3, as it was a hybrid carbon material made of carbon black and graphite, it would improve the cycle life by the two mechanisms.

4.1.8. Negative plates properties after the cycles at PSoC types 1

In order to confirm the failure mode of the cells, the cycled negative plates were removed from the cell, washed and dried (**section 0**), and the lead sulfate and carbon content were analyzed (**section 3.13.2**) as well as, the SEM micrographs were obtained (**section 3.13.6**), for LS2 mixtures.

The data confirmed that the failure mode was the sulfation of the negative plates (see **Table 23**). For the mixtures with micrometer size carbon materials (mixtures 1, 4 and 5) it was only needed around 30% of lead sulfate content to fail in the PSoC cycles. This amount can collapse the active sites located at the NAM skeleton for the Pb^{2+} reduction. In the case of mixture 6, the lead sulfate concentration was higher than 60%, i.e. when the carbon material was at the energetic surface of the NAM, the carbon material was covered by lead sulfate crystals creating a passivation phenomenon. The crystal growth was uncontrolled,

126

and the cell failed once the whole surface was covered by the crystals. The carbon content was consistent with the initial amount of carbon in the negative plate which was the sum of the carbon material and lignosulfonate dosage. It can be confirmed that the carbon material was not degraded during the PSoC cycle life test.

Table 23. Batch 1. Results for the PSoC cycles type 1. Carbon and lead sulfate content of the cycled negative plates.

Mixture	Cycles	Carbon content / wt. %*	PbSO$_4$ content / wt. %*
1	1525	1.58	26.0
2	673	**	**
3	1020	**	**
4	1080	1.80	30.2
5	1065	0.95	32.7
6	857	0.41	66.8

*Weighted percentage related to the total NAM mass. **Data were not available.

SEM micrographs (**Figure 50**) were taken for mixture 6 formed negative plates (**Figure 50. a, b**) and cycled negative plates (**Figure 50. c, d**). It can be appreciated how the negative plate has changed from formed to unformed conditions. When the negative plate was formed, small lead particles were found interconnected one to another, creating a multifold structure. These particles were part of the energetic structure and were supported by the lead skeleton. In the case of the cycled negative plates, we found what expected: big lead sulfates particles that impaired the PSoC cycle life test. These particles collapsed the entrance of acid sulfuric to the inner structure. In addition, at this lead sulfate concentration (66.8%) a great part of the lead skeleton has become sulfated and no hint of the lead skeleton can be seen in the micrograph. In contrast, for the cycled negative plates of the mixture 4 (**Figure 50. e, f**), we did not find any lead skeleton either, but the lead sulfate crystals were much more well-shaped and small in comparison to mixture 6. This was consistent to the lead sulfate concentration found for this plate (30.2%), corroborating the following theory: when the carbon material is integrated into the lead skeleton it can reduce the sulfation of the negative plate by controlling the crystal size of the lead sulfate, and leading to a longer PSoC cycle life.
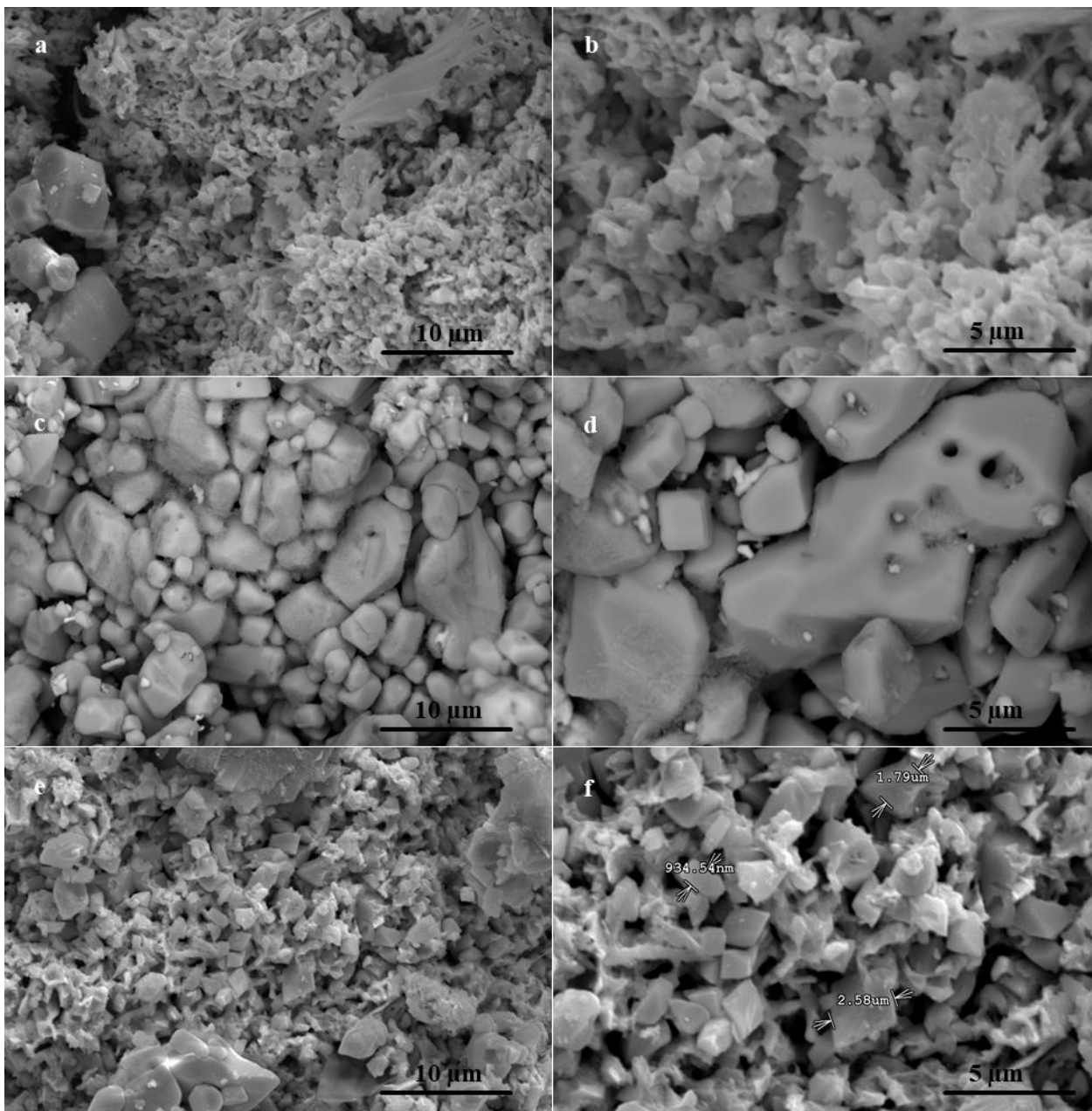
Figure 50. Batch 1. SEM micrographs. Mixture 6: formed negative plates (a, b) and cycled negative plates (847 cycles) (c, d). Mixture 4: cycled negative plates (e, f) (1080 cycles). Magnification: 3000x and 6000x.

The XRD analyses (**according to section 3.13.5**) of unformed, formed and cycled negative plates from mixtures 4 and 6 are showed in **Figure 51**. We analyzed different compounds at the three stages of the negative plates:

- Carbon diffraction peak (002): $2\theta = 26.50°$ (**Figure 51. a, d, g**) [84,85]. This peak was analyzed in order to confirm the presence of graphitic carbon materials. In this case, we

only expected high intensity of this peak for mixture 4 due to containing C3 (mix of graphite and carbon black). In the case of mixture 6, it contained a carbon black (C5), so a peak at 26.50° was not expected; carbons blacks do not have any graphitic structure. However, this peak was also high for mixture 6 in the case of the unformed negative plates. Why? During the mixing process another reaction can take place:

$$10Pb(OH)_2 + 6CO_2 \rightarrow PbO \cdot 6PbCO_3 \cdot 3Pb(OH)_2 + 7H_2O \text{ (R. 34)}$$
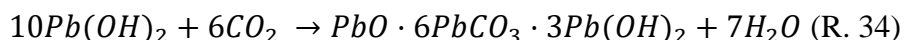
This reaction (R. 34) occurs when there is enough CO_2 in the mixer atmosphere and is called carbonization of the paste, and as a result, lead hydrocarbonate or hydrocerussite ($2PbCO_3 \cdot Pb(OH)_2$) is formed as part of $PbO \cdot 6PbCO_3 \cdot 3Pb(OH)_2$. In our case, not having any kind of vacuum system in the mixer favored the presence of CO_2 in direct contact with the paste, and thus the carbonization reaction [8]. Hydrocerussite shows different diffraction peaks, and we have focused on two: peak 1 / at 27.10° (015) and peak 2 / at 34.16° (110) [8]. Peak 1 can interfere with the carbon peak at 26.50° (**Figure 51. a)**. In order to prove this theory we analyzed also peak 2 (**Figure 51. c**) and saw the same tendency for both peaks. As conclusion, hydrocerussite was found in the unformed negative plates because of the carbonization of the paste. So, carbon peak at 26.50° for the unformed negative plates could not be representative, neither linked, to the graphitic carbon content.

Hydrocerussite was not found in the formed or in the cycled negative plates (**Figure 51. f, i**). During the soaking process the lead hydrocarbonate from the unformed negative plates reacted with the sulfuric acid and CO_2 gas was released [8]. **Figure 51. d** shows the carbon peak at 26.50° for the formed negative plates. In this case, this peak can be directly linked to the graphitic carbon content. As it is, the intensity for mixture 6 was almost zero, and for mixture 4 almost 200 cps, due to the graphitic nature of C4. The shape of this peak (carbon peak at 26.50°) was maintained in the cycled negative plates (**Figure 51. g**). These results corroborated the release of CO_2 gas was during the soaking process.

- Lead sulfate diffraction peak (021): $2\theta = 26.70°$. Lead sulfate was not found in the unformed negative plates (**Figure 51. a)** as main of the lead sulfate was part of the basic lead sulfates, in this case 3BS. In the formed plates (**Figure 51. d**) more lead sulfate was found for mixture 4 than for mixture 6, indicating that addition of C5 in mixture 6 improved the formation process. However, as in concordance with the lead sulfate content of the cycled plates (**Table 23**), and also the SEM micrographs (**Figure 50. c to f**), the lead sulfate peak was higher for mixture 6 than for mixtures 4 (**Figure 51. g).**

- Lead diffraction peak (111): $2\theta = 31.27°$. Lead content in the unformed negative plates (**Figure 51. b)** was directly linked to the curing process efficiency. During the curing

process the remaining unoxidized lead from the paste is oxidized to PbO at certain temperature and relative humidity conditions. As we can see in **Figure 51. b,** the same lead content was found for mixtures 4 and 6, so the same efficiency of the curing process. The lead content of the formed negative plates (**Figure 51. e)** was directly linked to the formation process efficiency. In this case, mixture 6 showed higher intensity lead peak, and therefore a higher formation process efficiency, as was seen also in the lead sulfate peak of the formed negative plates (**Figure 51. d)**. Finally, the lead peak for the cycled negative plates (**Figure 51. h)** was also in concordance with the lead sulfate peak of these cycled negative plates **(Figure 51. g):** higher lead sulfate content led to lower lead content, and vice versa. In this case, mixture 4, due to containing less amount of lead sulfate in the cycled negative plates, showed a higher lead peak.
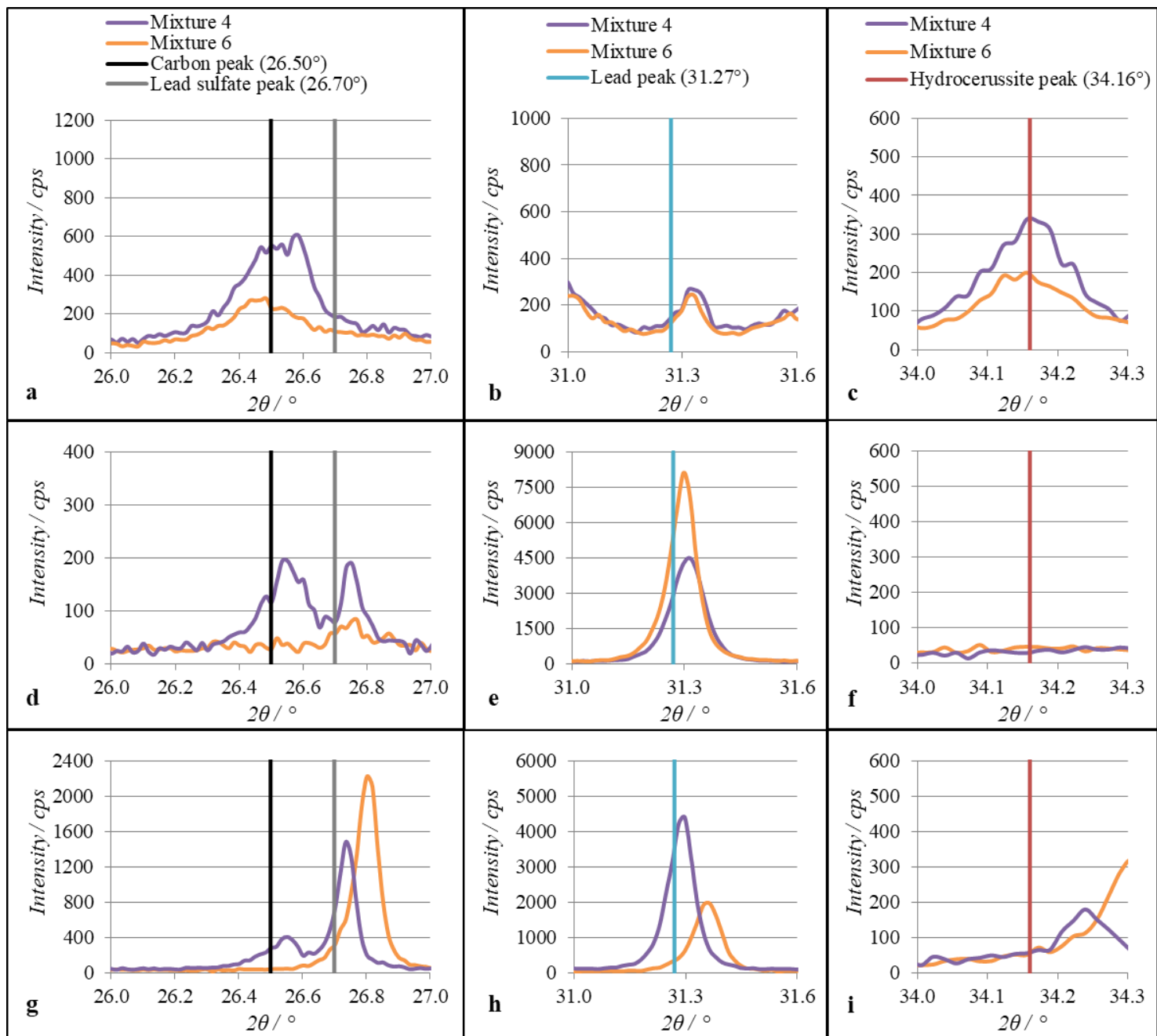
**Figure 51. Batch 1.** XRD patterns for negative plates of mixtures 4 and 6 in different states. **(a, b, c):** Unformed plates (after curing). **(d, e, f):** Formed plates (after cell formation process). **(g, h, i)**: Cycled plates (after cycling at PSoC). Represented diffraction peaks: Carbon (002): $2\theta = 26.50°$. $PbSO_4$ (021): $2\theta = 26.70°$. Pb (111): $2\theta = 31.27°$. Hydrocerussite (110): $2\theta = 34.16°$.

4.2. Research on the use of GANFg dispersed with LS as additives for the negative plates of LABs for Micro HEV

4.2.1. Aim of the study

After checking the well performance of the method for analyzing the influence of different carbon materials and OEs on the negative plate performance, we continued studying different types of carbon materials. In this case, for batch 2 we focused on nanocarbon materials.

For this batch, we chose graphitized carbon nanofibers (GANFg), a nanocarbon material supplied by the company Grupo Antolin [78]. The main attractive of these fibers was their high aspect ratio, as well as their low electrical resistivity ($1 \cdot 10^{-4}$ Ohm m). They had a diameter between 20 – 80 nm, and a maximum length of 30 µm. With this high aspect ratio they would be able to form an interconnected network inside the NAM. The main purpose of the whole batch was to know the optimum GANFg concentration, i.e. the concentration of GANFg needed to increase the cycle life of the LAB without increasing the HER rate. In addition, a new challenge came together with the addition of GANFg to the NAM: these fibers tend to be agglomerated together, as can be seen in **Figure 52**.
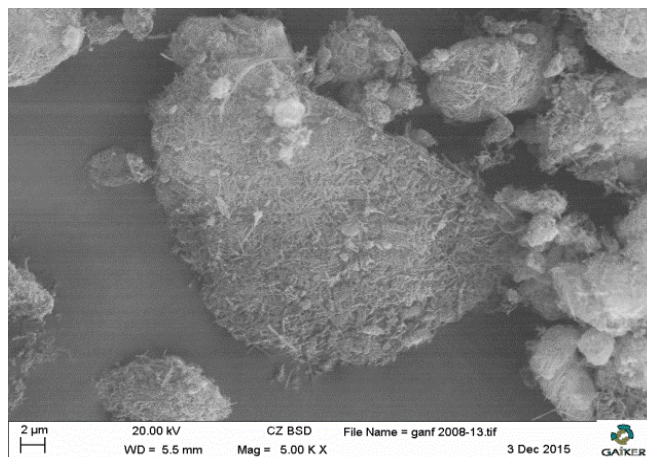
Figure 52. SEM micrograph of GANFg without any dispersant pretreatment. Analysis done by GAIKER.

Once GANFg are not able to be separated and spread through the negative plate, the conductive network will not be formed and the addition of GANFg to the NAM would be in vain. For this reason, it was needed to disperse the GANFg before adding them to the negative paste.

To sum up, the main targets of this batch was to find a way to disperse the GANFg in order to have them in a single way inside the NAM, and to know the optimum GANFg concentration that increased the cycle life keeping in a safe level the water consumption.

The whole study was summarized in the article "Graphitized Carbon Nanofibers: new additive for the Negative Active Material of Lead Acid Batteries" [77] located in the **annex ii.**

4.2.2. GANFg characteristics

GANFg were graphitized CNF where the walls were made of helical ribbons of graphene forming a spiral that ended in a tube. The hollow cores had a diameter between 20 – 60 nm, while the outside diameter can go from 40 to 140 nm. **Figure 53** shows a helical ribbon CNF, also called stacked-cup CNF. It can be appreciated how the graphene layer that comprised the whole fiber, came out of the fiber. The length of this fiber was exactly the same as the wall thickness of the CNF. CNF wall was made of stacks of graphene layers, which meant that π electrons from the p orbitals of the carbon atoms were completely delocalized along the whole fiber, conferring high electrical conductivity to this compound [86]. These fibers were industrially produced by catalytic Chemical Vapor Deposition (CVD) in the presence of a sulfur source, methane as the main carbon feedstock and a floating catalyst system, where the catalyst was made of Nickel at temperatures above 1100 °C [86].
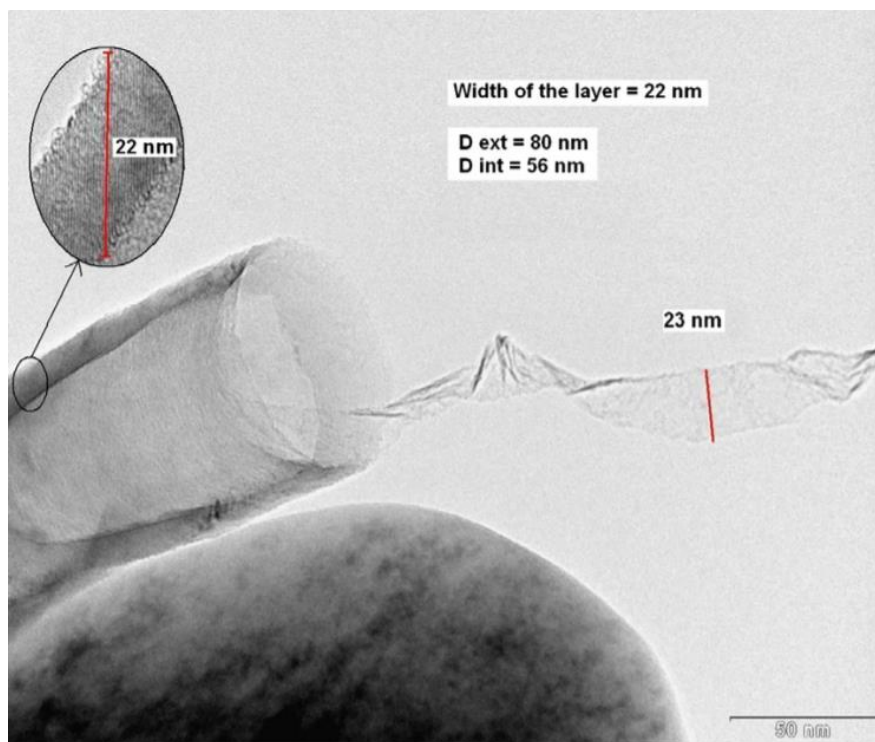
Figure 53. TEM image of a CNF from Grupo Antolin [86].

These fibers suffered a graphitization process at a temperature higher than 2500 °C in helium atmosphere which underwent the disappearance of most to the catalyst and the elimination of the CNF functionalities. In addition, the graphitization process also provoked

a change in the morphology of the fibers; it changed from circular to faceted polygonal cross section as can be seen in **Figure 54**. The carbon atoms were organized in an AB stacking structure, characteristic of graphite, after the graphitization process [87]. For the application of the GANFg as an additive for the NAM the graphitization process played an important role: this process reduced the Nickel content, and Nickel cannot be present in the NAM as it catalyzes the HER [70]. The final Ni concentration in GANFg was < 20 ppm; low enough for not increasing the HER rate substantially.
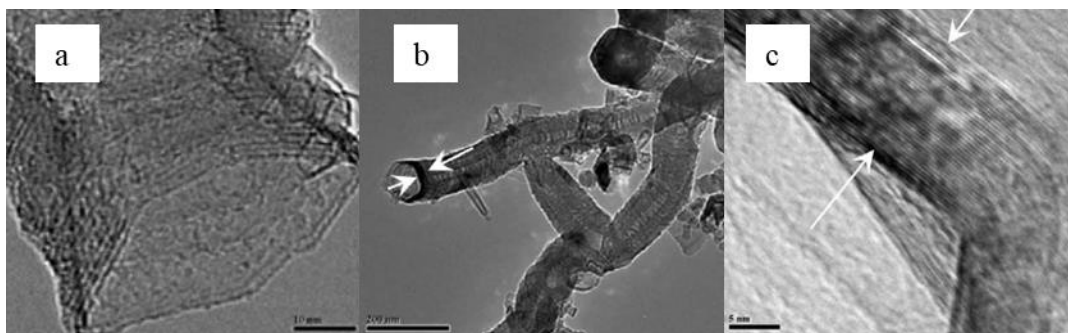
Figure 54. GANFg. Helical ribbon CNF from the Grupo Antolin after suffering a graphitization process at temperatures higher than 2400°C.

Table 24 summarized the properties of the GANFg used during this whole batch, as well as in Batch 3 and 4.

Table 24. Physicochemical characteristics of GANFg.

Physicochemical characteristic	Unit	Value
Fiber diameter	nm	20 – 80
Fiber length	μm	Up to 30
Bulk density	g cm^{-3}	1.9 – 2.0
Apparent density	g cm^{-3}	0.008 – 0.060
Solid percentage	%	>98
SSA	m^2 g^{-1}	105 - 115
Particle diameter	μm	0.005 – 0.200

GANFg will be located at the NAM skeleton, due to having micrometric size. As was explained before, those carbon materials out of the nanoscale are integrated into the lead skeleton during the formation process, acting as lead nucleating agents. Lead is formed on their surface until covering the whole surface and forming the NAM skeleton, which supports the NAM energetic structure throughout the whole plate. In this way, the resultant NAM skeleton will be more electrically conductive, and robust, as the GANFg network will serve as a support for the lead, and bring some stability to the NAM skeleton during the charge discharge reactions. Moreover, because of increasing the overall conductivity of

the NAM, the current is better distributed throughout the negative plates, reaching more active sites, and enhancing the Pb^{2+} reduction, therefore avoiding the sulfation of the negative plate and enhancing the cycle life of the negative plates. Based on all the theoretical advantages of GANFg addition, a set of mixtures was thought and tested during this batch of experiments.

4.2.3. Mixtures composition and GANFg dispersions

The first step of this batch was the design of the experiments. As we wanted to know the optimum concentration of GANFg, 4 mixtures listed in **Table 25** were prepared.

Table 25. Batch 2. Composition of the mixtures.

Mixture	GANFg / wt.%	OE1 / wt.%
NAM Control	0.00	0.30
S5	0.50	0.30
S6	0.20	0.30
S7	0.10	0.30

NAM Control mixture was used as a blank mixture for this batch. The only variable between the mixtures was the concentration of GANFg.
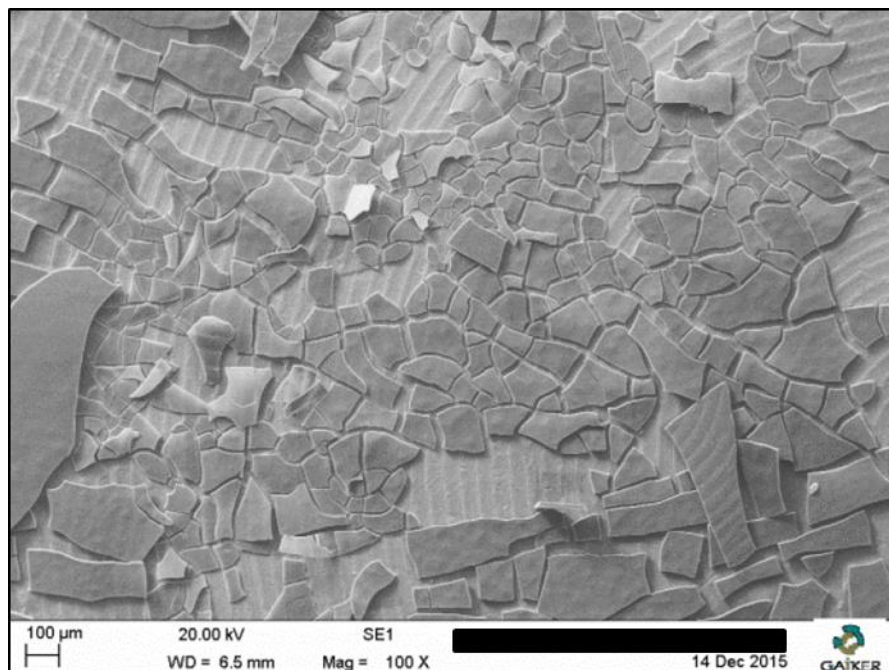
Figure 55. Batch 2. OE1 solution in the microscope. SEM micrograph taken by GAIKER.

The second step was the dispersion of the GANFg in water for having single fibers inside the NAM. In this way they could be homogeneously distributed along the negative plate. As one of the components of the negative paste was an active polymer, in this case the lignosulfonate OE1 (called LS2 for batch 1), we took advantage of the situation and dispersed the GANFg in water using this compound. GAIKER provided data from a dry solution of OE1 in order to see its aspect in the microscope (**Figure 55**).

This mother dispersion (called S4) contained: Water (100 g) + OE1 (7.5 g) + GANFg (12.5 g). The mother dispersion was diluted for preparing mixtures S5, S6 and S7. The composition of the final dispersions can be seen in **Table 27**. GAIKER provided data about the aspect, stability and particle size of the dispersions. **Figure 56** shows the SEM micrographs of dispersions S4, S5, S6 and S7. OE1 was covered by GANFg; in the case of higher GANFg concentrations, e.g. S4, the OE1 structures were not even well differentiated. The ratio GANFg / OE1 was 1.67, maintained for all the dispersions. The structure of OE1 can be well appreciated in **Figure 56.d.** The most important point was that the fibers were not agglomerated, so these dispersions were suitable for being used in the paste preparation.
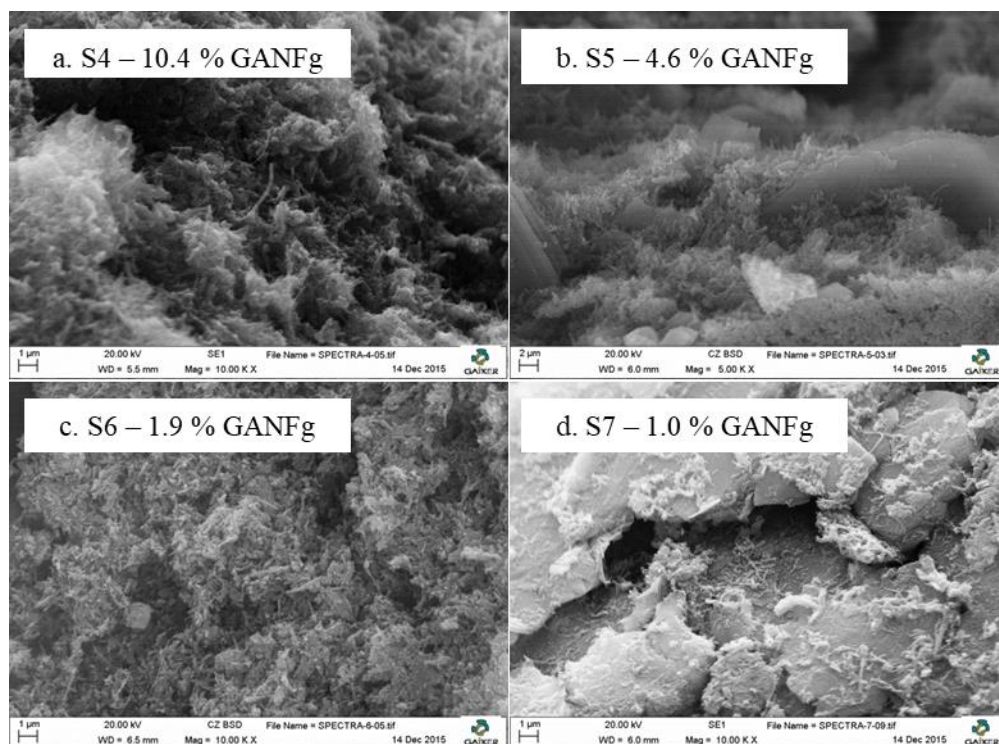
Figure 56. Batch 2. GANFg + OE1 dispersions SEM micrographs. **a.** S4. **b.** S5. **c.** S6. **d.** S7. GANFg percentage of each dispersion indicated in the figure. SEM micrographs taken by GAIKER.

The zeta potentials of the different dispersions were provided by GAIKER and are showed in **Table 26**. Zeta potentials higher than ± 20 mV indicate high stability of the dispersion. So we can conclude that the dispersions were stable.

Table 26. Batch 2. GANFg + OE1 dispersions: composition and zeta potential.

Sample	H2O: OE1:GANFg / g	Zeta Potential / mV
S4	100:7.5:12.5	-33.65 ± 3.56
S5	100:3.0:5.0	-38.67 ± 3.01
S6	100:1.2:2.0	-37.33 ± 1.83
S7	100:0.6:1.0	-52.56 ± 2.58

Once the dispersions were prepared and characterized, they were used for preparing the pastes. The pastes were prepared according to **section 3.5**, and the final amount of each component is showed in **Table 27**.

Table 27. Batch 2. Composition of the dispersions and negative mixtures.

Mixture		Dispersion / g			Components added during the mixing process / g					
Batch	Name	H$_2$O	GANFg	OE1	LO	H$_2$O	H$_2$SO$_4$*	PAC Fiber	BaSO$_4$	OE1
2	**NAM Control**				1000	116.2	54.0	2.2	10.0	3.0
	S5	100	5.0	3.0		15.0				0.0
	S6	100	2.0	1.2		15.0				1.8
	S7	100	1.0	0.6		12.0				2.4

*Acid density equal to 1.4 g cm^{-3}.

Notice in **Table 27** that the final amount of OE1 in all the mixture was equal to 3.0 g in order to have a final OE1 concentration of 0.30 wt. % (related to the LO mass).

4.2.4. Negative pastes and negative unformed plates characteristics

After preparing the pastes, the density of the pastes was measured. Results are showed in **Table 28**.

Table 28. Batch 2. Density of the pastes and carbon content, median pore diameter, porosity, apparent density and BET SSA of the unformed negative plates.

Mixture	Paste density / g cm^{-3}	Unformed negative plates				
		Carbon content / wt. %	Median pore diameter / μm	Porosity / %	Apparent density / g cm^{-3}	BET SSA / m^2 g^{-1}
NAM Control	4.63	0.60	0.18	41.10	4.63	*
S5	4.62	1.60	0.13	32.00	5.09	1.82
S6	4.64	1.40	0.15	32.20	5.10	1.57
S7	4.63	0.80	0.18	39.50	4.77	2.00

*Data not available.

No significant differences were found among the density values, meaning that the addition of GANFg did not cause effects on the rheology of the pastes. Once the density measurements were done, the negative plates were pasted (**section 3.6**) and cured (**section 3.7**). The positive plates were also prepared according to the same sections. However, as these plates were prepared according a standard procedure, and were not under study, their properties are not shown in this work.

The carbon content of the negative unformed plates was analyzed (according to **section 3.13.2**). Results are showed in **Table 28**. Results showed higher carbon amount than expected, as the only components that brought carbon to the mixtures were GANFg and LS, so a maximum amount around 0.90 wt. % should have been found in S5, in contrast to the result 1.60 wt. %. Similar facts happened for the rest of the mixtures, even for the NAM Control. This fact also happened for the unformed negative plates of the batch 1 (**section 4.1.3**). As was explained in that section (**4.1**) during the mixing process the carbon dioxide from the air can react with the lead hydroxide ($Pb(OH)_2$), forming which is known as Hydrocerussite ($2PbCO_3 \cdot 1PbO(OH)_2$), that can be found in the NAM as part of the lead Hydrocarbonate ($PbO \cdot 6PbCO_3 \cdot 3PbO(OH)_2$). This compound can be also detected by XRD, at the surroundings of 26.5° (2θ), where the carbon diffraction peak is located. This means that Hydrocerussite diffraction peak could be interfering with the carbon diffraction peak, masking the real result of the carbon peak. For corroborating this hypothesis, the XRD analyses of the unformed negative plates were done (according to **section 3.13.5**). **Figure 57** shows the XRD patterns for the unformed negative plates of batch 2. As expected, all the negative plates were made mainly of PbO, $PbSO_4$, 3BS and Pb. The carbon diffraction peak at 26.50° (2θ) had the same shape as the hydrocerussite diffraction peak 34.16° (2θ), confirming that hydrocerussite was present in the negative plates, and its peak at 27.1° (2θ) interfered the carbon diffraction peak.
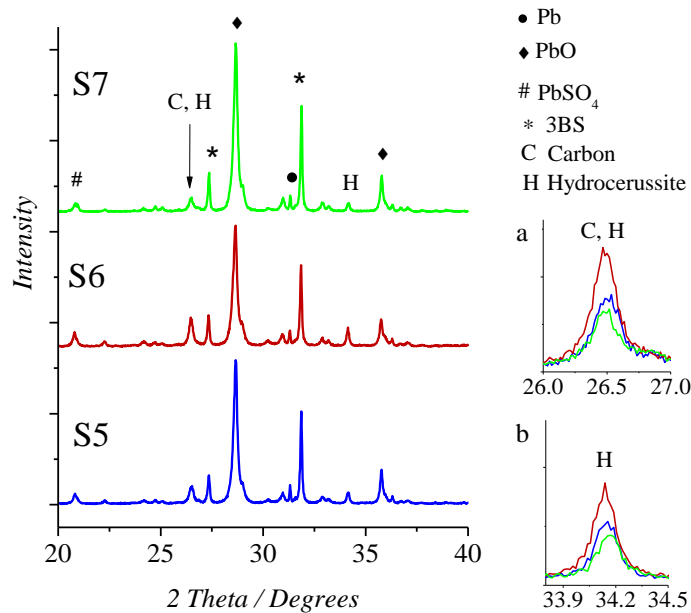
Figure 57. Batch 2. XRD patterns for the unformed negative plates for mixtures S5, S6 and S7. **a.** Zoom for the carbon (family of planes: 002) and Hydrocerussite (family of planes: 104) diffraction peaks around $2\theta = 25.6°$. **b.** Zoom for the Hydrocerussite (family of planes: 110) diffraction peak at $2\theta = 34.16°$.

Table 28 also shows the median pore diameter, porosity and apparent density of the unformed negative plates. These properties were analyzed following the porosity measurements procedure (**section 0**). Higher addition of GANFg led to lower pore diameter, and when GANFg were added at 0.10 wt. % the pore diameter was not affected. However, the differences were not very high, so these results can be considered as a change in the tendency of this property when GANFg were added. The porosity values of the unformed negative plates were in line with the median pore diameter: lower median pore diameter led to lower porosity, and again, addition of GANFg at 0.10 wt. % did not cause a reduction in the porosity of the unformed negative plates. However, in the case of the mixtures S5 and S6, with higher GANFg content, the porosity of the unformed negative plates was significantly reduced. Apparent density values were also similar for mixtures NAM control and S7, but higher for S5 and S6. Apparent density, or bulk density, was calculated as the amount of active material divided the volume occupied by the sample, including the voids inside the active material. Higher apparent densities meant a reduction in the total volume due to smaller pores present in the active material. And because of this, mixtures S5 and S6 showed lower apparent density values. The BET SSA of the unformed negative plates for the GANFg mixtures also appears in **Table 28**. The data shows higher BET SSA for the mixture S7, which also had the highest porosity among the GANFg mixtures. On the contrary, S5 showed higher BET SSA than S6, although both of these mixtures had similar porosity. Higher GANFg concentration led to lower medium pore

139

diameter, but to a higher amount of pores, and because of that the BET SSA of mixture S5 was higher than the one for mixture S6. If we compare these results to the batch 1 results (**Table 20**) we can conclude that addition of batch 1 carbon materials, due to having higher SSA than GANFg (in some cases) and being added at higher concentrations, led to higher BET SSA for the unformed negative plates.

4.2.5. Formed negative plates characteristics

After analyzing the unformed negative plates the 2 V / 1 Ah cells were assembled (**section 3.8**) and formed (**section 3.9**). After the formation of the cells, the negative plates from two cells per type were taken out of the cells, washed and analyzed (**section 0**). Carbon content and lead sulfate content were analyzed (**section 3.13.2**), as BET SSA (**section 3.13.4**) of the formed negative plates. Results are showed in **Table 29**. Carbon content values were lower after formation of the cells, in comparison with the unformed negative plates values (**Table 28**). These results confirmed the reaction between Hydrocerussite and sulfuric acid during the soaking process whereby CO_2 was released. In this way, the carbon content of the formed negative plates was consistent with the real amount of carbon added during the pasting process. The lead sulfate content was directly linked to the formation process efficiency. According to the results, addition of GANFg at concentrations higher than 0.10 wt. % led to a higher formation process efficiency. S5 showed the lowest lead sulfate content, i.e. the more amount of PbO, $PbSO_4$ and 3BS from the unformed negative plates of this mixture were converted to lead. The BET SSA of the formed negative plates supported the lead sulfate results: higher BET SSA meant that more and smaller lead particles have been formed at the energetic structure of the NAM, and thus less amount of lead sulfate should be found in these plates. S5 showed the highest BET SSA, followed by S6, so we can conclude that addition of GANFg at dosages higher than 0.10 wt. % improved the formation process efficiency and the BET SSA of the formed negative plates. When GANFg were added at 0.10 wt. % the formation process efficiency was not improved, either the BET SSA of the formed negative plates. During the formation process the NAM skeleton was formed, and GANFg were supposed to be part of this skeleton, as these single fibers had a length in the order of microns. Once the NAM skeleton was formed, the GANFg were integrated inside it. Luckily GANFg would be able to form an interconnected network inside the NAM skeleton, and conferring to this one beneficial mechanical and conductive properties. GANFg inside the NAM skeleton could provide more active sites where the lead sulfate was reduced to lead; this mechanism led to the formation of smaller lead crystals and higher BET SSA.

Table 29. Batch 2. Physicochemical properties of the formed negative plates: carbon content, lead sulfate content and BET SSA.

Mixture	Formed negative plates		
	Carbon content / wt. %*	PbSO$_4$ content / wt. %*	BET SSA / m^2 g^{-1}
NAM Control	0.36	4.80	0.66
S5	0.90	1.70	0.96
S6	0.48	4.00	0.80
S7	0.35	4.90	0.73

*Weighted percentage related to the total NAM mass.

4.2.6. Capacity test

After the formation, the first test done on the cells was the capacity test (**section 3.11.2**). This test was repeated twice. The second value was taken as reliable, as it was done after the first recharge of the cell. During this test the cells were discharged at 0.05 A (I$_{20}$) until they reached the cutoff voltage (1.75 V). The test was supposed to last 20 h, if the cell capacity at 20 hour was equal to 1 Ah. During this test, the LS played an important role, as it was responsible for avoiding the passivation of the negative plate surface, and increased the NAM utilization. However, in this case all the mixture contained the same amount and type of LS, so differences among the results could not be attributed to the LS. **Figure 58** shows the corresponding results. According to the improvement of the formation process efficiency, addition of GANFg at dosages higher than 0.10 wt. % improved slightly the capacity of the cells. Higher BET SSA of the formed negative plates led to a better utilization of the active material: the energetic structure of the NAM was more folded, and more active sites for the lead oxidation to lead sulfate were found. In anyway, differences among the results were not so high, and even lower for the second capacity test results. If we see at results from batch 1 (**Table 21**) the mixtures that comprised OE1 in their negative plates showed second capacities values from 0.80 Ah to 0.87 Ah, so similar results as obtained adding higher amount of carbon material can be obtained adding low amount of GANFg.
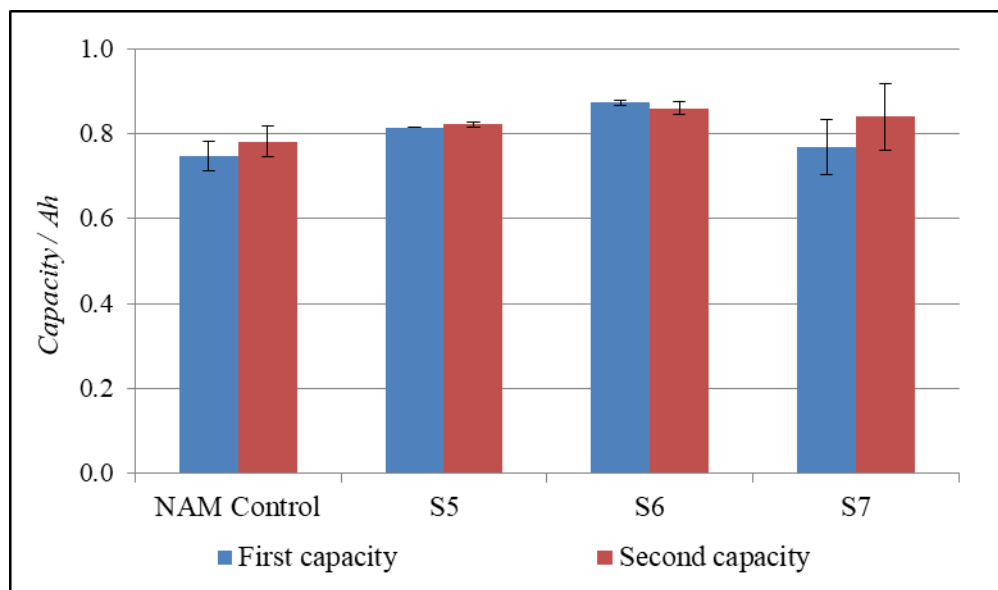
Figure 58. Batch 2. Results for the first and second capacity tests. Error bars related to the standard deviation of the measurements.

4.2.7. CCA test

After the first capacity test, and as well after the second capacity test, CCA tests were done (**section 3.11.3**). Results are showed in **Figure 59**. As was explained for the capacity results, although LS played a key role for suppressing the passivation layer, no differences among the results can be explained through this compound, as concentration and type of LS were the same for all the mixtures. Results for the CCA tests were very similar, as the results for the capacity tests. GANFg mixtures showed slightly better results than NAM Control, in this case S7 despite having only 0.10 wt. % of GANFg showed better results than NAM Control. Therefore, GANFg addition improved the CCA of the negative plates, most probably by increasing the overall conductivity of the negative plates. Again, if we compare these results with batch 1 ones for this test (**Figure 46**) just mixture 1 exceeded the 80 s in the first CCA, followed very close by mixtures 4 and 5. In batch 2 all GANFg mixtures reached or got very close to 80 s. This meant that similar results in the CCA test can be found when carbon materials or GANFg were added. The difference was that the carbon materials dosage in batch 1 was quite higher than in batch 2.
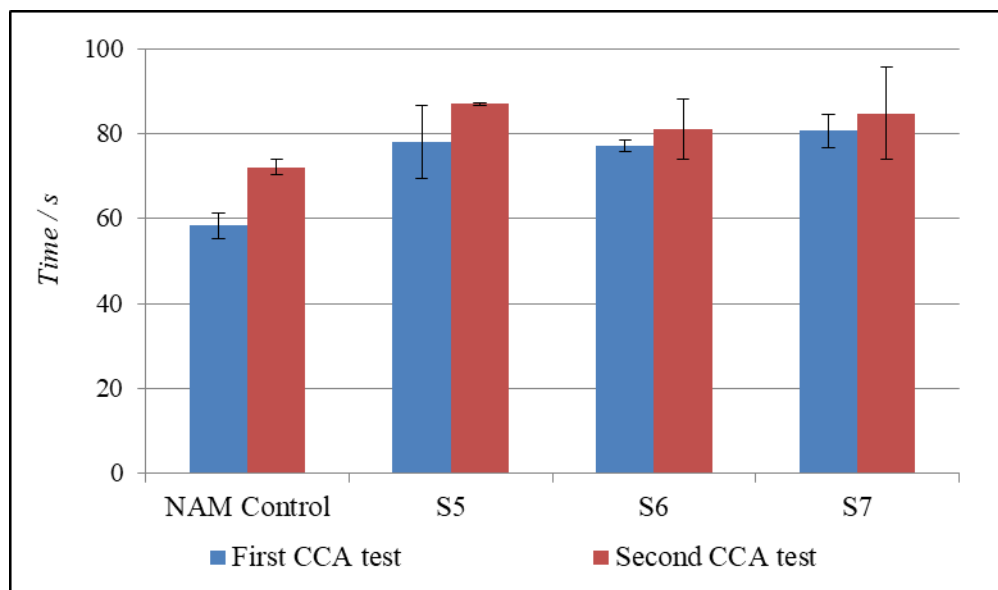
Figure 59. Batch 2. Results for the first and second CCA tests: time taken by the cell to reach 1 V during the discharge at 5 A and -18°C. Error bars related to the standard deviation of the measurements.

4.2.8. ICA test type 1

As one of the main features of the LAB installed in the Micro HEV is to recover the energy from the regenerative braking, the ICA test type 1 (**section 3.11.4**) was performed on the cells for analyzing how GANFg affected to the charge acceptance of the negative plates. During this test, the cells were discharged to 90% SoC, and then they were resting for a period of 72 h. For this period the sulfation of the negative plate was supposed to occur. When this phenomenon happens, the reduction of Pb^{2+} is hampered, as less activated sites are available, and the charge acceptance of the negative plates decays. After the 72 h, the cells were recharged at constant voltage (2.42 V) and the current passing through the cell was measured. As reference parameter we took the current passing through the cell at the 5th second of charge. Results are showed in **Figure 60**. GANFg at concentrations higher than 0.10 wt. % slightly improved the charge acceptance. However, these values were around 0.40 A, lower than the results obtained in batch 1 for the same test (**Figure 47**) which were above 0.60 A for all the mixtures containing OE1. Indeed, in batch 1 we found higher BET SSA values for the unformed negative plates than in batch 2 (**Table 20** vs **Table 28**). Batch 1 carbon materials increased in a higher way the BET SSA of the unformed negative plates, leading to a higher amount of activated sites where the reduction of Pb^{2+} can take place. This did not happen in the case of batch 2; as the BET SSA of the unformed negative plates was not at the same level of batch 1, batch 2 mixtures provided less active sites where the Pb^{2+} could have been reduced, and because of that the results in the ICA test were worse. In conclusion GANFg addition can increase a little bit the charge

acceptance of the negative plates, but this increase was higher when carbon materials of batch 1 were added.
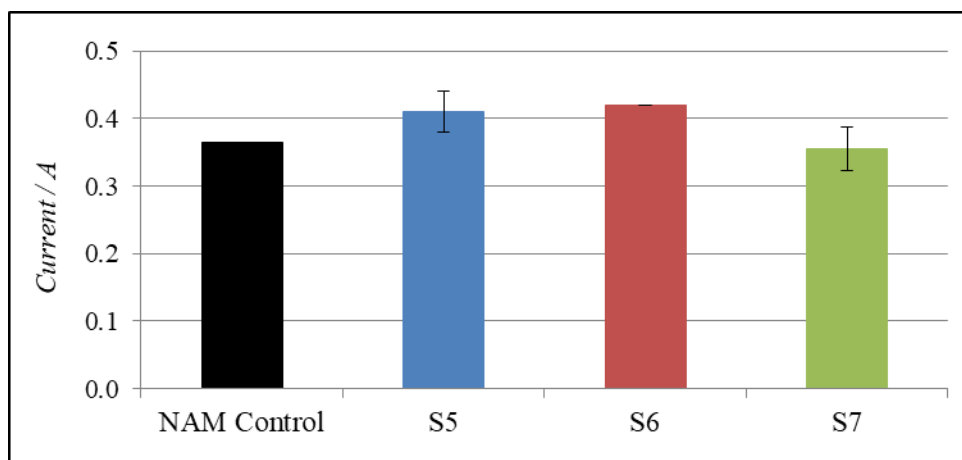
Figure 60. Batch 2. Results for ICA test type 1. Error bars related to the standard deviation of the measurements.

4.2.9. Water consumption study: float currents and negative polarization test

In order to evaluate the effect of GANFg addition on the water consumption in real batteries, different tests were performed: measurement of the float currents during the recharge after the first and the second capacity and the negative polarization study.

After each capacity test a recharge of 24 h was done according to **section 3.11.1**. This recharges was done at constant current of 0.25 A (step A) until the cell reached 2.67 V. Then the cell voltage was maintained at 2.67 V until the total recharge time was equal to 24 h (step B). During step B the current passing through the cells was decreasing, as the amount of $PbSO_4$ to recharge was getting lower. At the final period of step B the current remained steady, as all the $PbSO_4$ had been already converted to Pb, the only reaction taking place at the negative plates was the HER. At this point the steady current is also known as float current. Due to this argument, the float currents can be directly linked to the HER rate, and thus to the water consumption. For batch 2 the float currents were measured and they are showed in **Figure 61**. As was expected, GANFg addition increased the HER rate, as S5 and S6 showed higher float currents than NAM Control. Again, S7 showed similar, even lower float currents than NAM Control. This was expected due to the Nickel content of GANFg. As was mentioned before, GANFg were made using a catalyst base of Nickel. Part of the catalyst remained in the tip of the fiber when the production process was finished. After the production of the fiber, the graphitization process was done, but despite heating the fibers at temperatures higher than 2400°C not all the Nickel can be removed. The final amount of Nickel in the GANFg was lower than 20 ppm, but this 20 ppm were able to catalyzed the HER reaction and increased the water consumption of the cells when GANFg were added at concentrations higher than 0.10 wt. %.
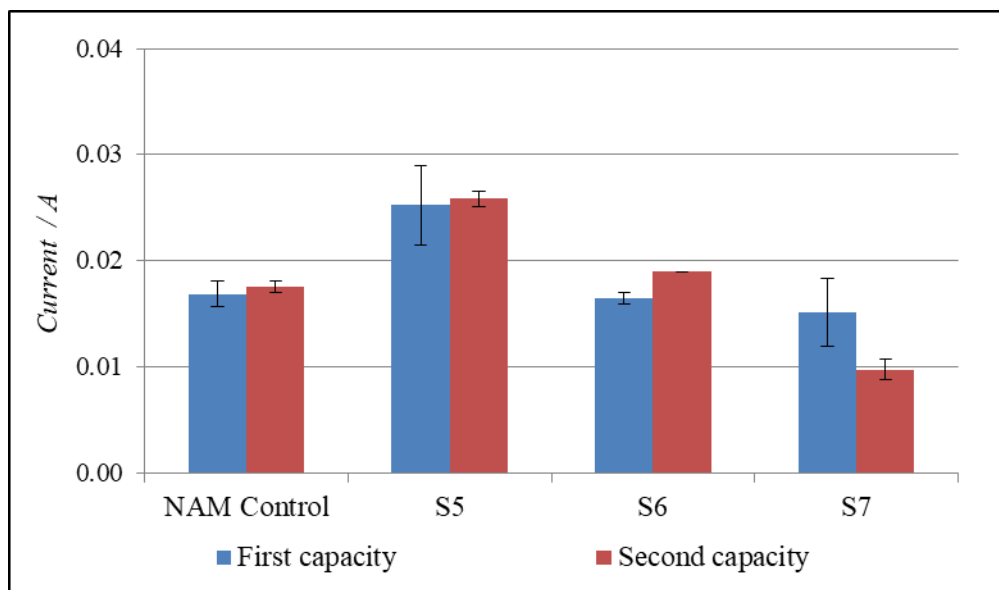
Figure 61. Batch 2. Float currents during the recharge of the cells after the first and the second capacity test. Error bars related to the standard deviation of the measurements.

The negative polarization study was also performed in order to see the effect of GANFg in the HER rate. This test was done according to **section 3.11.5**. Before starting the test, the potential of the negative plate inside the cell was measured with an Ag/AgCl reference electrode. During the test a set of charges at different constant currents were applied to the cells. At the end of each charging step, when the potential of the cell was constant, the potential of the negative plate was measured. Negative plate potentials for all the mixtures as a function of the current density passing through the cell are showed in **Figure 62**. As was explained in the former batch, just two reactions can take place in the negative plate while charging: lead sulfate reduction (R. 28) and HER (R. 29).

$$PbSO_4 + 2H^+ + 2e^- \leftrightarrow Pb + HSO^-_4 + H^+ \text{ (R. 28)}$$
$$2H^+ + 2e^- \leftrightarrow H_2 \text{ (R. 29)}$$
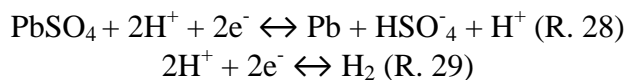
According to the relationship between the negative plate potential and the current density we can know which reactions were taking place at different current densities. Analyzing this relationship from **Figure 62** two zones can be differentiated in the graphic:

- **Zone A – j < 1 mA cm^{-2}**. No linear relationship between the potential and the current density was found. This meant the coexistence of two reactions at the same time: lead sulfate reduction (R. 28) and HER (R. 29).
- **Zone B – j > 1 mA cm^{-2}**. Linear relationship between the potential and the current density was found. This meant the predominance of just one reaction: HER (R. 29). At current densities higher than 1 mA cm^{-2} the HER starts, and had the predominance at higher current densities as well.

145
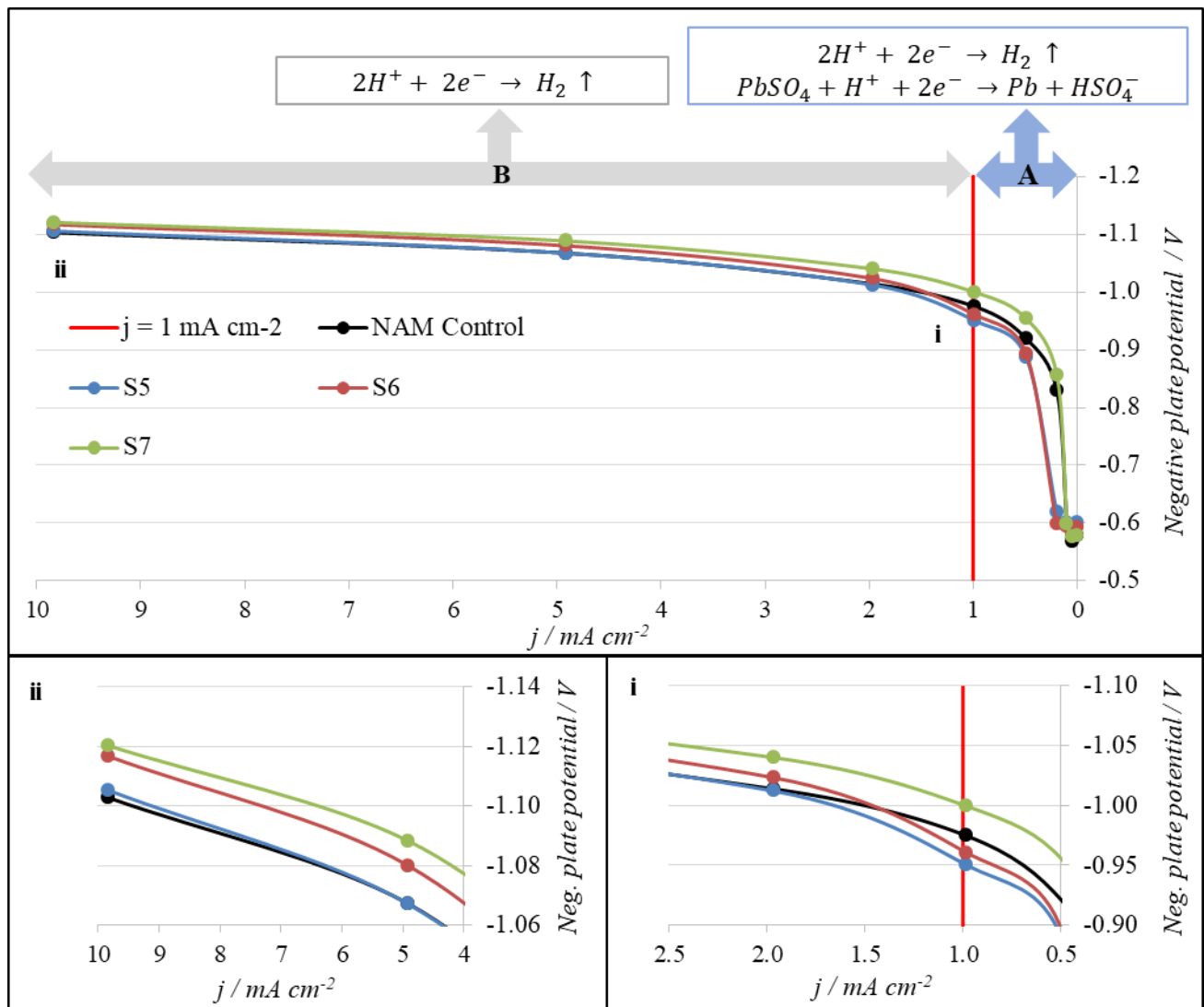
Figure 62. Batch 2. Negative polarization curves. The negative plate potential was measured vs Ag/AgCl reference electrode. **i)** Zoom for at $j = 0.5 – 2.5$ mA cm^{-2}. **ii)** Zoom for $j = 4 - 10$ mA cm^{-2}.

We can see in **Figure 62 i** how the relationship between the potential and the current density changed from no linear to linear from 1 to 2 mA cm^{-2} respectively. At higher currents densities (**Figure 62 ii**) the relation potential – current density was completely linear.

Figure 62 i can be contradictory, as the negative plate potential values were not following the same tendency at 1 and 2 mA cm^{-2}. However, if we plot the same type of graph for the negative plate overpotential (**Figure 63**) we see that the tendency is the same at both current densities.
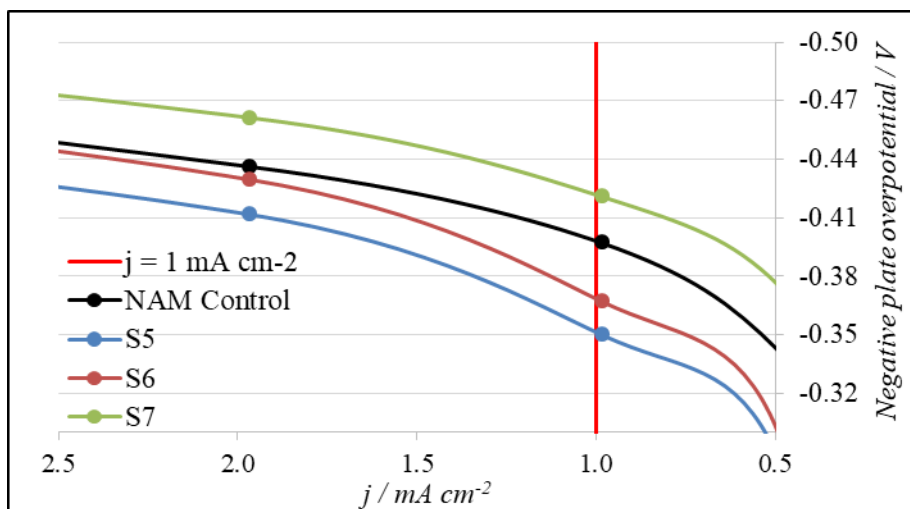
Figure 63. Batch 2. Negative plate overpotential at $j = 0.5 – 2.5$ mA cm^{-2}.
The negative plate potential was measured vs Ag/AgCl reference electrode.

According to these results, the reference current density, that was considered the point where HER was the only reaction taking place at the negative plate was 1 mA cm^{-2}. At this point, the negative plate overpotential, named $\eta_{app,H2}$, was calculated as:

$$\eta_{app,H2} = E_{1\ mA\ cm-2} - E_0$$

Where $E_{1\ mA\ cm-2}$ was the potential of the negative plate at current density equal to 1 mA cm^{-2}, and E_0 was the potential of the negative plate at current density equal to 0 mA cm^{-2}, i.e. at the beginning of the test, when no current was passing through the cell. The $\eta_{app,H2}$ are listed in **Table 30**, in ascending order (absolute value).

Table 30. Batch 2. $\eta_{app,\ H2}$ for all the mixtures. Values are
ordered from the lowest to the highest $\eta_{app,\ H2}$ (absolute value).
Water consumption degree is also showed.

Mixture	$\eta_{app\ H2}$ / V	Water consumption degree	
S5	-0.350		Highest
S6	-0.367		
NAM Control	-0.397		
S7	-0.421		Lowest

Lowest $\eta_{app,H2}$ were related to highest water consumption: lower overpotential indicates that the energy barrier that has to be overcome for producing hydrogen is low, so more hydrogen will be produced and the cell will have a higher water consumption.

In batch 2, S5 followed by S6 showed the lowest $\eta_{app,H2}$, i.e. GANFg added at concentrations higher than 0.10 wt. % increased the HER rate. This was exactly the same result obtained for the float currents analyses. So we can corroborate this statement. On the contrary and again, the addition of GANFg at 0.10 wt. % did not increased the HER rate. As was explained before, the content of Nickel inside the GANFg was the responsible for the water consumption increase in the case of mixtures S5 and S6. In comparison with batch 1 (**Table 22**), the highest $\eta_{app,H2}$ was showed by mixture 1 (-0.3338 V) which was even lowest than S5 value in batch 2 (-0.350 V). This meant that, although GANFg addition increased the water consumption, the carbon materials increased it in a further way. Carbon materials also increased the BET SSA of the unformed negative plates, something that did not happen in the case of GANFg. This increase of the BET SSA provided not only activated sites for the Pb^{2+} reduction, also brought activated sites for the H^+ reduction. In this way, GANFg would be more recommended as an additive for the negative plates if we want to strictly restrain the water consumption of the LAB.

4.2.10. Cycles at PSoC type 1

The cycle life test at PSoC type 1 (**section 3.11.6**) was performed for all the mixtures. Results are showed in **Figure 64**. It can be clearly appreciated that the GANFg addition improved the cycle life of the cells. This result was expected according to the behavior of the GANFg mixtures in the rest of the test: GANFg improve the BET SSA of the formed negative plate, and they slightly improved the capacity and the CCA of the cells. The charge acceptance was also slightly improved by the GANFg addition. As has been explained, GANFg due to their high length (up to 30 μm) were thought to be integrated into the bulk of the NAM skeleton during the formation process. This was possible because the GANFg have been previously dispersed, otherwise we would only found agglomerates of fibers inside the active material. From the NAM skeleton they were able to create more activated sites where the electrochemical reactions can take place. This was appreciated in the formed negative plates BET SSA results: GANFg improved the electrochemical active area of the NAM, by creating smaller Pb crystals that were more available for the later electrochemical reactions. It is important to notice that these activated sites can be used for the electrochemical reactions due to the low electrical resistivity of GANFg, which made possible the reduction or oxidation of the Pb species on their surface. The presence of GANFg inside the NAM skeleton provided a more electrical conductive NAM skeleton, which involved a better performance of the GANFg mixtures during the cycle life test. Coherently, higher GANFg addition led to higher cycle life. But the most important fact from this result was that mixture S7 cells, just containing GANFg at 0.10 wt. %, were able to perform 1139 cycles. If we compare this result with batch 1 results (**Figure 49**), only mixture 1 (among the mixtures containing OE1) exceeded this result with 1525 cycles. The rest of the mixtures containing OE1 performed fewer cycles, even when they contained more amount of carbon material, plus they showed better charged acceptance than S7. From this moment, we can say that the optimum amount of GANFg for seeing an effect of this additive in the cycle life was 0.10 wt. %.
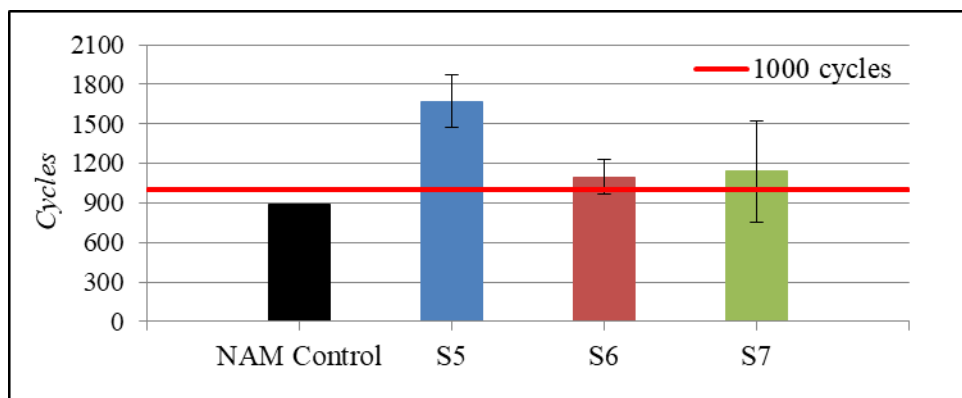
Figure 64. Batch 2. Results for the PSoC cycles type 1. Results: 893 (NAM Control), 1670 (S5), 1095 (S6), 1139 (S7). Error bars related to the standard deviation of the measurements.

After the cycle life test, the cells were recharged for 16 h (according to **section 3.11.1**) in order to study the amount of irreversible lead sulfate accumulated in the negative plates during the test. We wanted to study the recharge of the S7 cells, as the dosage of this mixture was defined as the optimum one. **Figure 65** showed the current and voltage of this recharge.
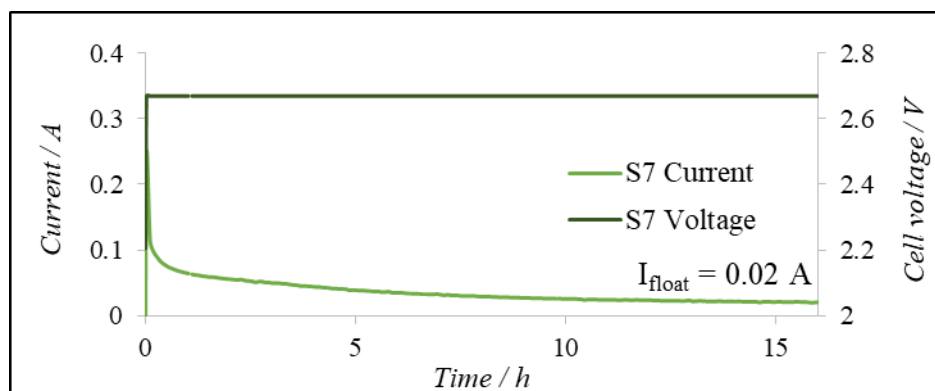
Figure 65. Batch 2. Recharge for 16 h of S7 cell after the cycle at PSoC test. Float current (I_{float}) = 0.02 A.

The analyses was done specially for comparing the float currents showed for the same mixture after the second capacity (**Figure 61**) and during the recharge after cycles (**Figure 65**). The results were 0.01 A vs 0.02 A, respectively. Higher float current value was found for the cycled plate. As more irreversible lead sulfate must be presented in the cycled cell due to the deposition of this one during the cycles, the current provided by the maintenance of the voltage had to be spent in the HER.

4.2.11. CV results

As an informative test, the CV was done for the S7 mixture, as 0.10 wt. % had been considered the optimum GANFg dosage.

CV is an electrochemical technique for studying the development of different electrochemical reactions at certain potential ranges. In the case of a lead wire submerged in sulfuric acid the negative polarization (potential goes from positive to negative values) leads firstly to the reduction of PbO_2 to $PbSO_4$, and secondly to the reduction of $PbSO_4$ to Pb. For the positive polarization (potential goes from negative to positive values), the Pb is oxidized firstly in $PbSO_4$, and secondly to PbO_2. These reactions are showed in **Figure 66**, where a voltammogram of a lead wire submerged in sulfuric acid ($\rho = 1.285$ g cm^{-3}). The measurements were done on a three electrodes cell, where the lead wire acted as working electrode. A Mercury / Mercurous Sulfate with saturated. K_2SO_4 reference electrode (named SMSE) was used. The potential range was from -1.90 V to 1.90 V, and the scan rate was 20 mV s^{-1}. HER reaction is showed at the most negative potentials and Oxygen Evolution Reaction is showed at the most positive potentials, both reactions defining the end of the potential range, as no more Pb species will react out of this potential range.

The interpretation of the CV is the following: each current peak is linked to an electrochemical reaction according the potential range; along this potential range current is being consumed for reducing or oxidizing one of the Pb substances. All these currents are considered faradaic currents, as they are generated by the reduction of Pb substances on the electrode surface. The area under the peak can be linked to the amount of charge involved in the electrochemical reaction.
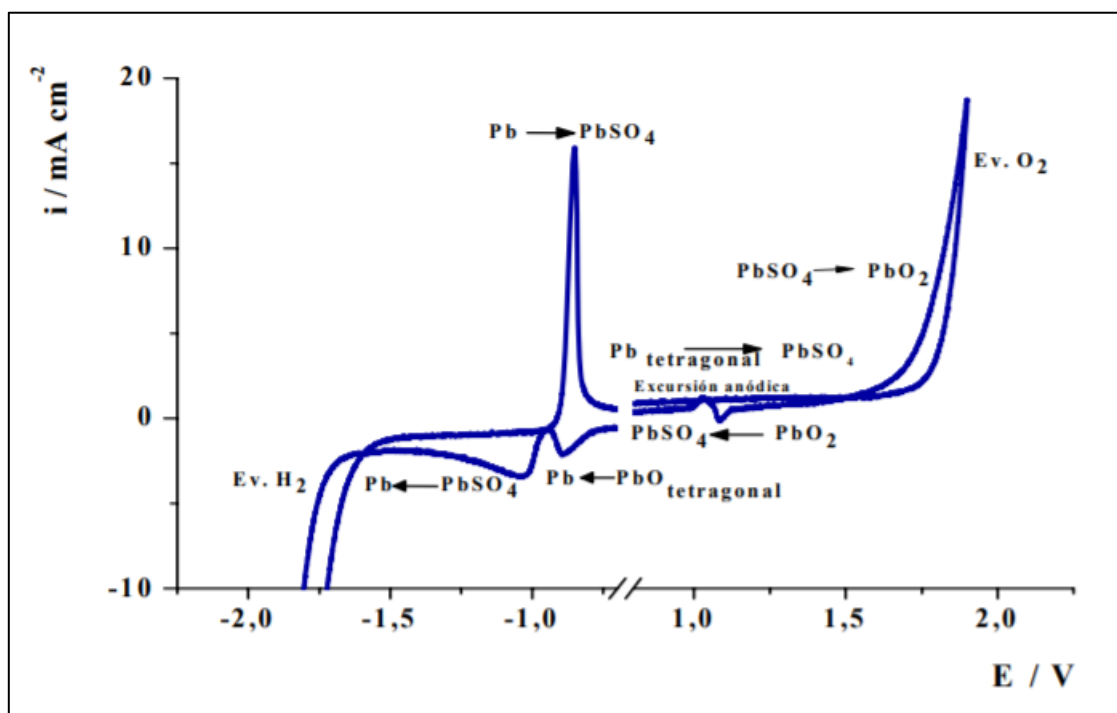
**Figure 66. Lead wire voltammogram**. Solution: sulfuric acid 1.285 g cm^{-3}. Reference electrode: SMSE. Voltage range: -1.90 V to 1.90 V. Scan rate: 20 mV s^{-1}. Temperature: 25ºC. Excursión anódica = anodic excursion. Figure from [88].

150

As all our studies were focused on the negative plate, we performed the CV in a potential range that covered the reactions occurring just in the negative plate: from -1.25 V to -2.00 V, referred to SMSE. In our case, as we worked with an Ag/AgCl reference electrode, the potential conversion was: -1.50 V to 0.50 V. This test was explained in **section 3.12**. The 2 V / 1 Ah cells were filled completely with acid, in order to ensure the whole plate soaking. Then the three electrodes cell was prepared: negative plate -> working electrode, positive plate -> counter electrode, Ag/AgCl reference electrode. The scan rate was 5 mV s^{-1}, and a total of 300 cycles were done. This test was only done for the mixture S7 in order to see the effect of the cycles in the reversibility of the electrochemical reactions. Results are showed in **Figure 67**. The difference between the oxidation and reduction peak for the scan 1st and 300th is also showed.

The main difference between **Figure 66** and **Figure 67** was the extension of the peaks area in the second one. This effect is called the capacitive effect of the carbon materials inside the NAM. When carbon materials are added, they exert a capacitive effect in the NAM. In this way the capacitive effect is linked to the double layer capacitance of the carbon material, which depends on the functional groups on the carbon materials surface and on their SSA.

The change in the shape of the peak linked to the Pb oxidation to PbSO$_4$ after 300 cycles indicated that the lead oxidation was more difficult, more positive potentials were needed for the oxidation. This could be related to the sulfation of the negative plate: as the lead sulfate was accumulated through the cycles, less amount of lead was available for its oxidation. In this way, the obtained lead sulfate amount was lower in the 300th cycle, and the area under this peak was smaller than the one under the 1st cycle peak. Less amount of charge has been used for this electrochemical reaction. In the case of the lead sulfate reduction, the shape of the peak was much more maintained. As the lead sulfate concentration increased with the number of cycles more reagent amount was available for this electrochemical reaction. This loss on the reversibility was also explained by the potential difference (ΔV) between the oxidation and reduction peak for the scan 1st and 300th. ΔV_{300} - ΔV_{100} was equal to 0.16 V, and most of the reversibility was lost due to the displacement of the oxidation peak; from scan 1st to 300th the peak was displaced by 0.176 V.

For the HER reaction, also indicated in **Figure 67**, the peak was more pronounced for the scan 1st. As in the case of scan 300th the negative plate was more sulfated, the internal resistance of the plate was increased, and the current took longer time to reach the places where the proton could be reduced. Because of that the slope for the scan 1st was higher, as the reaction started earlier in this cycle in comparison with scan 300th.
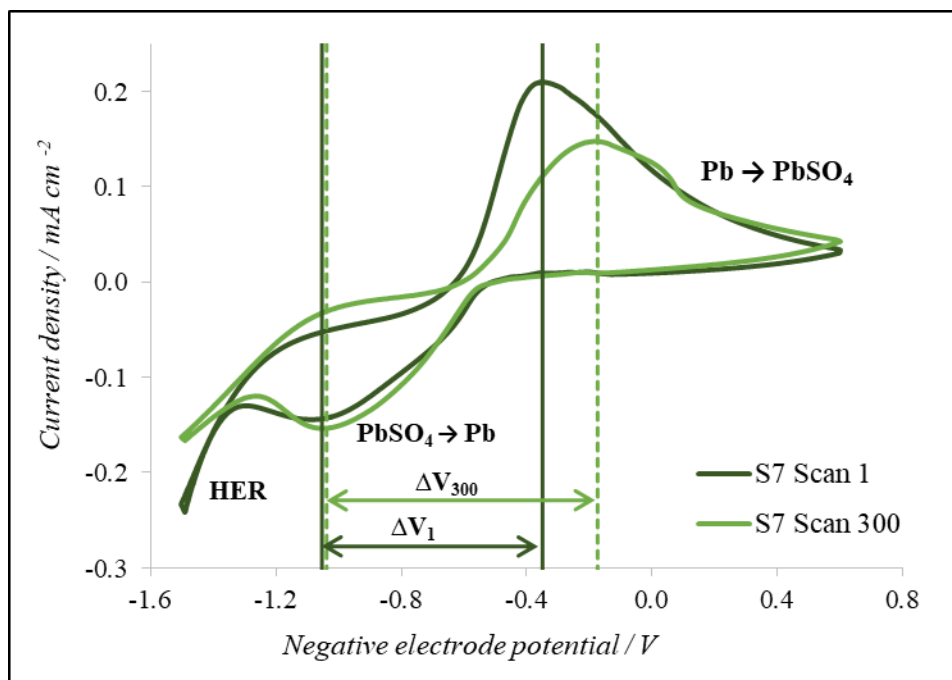
Figure 67. Batch 2. Voltammogram for the 2 V / 1 Ah cell for mixture S7. Scan 1st and 300th are represented. Active area: 20.36 cm^2. Solution: sulfuric acid 1.285 g cm^{-3}. Reference electrode: Ag/AgCl. Voltage range: -1.50 V to 0.50 V. Scan rate: 5 mV s^{-1}. Temperature: 25ºC.

The area under the oxidation and reduction peaks, i.e. the stored charged during the electrochemical reaction, was examined through the cycles. Results are showed in **Figure 68**. For Q_d it can be appreciated an increase at the 50th cycle, which was related to the activation of the Pb surface. In the case of Q_c this increase was also present but in a lower rate. It can be appreciated again how the charge reaction rate was almost maintained through the cycles, due to the high amount of lead sulfate available in the negative plate. For the discharge reaction, the drop of the stored charged was more pronounced, according also with the comparison between scan 1st and 300th from **Figure 68**.

152
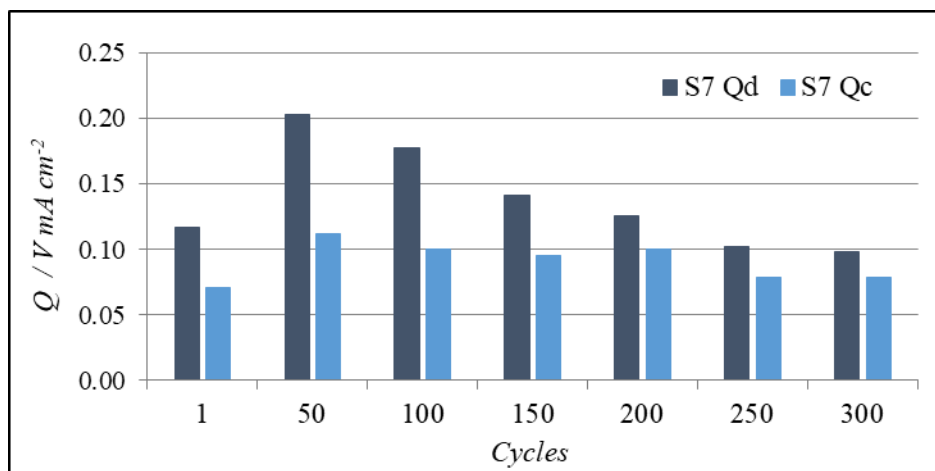
Figure 68. Batch 2. CV test for S7. Stored charge during discharge (Q_d) and charge (Q_c) reactions. Data represented every 50 cycles.

4.2.12. Properties of the negative plates after cell operation

The negative plates from cells after the ICA test type 1 and negative polarization study (**T**: tested cells) and the recharge after the PSoC cycles (**C**: cycled cells) were removed from the cells, washed and dried (**section 0**). Both types of plates were formed negative plates, as after the ICA test type 1 a recharged was applied to the cells, and during the negative polarization study just charges were applied to the cells.

For comparing these two types of plates, the XRD analyses (**section 3.13.5**) and SEM micrographs (**section 3.13.6**) were done. XRD patterns for tested negative plates for mixtures S5, S6 and S7, together with the cycled negative plates for mixture S7, are showed in **Figure 69.**

As expected in the XRD analyses, lead was present in all the mixtures. It was very interesting to see the presence of PbO in the tested negative plates. This compound was supposed to be present in the unformed negative plates, but it shouldn't be present in the formed negative plates. However, it has been establish that some materials that are able to reduce the pores diameter of the lead-carbon electrode provoke the lack of SO_4^{2-} inside the pores, and the rise of the pH due to the high proton concentration. In these conditions, α-PbO is formed [43]. So the presence of PbO in the formed negative plates can be linked to the reduction of the pore diameter induced by the GANFg addition. It happened in a higher rate for mixtures S5 and S6, as PbO diffraction peaks were higher for these mixtures, than for mixture S7. This result was in line with the porosity measurements done for the unformed negative plates (**Table 28**) where a decrease in the median pore diameter was seen when the GANFg concentration increased.

153
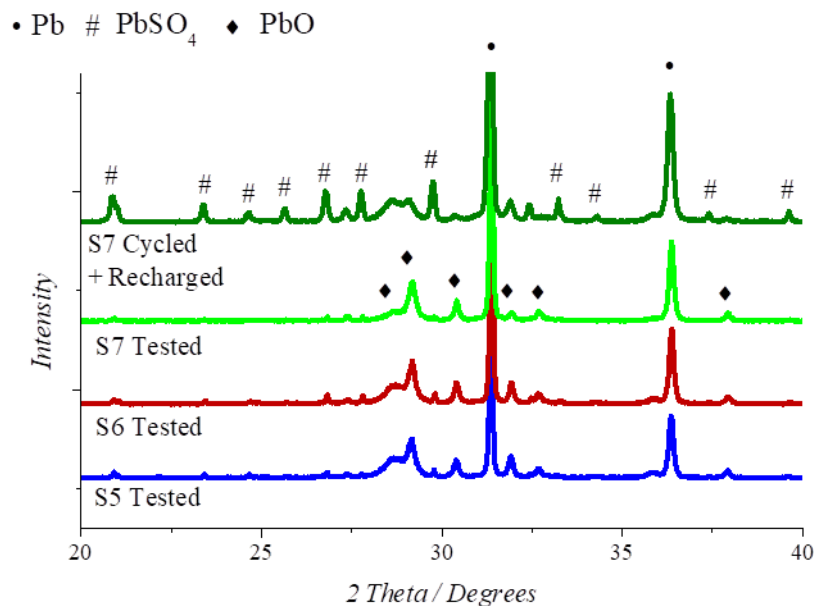
Figure 69. Batch 2. XRD patterns for the tested (T) and cycled + recharged (C) negative plates for mixtures S5, S6 and S7, and just mixture S7, respectively.

The main difference between the tested and the cycled negative plates was the presence of the lead sulfate in the S7 cycled negative plates. These lead sulfate particles were considered irreversible lead sulfate, as after the cycle life test the cells were recharged. It is clear that some of these particles, due to their high size became irreversible lead sulfate crystals. Through the discharges of the cycle life test the lead sulfate was accumulated on the negative plate. Those lead sulfate crystal with a bigger size shoed a low solubility in the sulfuric acid, and because of that they couldn't be converted to lead again, leading to the failure of the cell. Once the cells were recharged, these irreversible lead sulfate crystals were not able to be recovered, i.e. converted to lead. For confirming the existence of these irreversible lead sulfates, the lead sulfate content of the cycled negative plates was analyzed according to **section 3.13.2**. The carbon content was also analyzed. Results are showed in **Table 31**. The lead sulfate content of these cycled negative plates was much higher than the one for the formed plates (**Table 29**) where the highest lead sulfate concentration was 4.90 wt. %. In some cases the lead sulfate content was in line with the number of cycles; higher lead sulfate content was found for mixtures that performed a higher number of cycles. However, in the case of mixture S7 the lead sulfate content was higher than expected. The carbon content values were very similar to the formed negative plates ones (**Table 29**). This proved that GANFg were not degraded due to the cycle life test.

Table 31. Batch 2. Chemical properties of the cycled negative plates: carbon and lead sulfate content. The cells were recharged after the cycle life test. Number of cycles performed by each mixture is also indicated.

Mixture	Cycled negative plates		
	Cycles	Carbon content / wt. %	PbSO$_4$ content / wt. %
NAM Control	893	0.33	11.40
S5	1670	0.84	26.35
S6	1095	0.54	16.40
S7	1139	0.36	36.20

*Weighted percentage related to the total NAM mass.

The SEM micrographs of the tested and the cycled plates are showed in **Figure 70**.
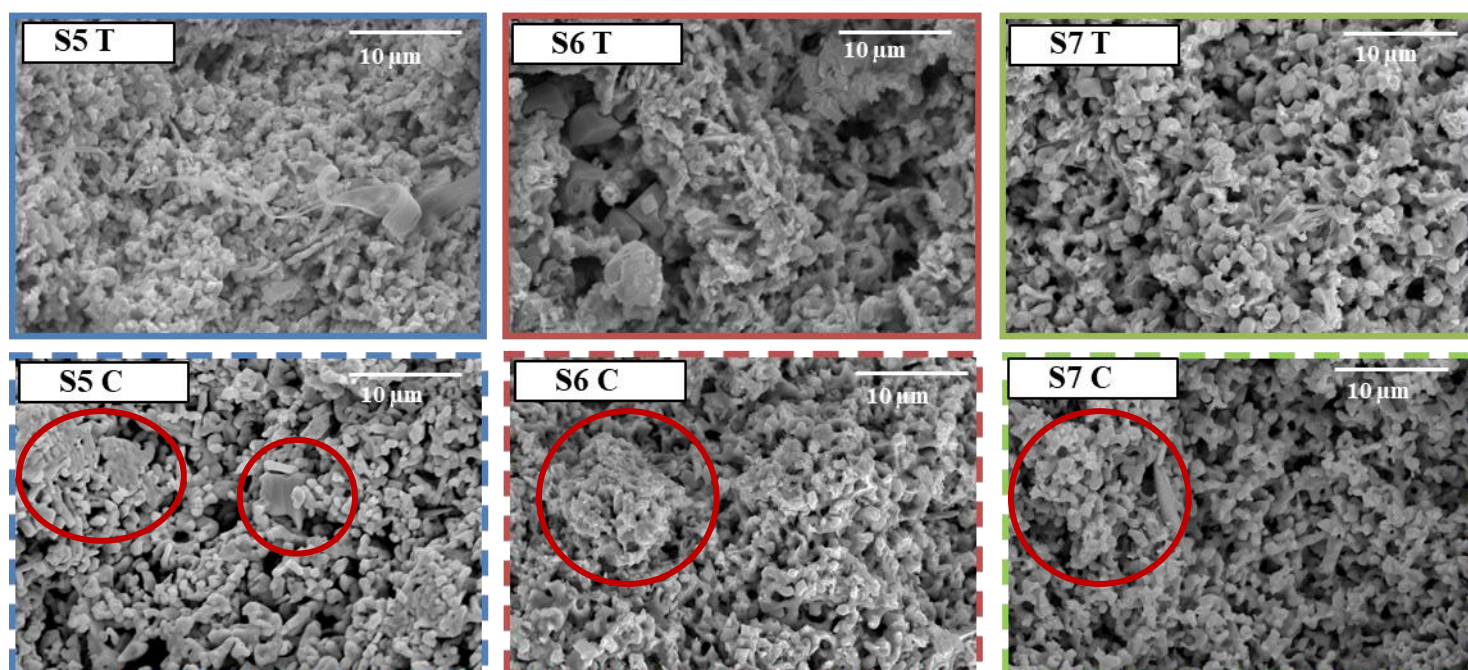
Figure 70. Batch 2. SEM micrographs for tested (T; solid line frame) and cycled (C; dotted line frame) negative plates for mixtures S5, S6 and S7. The cells were recharged after the cycle life test. Red circles: agglomerates. Magnification: x1000.

At first sight, the tested plates looked more condensed (more particles in the same space) than the cycled plates. It seems that the tested plates were less porous. This could be possible, as during the cycle life test, more specifically during the recharge of the cells, the HER took place, whereby H$_2$ gas abandoned the negative plate, improving the porosity of the plate. This fact was increased by the recharge that was applied to the cycled cells, which was much more intense than the one applied during the cycle life test. However, the particles for the tested plates were more interconnected than the ones for the cycled plates. This made sense, as in the tested plates at least the 95% of the active material was lead, and

the lead particles were all of them interconnected. The ones that we see in the **Figure 70** (tested plates) were the corresponding to the energetic structure of the NAM. In the cycled plates some agglomerates can be found, as a result of the accumulation of the lead sulfate

4.2.13. Conclusions

The main target for this batch, batch 2, was to move from the carbon materials of batch 1 to nanocarbon materials. This change was proposed due to the advantages of using nanocarbon materials instead of carbon materials such as graphite or carbon black: nanocarbon materials added at lower concentrations than graphite or carbon black in the negative plate of LAB, can improved the cycle life and maintain at a safe degree the water consumption.

The main conclusions are listed below:

- No significant differences were found among the density values, indicating that the addition of GANFg did not affect to the rheology of the pastes.
- Physicochemical properties of the negative plates indicated that addition of GANFg at concentrations higher than 0.10 wt. % reduced the median pore diameter of the unformed negative plates, reducing also their porosity.
- GANFg mixtures showed lower lead sulfate content (except mixture S7), so the formation process was improved by the addition of GANFg at concentrations higher than or equal to 0.20 wt. %.
- Addition of GANFg also improved the BET SSA of the formed negative plates.
- GANFg slightly improve the results on the capacity and CCA tests.
- The integration of GANFg inside the NAM skeleton increased its conductivity, distributing in a more homogeneously way the current along the negative plate and improving the discharge of the plates, even when GANFg were added at 0.10 wt. %.
- The charge acceptance of the negative plates was slightly improved by the addition of GANFg at concentrations higher than or equal to 0.20 wt. % by improving the BET SSA of the formed negative plates.
- Higher GANFg concentration led to higher HER rates. However, batch 1 mixtures showed higher HER rates than batch 2 mixtures.
- All GANFg mixtures showed longer cycle life than NAM Control, even mixture S7 (GANFg = 0.10 wt. %). Therefore low GANFg concentration was able to improve the cycle life of the cells.

As final conclusion, the optimum concentration of GANFg was 0.10 wt. % as with this amount of fibers the HER rate was controlled, whereas we achieved a higher cycle life adding GANFg than adding batch 1 carbon materials. However, we need to work more on the improvement of the charge acceptance.

4.3.1. Aim of the study

After the former study, the optimum GANFg concentration in NAM was clear: 0.10 wt. %. It was also clear that it is necessary to disperse the GANFg with the help of OEs, in order to have single fibers inside the NAM. These considerations gave rise the lowest dosage of GANFg (0.10 wt. %) which induced an increase in the cycle life of the 2 V / 1 Ah cells keeping at a safe degree the water consumption. Knowing this, we focused on two targets for batch 3:

- Addition of a mix of OEs in the NAM. One of the OEs was OE1 which was used in batch 1 and 2 (named also LS2 in batch 1). According to this target, a new OE, OE2, was chosen for dispersing the GANFg as well as acting as OE delaying the passivation phenomena at the negative plate surface. Furthermore, OE2 was also expected to increase the charge acceptance based on other experiments not showed in this document.
- In order to study the effect of the final amount of OEs mix in NAM, two OEs mix dosages were selected: 0.30 wt. % and 0.20 wt. %. A reduction in the final content of OE was expected to bring better results in the charge acceptance test.

The whole study was summarized in the article "Improvement of the lead acid battery performance by the addition of graphitized carbon nanofibers together with a mix of OEs in the negative active material" [89] located in the **annex iii**.

4.3.2. GANFg, OE1 and OE2 characteristics

The properties of GANFg were widely explained in **section 4.2.2**.

This OE1 was a sodium salt lignosulfonate, a derivate from the lignin. It has been seen in this document its efficiency on delaying the passivation phenomena suffered by the negative plate surface during the discharge of the battery. It also showed a good performance for dispersing the GANFg. Its degree of sulfonation, i.e. the number of sulfonic acid groups per 1000 unit weight lignin, was 0.9.

OE2 was a more highly polymerized naphthalene sulfonate that work as dispersant. It is supplied as a sodium salt and it is available as fine tan powders easily dispersed in water. It ensures high solid-water dispersions with low viscosities. Its degree of sulfonation of OE2 is 1.2%, higher than the one for OE1. It is important to keep in mind here that higher concentration of sulfonic groups means a better performance of the OE in the negative plates of LAB [8].

Figure 71 shows the molecular structures for OE1 (right side) and OE2 (left sided). In the case of OE2 the structure is a linear polymer where the only functional group is the sulfonic

group. For OE1 the structure is more complicated as different functional groups are present, such as carboxylic (-COOH), phenolic (Ar-OH), methoxyl groups (-O·CH$_3$)… The influence of the different functional groups on the negative plate performance has been widely investigated [53,54] concluding that carboxylic and phenolic groups increased the cycle life of the SLI batteries, while decreased the charge acceptance and accelerate the self-discharge of the battery.
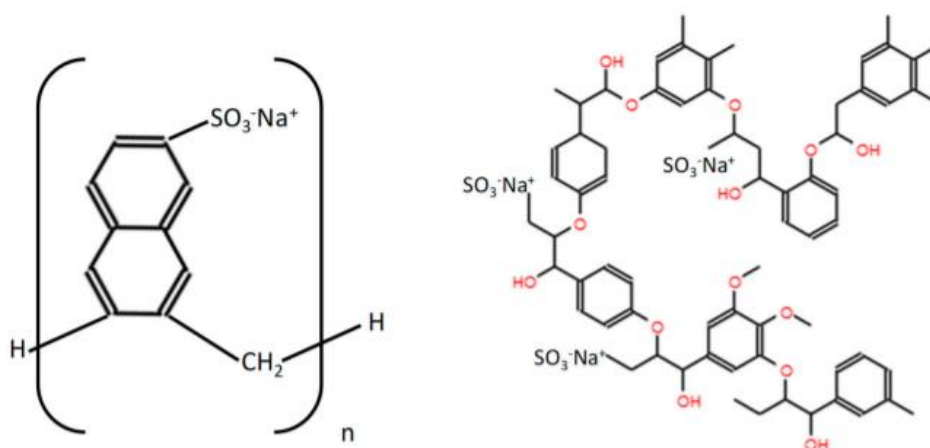
Figure 71. Molecular structures for sodium highly polymerized naphthalene sulfonate (left) and Sodium lignosulfonate (right) [90].

As was done for OE1 in the batch 2 (**section 4.2.3**), GAIKER [74] prepared the OE2 water solution and took the corresponding SEM micrographs, which are showed in **Figure 72**. The agglomerates for OE2 were much bigger than the ones obtained for OE1 (**Figure 55**). This finding was inline with the molecular weight of the OE:

- OE1 molecular weight = 6000 – 9000 g mol^{-1}.
- OE2 molecular weight = 10200 g mol^{-1}.

Higher molecular weight led to bigger agglomerates.
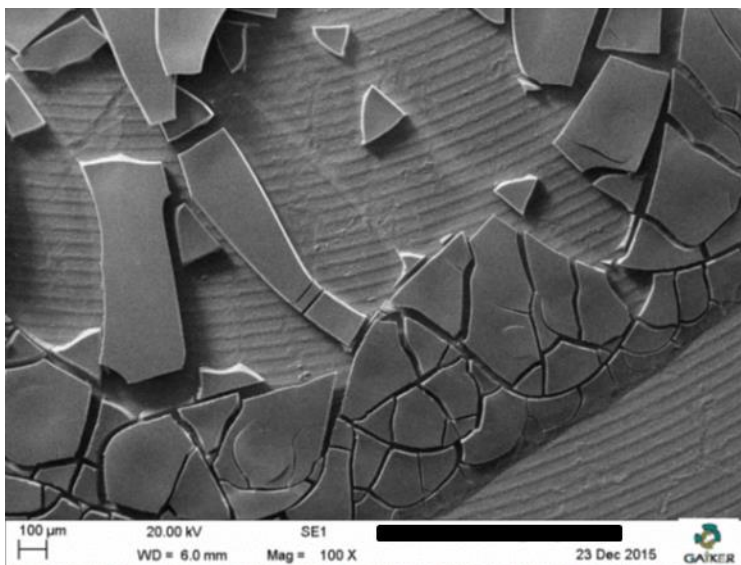
Figure 72. Batch 3. OE2 solution in the microscope. SEM micrograph taken by GAIKER.

In addition GAIKER also prepared 4 dispersions of GANFg and OE2 (according to **section 3.3**): S12 (mother dispersion), S13, S14 and S15. The dispersions were done with the Dispermat ® CN 10 from VMA-GETZMANN GMBH (**Figure 19**); some of its accessories were used also (everything is summarized in the **section 3.3**) at GAIKER facilities.

S12 dispersion (mother dispersion) contained: Water (100 g) + OE2 (7.5 g) + GANFg (12.5 g). The mother dispersion was diluted for preparing mixtures S13, S14 and S15. The composition of the final dispersions can be seen in **Table 32**. GAIKER provided data about the aspect and stability of the dispersions.

Zeta potentials (see **Table 32**) higher than $\pm$ 20 mV indicate high stability of the dispersion. So we can conclude that the dispersions were stable.

Table 32. GANFg + OE2 dispersions: composition and zeta potential (analysis made by GAIKER).

Sample	H_2O:OE2:GANFg / g	Zeta Potential / mV
S12	100:7.5:12.5	-29.23 ± 2.56
S13	100:3.0:5.0	-24.92 ± 1.95
S14	100:1.2:2.0	-37.60 ± 0.53
S15	100:0.6:1.0	-36.23 ± 1.26

Figure 73 shows the SEM micrographs of dispersions S12, S13, S14 and S1. In comparison with **Figure 56** (same micrographs taken for OE1 dispersions) the presence of the OE2 is more noticeable when GANFg concentration was equal to 1.9%, corroborating again the higher molecular weight for OE2. Again, it can be seen that the fibers were not

159

agglomerated, so these dispersions were suitable for being used in the paste preparation, i.e. OE2 can be used as GANFg dispersant.
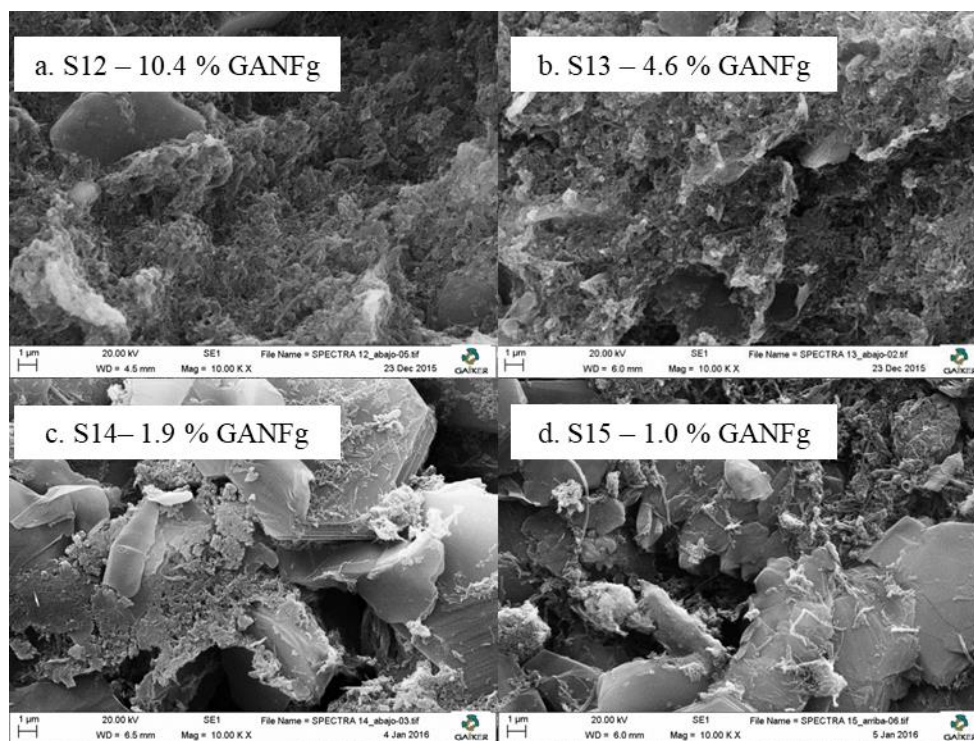
Figure 73. Batch 3. GANFg and OE2 dispersions SEM micrographs. **a.** S12. **b.** S13. **c.** S14. **d.** S15. GANFg percentage of each dispersion indicated in the figure. SEM micrographs taken by GAIKER.

4.3.3. GANFg dispersions and mixtures compositions

The GANFg dispersions prepared for this batch were based on the mix of OE1 and OE2, according to the final mixture compositions showed in **Table 33**.

Table 33. Batch 3. Composition of the mixtures.

Mixture	GANFg / wt.%	OE1 / wt.%	OE2 / wt.%
Blank	0.00	0.00	0.00
S25B	0.00	0.15	0.15
S25	0.10	0.15	0.15
S26B	0.00	0.10	0.10
S26	0.10	0.10	0.10

As can be seen in **Table 33**, five mixtures were prepared, but just two of them contained GANFg. The blank mixture was prepared for seeing the effect of the OEs as well as

GANFg addition, as it did not contain any of these compounds. Mixtures S25B and S25B were the reference mixtures for mixtures S25 and S26, respectively. The first ones did not contain GANFg in contrast to the second ones. Furthermore, the final amount of OEs was 0.30 wt. % for S25B and S25, and 0.20 wt. % for S26B and S26. For preparing mixtures S25 and S26 the GANFg dispersions were needed. In this case as both dispersions contained the same amount of GANFg, and the only difference was the amount of OEs, the same type of GANFg dispersion was used to prepare both mixtures: S25.

S25 dispersion was prepared by GAIKER following the procedure from **section 3.3.** Firstly the mother dispersion S24 was prepared, and then diluted to give rise to S25. The composition of these dispersions is showed in **Table 34**.

Table 34. Batch 3. GANFg + OE1 + OE2 dispersions S24 and S25: dispersions composition, zeta potential and particle size of the agglomerates inside the dispersion. Analyses made by GAIKER.

Sample	H$_2$O:OE1: OE2:GANFg / g	Zeta Potential / mV	d / μm	d$_{50}$ / μm	d$_{90}$ / μm
S24	200:7.5:7.5:25		3.53 ± 0.84	1.04 ± 0.03	8.53 ± 1.04
S25	100:0.3:0.3:1	45.93 ± 7.84			

The zeta potential of the S25 dispersion was provided by GAIKER and is showed in **Table 34**. Zeta potentials higher than ± 20 mV indicate high stability of the dispersion. So we can conclude that the dispersion was stable.

Table 34 shows the particle size of the dispersion S24, measured with the equipment MASTERSIZER (**section 3.2.4**). **Figure 74** shows the corresponding graphic regarding the particle size of dispersion S24. These results can be extrapolated to dispersion S25, as from dispersion S24 to dispersion S25 the solution was only dispersed, so no forces were applied to reduce the particle size of the agglomerates inside the dispersion. It can be seen in the graphic that the dispersion mainly contained two types of particles size: 0.1 μm and 1.0 μm. Some bigger particles were also found. As GANFg can reach a length up to 30 μm we can ensure that the fibers were not cut, and the ones with the highest length remained in the same size after the dispersion preparation.
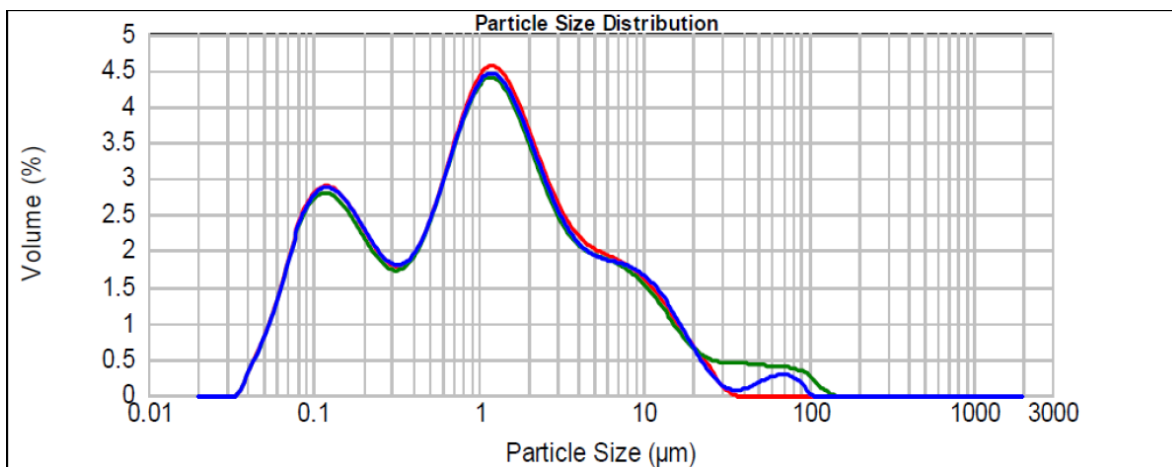
Figure 74. Batch 3. Particle size distribution for the dispersion S24. Analysis made by GAIKER.

Table 35 shows the final composition of the mixtures, i.e. the final amount of each ingredient used for preparing the negative pastes. At the "Dispersion" column we can see that the same dispersions (S25) was used for the GANFg mixtures of this batch: S25 and S26. Knowing the amount of OEs contained in the dispersion S25 we adjusted the amount of OEs that had to be added in dry conditions in order to reach the final and desires concentration of OEs in the negative mixtures S25 and S26.

Table 35.Batch 3. Composition of the dispersions and negative mixtures.

Mixture		Dispersion / g				Components added during the mixing process / g						
Batch	Name	H_2O	GANFg	OE1	OE2	LO	H_2O	H_2SO_4*	PAC Fiber	$BaSO_4$	OE1	OE2
3	Blank					1000	147	46.0	2.2	10.0	-	-
	S25B						135				1.5	1.5
	S25	100	1	0.3	0.3		35				1.2	1.2
	S26B						137				1.0	1.0
	S26	100	1	0.3	0.3		27				0.7	0.7

*Acid density equal to 1.4 g cm^{-3}.

4.3.4. Negative pastes and negative unformed plates characteristics

The negative pastes were prepared according to **section 3.5**. It is interesting to notice in **Table 35** the different amount of water added in each mixtures; the highest amount of water was added for the blank mixtures. This mixture did not contain any OE that facilitated the mixing process, so more water had to be added in order to mix all the compounds properly. In addition, blank mixture showed the lowest penetration. After the mixing process the density of the pastes were measured (see **Table 36**). Among the density values, the blank mixture showed higher values in comparison with mixtures S25B and

S26B, even when blank mixture needed more water to be properly prepared. So, the presence of OEs in the mix reduced the paste density, and facilitated the mixing process. GANFg mixtures, S25 and S26, showed lower densities than the corresponding reference mixtures, S25B and S26B. The dispersion addition also reduced the paste density; this fact was linked to the predispersion of the OEs.
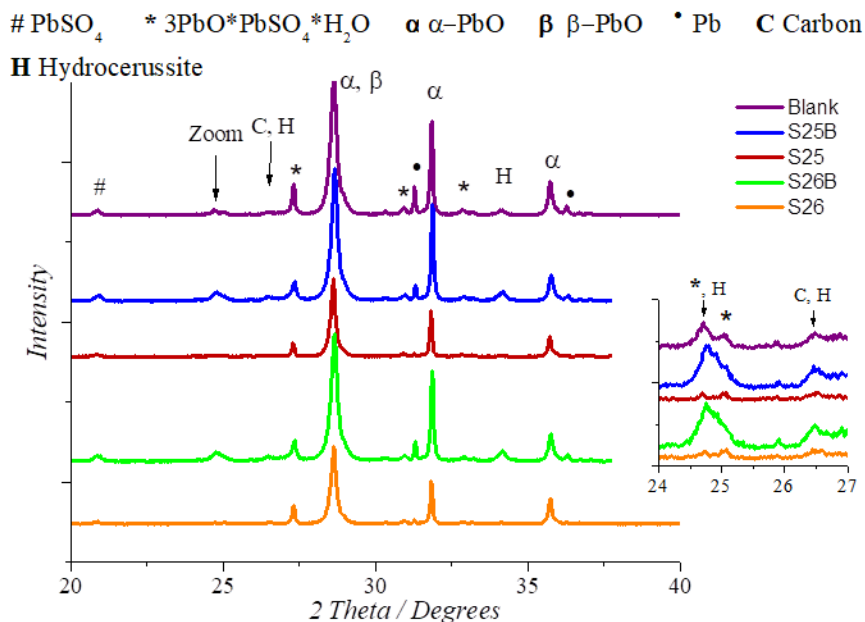
Table 36. Batch 3. Density of the pastes after the mixing process. Physicochemical properties of the unformed negative plates: carbon content, lead sulfate content and BET SSA.

Mixture	Paste density / g cm^{-3}	Unformed negative plates		
		Carbon content / wt. %	PbSO$_4$ content / wt. %	BET SSA / m^2 g^{-1}
Blank	4.54	0.40	6.30	1.42
S25B	4.63	0.90	6.10	1.92
S25	4.40	0.45	5.80	2.33
S26B	4.64	0.80	6.30	1.88
S26	4.29	0.43	6.25	2.18

*Weighted percentage related to the total NAM mass.

After preparing the pastes, the grids were pasted to prepare the 1 Ah negative plates according to **section 3.6**, and then the plates were cured according **to section 3.7**. The positive plates were also prepared according to the same sections. However, as these plates were prepared according a standard procedure, and were not under study, their properties are not shown in this work.

The carbon content of the negative unformed plates was analyzed (according to **section 3.13.2**). Results are showed in **Table 36**. Results showed higher carbon amount than expected for mixtures Blank, S25B and S26B, as in the case of the Blank mixtures none carbon material was added to the mixture; for mixtures S25B and S26B a maximum of 0.30 wt. % was expected, not a value around 0.80 – 0.90 wt. %. This fact also happened for the unformed negative plates of the batch 1 (**section 4.1.3**) and batch 2 (**section 4.2.4**). As was explained in those sections during the mixing process the carbon dioxide from the air can react with the lead hydroxide (Pb(OH)$_2$), forming which is known as Hydrocerussite (2PbCO$_3$·1PbO(OH)$_2$), that can be found in the NAM as part of the lead Hydrocarbonate (PbO·6PbCO$_3$·3PbO(OH)$_2$). This compound can be also detected by XRD, at the surroundings of 26.5° (2θ), where the carbon diffraction peak is located. This means that Hydrocerussite diffraction peak could be interfering with the carbon diffraction peak, masking the real result of the carbon peak. For corroborating this hypothesis, the XRD analyses of the unformed negative plates were done (according to **section 3.13.5**).

Figure 75. Batch 3. XRD patterns for the unformed negative plates. ***(3BS), C, H peak (2θ: 24.0 – 27.0). Zoom: 1st peak -** Hydrocerussite (family of planes: 104) and 3BS (family of planes: 002) diffraction peaks at 2θ = 24.7°. **2nd peak** - 3BS (family of planes: 210) diffraction peaks at 2θ = 25.1°. **3rd peak** - for the carbon (family of planes: 002) and Hydrocerussite (family of planes: 015) diffraction peaks around 2θ = 26.5°.

Figure 75 shows the XRD patterns for the unformed negative plates of batch 3. As expected, all the negative plates were made mainly of α-PbO, β-PbO, $PbSO_4$, 3BS and Pb. The carbon diffraction peak at 26.50° (2θ) had the same shape as the hydrocerussite diffraction peak 24.70° (2θ), confirming that hydrocerussite was present in the negative plates, and its peak at 27.1° (2θ) interfered the carbon diffraction peak.

Table 36 also shows the lead sulfate content of the unformed negative plates; analyses made according to **section 3.13.2**. No significant differences were found among the difference mixtures, as the same amount of sulfuric acid was used for preparing all the pastes. The BET SSA of the unformed negative plates for all the mixtures appears also in **Table 36**. The data shows higher BET SSA for the mixture GANFg mixtures, S25 and S26, followed by mixtures S25B and S26B. The lowest value was obtained by the blank mixtures. According to the results, OEs as S25B and S26B showed higher BET SSA values than the Blank mixture. Furthermore, S25B showed higher BET SSA values than S26B, so an increase of 0.10 wt. % in content of OEs increased the BET SSA.

4.3.5. Negative formed plates characteristics

After analyzing the unformed negative plates the 2 V / 1 Ah cells were assembled (**section 3.8**) and formed (**section 3.9**). After the formation of the cells, the negative plates from two cells per type were taken out of the cells, washed and analyzed (**section 0**). Carbon content

and lead sulfate content were analyzed (**section 3.13.2**), as BET SSA (**section 3.13.4**) of the formed negative plates. Results are showed in **Table 37**. Carbon content values were lower after formation of the cells, in comparison with the unformed negative plates values (**Table 36**). These results confirmed the reaction between Hydrocerussite and sulfuric acid during the soaking process whereby CO_2 was released. In this way, the carbon content of the formed negative plates was consistent with the real amount of carbon added during the pasting process.

The lead sulfate content of the formed negative plates (**Table 37**) was lower than the one found for the unformed negative plates (**Table 36**). This made sense, as during the formation process of the negative plate the lead sulfate was converted to lead. However, in this case Blank, S25 and S26 mixtures showed the highest results, while it was expected a lower lead sulfate content for the GANFg mixtures, as happened in Batch 2 (**Table 29**).

Table 37. Batch 3. Physicochemical properties of the formed negative plates: carbon content, lead sulfate content and BET SSA.

Mixture	Formed negative plates		
	Carbon content / wt. %	PbSO$_4$ content / wt. %	BET SSA / m^2 g^{-1}
Blank	0.10	4.50	0.25
S25B	0.30	2.80	0.50
S25	0.41	4.25	0.72
S26B	0.30	2.40	0.54
S26	0.39	4.45	0.66

*Weighted percentage related to the total NAM mass.

The BET SSA of the formed negative plates is also showed in **Table 37**. This magnitude has been reduced from the unformed (**Table 36**) to the formed negative plates. The unformed negative plates showed higher values as they were made of α-PbO, β-PbO, $PbSO_4$, 3BS and Pb, bigger molecules with larger surfaces. However the trend was similar for the unformed and formed negative plates: blank mixtures showed the lowest results, followed by the reference mixtures, S25B and S26B, and by the GANFg mixtures, S25 and S26. There was not significant difference among the 0.30 wt. % OEs mixtures, S25B and S25, and the 0.20 wt. % OEs mixtures, S26B and S26. Leading to the conclusion that higher OEs concentration did not improved the BET SSA of the formed negative plates. Again, the GANFg mixtures showed the highest BET SSA. As was explained in Batch 2 (**section 4.2.5**) during the formation process, GANFg due to their low electrical resistivity and high length (of microns) were able to act as lead nuclei, and became part of the NAM skeleton. As a result small lead crystals were covering the GANFg and the BET SSA of the

S25 and S26 mixtures was higher. In addition, no significant differences were found among S25 and S26 mixtures, suggesting that just GANFg were responsible of the increase in the BET SSA.

Figure 76 shows the XRD patterns for the formed negative plates of batch 3.
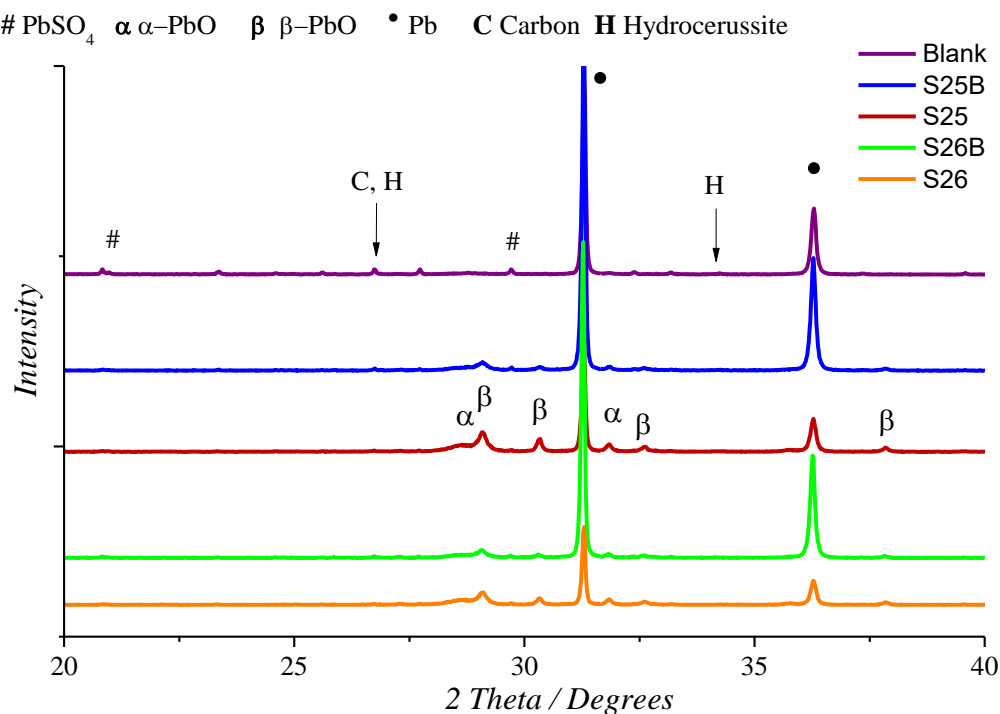
Figure 76. Batch 3. XRD patterns for the formed negative plates.

As expected, no hydrocerussite was found in the formed negative plates, according to the flat area found at the surroundings of hydrocerussite diffraction peak at 34.16° (2θ). The formed negative plates were made of Pb mainly, but other species were also found: α-PbO, β-PbO, $PbSO_4$. The presence of $PbSO_4$ was also found in the chemical analyses of the formed negative plates (**Table 37**). α-PbO and β-PbO were present in the formed negative plates (**Figure 76**). This fact was also seen for the GANFg mixtures of Batch 2 (**Figure 69**). It has been establish that some materials that are able to reduce the pore diameter of the lead-carbon electrode provoke the lack of SO_4^{2-} inside the pores, and the rise of the pH due to the high proton concentration. In these conditions, α-PbO is formed [43]. As was seen in the batch 2, GANFg were able to reduce the median pore diameter of the NAM (**Table 28**). So again, the presence of α-PbO (in this case also β-PbO) in the formed negative plates can be linked to the reduction of the pore diameter induced by the GANFg addition. We also found α-PbO and β-PbO in the mixtures S25B and S26B, although the intensity of the peaks was lower than in the case of the GANFg mixtures. This fact suggested that the addition of OEs also reduced the pore diameter of the NAM which led to the absence of

166

SO_4^{2-} inside the pores, and thus the formation of PbO instead of $PbSO_4$. The reduction of the median pore diameter of the NAM when OEs were added was in line with the increase of the BET SSA when these compounds were added to the NAM (**Table 36**).

4.3.6. Capacity test

After the formation, the first test done on the cells was the capacity test (**section 3.11.2**). This test was repeated twice. The second value was taken as reliable, as it was done after the first recharge of the cell. During this test the cells were discharged at 0.05 A (I_{20}) until they reached the cutoff voltage (1.75 V). The test was supposed to last 20 h, if the cell capacity at 20 hour was equal to 1 Ah. During this test, the OEs played an important role, as they were responsible for avoiding the passivation of the negative plate surface, and increased the NAM utilization. **Figure 77** shows the corresponding results.

The blank mixture showed the lowest capacity, this result was expected, as this mixture did not contain any OE, so the passivation layer was formed in an easier way on the negative plate surface, avoiding the continuity of the discharge. The increase of 0.10 wt. % of OEs concentration did not improve the capacity of the plates. However, the GANFg addition led to higher capacities, and a better NAM utilization. This result was also observed in Batch 2 (**Figure 58**), where was linked to the higher BET SSA of the GANFg mixtures: NAM was more folded, and more active sites for the lead oxidation to lead sulfate were found. Maybe, the predispersion of the OEs also improved the performance of the OE in the negative plate.
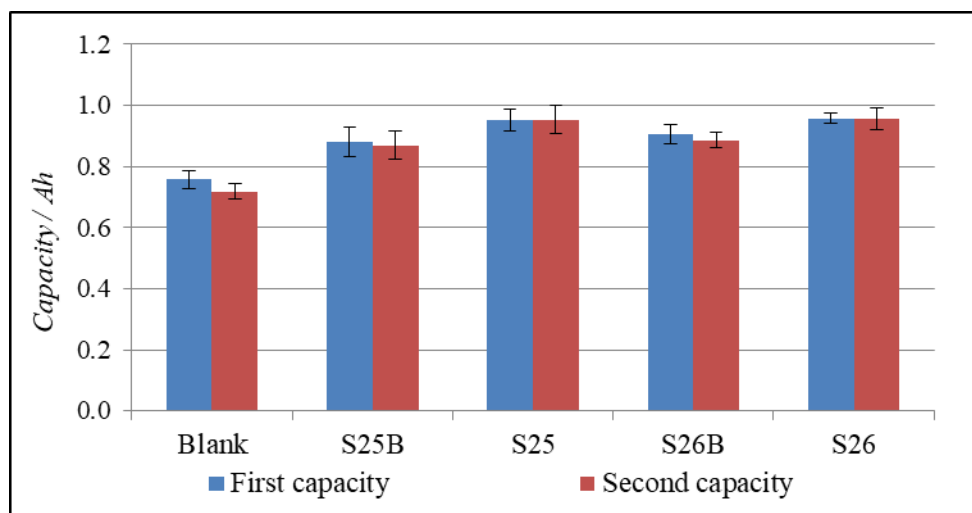
Figure 77. Batch 3. Results for the first and second capacity tests. Error bars related to the standard deviation of the measurements.

4.3.7. CCA test

After the first capacity test, and as well after the second capacity test, CCA tests were done (**section 3.11.3**). Results are showed in **Figure 78**. Again, the results of this test were linked to the OE performance, as in this case the test was a high rate discharge at extremely low temperature. This type of test involves a faster formation of the passivation layer, as the solubility of lead sulfate crystals decreased at lower temperatures collapsing the pores and impeding the continuity of the discharge. As can be seen in the figure, Blank mixture showed the lowest CCA duration, in line with the fact that this mixture did not contain any OEs, so the formation of the passivation layer was facilitated. In contrast to the capacity test results (**Figure 77**), in this case higher OEs concentration led to an improvement in the CCA duration. Accordingly, mixture S25B showed better results than mixture S26B, and the same for S25 and S26 respectively. So we can corroborate that the role of the OEs was more pronounced in the CCA test. Again, we can see in the figure that GANFg mixture showed better results due to the same reasons explained for the capacity test: better NAM utilization when GANFg were added plus predispersion of the OEs.
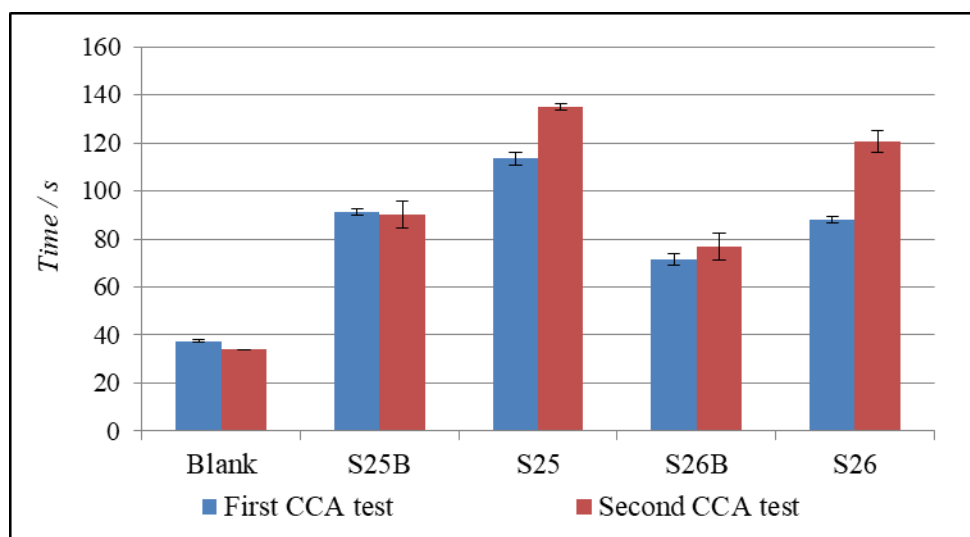
Figure 78. Batch 3. Results for the first and second CCA tests: time taken by the cell to reach 1 V during the discharge at 5 A and -18°C. Error bars related to the standard deviation of the measurements.

4.3.8. ICA test type 2

As one of the main features of the LAB installed in the Micro HEV is to recover the energy from the regenerative braking, the ICA test type 2 (**section 3.11.4**) was performed on the cells for analyzing how GANFg and OEs concentration affected to the charge acceptance of the negative plates. During this test, the cells were discharged to 90% SoC, and then they were resting for a period of 24 h (for batches 1 and 2 the duration of the pause was 72 h).

For this period the sulfation of the negative plate was supposed to occur. When this phenomenon happens, the reduction of Pb^{2+} is hampered, as less activated sites are available, and the charge acceptance of the negative plates decays. After the 24 h, the cells were recharged at constant voltage (2.42 V) and the current passing through the cell was measured. As reference parameter we took the current passing through the cell at the 5th second of charge. Results are showed in **Figure 79**. For understanding these results it is important to take into consideration that the Pb^{2+} reduction can take place at two different surfaces of the negative plate: on the GANFg surface (in this case) and on the lead surface [38]. However, it is also known that the Pb^{2+} reduction also depends on the migration of the Pb^{2+} ions through the porous $PbSO_4$ layer and the OE layer, which means that higher OEs concentration leads to lower Pb^{2+} migration, and thus lower charge acceptance [8]. This theory explains the good charge acceptance obtained by the Blank mixture: the Pb^{2+} migration was facilitated for this mixture, as it did not contain any OEs, resulting in a higher charge acceptance. According again to this theory, S25B and S25 due to containing higher OEs concentration, showed lower charge acceptance than S26B and S26B. For this test, the GANFg addition did not have any beneficial effect. It was also seen in batch 2 results (**Figure 60**) that GANFg only improved slightly the charge acceptance when they were added at concentrations equal to or higher than 0.20 wt. %.
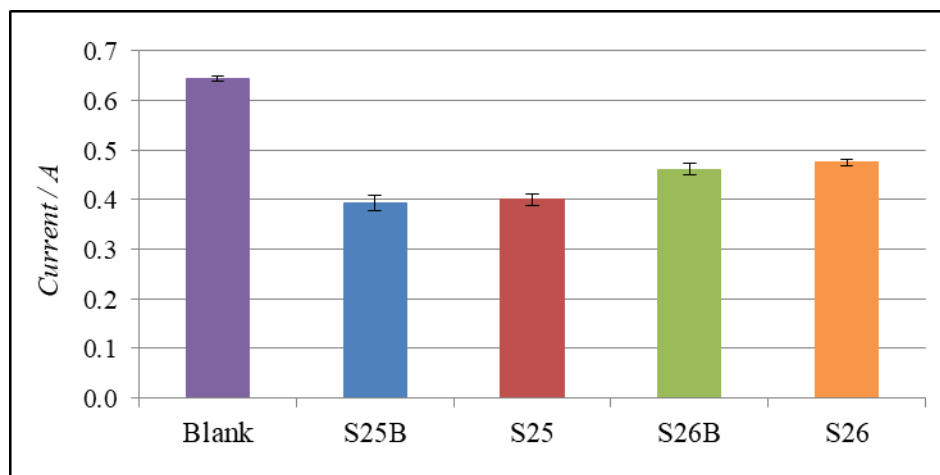
Figure 79. Batch 3. Results for ICA test type 2. Error bars related to the standard deviation of the measurements.

4.3.9. Water consumption study: float currents and negative plate polarization test

In order to evaluate the effect of GANFg addition and OEs concentration on the water consumption in real batteries, different tests were performed: measurement of the float currents during the recharge after the first and the second capacity and the negative polarization study.

After each capacity test a recharge of 24 h was done according to **section 3.11.1**. This recharges was done at constant current of 0.25 A (step A) until the cell reached 2.67 V. Then the cell voltage was maintained at 2.67 V until the total recharge time was equal to 24 h (step B). During step B the current passing through the cells was decreasing, as the amount of $PbSO_4$ to recharge was getting lower. At the final period of step B the current remained steady, as all the $PbSO_4$ had been already converted to Pb, the only reaction taking place at the negative plates was the HER. At this point the steady current is also known as float current. Due to this argument, the float currents can be directly linked to the HER rate, and thus to the water consumption. For batch 3 the float currents were measured and they are showed in **Figure 80.**

As was expected, GANFg addition increased the HER rate, as S25 and S26 showed higher float currents than S25B and S26B. This was expected due to the Nickel content of GANFg, as was explained in **section 4.2.9** for Batch 2. The final amount of Nickel in the GANFg was lower than 20 ppm. There were no significant difference between the 0.30 wt. % OEs mixtures and 0.20 wt. % OEs mixtures. However, the blank mixture did show higher float currents than mixtures S25B and S26B, suggesting that addition of OEs reduced the HER rate. As happened in the case of the charge acceptance, the proton must also go through the OE layer for reaching the lead surface and be reduced, and indeed, this migration can be impeded by this layer, and thus the HER rate would be reduced by the addition of OEs.
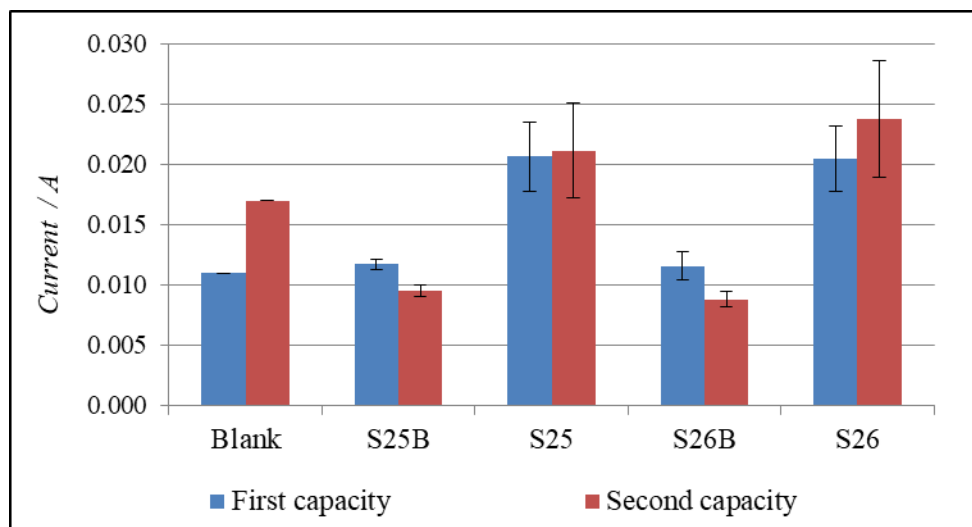
Figure 80. Batch 3. Float currents during the recharge of the cells after the first and the second capacity test. Error bars related to the standard deviation of the measurements.

The negative polarization study was also performed according to **section 3.11.5**. The negative polarization study was also performed in order to see the effect of GANFg and the use of different OEs concentration on the HER rate. Before starting the test, the potential of

the negative plate inside the cell was measured with an Ag/AgCl reference electrode. During the test a set of charges at different constant currents were applied to the cells. At the end of each charging step, when the potential of the cell was constant, the potential of the negative plate was measured. Negative plate potentials for all the mixtures as a function of the current density passing through the cell are showed in **Figure 81**. As was explained in the former batch, just two reactions can take place in the negative plate while charging: lead sulfate reduction (R. 28) and HER (R. 29).

$$PbSO_4 + 2H^+ + 2e^- \leftrightarrow Pb + HSO^-_4 + H^+ \text{ (R. 28)}$$
$$2H^+ + 2e^- \leftrightarrow H_2 \text{ (R. 29)}$$
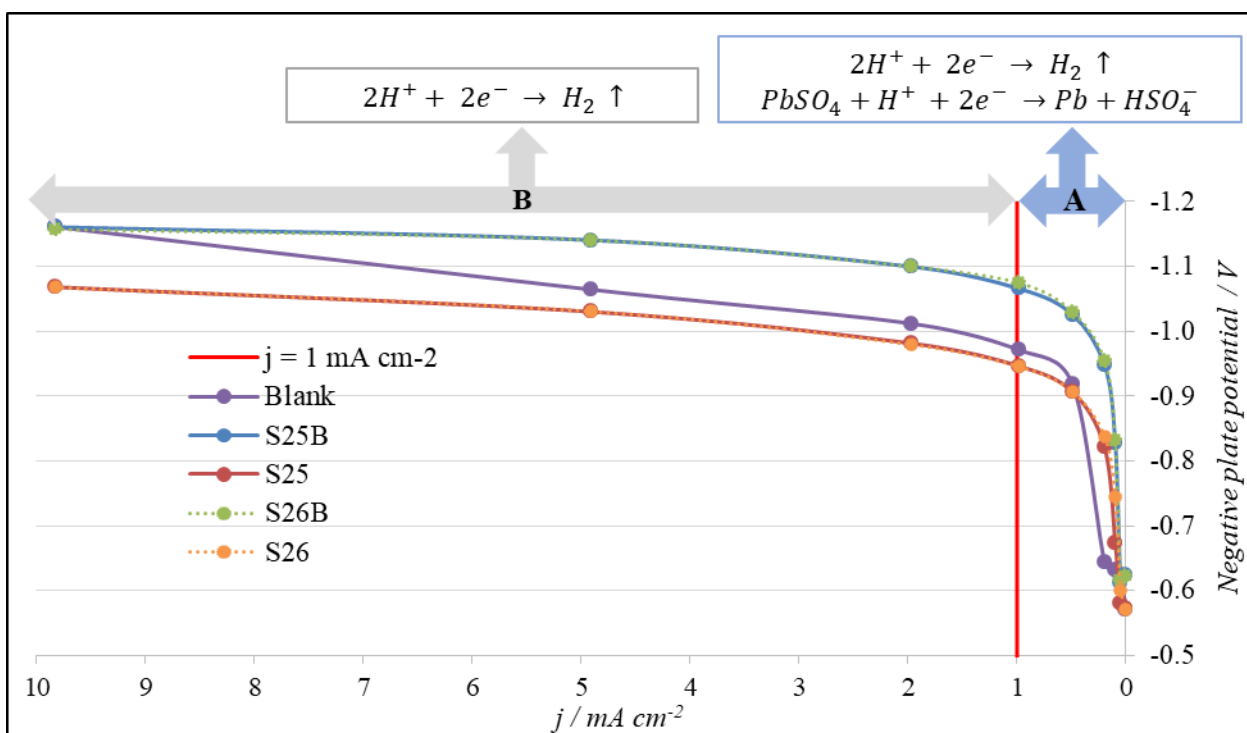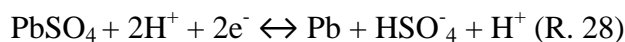
Figure 81. Batch 3. Negative polarization curves. The negative plate potential was measured vs Ag/AgCl reference electrode.

According to the relationship between the negative plate potential and the current density we can know which reactions were taking place at different current densities. Analyzing this relationship from **Figure 81** two zones can be differentiated in the graphic:

- **Zone A – j < 1 mA cm^{-2}**. No linear relationship between the potential and the current density was found. This meant the coexistence of two reactions at the same time: lead sulfate reduction (R. 28) and HER (R. 29).
- **Zone B – j > 1 mA cm^{-2}**. Linear relationship between the potential and the current density was found. This meant the predominance of just one reaction: HER (R. 29). At current

171

densities higher than 1 mA cm^{-2} the HER starts, and had the predominance at higher current densities as well.

According to these results, the reference current density, that was considered the point where HER was the only reaction taking place at the negative plate was 1 mA cm^{-2}. At this point, the negative plate overpotential, named as $\eta_{app,H2}$, was calculated as:

$$\eta_{app,H2} = E_{1\ mA\ cm-2} - E_0$$

Where $E_{1\ mA\ cm-2}$ was the potential of the negative plate at current density equal to 1 mA cm^{-2}, and E_0 was the potential of the negative plate at current density equal to 0 mA cm^{-2}, i.e. at the beginning of the test, when no current was passing through the cell. The $\eta_{app,H2}$ are listed in **Table 38**, in ascending order (absolute value).

The lowest $\eta_{app,H2}$ were related to highest water consumption: low overpotential indicated that the energy barrier that has to be overcome for producing hydrogen is low, so more hydrogen will be produced and the cell will have a higher water consumption.

In batch 3, GANFg mixtures, S25 and S26 showed practically equal $\eta_{app,H2}$, values as well as the lowest ones, i.e. GANFg addition increased the HER rate. Blank mixture showed higher water consumption degree than mixtures S25B and S26B, and lower water consumption degree than S25 and S26. So again, addition of OE decreased the HER rate, due to the migration problems of the protons when they were trying to reach the lead surface through the OE layer to reach the lead surface to be reduced. Addition of GANFg increased the HER rate, because of the impurities content of GANFg, which catalyzed the HER reaction. These were exactly the same results obtained for the float currents analyses. Therefore, we can corroborate these statements.

Table 38. Batch 3. $\eta_{app,\ H2}$ for all the mixtures. Values are
ordered from the lowest to the highest $\eta_{app,\ H2}$ (absolute value).
Water consumption degree is also showed.

Mixture	$\eta_{app\ H2}$ / V	Water consumption degree
S25	-0.374	Highest
S26	-0.375	
Blank	-0.401	
S25B	-0.423	
S26B	-0.431	Lowest

If we compare these results with Batch 2 results (**Table 30**) we can see that the S7 $\eta_{app,\ H2}$ was higher in that case, suggesting the increase of the water consumption when OE2 was added to the NAM, instead of just OE1.

4.3.10. Cycles at PSoC type 2

The cycle life test at PSoC type 2 (**section 3.11.6**) was performed for all the mixtures. Results are showed in **Figure 82**. Before doing any comparison between batch 3 and batches 1 and 2, it is important to notice that in the case of batch 3 the test was performed in different conditions; because of that it was called "cycle life test at PSoC type 2". In the case of the test type 2, the 2 V / 1 Ah cells started the test at 50% of SoC, so no comparison can be done between batch 3 and batches 1 and 2.

Results in **Figure 82** showed that the GANFg mixtures, S25 and S26, fulfilled the highest number of cycles. So the first conclusion was that GANFg addition improved the cycle life of the 2 V / 1 Ah cells. This result was expected: when GANFg were added to the NAM they became part of the NAM skeleton during the formation process. In this way, the NAM skeleton electrical conductivity was increased which was essential when the plate was highly discharged. Why? GANFg electrical resistivity was equal to $1 \cdot 10^{-4}$ Ohm m, whereas lead electrical resistivity was $2.08 \cdot 10^{-7}$ Ohm m, so when the plate was charged, the lead was more conductive than the GANFg, and no effect of GANFg addition can be appreciated. However, when the plate was sulfated, there were three species in the NAM: $PbSO_4$, an insulator, Pb and GANFg, conductive materials. In these conditions the current could pass through the Pb and GANFg, and being better distributed throughout the negative plate. This led to a better charge acceptance, i.e. an increase of the Pb^{2+} reduction rate, and a longer cycle life.
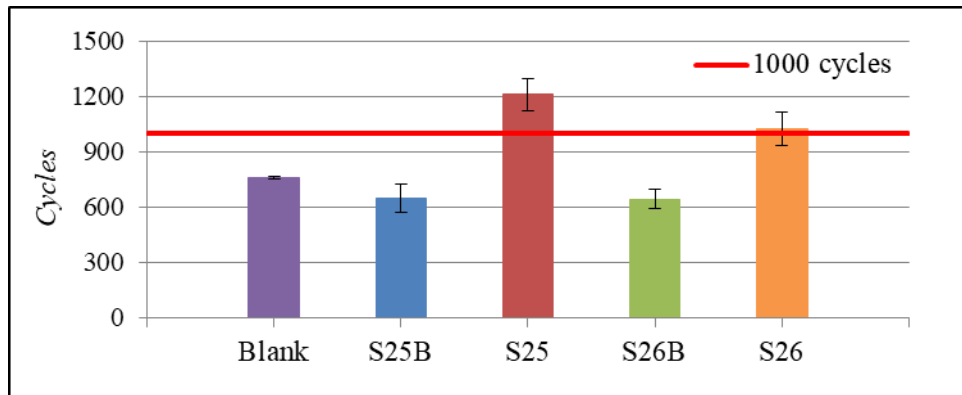
Figure 82. Batch 3. Results for the PSoC cycles type 2. Results: 762 (Blank), 649 (S25B), 1209 (S25), 644 (S26B), 1025 (S26). Error bars related to the standard deviation of the measurements.

As mixture S26 fulfilled less number of cycles than mixture S25, lower OEs concentration led to a reduction in cycle life. Although, this difference was not appreciated for mixtures S25B and S26B, giving rise to the theory that when a carbon material was added the OE behaved differently. This fact was not new: it is known that the OE can be adsorbed on the carbon material surface due to the interaction of the organic groups [91], and in this case, its performance is impaired. So in this case, when GANFg and OEs were added, some OE can remain attached to the GANFg surface leading to a decrease in the cycle life.

In the case of the blank mixture, it can be observed that this mixture performed more number of cycles than OEs mixtures, S25B and S26B. Again the non-beneficial effect of the addition of OEs in the charge acceptance of the negative plates came out. In the case of the blank mixture, the Pb^{2+} had no OEs layer to cross, so the Pb^{2+} reduction rate was higher in comparison with mixtures S25B and S26B, as well as the cycle life.

4.3.11. Cycled plates physcochemical properties

After the cycles at PSoC type 2, the 2 V / 1 Ah cells were recharged according to **section 3.11.1.** This recharge was done in order to see the amount of irreversible lead sulfate crystals remaining in the plates. After the recharge, the cycled negative and positive plates were removed from the cells, washed and dried (**section 0**).

The XRD analyses (**section 3.13.5**) of the negative cycle plates were done. XRD patterns are showed in **Figure 83**.
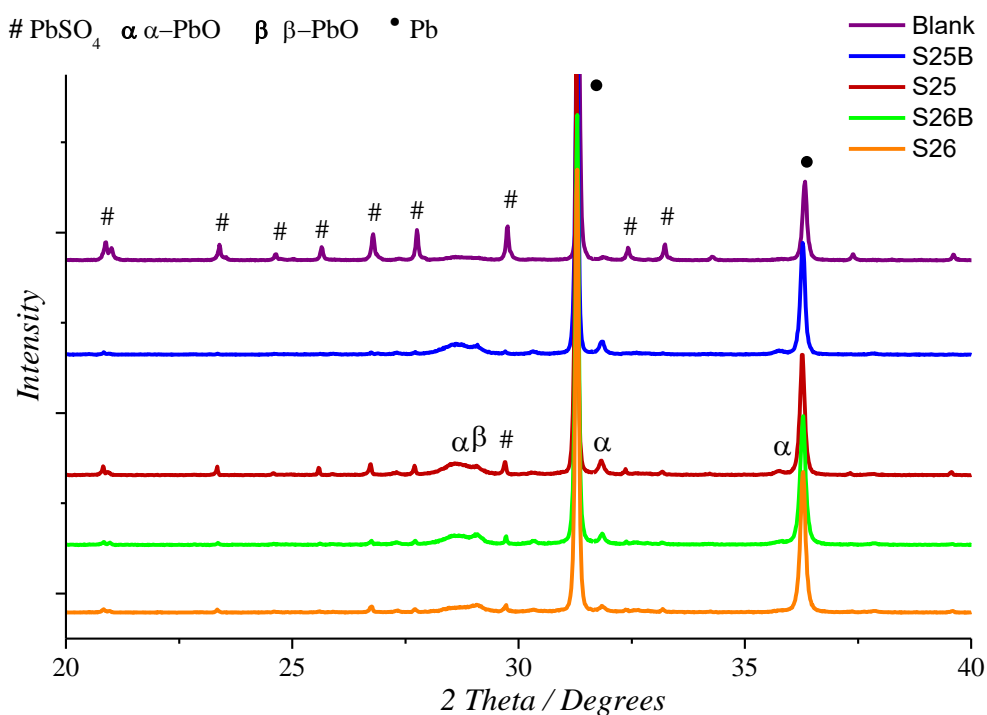
Figure 83. Batch 3. XRD patterns for the cycled negative plates.

The cycled negative plates were made of Pb mainly, but other species were also found: α-PbO, β-PbO, $PbSO_4$. In these conditions, the presence of $PbSO_4$ was more pronounce that in the case of the formed negative plates (**Figure 76**), completely expected due to the cycle life test. Again, α-PbO and β-PbO were also present in the cycled negative plates for all mixtures except for the Blank mixture. These compounds were already found in the formed negative plates (**Figure 76**), and it was already explained in that sections that GANFg and OEs were able to reduce the median pore diameter of the NAM, leading to the absence of

174

SO_4^{2-} inside the pores. In this way, when lead was being reduced to Pb^{2+}, PbO was formed instead of $PbSO_4$. According to the XRD patterns, Blank mixture showed the highest $PbSO_4$ concentration, so the highest amount of irreversible $PbSO_4$ crystals.

For confirming the existence of these irreversible lead sulfates, the lead sulfate content of the cycled negative plates was analyzed according to **section 3.13.2**. The carbon content was also analyzed, as well as the BET SSA (**section 3.13.4**). Results are showed in **Table 39**.

The carbon content did not change from the formed (**Table 37**) to the cycled negative plates. This meant that the carbon can resist the oxidant conditions suffered during the discharges of the cycle life test without degrading. In the case of the Blank mixture, the carbon content was higher for the cycled negative plates (0.10 wt. % higher). This difference was not taken into consideration due to equipment limitations.

The lead sulfate content results were as expected after the XRD analyses. Blank mixture showed the highest lead sulfate concentration. So the biggest lead sulfate crystals were formed in this type of plate: through the cycles more lead sulfate has been accumulated on the surface of these negative plates. This is in line with the fact that this mixture did not contain any OEs that suppressed the formation of the lead sulfate passivating layer. The other mixtures showed lower lead sulfate concentrations, higher for the GANFg mixtures, S25 and S26: these mixtures fulfilled higher number of cycles, so more irreversible lead sulfate was formed in these plates. However, the irreversible lead sulfate amount did not seem enough to impair the cycle life test. In order to find the failure mode of this test the lead sulfate content of the positive plates was also analyzed (see **Table 37**). As can be seen in the table the cycled positive plates were more sulfated than the negative ones. It has been also established by J. Albers [92] that the softening of the PAM leads to the sulfation of the plates and the failure of the AGM and Flooded LABs during this type of test (cycles at PSoC type 2). Even if the positive plates were the responsible of the failure of the cells, the same positive plates were used for all the mixtures, so the differences among the number of cycles can only be related to the negative plate's properties.

The BET SSA of the cycled negative plates is showed in **Table 39**. In comparison with the BET SSA values obtained for the formed negative plates (see **Table 37**), the BET SSA has been reduced for all the mixtures because of the cycle life test. However, this reduction was only significant for GANFg mixtures, from 0.72 to 0.41 m^2 g^{-1}, in the case of S25, and from 0.66 to 0.38 m^2 g^{-1}. A lower BET SSA means bigger lead crystals, so accumulation of these crystals during the charge process. In this case bigger lead crystals have been formed due to the reduction of the active sites where lead can be reduced. As was explained for the formed negative plates, GANFg increased the number of activated sites where Pb^{2+} can be formed. After the cycle life test, some of these sites can be covered by the irreversible lead

sulfate crystals, and fewer amounts of small Pb crystals were formed. As a result the BET SSA decreased.

Table 39. Batch 3. Physicochemical properties of the cycled negative plates: carbon and lead sulfate content, and BET SSA. Lead sulfate content of the cycled positive plates. The cells were recharged after the cycle life test. Number of cycles performed by each mixture is also indicated.

Mixture	Cycles	Negative cycled plates			Positive cycled plates
		Carbon content / wt. %	$PbSO_4$ content / wt. %	BET SSA / $m^2 \, g^{-1}$	$PbSO_4$ content / wt. %
Blank	762	0.20	10.60	0.22	15.60
S25B	649	0.28	2.45	0.44	23.00
S25	1209	0.34	4.40	0.41	6.60
S26B	644	0.30	2.45	0.45	27.80
S26	1025	0.38	3.30	0.38	14.10

*Weighted percentage related to the total NAM mass.

4.3.12. NAM structure analyses after cell operation

The SEM micrographs of the formed and the cycled negative plates were obtained according to **section 3.13.6.** SEM micrographs are showed in **Figure 84.** The main difference among the SEM micrographs of the negative formed plates was between the Blank mixture and the rest of the mixtures: it was so clear that the absence of OEs led to a lower porous structure, made of big lead particles. The NAM structure of this mixture (Blank – F) was made of flat lead particles, which explained its low BET SSA (**Table 37**). Smaller lead particles can be observed for the 0.30 wt. % OEs mixtures (S25 – F and S25B – F), in contrast to the 0.20 wt. % OEs mixtures (S26 – F and S26B – F). It can be observed for the GANFg mixtures (S25 – F and S26 – F) a more condensed surface, suggesting a more activated surface for these mixtures.

For the cycled plates of mixtures Blank, S25B and S26B (Blank – C, S25B – C and S26B – C) it can be appreciated how the small particles from the surface has been lost due to the cycle life test, becoming part of the skeleton that supported these particles in the case of the formed plates. However, for the GANFg mixtures (S25 – C and S26 – C), the energetic structure was maintained but more agglomerates were found on the surface.
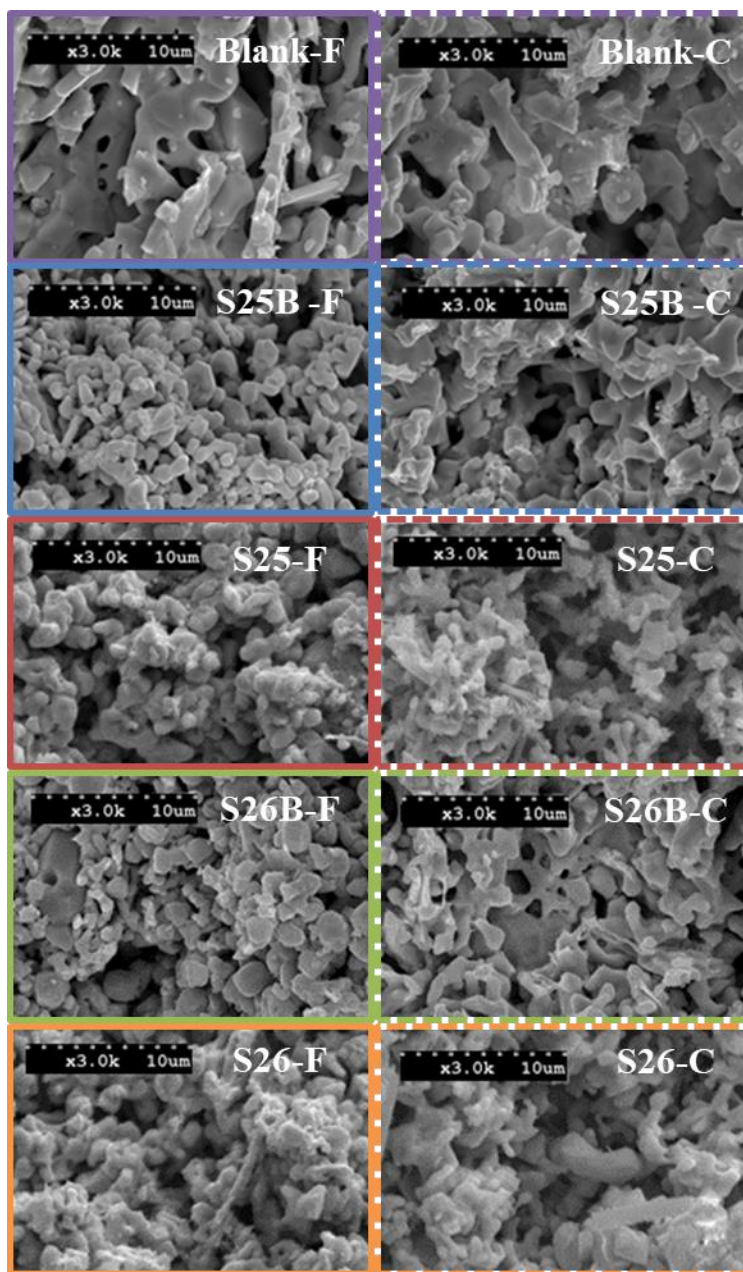
Figure 84. Batch 3. Negative plates SEM micrographs. **Left side (F – solid lines)**: formed negative plates (NAM after the formation process). **Right side (C – dashed lines)**: cycled negative plates (NAM after the 17.5% DoD cycle life test 2). Magnification: x3000.

4.3.13. Conclusions

The main target for batch 3, was to see the effect of a new type of OE, OE2, in the performance of the negative plate while adding also the optimum amount of GANFg (0.10 wt. %) in order to achieve high cycle life of the 2 V / 1 Ah cells while the water consumption was kept at a safe degree.

The main conclusions are listed below:

-   OEs and GANFg increased the BET SSA of the formed and unformed negative plates.
-   GANFg addition slightly improved the BET SSA of the formed negative plates. This result was linked to the introduction of GANFg in the bulk of the NAM skeleton. In this way a more electrical conductive system was created, which induced a higher amount of activated sites where Pb^{2+} can be reduced to give rise to many small lead crystals.
-   OEs reduced the passivation phenomena suffered by the negative plates during the capacity test and the CCA test where the OEs effect was more pronounced.
-   GANFg did not improve the charge acceptance. However, the absence of OEs in the blank mixture resulted in a high charge acceptance. Confirming the OEs impaired the charge acceptance due to delaying the migration of the Pb^{2+} ions.
-   GANFg increased the HER rate, and thus the water consumption because of their impurities content. OEs reduced the water consumption, due to delaying the migration of the H^+ ions.
-   OE2 increased the HER rate in a higher degree than OE1, according to Batch 2 results.
-   GANFg increased the cycle life of the 2 V / 1 Ah cells working in PSoC conditions. GANFg were able to act as a current carrier when the negative plate was extremely sulfated. The OEs performance during the cycle life test was impaired by the GANFg addition, most probably because the OE remained adsorbed on the GANFg surface.

As main conclusion, the optimum OEs concentration to be used for dispersing the GANFg and to work as an active polymer in the negative plate was 0.30 wt. %. The use of the mix of OEs together with GANFg improved the cycle life of the 2 V / 1 Ah cells, but did fail to improve the charge acceptance of the negative plates.

4.4.1. Aim of the study

As the charge acceptance of the negative plates was not improved by the addition of another type of OE, the next step was focused on improving the charge acceptance of the negative plates by adding carbon materials C1 and C4 used in the batch 1. On this purpose we maintained the GANFg dosage, and additionally add these carbon materials.

4.4.2. GANFg, OE1, Carbon C4 and Graphite C1 characteristics

The properties of GANFg were widely explained in **section 4.2.2**, as well as the properties C4 and C1 (**section 4.1.2**) and the properties of OE1 (**section 4.1.2 and section 4.3.2**). As a reminder, C4 was a carbon black with high BET SSA and C1 was an expanded graphite.

Table 40 shows the physicochemical properties of GANFg, C4 and C1. The BET SSA of the three carbon materials is showed in the table. GANFg and C4 showed similar BET SSA, in contrast to the expanded graphite C1. In the case of the particle size, both, C1 and C4, had higher particle size then GANFg, however GANFg had a fiber length of 30 μm, so finally the three carbon materials were considered high particle size carbon materials. This condition is important for the interaction of these materials with the NAM: high particle size carbon materials are introduced in the bulk of the NAM skeleton, independently of their concentration in NAM. Therefore the three carbon materials were expected to be found into the bulk of the NAM skeleton. In the case of the conductivity, we knew the exact electrical resistivity of the GANFg. For the C4, a carbon black, we have considered standard values showed in [93]. According to the explanation in [93] we have considered that the C1, an expanded graphite, had the same or lower electrical resistivity as the graphite [91]. So the most conductive material was C1.

Table 40. Batch 4. Physicochemical characteristics of GANFg, C4 and C1.

Carbon material	SSA / $m^2\,g^{-1}$	Particle size D_{50} / μm	Fiber diameter / μm	Fiber length / μm	Conductivity	Electrical resistivity / Ohm m
GANFg	105 – 115	0.005 – 0.200	20 – 80	Up to 30	Excellent	$1\cdot10^{-4}$
C4	120 – 180	11			Low	0.10 – 0.01
C1	18	28			Excellent	$\leq3\cdot10^{-7}$ (c-axis) $\leq4\cdot10^{-6}$ (a-axis)

4.4.3. Mixtures compositions and GANFg dispersions

Below we can see the final composition of the mixtures used for this batch:
- S44B: GANFg (0.10%) + OE1 (0.30%)
- S39: GANFg (0.10%) + OE1 (0.30%) + C4 (0.5%)
- S40: GANFg (0.10%) + OE1 (0.30%) + C1 (1.0%)

Different GANFg dispersions were prepared for each mixture of this batch. The dispersions were made by GAIKER following the procedure from **section 3.3.** In the case of dispersions S39 and S40 the procedure named "Dispersion made of GANFg, carbon materials and OE" was used, and no mother dispersion was needed as the initial amount of carbon material was high enough. All the dispersions were made using OE1 as a surfactant, and the same OE was used for the preparation of the negative pastes. The concentration of the carbon materials C4 and C1 was chosen according to the results obtained in batch 1: best results were found when C4 was added at 0.8% and C1 at 1.5%. As for this batch GANFg were also added we decided to low the carbon material concentration for this batch to 0.5% in the case of C4, and 1.0% in the case of C1. With these concentrations we expected to maintain the cycle life result obtained when GANFg were added at 0.10% in batches 2 and 3, and the charge acceptance obtained when C4 and C1 were added in batch 1.

The final composition of the dispersions is showed in **Table 41**. At first sight, it can be seen that just part of the carbon material was added to the dispersion. The rest was added during the mixing process.

Table 41. Batch 4. GANFg + OE1 + Carbon material dispersions: zeta potential and particle size.

Sample	H2O:OE1:C:GANFg / g*	Zeta Potential / mV	d / μm	d_{50} / μm	d_{90} / μm
S44B	100:0.6:1.0	-52.56 ± 2.58			
S39	100:0.6:3.0(**C4**):1.0	-49.58 ± 8.16	0.199 ± 0.015	0.090 ± 0.009	0.533 ± 0.013
S40	100:0.6:3.0(**C4**):1.0	-65.48 ± 2.29	12.682 ± 0.358	10.606 ± 0.411	28.403 ± 3.365

*C: Carbon material. C4 was used for S39 dispersion, and C1 was used for S40 dispersion.

The zeta potentials of the dispersions were provided by GAIKER and are showed in **Table 41**. Zeta potentials higher than ± 20 mV indicate high stability of the dispersion. So we can conclude that the dispersions were stable. In addition GAIKER analyzed the particle size of the dispersions S39 and S40. A summary of the particle size of these dispersions is showed in **Table 41**.

Figure 85 shows the particle size of the dispersion S39, measured with the equipment MASTERSIZER (**section 3.2.4**). It can be observed a bimodal particle size distribution, were the two peaks are located at 0.07 μm and 0.45 μm. These particles size were lower than the single carbon material particle sizes: GANFg had a length up to 30 μm, and C4 a particle size equal to 11 μm. This meant that these carbon materials were broken when they were dispersed together, as in the case of the dispersion S24 from batch 3, when GANFg were dispersed together with the OE1 and OE2 (**Figure 74**) the particle size distribution was also bimodal, but the peaks were located approximately at 0.1 μm and 1.0 μm.

This result was not surprising: C4 due to having a high particle size showed more difficulties to be dispersed. Actually, special procedure was performed for making this dispersion (also showed in **section 3.3**) because the viscosity increased a lot when C4 was used. This fact happened due to the high BET SSA of the C4. In this way, when it was added to the dispersion it adsorbed on its surface a big amount of water, drying the dispersion and increasing its viscosity. The friction between the particles occurred in a higher rate, and the final particle size was lower.
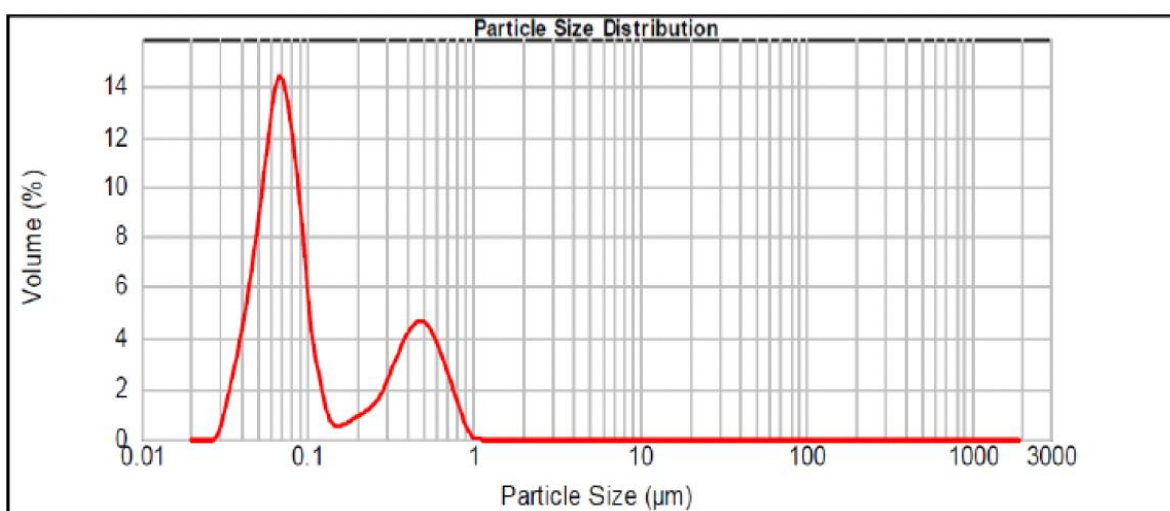
Figure 85. Batch 4. Particle size distribution for the dispersion S39. Analysis made by GAIKER.

Figure 86 shows the particle size of the dispersion S40, measured with the equipment MASTERSIZER (**section 3.2.4**). In this case the particle size distribution was almost monomodal, although there were also a small fraction of particles with sizes between 0.05 μm and 0.5 μm. The maximum peak is located at 13 μm. This particle size was closer to the C1 particle size, 28 μm and GANFg length (up to 30 μm), but in this case the dispersion method was also responsible for breaking the particles but in a lower rate than in the case of dispersion S39. Moreover the incorporation of C1 to the dispersion was clear after the particle size distribution results, as the particles size for S40 were higher than the ones found for the dispersion S24 (**Figure 74**).

181
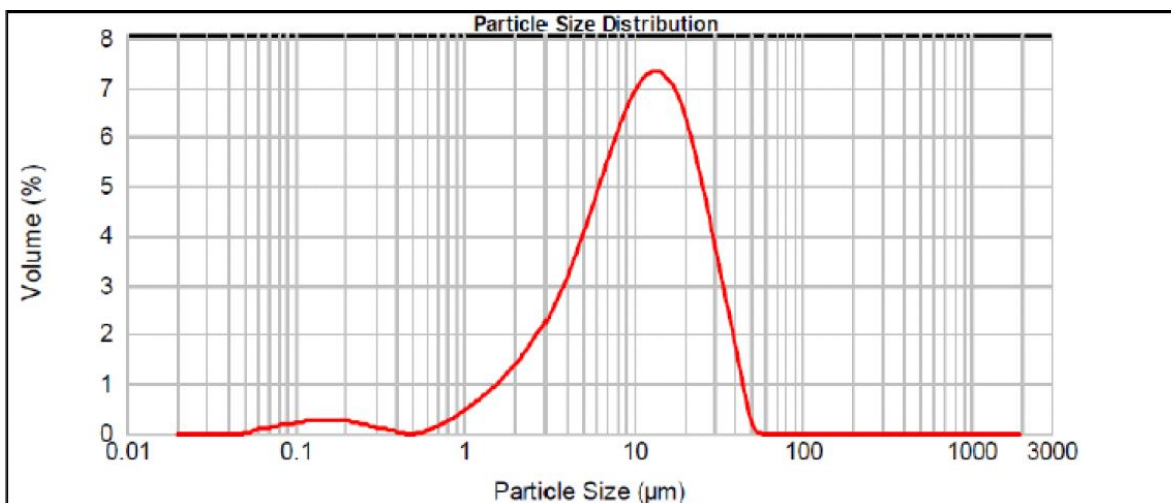
Figure 86. Batch 4. Particle size distribution for the dispersion S40. Analysis made by GAIKER.

4.4.4.Negative pastes and negative unformed plates characteristics

The negative pastes were prepared according to **section 3.5**. **Table 42** shows the final composition of the mixtures, i.e. the final amount of each ingredient used for preparing the negative pastes. In can be seen at the left column "Components added during the mixing process" the amount of carbon material added during the mixing process to reach their desired concentration in GANFg defined above.

Table 42. Batch 4. Composition of the dispersions and negative mixtures.

Mixture		Dispersion / g					Components added during the mixing process / g							
Batch	Name	H$_2$O	GANFg	OE1	Carbon		LO	H$_2$O	H$_2$SO$_4$*	PAC Fiber	BaSO$_4$	OE1	Carbon	
4	S44B	100	1.0	0.6			1000	35	46	2.2	10	2.4		
	S39				C4	3.0		35					C4	2.0
	S40				C1	3.0		35					C1	7.0

*Acid density equal to 1.4 g cm^{-3}.

After the mixing process the density of the pastes were measured (see **Table 43**). Among the density values, S44B mixture showed lowest values in comparison with mixtures S39 and S40. Carbon materials uptook more amount of water on their surface, increasing the paste density. The uptaken water was directly related to the BET SSA of the carbon material, therefore S39 showed higher paste density due to containing a higher BET SSA carbon material.

After preparing the pastes, the grids were pasted to prepare the 1 Ah negative plates according to **section 3.6**, and then the plates were cured according **to section 3.7**. The positive plates were also prepared according to the same sections. However, as these plates

182

were prepared according a standard procedure, and were not under study, their properties are not shown in this work.

The carbon content of the negative unformed plates was analyzed (according to **section 3.13.2**). Results are showed in **Table 43**. The final amount of carbon content depends on the OE, GANFg and carbon material of the mixture. For this batch, the mixtures were expected to contain a carbon content equal to: 0.40% for S44B, 0.90% for S39, and 1.40% for S40. Carbon content were very close to this values, so we did not expect to found hydrocerussite in the unformed negative plates as happened in the other batches. As a reminder: the carbon dioxide from the air can react with the lead hydroxide ($Pb(OH)_2$), forming which is known as Hydrocerussite ($2PbCO_3 \cdot 1PbO(OH)_2$), that can be found in the NAM as part of the lead Hydrocarbonate ($PbO \cdot 6PbCO_3 \cdot 3PbO(OH)_2$).

Table 43. Batch 4. Density of the pastes. Carbon and lead sulfate content, and BET SSA of the unformed negative plates.

Mixture	Paste density / g cm^{-3}	Unformed negative plates		
		Carbon content / wt. %	$PbSO_4$ content / wt. %	BET SSA / $m^2 g^{-1}$
S44B	4.12	0.50	5.50	2.37
S39	4.41	1.00	6.10	2.42
S40	4.33	1.45	6.10	2.30

*Weighted percentage related to the total NAM mass.

Nevertheless, the XRD analyses of the unformed negative plates were done (according to **section 3.13.5**). Results are showed in **Figure 87**. As expected, all the negative unformed plates were made mainly of α-PbO, β-PbO, $PbSO_4$, 3BS and Pb. In this case, for mixtures S39 and S40, the carbon diffraction peak at 26.50° (2θ) had different shape as the Hydrocerussite diffraction peak 34.16° (2θ), but the last one showed low intensities, confirming the existence of this compound in these plates at small concentrations. In the case of mixture S44B, the carbon diffraction peak at 26.50° (2θ) and the Hydrocerussite diffraction peak 34.16° (2θ) had a similar shape, confirming the formation of this compound during the mixing process for this mixture. It was very noticeable the high intensity of the carbon diffraction peak at 26.50° (2θ) for mixture S40: the intensity of this peak is directly related to the graphitization degree of the carbon. As mixture S40 contained 1.0% of C1, an expanded graphite, this peak showed a high intensity.
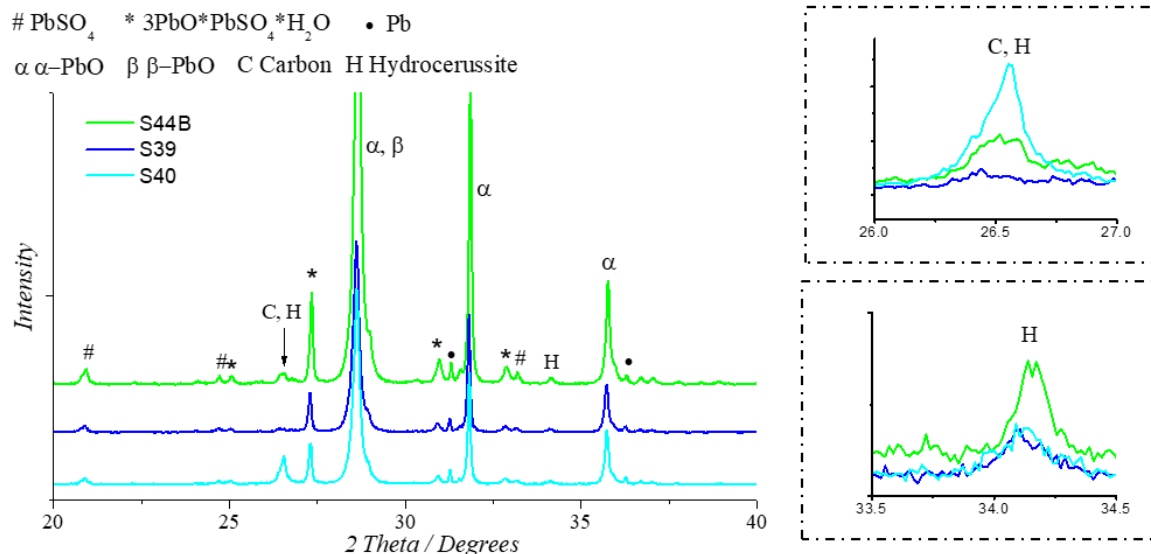
Figure 87. Batch 4. XRD patterns for the unformed negative plates for mixtures S44B, S39 and S40. **C, H peak (2θ: 26.0 – 27.0).** Zoom for the carbon (family of planes: 002) and Hydrocerussite (family of planes: 104) diffraction peaks around 2θ = 25.6°. **H peak (2θ: 33.5 – 34.5).** Zoom for the Hydrocerussite (family of planes: 110) diffraction peak at 2θ = 34.16°.

Table 43 also shows the lead sulfate content of the unformed negative plates; analyses made according to **section 3.13.2**. No significant differences were found among the difference mixtures, as the same amount of sulfuric acid was used for preparing all the pastes. The BET SSA of the unformed negative plates for all the mixtures appears also in **Table 43**. The data shows similar BET SSA for all the mixtures.

4.4.5. Negative formed plates characteristics

After analyzing the unformed negative plates the 2 V / 1 Ah cells were assembled (**section 3.8**) and formed (**section 3.9**). After the formation of the cells, the negative plates from two cells per type were taken out of the cells, washed and analyzed (**section 0**). Carbon content and lead sulfate content were analyzed (**section 3.13.2**), as BET SSA (**section 3.13.4**) of the formed negative plates. Results are showed in **Table 44**. Carbon content values were a little but lower after formation of the cells, in comparison with the unformed negative plates values (**Table 43**). This carbon content reduction was related to the reaction between Hydrocerussite and sulfuric acid during the soaking process whereby CO_2 was released. The carbon content differences were very low, as Hydrocerussite was found in the unformed negative plates (**Figure 87**) but at low concentrations. The XRD analyses were performed for confirming this theory.

The lead sulfate content of the formed negative plates (**Table 44**) was lower than the one found for the unformed negative plates (**Table 43**). This made sense, as during the formation process of the negative plate the lead sulfate was converted to lead. The lead sulfate content was higher for the mixture S44B, suggesting that the addition of C1 and C4 improved the efficiency of the formation process.

Table 44. Batch 4. Physicochemical properties of the formed negative plates: carbon content, lead sulfate content and BET SSA.

Mixture	Formed negative plates		
	Carbon content / wt. %	$PbSO_4$ content / wt. %	BET SSA / $m^2 g^{-1}$
S44B	0.40	4.20	0.80
S39	0.90	1.50	0.95
S40	1.30	2.00	0.86

*Weighted percentage related to the total NAM mass.

Figure 88 shows the XRD patterns for the formed negative plates of batch 4. As expected, no hydrocerussite was found in the formed negative plates, according to the flat area found at the surroundings of hydrocerussite diffraction peak at 34.16° (2θ). The formed negative plates were made of Pb mainly, but other species were also found: α-PbO, β-PbO, $PbSO_4$. The presence of $PbSO_4$ was also found in the chemical analyses of the formed negative plates (**Table 44**). As was showed in the table, mixture S44B contained a higher amount of lead sulfate, as it is corroborated by the XRD analyses: we can see in **Figure 88** that the $PbSO_4$ diffraction peak at 2θ = 26.7° was only intense for the mixture S44B. Moreover, carbon diffraction peak at 2θ = 26.5° was only intense for mixture S40. As was explained for the unformed negative plates, this mixture contained the carbon material C1, which was an expanded graphite. Therefore it was logical to find an intense carbon diffraction peak, as this peak is directly related with the graphitization degree of the carbon material. Although GANFg were also graphitized carbon materials, their content did not influence on the intensity of the carbon diffraction peak due to the low content of GANFg in NAM. α-PbO and β-PbO were present in the formed negative plates (**Figure 88**). This fact has been seen in batches 2 and 3, and it was related to the decrease of the median pore diameter of the NAM when GANFg were added (**section 4.3.5**). Higher amounts of α-PbO and β-PbO were found for mixtures S39 and S40, suggesting the further decrease of the median pore diameter of NAM when C1 and C4 were added. Among these two mixtures, S39 showed higher intensities for these peaks, so the median pore diameter of the NAM was lower when C4 was added. This finding was in line with the particle size of C4, lower than the particle size of C1. Moreover, dispersion S39 also showed lower particle sizes than dispersion S40. Smaller carbon material particles led to lower median pore diameters.
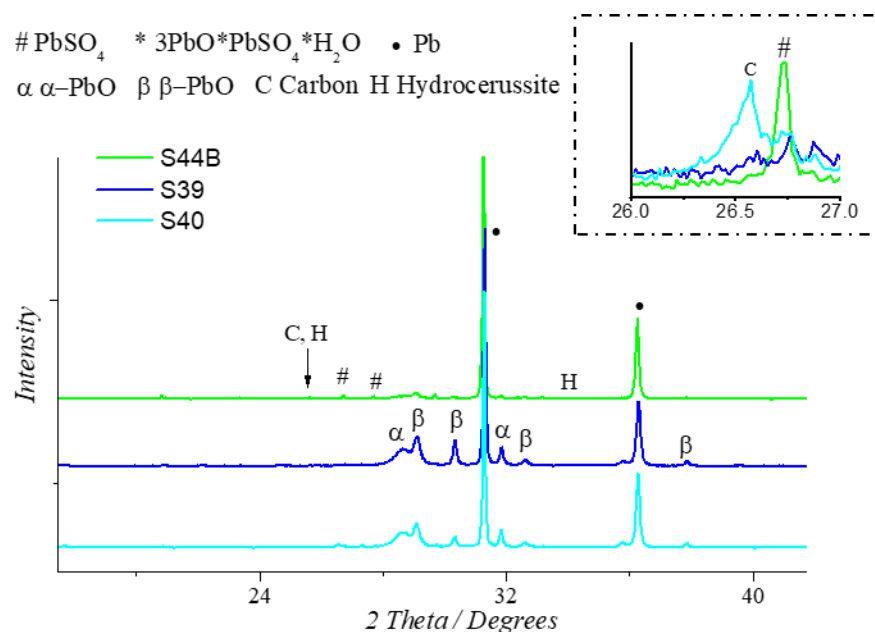
Figure 88. Batch 4. XRD patterns for the formed negative plates for mixtures S44B, S39 and S40. **C, PbSO$_4$ peak (2θ: 26.0 – 27.0).** Zoom for the carbon (family of planes: 002) diffraction peak at 2θ = 26.5° and PbSO$_4$ (family of planes: 021) diffraction peak at 2θ = 26.7°.

The BET SSA of the formed negative plates is also showed in **Table 44**. This magnitude has been reduced from the unformed (**Table 43**) to the formed negative plates. The unformed negative plates showed higher values as they were made of α-PbO, β-PbO, PbSO$_4$, 3BS and Pb, bigger molecules with larger surfaces. However the trend was similar for the unformed and formed negative plates: no significant differences were found, just a little bit higher BET SSA was found for mixture S39. The addition of carbon materials besides the addition of GANFg did not cause a very noticeable effect on the BET SSA of the formed negative plates. During the formation process these particles, GANFg, C1 and C4 due to having a high particle size acted as active sites for the Pb^{2+} reduction. In this way they became part of the NAM skeleton, being completely covered by lead particles. This behavior of these carbon materials in NAM did not contribute to the energetic structure of the NAM, and because of that no increase of the BET SSA of the formed negative plates was appreciated. Just a little bit higher BET SSA was appreciated for mixture S39, due to containing the highest surface area carbon material (C4). Some particles of this material could have been pushed to the surface increasing a little bit the surface area of the NAM.

4.4.6. Capacity test

After the formation, the first test done on the cells was the capacity test (**section 3.11.2**). This test was repeated twice. The second value was taken as reliable, as it was done after the first recharge of the cell. During this test the cells were discharged at 0.05 A (I$_{20}$) until

they reached the cutoff voltage (1.75 V). The test was supposed to last 20 h, if the cell capacity at 20 hour was equal to 1 Ah. During this test, the OEs played an important role, as they were responsible for avoiding the passivation of the negative plate surface, and increased the NAM utilization. As all the mixtures contained the same type and amount of OE, we did not expect significant differences among the mixtures. **Figure 89** shows the corresponding results. As can be seen no significant differences were found.
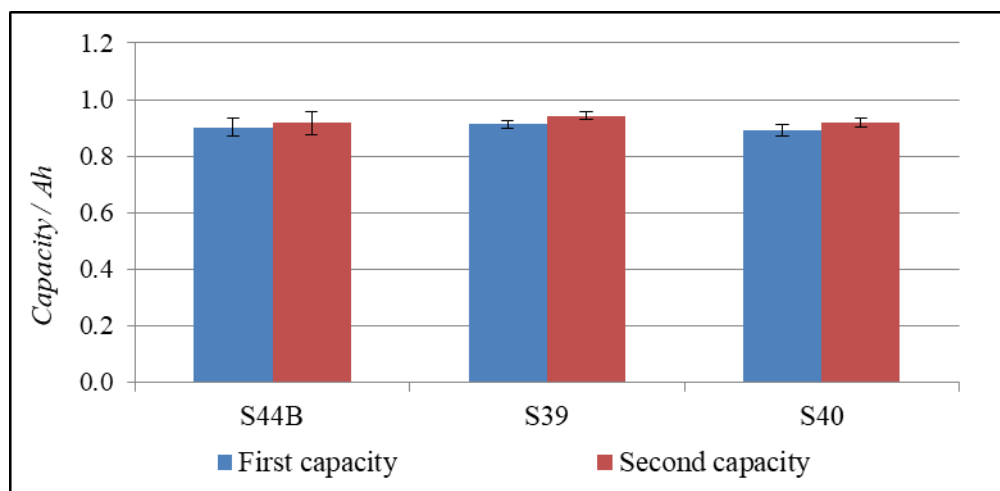
Figure 89. Batch 4. Results for the first and second capacity tests. Error bars related to the standard deviation of the measurements.

4.4.7. CCA test

After the first capacity test, and as well after the second capacity test, CCA tests were done (**section 3.11.3**). Results are showed in **Figure 90**. Again, the results of this test were linked to the OE performance, as in this case the test was a high rate discharge at extremely low temperature. This type of test involves a faster formation of the passivation layer, as the solubility of lead sulfate crystals decreased at lower temperatures collapsing the pores and impeding the continuity of the discharge. However, in this case the addition of carbon materials also played a key role: the OEs can adsorb on the carbon surfaces, which impairs the performance of the OE. As can be seen in the figure, carbon material mixtures, S39 and S40, showed lower results due to impairing the performance of the OE. In this case, mixture S40 showed the lowest results, due to containing the highest amount of carbon material.
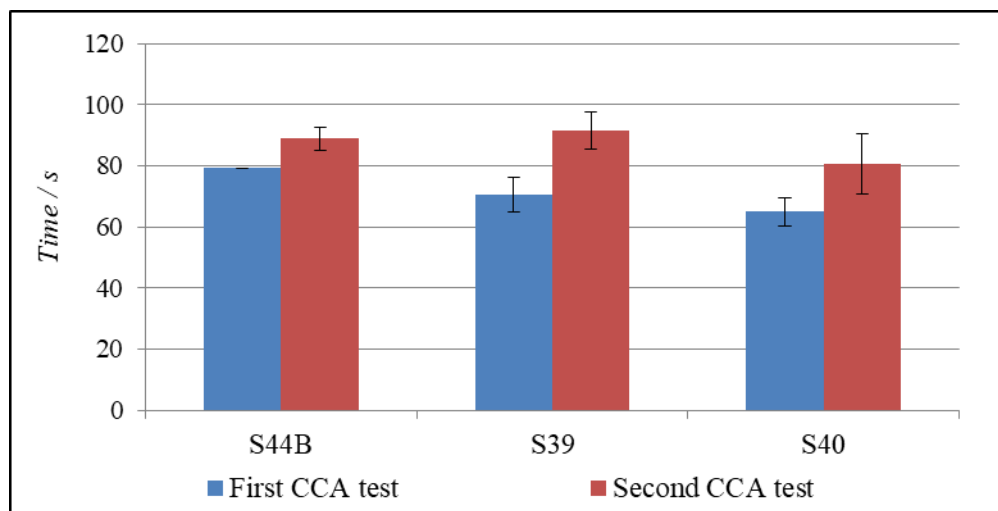
Figure 90. Batch 4. Results for the first and second CCA tests: time taken by the cell to reach 1 V during the discharge at 5 A and -18°C. Error bars related to the standard deviation of the measurements.

4.4.8. ICA test type 2

ICA test type 2 (**section 3.11.4**) was performed on the cells for analyzing how GANFg and carbon materials addition affected to the charge acceptance of the negative plates. This feature is important for the LAB in HEV, as they need to be efficiently recharged during the regenerative braking of the vehicle. During this test, the cells were discharged to 90% SoC, and then they were resting for a period of 24 h (for batches 1 and 2 the duration of the pause was 72 h). For this period the sulfation of the negative plate was supposed to occur. When this phenomenon happens, the reduction of Pb^{2+} is hampered, as less activated sites are available, and the charge acceptance of the negative plates decays. After the 24 h, the cells were recharged at constant voltage (2.42 V) and the current passing through the cell was measured. As reference parameter we took the current passing through the cell at the 5th second of charge. Results are showed in **Figure 91**. For understanding these results it is important to take into consideration that the Pb^{2+} reduction can take place at two different surfaces of the negative plate: on the GANFg, C1 and C4 surfaces (in this case) and on the lead surface [38]. For this batch it was also important to analyze the BET SSA results for the formed negative plates: as the similar BET SSA was found for all the mixtures, a little bit higher for mixture S39, the same charge acceptance was expected. Indeed, in **Figure 91** we can see the same trend as was seen in the case of the BET SSA of the formed negative plates (**Table 44**), no significant differences among the mixtures, and just a little bit higher result for mixture S39 due to containing the highest surface area carbon material. So the extra addition of carbon materials did not improve the charge acceptance of the plates. As was explained above, these materials (GANFg, C1 and C4) were expected to be located at the NAM skeleton, and not at the surface where they can improve the charge acceptance in a higher degree. In addition, it could be possible that the optimum dosage of the carbon

188

materials in NAM was not reach, and because of that it was not possible to notice a better performance of these materials during the charge acceptance test.
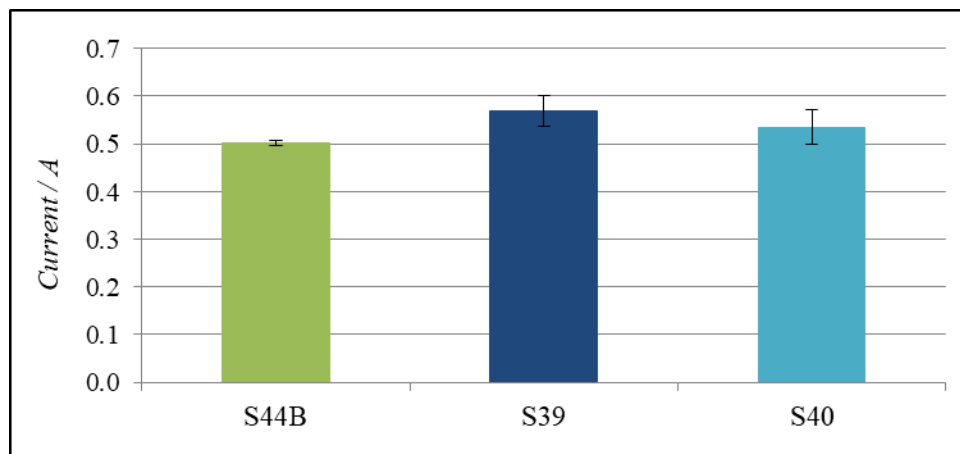
Figure 91. Batch 4. Results for ICA test type 2. Error bars related to the standard deviation of the measurements.

4.4.9. Water consumption study: float currents and negative plate polarization test

In order to evaluate the effect of GANFg and carbon materials addition on the water consumption in real batteries, different tests were performed: measurement of the float currents during the recharge after the first and the second capacity and the negative polarization study.

After each capacity test a recharge of 24 h was done according to **section 3.11.1**. This recharges was done at constant current of 0.25 A (step A) until the cell reached 2.67 V. Then the cell voltage was maintained at 2.67 V until the total recharge time was equal to 24 h (step B). During step B the current passing through the cells was decreasing, as the amount of $PbSO_4$ to recharge was getting lower. At the final period of step B the current remained steady, as all the $PbSO_4$ had been already converted to Pb, the only reaction taking place at the negative plates was the HER. At this point the steady current is also known as float current. Due to this argument, the float currents can be directly linked to the HER rate, and thus to the water consumption. For batch 3 the float currents were measured and they are showed in **Figure 92**.

Figure 92. Batch 4. Float currents during the recharge of the cells after the first and the second capacity test. Error bars related to the standard deviation of the measurements.

As can be seen in the figure, addition of carbon materials increased the HER rate. Even when these materials did not contribute to the charge acceptance of the plates, due to not contributing to the BET SSA of the formed negative plates, they were still present in the plates, where they can catalyze the HER reaction. In this way the HER rate was directly linked to the carbon material concentration in NAM. **Figure 93** shows the relationship between the float currents and the carbon concentration in NAM for the different mixtures, as well as the tendency line equation with the correlation coefficient (R^2). In this way it was clear the direct relation between the carbon content in NAM and the HER rate.
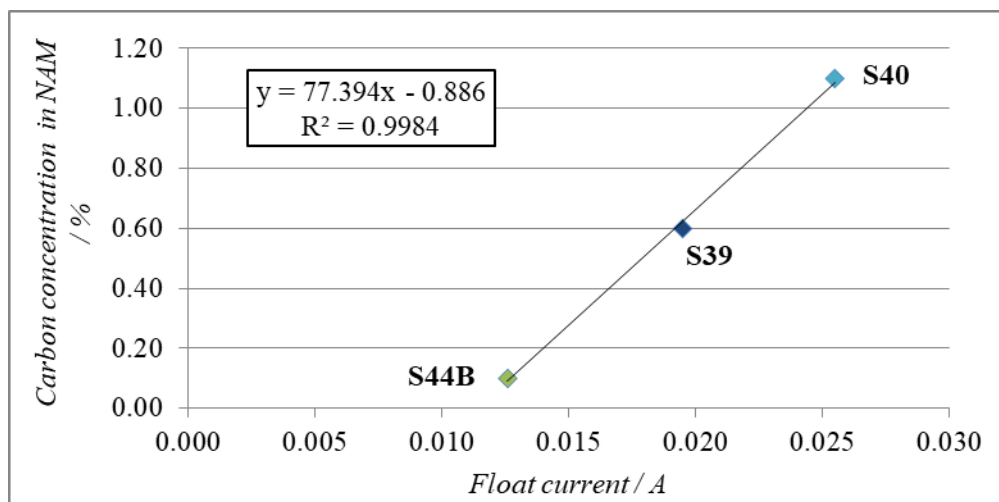
Figure 93. Batch 4. Carbon concentration vs float currents.

The negative polarization study was also performed according to **section 3.11.5**. The negative polarization study was also performed in order to see the effect of GANFg and carbon material addition on the HER rate. Before starting the test, the potential of the

negative plate inside the cell was measured with an Ag/AgCl reference electrode. During the test a set of charges at different constant currents were applied to the cells. At the end of each charging step, when the potential of the cell was constant, the potential of the negative plate was measured. Negative plate potentials for all the mixtures as a function of the current density passing through the cell are showed in **Figure 94**. As was explained in the former batch, just two reactions can take place in the negative plate while charging: lead sulfate reduction (R. 28) and HER (R. 29).

$$PbSO_4 + 2H^+ + 2e^- \leftrightarrow Pb + HSO^-_4 + H^+ \text{ (R. 28)}$$
$$2H^+ + 2e^- \leftrightarrow H_2 \text{ (R. 29)}$$
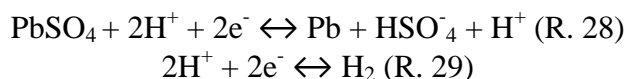
According to the relationship between the negative plate potential and the current density we can know which reactions were taking place at different current densities. Analyzing this relationship from **Figure 94** two zones can be differentiated in the graphic:

- **Zone A – j** < 1 mA cm^{-2}. No linear relationship between the potential and the current density was found. This meant the coexistence of two reactions at the same time: lead sulfate reduction (R. 28) and HER (R. 29).
- **Zone B – j** > 1 mA cm^{-2}. Linear relationship between the potential and the current density was found. This meant the predominance of just one reaction: HER (R. 29). At current densities higher than 1 mA cm^{-2} the HER starts, and had the predominance at higher current densities as well.
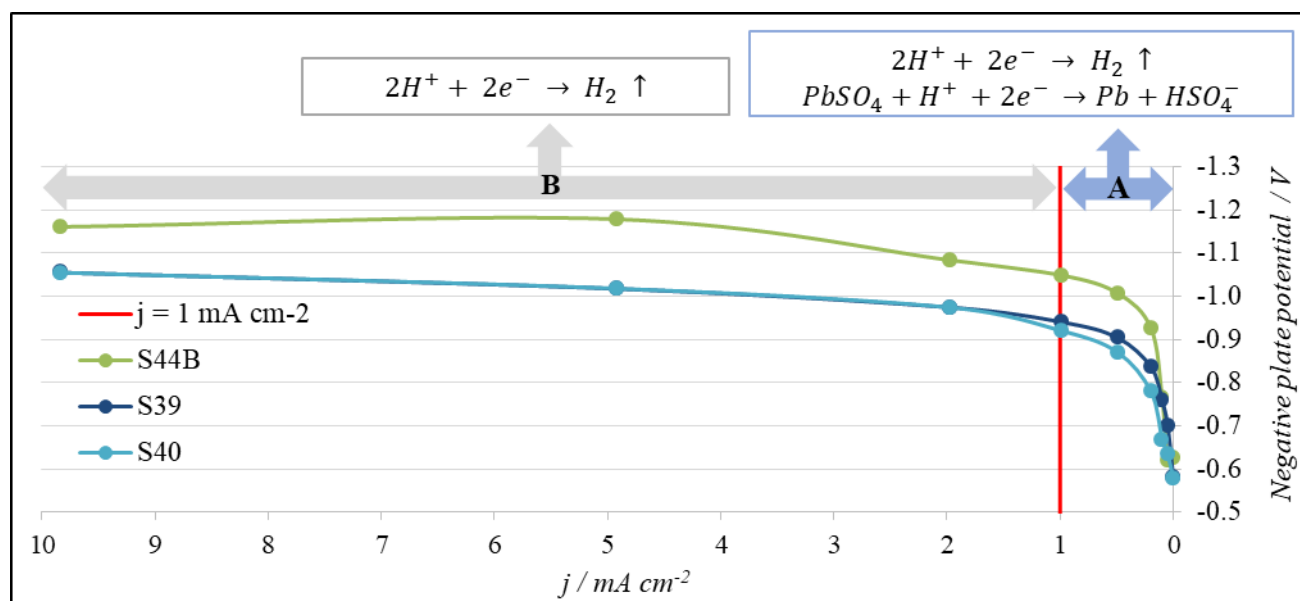
Figure 94. Batch 4. Negative polarization curves. The negative plate potential was measured vs Ag/AgCl reference electrode.

According to these results, the reference current density, that was considered the point where HER was the only reaction taking place at the negative plate was 1 mA cm^{-2}. At this point, the negative plate overpotential, named as $\eta_{app,H2}$, was calculated as:

$$\eta_{app,H2} = E_{1\ mA\ cm-2} - E_0$$

Where $E_{1\ mA\ cm-2}$ was the potential of the negative plate at current density equal to 1 mA cm^{-2}, and E_0 was the potential of the negative plate at current density equal to 0 mA cm^{-2}, i.e. at the beginning of the test, when no current was passing through the cell. The $\eta_{app,H2}$ are listed in **Table 45**, in ascending order (absolute value).

The lowest $\eta_{app,H2}$ were related to highest water consumption: low overpotential indicated that the energy barrier that has to be overcome for producing hydrogen is low, so more hydrogen will be produced and the cell will have a higher water consumption.

According to the table, mixture S40 developed the highest HER rate, although it showed practically equal $\eta_{app,H2}$ value as mixture S39. In the case of the float currents this difference was more noticeable. Mixture S44B showed the highest $\eta_{app,H2}$ (absolute value), so the lowest HER rate, therefore the lowest water consumption, as was already seen in the float currents analysis. So we can confirm that addition of carbon materials besides GANFg involved a higher HER rate, and higher carbon material dosage led to higher HER rate as well.

Table 45. Batch 4. $\eta_{app,\ H2}$ for all the mixtures. Values are ordered from the lowest to the highest $\eta_{app,\ H2}$ (absolute value). Water consumption degree is also showed.

Mixture	$\eta_{app\ H2}$ / V	Water consumption degree
S40	-0.3121	Highest
S39	-0.3169	
S44B	-0.4240	Lowest

4.4.10. Cycles at PSoC type 2

The cycle life test at PSoC type 2 (**section 3.11.6**) was performed for all the mixtures. Results are showed in **Figure 95**. These results can be compared to batch 2 results, as both batches performed exactly the same, which was not the case for batches 1 and 2.
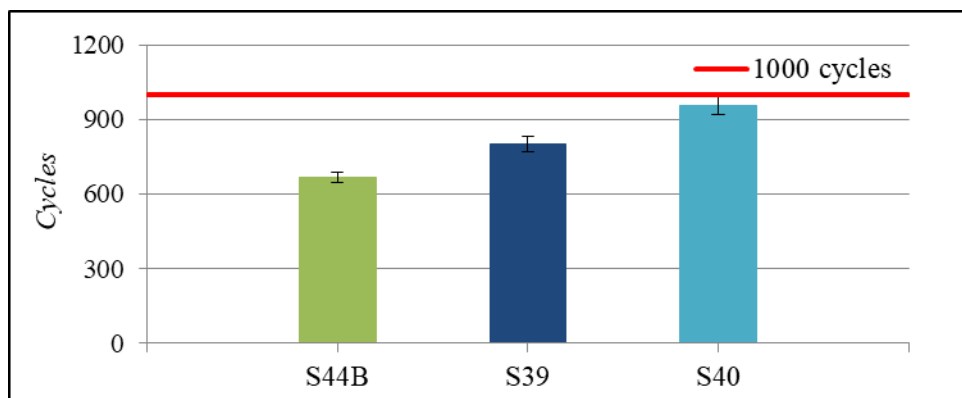
Figure 95. Batch 4. Results for the PSoC cycles type 2. Results: 667 (S44B), 801 (S39), 957 (S40). Error bars related to the standard deviation of the measurements.

Results in **Figure 95** showed that the carbon mixtures, S39 and S40, increased the cycle life of the 2 V / 1 Ah cells. In addition, as happened with the float currents, the number of cycles was directly proportional with the concentration of carbon materials in NAM (see **Figure 96**).
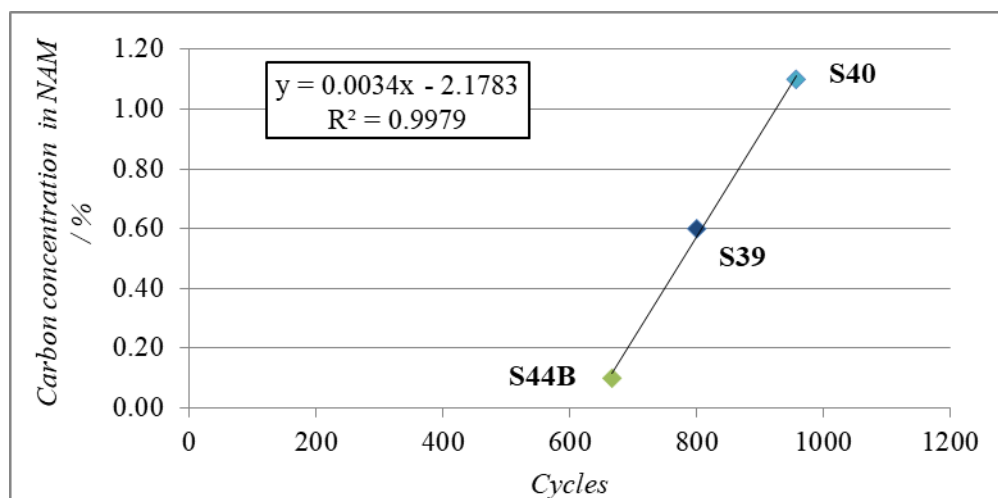
Figure 96. Batch 4. Carbon concentration vs number of cycles performed by the mixtures.

These results were very linked to the interaction of these carbon materials with the NAM. In this batch all carbon materials were located into the NAM skeleton, creating a more dynamic electrical and electrical conductive system. Carbon materials in the NAM skeleton, a part of improving the conductivity of the NAM skeleton, can act as electro osmotic pumps: the pores of the carbon materials are filled or emptied by H^+ and SO_4^{2-} ions during charge and discharge reactions. In this way the distribution of the electrolyte inside the negative plate is improved, as well as the formation of lead sulfate throughout the plate. In this way no big lead sulfate crystals are formed, and the sulfation of the negative plate is delayed.

193

The above explanation can be applied to the mixtures of this batch. Higher dosage of carbon increased the electro-osmotic effect of the carbon material in the NAM skeleton, leading to a higher cycle life. However, C1 and C4 had different BET SSA, so a linear relationship couldn't be expected as these materials should behave in a different way inside the NAM. In this case the electro-osmotic effect would be more remarkable for C4 mixture (S39) due to the higher BET SSA of this carbon material. However, there is another important property of the carbon materials: the electrical conductivity. While C1 acted in a lower degree as an electro-osmotic pump, it improved in a higher degree than C4 the conductivity of the NAM, leading to an increase of the electrochemical reactions yield.

4.4.11. Cycled plates characteristics

After the cycles at PSoC type 2, the 2 V / 1 Ah cells were recharged according to **section 3.11.1.** This recharge was done in order to see the amount of irreversible lead sulfate crystals remaining in the plates. After the recharge, the cycled negative and positive plates were removed from the cells, washed and dried (**section 0**).
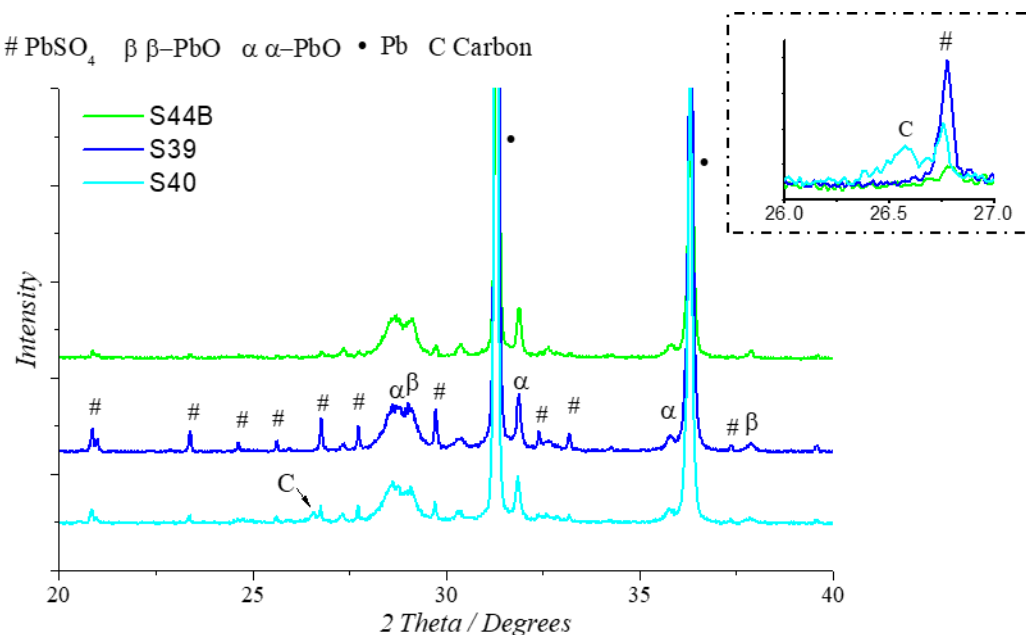
Figure 97. Batch 4. XRD patterns for the cycled negative plates for mixtures S44B, S39 and S40. **C, PbSO$_4$ peak (2θ: 26.0 – 27.0).** Zoom for the carbon (family of planes: 002) diffraction peak at 2θ = 26.5° and PbSO$_4$ (family of planes: 021) diffraction peak at 2θ = 26.7°.

The XRD analyses (**section 3.13.5**) of the negative cycle plates were done. XRD patterns are showed in **Figure 97**. The cycled negative plates were made of Pb mainly, but other species were also found: α-PbO, β-PbO, PbSO$_4$. Again, α-PbO and β-PbO were also present in the cycled negative plates for all mixtures. These compounds were already found in the formed negative plates (**Figure 88**), and it was already explained in that sections that GANFg and carbon materials were able to reduce the median pore diameter of the NAM, leading to the formation of PbO due to the absence of SO$_4^{2-}$ in the pores. According to the

194

XRD patterns, S39 mixture showed the highest $PbSO_4$ concentration, so the highest amount of irreversible $PbSO_4$ crystals. The carbon diffraction peak was still noticeable for mixture S40, corroborating that the graphitic structure of C1 was not lost during the cycles.

For confirming the existence of these irreversible lead sulfates, the lead sulfate content of the cycled negative plates was analyzed according to **section 3.13.2**. The carbon content was also analyzed, as well as the BET SSA (**section 3.13.4**). Results are showed in **Table 46**.

The carbon content did practically not change from the formed (**Table 44**) to the cycled negative plates. This meant that the carbon can resist the oxidant conditions suffered during the discharges of the cycle life test without degrading.

The lead sulfate content was relatively low and very similar for all the mixtures. This led to the conclusion that the negative plates were perfectly recharged after the cycle life test, as the amount of irreversible lead sulfate was so low. As happened in batch 3, the sulfation of the negative plate was not the failure mode of the test. Again we analyzed the positive plate lead sulfate content in order to prove that the sulfation of the positive plate was in this case the failure mode of the test (**Table 44**). As can be seen in the table the cycled positive plates were more sulfated than the negative ones, as happened in the batch 3. Therefore the sulfation of the positive plates was the failure mode of the test, as happened for AGM and Flooded LABs during this type of test [92]. Even if the positive plates were the responsible of the failure of the cells, the same positive plates were used for all the mixtures, so the differences among the number of cycles can only be related to the negative plate's properties.

Table 46. Batch 4. Physicochemical properties of the cycled negative plates: carbon and lead sulfate content, and BET SSA. Lead sulfate content of the cycled positive plates. The cells were recharged after the cycle life test. Number of cycles performed by each mixture is also indicated.

Mixture	Cycles	Negative cycled plates			Positive cycled plates
		Carbon content / wt. %	$PbSO_4$ content / wt. %	BET SSA / $m^2 g^{-1}$	$PbSO_4$ content / wt. %
S44B	667	0.45	2.95	0.72	18.30
S39	801	0.80	2.93	0.88	5.20
S40	957	1.25	2.50	0.79	8.50

*Weighted percentage related to the total NAM mass.

The BET SSA of the cycled negative plates is showed in **Table 46**. In comparison with the BET SSA values obtained for the formed negative plates (see **Table 44**), the BET SSA has

been slightly reduced for all the mixtures because of the cycle life test, but the tendency was exactly the same as in the formed negative plates. This also confirmed that the negative plates did not suffer during the test, and that the carbon materials were able to maintain the physicochemical properties of the negative plates.

4.4.12. NAM structure analyses after cell operation

The SEM micrographs of the formed and the cycled negative plates were obtained according to **section 3.13.6.** SEM micrographs are showed in **Figure 98.** The was not a big difference between the formed and the cycled negative plates, as the negative plates did not suffered a lot during the cycle life test.

S40 micrographs from formed to cycled negative plates were very similar; perhaps the surface of the formed plates looked more active than the one related to the cycled plates. In the case of S44B mixtures a more consolidated NAM skeleton was showed, in contrast to mixtures S39 and S40 where the NAM skeleton was made by interconnected agglomerates. This happened due to the introduction of the carbon materials in the NAM skeleton, which led to the formation of different structures inside the NAM skeleton. It could be observed also smaller particles on the surface of mixture S39. These small particles were the carbon particles that were pushed to the surface during the formation process.
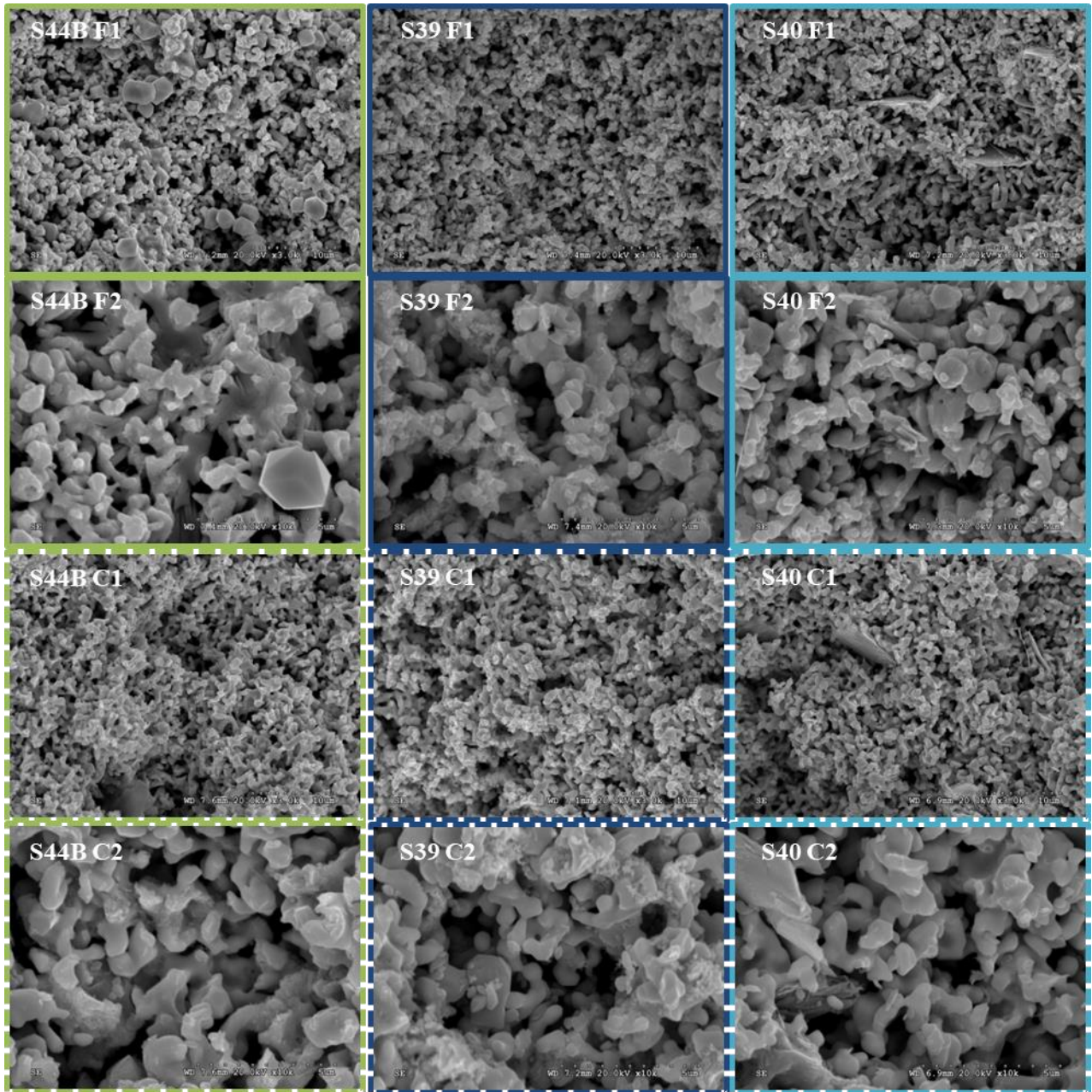
Figure 98. Batch 4. Negative plates SEM micrographs. **F – Solid lines:** formed negative plates (NAM after the formation process). **F1:** x3000. **F2:** x10000. **C – Dashed lines:** cycled negative plates (NAM after the 17.5% DoD cycle life test 2). **C1:** x3000. **C2**: x10000.

4.4.13. Conclusions

The main target for batch 4, was to see the effect if the extra addition of the carbon materials to the negative plates besides GANFg at 0.10% induced a higher charge acceptance of the negative plates.

The main conclusions are listed below:

- Addition of C1 and C4, besides GANFg slightly improved the BET SSA of the formed and unformed negative plates.
- C1, C4 and GANFg were introduced into the NAM skeleton. Their addition did not cause any effect on the energetic structure of NAM, just some C4 particles were pushed to the surface. Because of that the BET SSA of the formed negative plates was similar for all the mixtures.
- Addition C1 and C4 adsorbed the OE on their surfaces leading to a worse results during the CCA test. Higher carbon material concentration led to worse results in the CCA test.
- Addition C1 and C4 besides GANFg did not improve the charge acceptance. This was linked to the introduction of these carbon materials in the NAM skeleton, from where they were not able to improve this parameter.
- Addition of carbon materials increased the HER rate, and this increase was directly proportional to the carbon material concentration.
- Addition C1 and C4 besides GANFg increased the cycle life of the 2 V / 1 Ah cells working in PSoC conditions. This increase was directly proportional to the carbon material concentration. C1 increased the cycle life by improving the electrical conductivity of the NAM skeleton favoring the electrochemical reactions, and C4 was able to act as an electro-osmotic pump favoring the non-faradaic reactions.

As main conclusion, the charge acceptance of the negative plates was not improved with the addition of carbon materials besides GANFg. These findings meant that carbon material dosages must be higher for being noticeable in the charge acceptance of the plates. Addition of GANFg together with carbon materials led to higher cycle life, but after knowing that the charge acceptance was not improved, the addition of these materials will not be helpful for the LAB business.

5. Final conclusions / Conclusiones finales

The conclusions of the influence of the addition of carbon materials and organic expanders on the performance of the negative plate of EFB were the following:

1. Depending on the size and concentration of the carbon materials their performance on the negative plate changed. Those carbon materials with micrometer sizes were integrated into the lead skeleton, and were able to improve the cycle life of the 2 V / 1 Ah. The carbon material with nanometer size was pushed to the surface of the NAM becoming part of the energetic structure. This carbon material failed to improve the cycle life of the cells because of it was covered by lead sulfate crystals during the test.

2. Each type of carbon material had an optimum dosage that should be added to the NAM in order to see beneficial effects on the charge acceptance and the cycle life.

3. The best performance was obtained for the addition of expanded graphites. These materials were able to avoid the sulfation of the negative plate efficiently during the cycle life test, by improving the conductivity of the NAM skeleton and / or by inducing a hindrance effect that impeded the accumulation of lead sulfate crystals.

4. Addition of carbon nanofibers (GANFg) previously dispersed with organic expanders increased the cycle life of the 2 V / 1 Ah. Nanofibers failed to improve the charge acceptance of the cells because of they did not improve the electrochemical surface area of the NAM. Higher nanofibers dosages led to longer cycle life.

5. Carbon nanofibers were incorporated into the NAM skeleton because of having a length in the scale of micrometers. Due to their low electrical resistance, they increased the conductivity of the NAM skeleton. This fact led to an improvement in the current distribution throughout the negative plate during the cycle life test, impeding the accumulation of lead sulfate crystals.

6. The optimum nanofibers dosage was 0.10 wt. % related to the amount of leady oxide of the paste.

7. The optimum organic expanders concentration for dispersing the fibers and for working as an active polymer in the negative plate was 0.30 wt. %.

8. The use of the mix of organic expanders together with carbon nanofibers improved the cycle life of the 2 V / 1 Ah cells, but failed to improve the charge acceptance of the negative plates.

9. The charge acceptance of the negative plates was not significantely improved by the addition of carbon black or expanded graphite besides GANFg. This finding meant that the dosages of the expanded graphite or the carbon black must be higher for having a beneficial effect on the charge acceptance of the plates.

10. The addition of carbon materials always led to a higher hydrogen evolution reaction rate, which was directly proportional to the carbon material dosage. All carbon materials catalyzed the hydrogen evolution.

11. Addition of GANFg together with carbon materials led to higher cycle life, but after knowing that the charge acceptance was not improved, the addition of these materials together will not be helpful for the EFB business.

12. Organic expanders delayed the migration of the lead ions (II) during the charge of the cells, leading to a lower charge acceptance of the negative plates. Organic expanders can be adsorbed on the carbon materials surface, which impedes their beneficial effect.

Las conclusiones de la influencia de la adición de materiales de carbono y expanders orgánicos en el rendimiento de la placa negativa de las EFB fueron las siguientes:

1. El comportamiento de los materiales de carbono en la placa negativa depende del tamaño de partícula y de la concentración de los mismos. Los materiales de carbono de tamaño micrométrico se integraron en el esqueleto de plomo y aumentaron el número de ciclos de vida de las celdas de 2 V / 1 Ah. El material de carbono con tamaño nanométrico fue empujado a la superficie de la MAN, convirtiéndose en parte de la estructura energética. Este material de carbono se recubrió por cristales de sulfato de plomo durante el test de ciclos de vida, por lo que no logró mejorar el número de ciclos realizados por esta formulación.

2. Cada tipo de material de carbono debe ser añadido en una dosis óptima para ver efectos beneficiosos tanto en la aceptación de carga como en los ciclos de vida.

3. Los grafitos expandidos mostraron los mejores resultados. Estos materiales fueron capaces de evitar la sulfatación de la placa negativa de manera eficiente durante los ciclos de vida, mejorando la conductividad del esqueleto de plomo y / o induciendo un efecto estérico que impidió la acumulación de cristales de sulfato de plomo.

4. La adición de nanofibras de carbono (GANFg) previamente dispersadas con expanders orgánicos aumentó el número de ciclos de vida de las celdas de 2 V / 1 Ah. Las nanofibras no mejoraron la aceptación de carga de las celdas, debido a que no aumentaron la superficie específica de la MAN. Una mayor dosis de nanofibras condujo a la realización de un mayor número de ciclos.

5. Las nanofibras se incorporaron al esqueleto de plomo debido a mostrar una longitud del orden de micrómetros. Dada su baja resistencia eléctrica, aumentaron la conductividad de dicho esqueleto. Este hecho condujo a una mejora en la distribución de la corriente en toda la placa negativa durante los ciclos, impidiendo la acumulación de cristales de sulfato de plomo.

6. La dosis óptima de nanofibras fue de 0.10 wt. % en relación a la cantidad de óxido de plomo.

7. La concentración óptima de expanders orgánicos para dispersar las nanofibras y para trabajar como como un polímero activo en la placa negativa fue de 0.30 wt. %.

8. La mezcla de expanders orgánicos junto las nanofibras de carbón condujo a un aumento de los ciclos de vida de las celdas de 2 V / 1 Ah, pero no mejoró la aceptación de carga de las placas negativas.

9. La aceptación de carga de las placas negativas no mejoró significativamente con la adición de carbón black o grafito expandido además de GANFg. Este descubrimiento

significó que la concentración del grafito espandido o del carbón black ha de ser aumentada si se quiere ver un efecto beneficioso en la aceptación de carga de las placas negativas.

10. La adición de materiales de carbono siempre condujo a un mayor rendimiento de la reacción de evolución de hidrógeno. Dicho ratio fue directamente proporcional a la cantidad de carbón. Todos los materiales de carbón catalizan dicha reacción.

11. La adición de nanofibras de carbono conllevó la mejora de los ciclos de vida. Sin embargo, después de saber que este aditivo no mejoraba la aceptación de carga, se descartó su uso en las EFBs.

12. Los expanders orgánicos retrasan la migración de los iones de plomo (II) durante la carga de las celdas, conduciendo a una baja aceptación de carga de las placas negativas. Estos aditivos pueden ser absorbidos en la superficie de los materiales de carbono, lo que impediría su buen funcionamiento.

6. References

[1] OECD, OECD Glossary of Statistical Terms, (n.d.).
https://stats.oecd.org/glossary/about.asp.

[2] European Commission, EUROSTAT, (n.d.). https://ec.europa.eu/eurostat.

[3] European Environment Agency, Explaining road transport emissions. A non-technical guide, Luxembourg, 2016. doi:10.2800/71804.

[4] J.D. Naber, J.E. Johnson, Internal combustion engine cycles and concepts, Altern. Fuels Adv. Veh. Technol. Improv. Environ. Perform. (2014) 197–224. doi:10.1533/9780857097422.2.197.

[5] G. Fontaras, N.-G. Zacharof, B. Ciuffo, Fuel consumption and CO2 emissions from passenger cars in Europe – Laboratory versus real-world emissions, Prog. Energy Combust. Sci. 60 (2017) 97–131. doi:10.1016/J.PECS.2016.12.004.

[6] N. Hooftman, M. Messagie, J. Van Mierlo, T. Coosemans, A review of the European passenger car regulations – Real driving emissions vs local air quality, Renew. Sustain. Energy Rev. 86 (2018) 1–21. doi:10.1016/J.RSER.2018.01.012.

[7] I. Meyer, M. Leimbach, C.C. Jaeger, International passenger transport and climate change: A sector analysis in car demand and associated CO2 emissions from 2000 to 2050, Energy Policy. 35 (2007) 6332–6345. doi:10.1016/J.ENPOL.2007.07.025.

[8] D. Pavlov, Lead-Acid Batteries: Science and Technology, 2011.

[9] Macomb Community College, Center for Advanced Automotive Technology (CAAT), (n.d.). http://autocaat.org.

[10] C.Ş. Ioan-Adrian VIOREL, Loránd SZABÓ, Lars LÖWENSTEIN, INTEGRATED STARTER-GENERATORS FOR AUTOMOTIVE APPLICATIONS, Acta Electroteh. 45 (2004) 255–260. https://ie.utcluj.ro/acta-electrotehnica.html.

[11] A. Sakai, T. Miyazaki, T. Okano, K. Nimura, D. Nakata, Regenerative Braking Systems, in: Encycl. Automot. Eng., American Cancer Society, 2014: pp. 1–15. doi:10.1002/9781118354179.auto053.

[12] CARMAX, Rank. 8 Best Electr. Cars 2019 Rev. Photos, More. (2019). https://www.carmax.com/articles/best-electric-cars.

[13] C. Chumchal, D. Kurzweil, Lead–acid battery operation in micro-hybrid and electrified vehicles, Lead-Acid Batter. Futur. Automob. (2017) 395–414. doi:10.1016/B978-0-444-63700-0.00013-1.

[14] G. Planté, Nouvelle pile secondaire d'une grande puissance, in: Comptes rendus hebdomadaires des séances de l'Académie des sciences, Paris, La France, 1860: pp. 640–642. https://gallica.bnf.fr/ark:/12148/bpt6k3007r/f652.item.

[15] D.W.J. Sinsteden, Versuche über den Grad der Continuität und die Stärke des Stroms eines gröfsern magneto-elektrischen Rotations - Apparats und über die eigenthümliche Wirkung der Eisendrahtbündel in den Inductionsrollen dieser Apparate, Ann. Der Phys. Und Chemie. XCII (1854) 1–21.

https://gallica.bnf.fr/ark:/12148/bpt6k151777/f11.image.langDE.

[16]   J. Garche, On the historical development of the lead/acid battery, especially in Europe, J. Power Sources. 31 (1990) 401–406. doi:10.1016/0378-7753(90)80095-U.

[17]   G. Planté, Note sur la polarisation voltaïque, in: C. R. Hebd. Seances Acad. Sci., Paris, La France, 1859: pp. 402–405. https://gallica.bnf.fr/ark:/12148/bpt6k3006f/f404.image.

[18]   J.H. GLADSTONE, A. TRIBE, The Chemistry of the Planté and Faure Accumulators, Nature. 25 (1882) 221–223. doi:10.1038/025221a0.

[19]   H. Aron, Theorie der Akkumulatoren und Erfahrungen mit denselben, 2019.

[20]   O.S. Burheim, O.S. Burheim, Secondary Batteries, Eng. Energy Storage. (2017) 111–145. doi:10.1016/B978-0-12-814100-7.00007-9.

[21]   C.-H. Dustmann, Advances in ZEBRA batteries, J. Power Sources. 127 (2004) 85–92. doi:10.1016/J.JPOWSOUR.2003.09.039.

[22]   E.D. Wachsman, C.A. Marlowe, K.T. Lee, Role of solid oxide fuel cells in a balanced energy strategy, Energy Environ. Sci. 5 (2012) 5498–5509. doi:10.1039/C1EE02445K.

[23]   M. Gelbke, C. Mondoloni, Flooded starting-lighting-ignition (SLI) and enhanced flooded batteries (EFBs): State-of-the-art, Lead-Acid Batter. Futur. Automob. (2017) 149–184. doi:10.1016/B978-0-444-63700-0.00005-2.

[24]   J.R. Anderson, V.B. Tare, Reaction of Oxygen with Evaporated Films of Lead, J. Phys. Chem. 68 (1964) 1482–1489. doi:10.1021/j100788a036.

[25]   EIRICH, (n.d.). https://www.eirich.com/en/.

[26]   H.-J. Vogel, Vacuum- and air-cooled mixing of lead/acid battery paste: a comparison of the production results, J. Power Sources. 53 (1995) 269–271. doi:10.1016/0378-7753(94)02021-T.

[27]   MAC Engineering and Equipment Company (USA), (n.d.). https://www.mac-eng.com/.

[28]   HADI Maschinenbau, (n.d.). https://www.hadi.at/en/frontpage/.

[29]   N. Duc Hung, J. Garche, K. Wiesener, Beitrag zum mechanismus der oxydation von freiblei in bleiakkumulatorpaste bei der reifung, J. Power Sources. 17 (1986) 331–344. doi:10.1016/0378-7753(86)80054-4.

[30]   ENTEK, (n.d.). http://entek.com/.

[31]   DARAMIC, (n.d.). https://www.daramic.com/.

[32]   MICROPOROUS, (n.d.). https://microporous.net/.

[33]   Hollingsworth & Vosen, (n.d.). https://www.hollingsworth-vose.com/.

[34]   Exide Technologies, (n.d.). www.exide.com.

[35]   K. Peters, D.A.J. Rand, P.T. Moseley, Performance-enhancing materials for lead-acid battery negative plates, in: Lead-Acid Batter. Futur. Automob., Elsevier Inc., 2017: pp. 213–234. doi:10.1016/B978-0-444-63700-0.00007-6.

[36]   J. Settelein, J. Oehm, B. Bozkaya, H. Leicht, M. Wiener, G. Reichenauer, G. Sextl, The external surface area of carbon additives as key to enhance the dynamic charge acceptance of lead-carbon electrodes, J. Energy Storage. 15 (2018) 196–204. doi:10.1016/J.EST.2017.11.016.

[37]   Consequences of including carbon in the negative plates of Valve-regulated Lead–Acid batteries exposed to high-rate partial-state-of-charge operation, J. Power Sources. 191 (2009) 134–138. doi:10.1016/J.JPOWSOUR.2008.08.084.

[38]   T. Rogachev, P. Nikolov, G. Petkova, Mechanism of action of electrochemically active carbons on the processes that take place at the negative plates of lead-acid batteries, J. Power Sources. 191 (2009) 58–75. doi:10.1016/j.jpowsour.2008.11.056.

[39]   D. Pavlov, T. Rogachev, P. Nikolov, G. Petkova, Mechanism of action of electrochemically active carbons on the processes that take place at the negative plates of lead-acid batteries, J. Power Sources. 191 (2009) 58–75. doi:10.1016/j.jpowsour.2008.11.056.

[40]   P. Bača, K. Micka, P. Křivík, K. Tonar, P. Tošer, Study of the influence of carbon on the negative lead-acid battery electrodes, J. Power Sources. 196 (2011) 3988–3992. doi:10.1016/J.JPOWSOUR.2010.11.046.

[41]   K. Micka, M. Calábek, P. Bača, P. Křivák, R. Lábus, R. Bilko, Studies of doped negative valve-regulated lead-acid battery electrodes, J. Power Sources. 191 (2009) 154–158. doi:10.1016/J.JPOWSOUR.2009.01.014.

[42]   P. Křivík, K. Micka, P. Bača, K. Tonar, P. Tošer, Effect of additives on the performance of negative lead-acid battery electrodes during formation and partial state of charge operation, J. Power Sources. 209 (2012) 15–19. doi:10.1016/J.JPOWSOUR.2011.11.058.

[43]   D. Pavlov, P. Nikolov, Capacitive carbon and electrochemical lead electrode systems at the negative plates of lead–acid batteries and elementary processes on cycling, J. Power Sources. 242 (2013) 380–399. doi:10.1016/J.JPOWSOUR.2013.05.065.

[44]   J. Xiang, P. Ding, H. Zhang, X. Wu, J. Chen, Y. Yang, Beneficial effects of activated carbon additives on the performance of negative lead-acid battery electrode for high-rate partial-state-of-charge operation, J. Power Sources. 241 (2013) 150–158. doi:10.1016/J.JPOWSOUR.2013.04.106.

[45]   A.M.F. L.A. Riley, A.J. Sakshaug, Characterization of Carbons and Understanding Their Hydrogen Gassing Properties in Lead–acid Battery Negative Plates, ALABC Research Project 1012L Final Report, ALABC, Durham, NC, USA, (2012)., n.d.

[46]   M.O. A. DuPasquier, A. Korchev, D. Miller, B. Merritt, P. Atanassova, Carbon

Black Surface Modifications for Reduced Hydrogen Evolution, LABAT' 2017, Golden Sands Resort, Bulgaria, 13–16 June (2017)., in: Carbon Black Surf. Modif. Reduc. Hydrog. Evol., 2017. http://labatscience.com/f/publications/o/0/4ad3d749f39bd051f527cf43aa133cb8.pdf.

[47]   D. Pavlov, P. Nikolov, T. Rogachev, Influence of carbons on the structure of the negative active material of lead-acid batteries and on battery performance, J. Power Sources. 196 (2011) 5155–5167. doi:10.1016/j.jpowsour.2011.02.014.

[48]   S.E. Lebo Jr., J.D. Gargulak, T.J. McNally, Lignin, in: Kirk-Othmer Encycl. Chem. Technol., American Cancer Society, 2001. doi:10.1002/0471238961.12090714120914.a01.pub2.

[49]   D. von Borstel, G. Hoogestraat, W. Ziechmann, Efficiency of lignosulfonates and humic-related substances as expanders in negative electrodes of the lead/acid system, J. Power Sources. 50 (1994) 131–140. doi:10.1016/0378-7753(93)01892-L.

[50]   B.D. McNicol, D.A.J. Rand, Power sources for electric vehicles, in: Elsevier, Amsterdam; New York, 1984.

[51]   E.J. Ritchie, Addition Agents for Negative Plates of Lead-Acid Storage Batteries: II . Pure Organic Compounds , J. Electrochem. Soc. . 100 (1953) 53–59. doi:10.1149/1.2781082.

[52]   A.C. Zachlin, Functions and Behavior of the Components of Expanders for the Negative Plates of Lead-Acid Storage Batteries, J. Electrochem. Soc. 98 (1951) 325–333. doi:10.1149/1.2778215.

[53]   D. Pavlov, B.. Myrvold, T. Rogachev, M. Matrakova, A new generation of highly efficient expander products and correlation between their chemical composition and the performance of the lead–acid battery, J. Power Sources. 85 (2000) 79–91. doi:10.1016/S0378-7753(99)00386-9.

[54]   M. Matrakova, T. Rogachev, D. Pavlov, B.. Myrvold, Influence of phenolic group content in lignin expanders on the performance of negative lead–acid battery plates, J. Power Sources. 113 (2003) 345–354. doi:10.1016/S0378-7753(02)00547-5.

[55]   K. Nakamura, M. Shiomi, K. Takahashi, M. Tsubota, Failure modes of valve-regulated lead/acid batteries, J. Power Sources. 59 (1996) 153–157. doi:10.1016/0378-7753(95)02317-8.

[56]   L.H.V. A.F. Hollenkamp, W.G.A. Baldsing, S. Lau, O.V. Lim, R.H. Newnham, D.A.J. Rand, J.M. Rosalie, D.G. Vella, Overcoming Negative-Plate Capacity Loss in VRLA Batteries Cycled Under Partial State-of-Charge Duty, ALABC Project N1.2 Final Report, July 2000–June 2002, n.d.

[57]   D.P. Boden, D.V. Loosemore, M.A. Spence, T.D. Wojcinski, Optimization studies of carbon additives to negative active material for the purpose of extending the life of VRLA batteries in high-rate partial-state-of-charge operation, J. Power Sources. 195 (2010) 4470–4493. doi:10.1016/j.jpowsour.2009.12.069.

[58] J. Valenciano, A. Sánchez, F. Trinidad, A.F. Hollenkamp, Graphite and fiberglass additives for improving high-rate partial-state-of-charge cycle life of valve-regulated lead-acid batteries, J. Power Sources. 158 (2006) 851–863. doi:10.1016/j.jpowsour.2005.11.058.

[59] P.T. Moseley, High rate partial-state-of-charge operation of VRLA batteries, J. Power Sources. 127 (2004) 27–32. doi:10.1016/j.jpowsour.2003.09.005.

[60] M.L. Soria, J.C. Hernández, J. Valenciano, A. Sánchez, F. Trinidad, New developments on valve-regulated lead–acid batteries for advanced automotive electrical systems, J. Power Sources. 144 (2005) 473–485. doi:10.1016/j.jpowsour.2004.11.005.

[61] E. Ebner, D. Burow, J. Panke, A. Börger, A. Feldhoff, P. Atanassova, J. Valenciano, M. Wark, E. Rühl, Carbon blacks for lead-acid batteries in micro-hybrid applications – Studied by transmission electron microscopy and Raman spectroscopy, J. Power Sources. 222 (2013) 554–560. doi:10.1016/j.jpowsour.2012.08.089.

[62] M. Calábek, K. Micka, P. Křivák, P. Bača, Significance of carbon additive in negative lead-acid battery electrodes, 2006. doi:10.1016/j.jpowsour.2005.11.022.

[63] P. Tong, R. Zhao, R. Zhang, F. Yi, G. Shi, A. Li, H. Chen, Characterization of lead (II)-containing activated carbon and its excellent performance of extending lead-acid battery cycle life for high-rate partial-state-of-charge operation, J. Power Sources. 286 (2015) 91–102. doi:10.1016/j.jpowsour.2015.03.150.

[64] S.W. Swogger, P. Everill, D.P. Dubey, N. Sugumaran, Discrete carbon nanotubes increase lead acid battery charge acceptance and performance, J. Power Sources. 261 (2014) 55–63. doi:10.1016/j.jpowsour.2014.03.049.

[65] N. Sugumaran, P. Everill, S.W. Swogger, D.P. Dubey, Lead acid battery performance and cycle life increased through addition of discrete carbon nanotubes to both electrodes, J. Power Sources. 279 (2015) 281–293. doi:10.1016/j.jpowsour.2014.12.117.

[66] R. Marom, B. Ziv, A. Banerjee, B. Cahana, S. Luski, D. Aurbach, Enhanced performance of starter lighting ignition type lead-acid batteries with carbon nanotubes as an additive to the active mass, J. Power Sources. 296 (2015) 78–85. doi:10.1016/j.jpowsour.2015.07.007.

[67] Q. Long, G. Ma, Q. Xu, C. Ma, J. Nan, A. Li, H. Chen, Improving the cycle life of lead-acid batteries using three-dimensional reduced graphene oxide under the high-rate partial-state-of-charge condition, J. Power Sources. 343 (2017) 188–196. doi:10.1016/j.jpowsour.2017.01.056.

[68] S. Logeshkumar, R. Manoharan, Influence of some nanostructured materials additives on the performance of lead acid battery negative electrodes, Electrochim. Acta. 144 (2014) 147–153. doi:10.1016/j.electacta.2014.08.080.

[69] L. Wang, W. Zhang, L. Gu, Y. Gong, G. Cao, H. Zhao, Y. Yang, H. Zhang,

Tracking the morphology evolution of nano-lead electrodeposits on the internal surface of porous carbon and its influence on lead-carbon batteries, Electrochim. Acta. 222 (2016) 376–384. doi:10.1016/j.electacta.2016.10.189.

[70] L.T. Lam, H. Ceylan, N.P. Haigh, T. Lwin, Influence of residual elements in lead on oxygen- and hydrogen-gassing rates of lead-acid batteries, J. Power Sources. 195 (2010) 4494–4512. doi:10.1016/j.jpowsour.2009.12.020.

[71] Yuasa, YUASA - AGM & EFB Automotive Batteries Explained, (n.d.). https://www.yuasa.co.uk/info/technical/agm-efb-explained/.

[72] A. Cooper, J. Furakawa, L. Lam, M. Kellaway, The UltraBattery—A new battery design for a new beginning in hybrid electric vehicle energy storage, J. Power Sources. 188 (2009) 642–649. doi:10.1016/J.JPOWSOUR.2008.11.119.

[73] Grupo Antolin, (n.d.). http://www.grupoantolin.com.

[74] GAIKER, Technological center GAIKER, (n.d.). http://www.gaiker.es/ing/index.aspx.

[75] Universidad Autónoma de Madrid, Department of Applied Physical Chemistry, (n.d.). http://www.uam.es/ss/Satellite/Ciencias/en/1234888218714/1242652474305/generic o/detalle/Department_of_Applied_Physical_Chemistry.htm.

[76] M. Blecua, E. Fatas, P. Ocon, J. Valenciano, F. de la Fuente, F. Trinidad, Influences of carbon materials and lignosulfonates in the negative active material of lead-acid batteries for microhybrid vehicles, J. Energy Storage. 11 (2017) 55–63. doi:10.1016/j.est.2017.01.005.

[77] M. Blecua, E. Fatas, P. Ocon, B. Gonzalo, C. Merino, F. de la Fuente, J. Valenciano, F. Trinidad, Graphitized Carbon Nanofibers: new additive for the Negative Active Material of Lead Acid Batteries, Electrochim. Acta. 257 (2017) 109–117. doi:10.1016/J.ELECTACTA.2017.10.067.

[78] G. ANTOLIN, GUPO ANTOLIN, (n.d.). http://www.grupoantolin.com/en.

[79] Metrohm, Autolab PGSTAT204, (n.d.). https://www.metrohm.com/en/products/electrochemistry/autolab-compact-line/PGSTAT204.

[80] IKA, Tube Mill control, (n.d.). https://www.ika.com/en/Products-Lab-Eq/Mills-Lab-mills-Grinding-mill-csp-194/Tube-Mill-control-cpdt-4180000/.

[81] ELTRA ELEMENTAL ANALYZERS, ELTRA CS-800, (n.d.). http://www.metalco.cz/user/related_files/carbon--sulfur-analyzer-cs-800.pdf.

[82] E.W. Washburn, The Dynamics of Capillary Flow, Phys. Rev. 17 (1921) 273–283. doi:10.1103/PhysRev.17.273.

[83] S. Brunauer, P.H. Emmett, E. Teller, Adsorption of Gases in Multimolecular Layers, J. Am. Chem. Soc. 60 (1938) 309–319. doi:10.1021/ja01269a023.

[84] R.J. Hill, Calculated X-ray powder diffraction data for phases encountered in lead/acid battery plates, J. Power Sources. 9 (1983) 55–71. doi:10.1016/0378-7753(83)87015-3.

[85] N. Iwashita, C.R. Park, H. Fujimoto, M. Shiraishi, M. Inagaki, Specification for a standard procedure of X-ray diffraction measurements on carbon materials, Carbon N. Y. 42 (2004) 701–714. doi:10.1016/j.carbon.2004.02.008.

[86] J. Vera-Agullo, H. Varela-Rizo, J.A. Conesa, C. Almansa, C. Merino, I. Martin-Gullon, Evidence for growth mechanism and helix-spiral cone structure of stacked-cup carbon nanofibers, Carbon N. Y. 45 (2007) 2751–2758. doi:10.1016/j.carbon.2007.09.040.

[87] M. Weisenberger, I. Martin-Gullon, J. Vera-Agullo, H. Varela-Rizo, C. Merino, R. Andrews, D. Qian, T. Rantell, The effect of graphitization temperature on the structure of helical-ribbon carbon nanofibers, Carbon N. Y. 47 (2009) 2211–2218. doi:10.1016/j.carbon.2009.03.070.

[88] A. Muñoz Babiano, Estudio de la influencia de aditivos de base sílice en baterías de plomo-ácido. Mejora del funcionamiento en estado parcial de carga, Universidad Autónoma de Madrid, 2008. https://repositorio.uam.es/bitstream/handle/10486/1588/14790_muñoz_babiano_almudena.pdf?sequence=1&isAllowed=y.

[89] M. Blecua, A.F. Romero, P. Ocon, E. Fatas, J. Valenciano, F. Trinidad, Improvement of the lead acid battery performance by the addition of graphitized carbon nanofibers together with a mix of organic expanders in the negative active material, J. Energy Storage. 23 (2019) 106–115. doi:10.1016/J.EST.2019.03.012.

[90] A. Duran, J.F. González-Sánchez, J.M. Fernández, R. Sirera, Í. Navarro-Blasco, J.I. Alvarez, Influence of Two Polymer-Based Superplasticizers (Poly-naphthalene Sulfonate, PNS, and Lignosulfonate, LS) on Compressive and Flexural Strength, Freeze-Thaw, and Sulphate Attack Resistance of Lime-Metakaolin Grouts, Polymers (Basel). 10 (2018). doi:10.3390/polym10080824.

[91] P.T. Moseley, D.A.J. Rand, A. Davidson, B. Monahov, Understanding the functions of carbon in the negative active-mass of the lead–acid battery: A review of progress, J. Energy Storage. (2018). doi:10.1016/j.est.2018.08.003.

[92] J. Albers, E. Meissner, 6 - Automotive absorptive glass-mat lead–acid batteries: State of the art, in: J. Garche, E. Karden, P.T. Moseley, D.A.J. Rand (Eds.), Lead-Acid Batter. Futur. Automob., Elsevier, Amsterdam, 2017: pp. 185–211. doi:https://doi.org/10.1016/B978-0-444-63700-0.00006-4.

[93] R. Taherian, A. Kausar, R. Taherian, Application of Polymer-Based Composites: Bipolar Plate of PEM Fuel Cells, Electr. Conduct. Polym. Compos. (2019) 183–237. doi:10.1016/B978-0-12-812541-0.00007-0.

Annexes

i. *Influences of carbon materials and lignosulfonates in the negative active material of lead-acid batteries for microhybrid vehicles.*

ii. *Graphitized Carbon Nanofibers: new additive for the Negative Active Material of Lead Acid Batteries.*

iii. *Improvement of the lead acid battery performance by the addition of graphitized carbon nanofibers together with a mix of organic expanders in the negative active material.*

iv. *Loss on Ignition – How to check the purity level of a carbon material. Optimization of the method.*
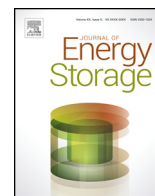
Influences of carbon materials and lignosulfonates in the negative active material of lead-acid batteries for microhybrid vehicles

M. Blecua[a], E. Fatas[a], P. Ocon[a,*], J. Valenciano[b], F. de la Fuente[b], F. Trinidad[b]

[a] Universidad Autónoma de Madrid, Departamento de Química Física Aplicada, C/Francisco Tomás y Valiente 7, 28049 Madrid, Spain
[b] Exide Technologies, R&D Centre, 19200 Azuqueca de Henares, Spain

A B S T R A C T

Lead-Acid batteries have been in continuous upgrade as they are required for new applications, such as stop-start function and regenerative braking for Micro-Hybrid vehicles. These issues are closely linked to cyclability and charge acceptance whose failure is directly related to a high sulfation of the negative plates. Carbon materials can be added to the negative active material to delay this sulfation, and other organic compounds, such as lignosulfonates, take part also in the improvement of these features. In this study, different types of carbon materials and lignosulfonates were used as additives for the negative active material, and negative plates have been prepared to assembly 2 V/1 Ah small lead acid cells. The cells performed several electrical tests: capacity, cold cranking, initial charge acceptance test, negative polarization study and cycling life in Partial State of Charge. At the same time, continuous physicochemical analyses of negative plates were carried out in order to evaluate their structure and composition. As a conclusion, those carbon materials that were are able to be introduced into the lead skeleton showed performance on charge acceptance by acting as super-capacitors, and on cycle life by reducing negative plate sulfation. The carbon material that was able to remain on the lead surface was able to increase charge acceptance, but failed to complete the cycle life test due to a high sulfation on its negative plates. The type of lignosulfonate and the electrochemical surface area supplied with the carbon materials had a strong influence on hydrogen evolution.

© 2017 Elsevier Ltd. All rights reserved.

1. Introduction

Micro-Hybrid vehicles have become a new opportunity for reducing fuel consumption and air pollution. Its technology is based on automatic start and stop functions and brake energy regeneration. In order to achieve this goal, 12 V batteries, denominated Enhanced Flooded Batteries (EFB), are continuously introducing new design changes [1]. EFB must be prepared to work at a High Rate Partial State of Charge (HRPSoC), taking into account that this condition provokes formation of big lead sulfate (PbSO$_4$) crystals, in the negative plates, which can't be converted efficiently to lead (Pb) leading to battery failure [2]. This sulfation is partially avoided by a group of additives denominated *expanders: lignosulfonate, carbon and barium sulfate*. In some cases, batteries also have to recover energy from braking; where charge acceptance becomes a critical parameter which also is limited by sulfation in the negative plate.

On the one hand, lignosulfonates avoid continuous formation of a PbSO$_4$ layer, acting as a surface active polymer [3]. They also take part in carbon degradation by oxygen from positive plate, which is strongly associated with water consumption [4]. Two types of lignosulfonates, with different dosages, are utilized in this paper. On the other hand, carbon materials are able to confer some properties to the Negative Active Material (NAM), such as increasing conductivity and/or surface area [5].

Due to the addition of carbon materials, the NAM electrochemical surface area is increased and the creation of isolated PbSO$_4$ crystals is facilitated, preventing the formation of a PbSO$_4$ continuous layer and increasing cycle life at HRPSoC. Increasing overall conductivity of NAM involves an increase of charge acceptance due to proper current flow through the plate. Furthermore, the addition of carbon materials with high specific surface area enhances charge acceptance by introducing a super-capacitor effect of the carbon [6,7].

Moseley et al. [5] also indicate that carbon materials act as an electroosmotic pump facilitating acid diffusion in the inner NAM. D. Pavlov et al. [8] establish that these additives must have high affinity for lead in order to be involved in battery performance.

They can be incorporated into the NAM by two ways: into the bulk of lead skeleton branches or on the lead phase surface, depending on particle size and concentration in NAM, respectively. Both ways can result beneficial for battery performance if these parameters are relatively low [8]. In addition, it has been proposed that electrochemical reduction of lead ions to lead in sulfuric acid is preferentially performed on electrochemically activated carbon surface [3].

Reactions of carbon materials [4] in Valve-Regulated Lead-Acid (VRLA) batteries indicate that at HRPSoC conditions, carbon can compete with lead to react with oxygen (oxygen cycle in positive plate) and water. As a result of carbon oxidation, the NAM electro-conductive system is lost (when carbon is incorporated into the bulk) and charge acceptance is impaired [8]. Products of the above reaction can be used to produce hydrogen (and raise water consumption) or recharge lead sulfate in the negative plate [4].

The addition of carbon materials can lower hydrogen evolution reaction (HER) overpotential in the negative plate [2], leading to water loss, which finally accelerates battery failure. For this reason, adequate type and dosage of the carbon materials are an important factor for water consumption prevention. Some studies based on activated carbon and carbon black addition, demonstrate the existence of an optimized dosage of carbon, which shows the best battery performance working at HRPSoC [7,9].

Different types of carbon materials at several concentrations have been tested as additives for the negative plate, confirming that both, the amount and the type of carbon material, are decisive for providing beneficial effects to the negative plates [10]. CSIRO laboratories in Australia have demonstrated that carbon black at concentrations from 0.2 to 2.0 wt.% in the negative plates increases the conductivity by some five orders of magnitude [11]. Low concentrations of graphite (1 wt.%) [12] and mixtures of flake graphite and carbon black [13] enhance cycle life at Partial-State of Charge (PSoC). However, flake graphite with low surface area does not improve cycle life at PSoC [7]. Differences between carbon black and graphite as additives for the negative plate have been studied by P.T. Moseley. This study shows better performance on HEV duty by those cells which contain graphite at 2.0 wt.% [14]. Other study shows that the optimum amount of expanded graphite is 1.50 wt.%, which makes possible to double the PSoC life of the battery by increasing charge acceptance [15]. New materials called Pb@C [2], made by high adhesion of Pb to carbon, are able to restraint hydrogen evolution while improving performance of the battery. Among other types of carbon materials, discrete Carbon NanoTubes (dCNT) have been used as an additive for NAM. They enhance charge acceptance, but hamper capacity and cold cracking performance; furthermore, a proper dispersion of this additive is completely necessary for a good performance [16]. Multi Wall Carbon Nano Tubes have also been tested as NAM additive for flooded lead acid battery Start Light Ignition (SLI). They are able to double the cycle life of real batteries [17].

In this paper, six mixtures that combine different types of carbon materials and two lignosulfonates were prepared in order

to study the influence of NAM in 2 V/1 Ah small lead acid cell performance. The electrical and structural characterizations were made and the different mixtures were compared depending on their performance on capacity, cold-cracking ability, charge acceptance, water consumption and cycle life at PSoC tests.

2. Experimental

2.1. Carbon additives and lignosulfonates to the negative active material

Five different carbon materials and two lignosulfonates (LS1 and LS2) were selected for this experiment. The BET Specific Surface Area (BET SSA) and particle size characteristics of the carbon materials and the sulfonation degree of the lignosulfonates were summarized in Table 1. Finally, six mixtures were selected in order to study their performance as NAM electrodes (Table 2). Also, BET SSA for the unformed negative plates of the different mixtures was included in Table 2.

2.2. Preparation of negative plates

Negative plates were prepared using lead oxide powder, Polyacrylic fiber (PAC), barium sulfate, deionized water, H_2SO_4 (1.40 g cm^{-3}), and different amounts of each carbon and lignosulfonate types; see Table 2. The weight percentage of Pb in leady oxide was $28 \pm 4\%$. Contents of PAC fiber, barium sulfate, deionized water and H_2SO_4 (1.40 g cm^{-3}) were 0.22 wt.%, 1 wt.%, 11.62 wt.% and 5.4 wt.% (weighted percentage is related to leady oxide), respectively. Paste preparation was carried out in a laboratory mixing machine. The procedure was as follows: firstly, leady oxide, PAC fiber, lignosulfonate and carbon material were stirred for a few minutes; then, deionized water was added and mixed for 5 min. Finally, H_2SO_4 was added to the mixture dropwise, and deionized water was used to adjust the consistency of the lead paste. A certain amount of paste was coated on a concast Pb-Sn grid with an area of around 10 cm^2 to prepare the negative plates. In order to complete the process, negative plates were introduced in a curing chamber for 24 h at 55 °C and 85% of relative humidity, during the first stage. In a second stage, temperature and relative humidity were set to 30 °C and 100%, respectively, for 24 h. After that, plates were dried at room temperature.

2.3. Assembly and formation of test cells

2 V/1 Ah small lead acid cells were prepared by one negative, and two positive plates, and a glass mat separator. All plates were compressed between two methacrylate sheets, and this assembly was partially submerged in H_2SO_4 (1.28 g cm^{-3}). The formation process was carried out at 40 °C, and was composed by an initial charge at constant current (0.35 A) for 13 h followed by several charges and discharges (−0.12 A/4.7 h, 0.24 A/3.0 h, 0.16 A/6.3 h, −0.24 A/2.5 h, 0.24 A/3.2 h, 0.12 A/4.2 h), in order to complete the

Table 1
Characteristics of the carbon materials and lignosulfonates added to NAM.

Carbon material	BET specific surface area/m^2 g^{-1}	Mean particle size D_{50}/μm	Conductivity
C1	18	28.0	Excellent
C2	25	11.6	Outstanding
C3	125	14.4	High
C4	120–180	11.0	Low
C5	1300–1550	<1	Low
Lignosulfonate		Degree of sulfonation[a]	
LS1		1.4	
LS2		0.9	

[a] Number of sulfonic acid groups per 1000 unit weight lignin.

Table 2
Carbon and lignosulfonate content for each mixture. BET specific surface area of unformed negative plates. Carbon factor and internal resistance after cell formation.

Mixture	Additive/wt.%[a]	Lignosulfonate/wt.%[a]	BET specific surface area/ $m^2 g^{-1}$	Internal resistance/$m\Omega$	Carbon factor/ $(m^2 g^{-1}) \cdot (wt.\%)$[a]
1	C1 (1.50)	LS2 (0.30)	2.14	11.55	27
2	C1 (1.50)	LS1 (0.35)	2.71	14.85	27
3	C2 (1.50)	LS1 (0.35)	2.36	15.25	38
4	C3 (1.80)	LS2 (0.30)	2.53	13.82	225
5	C4 (0.80)	LS2 (0.30)	2.54	12.32	120
6	C5 (0.15)	LS2 (0.30)	2.85	13.30	214

[a] Weighted percentages related to the weight of leady oxide.

cell formation. Main electrical parameters of the cells were $C_{20} = 1$ Ah and $I_{20} = 0.05$ A. After formation, the internal resistance of all cells was measured by a Battery HiTESTER 3554 (HIOKI device); the values were included in Table 2. Formation process was performed using an ARBIN BT2543 potentiostat/galvanostat.

2.4. Electrical tests

Cells carried out several electrical tests in order to evaluate their electrical performance. For all tests an ARBIN BT2543 potentiostat/galvanostat was used.

2.4.1. Capacity test

In order to check the low discharge rate performance (C_{20} capacity), cells were discharged at 0.05 A until a voltage of 1.75 V was reached. Time was measured and the cells were recharged for 24 h at 2.67 V with a current limit of 0.25 A. This test was performed twice.

2.4.2. Cold-cranking ability test

Cells were discharged at 5 A (5C) at (-18 ± 1) °C with a cutoff voltage of 1 V. Additionally, the time required by the cells to reach 1 V was also measured. After the test, cells were recharged for 16 h at 2.67 V with a current limit of 0.25 A.

2.4.3. Initial charge acceptance

Fully charged cells were discharged from 100% to 90% of their State of Charge (SoC) (discharge at 0.05 A for 2 h) at (27 ± 2) °C. After a rest period of 72 h, cells were charged at a constant voltage of 2.42 V for 1 min; current input was recorded every 0.1 s. Current through cells at 5 s of charge at constant voltage was studied. After that, cells were recharged until 100% SoC.

2.4.4. Negative polarization study

In constant current studies, a set of fixed currents passed through the fully charged cells for a certain period of time; steps were defined as follows: 0.2A/50 min, 0.1A/20 min, 0.04A/20 min, 0.02A/20 min, 0.01A/20 min, 0.004A/15 min, 0.002A/10 min and 0.001A/10 min. The voltage of the negative electrode was measured with an Ag/AgCl reference electrode at steady-state conditions at the beginning of the test and at the end of every charge. This test was performed at (27 ± 2) °C.

2.4.5. Cycle at partial state of charge (PSoC)

The fully charged cells were charged for 40 min at 0.35 A in order to ensure 100% SoC; limit voltage of 2.4 ± 0.05 V. After that, they were discharged for 30 min at 0.35 A until reaching 82.5% SoC. This charge-discharge cycling was performed until the discharging voltage was <1.66 V. More than 1000 cycles could be linked to a good battery performance at PSoC.

2.5. Physicochemical characterization

NAM morphology and particle size studies were determined by scanning electron microscope (SEM, S-3000N). Two magnifications of the samples were available: 3000× and 6000×. The crystalline phase of the negative electrode sheets was examined by powder X-ray diffraction (XRD) polycrystalline between 10–90° θ using Cu-Kα radiation on a Siemens D-5000 X-ray generator. BET SSA was evaluated using nitrogen adsorption measurements. Carbon and $PbSO_4$ content was determined by an ELTRA CS-800 analyzer.

3. Results and discussion

3.1. Effects of additives on unformed NAM properties and internal resistance

Five carbon materials, with BET SSA between 18 and 1550 $m^2 g^{-1}$, were selected according to material type and the properties that they could confer to the NAM (Table 1). Carbon materials can be classified by their particle size: high particle size (C1, C2, C3 and C4) and low particle size (C5) (Table 1). As was mentioned in the introduction, depending on their particle size and concentration in NAM, carbon materials merge in different ways with the lead skeleton [8]. In this case, C1, C2, C3 and C4, because their high particle size (micrometers) would be incorporated into the bulk negative skeleton branches and would form a lead-carbon electrode. Unlike C5, it could merge with the lead skeleton by two ways. At loads higher than 0.5 wt.%, this carbon material would form a lead-carbon electrode, as carbon materials mentioned above. However, at concentrations lower than 0.5 wt.%, this material would be pushed to the lead skeleton branches and increases the electrochemical active area [18]. A qualitative approach of the carbon materials conductivities is shown in Table 1. After these considerations, carbon material type and concentration in NAM were selected in order to cover six different mixtures that have performed several electrochemical tests (Table 2). Two types of lignosulfonates with a different sulfonation degree were also selected (Table 1). Sulfonation degree implies a higher number of SO_3H groups which exert a beneficial effect in the lignosulfonate performance. Apparently, a higher sulfonation degree involves a delay of the passivation phenomena caused by the $PbSO_4$ layer [19]. These lignosulfonates were added at two concentrations: 0.30 and 0.35 wt.% (Table 2).

Table 2 summarizes the composition of the different mixtures. C1 and C2 were added at 1.5 wt.% to NAM following the best recommendation [15]. C3 is a carbon material that combines the properties of a conductive carbon black and graphite, resulting in a good electrical conductivity. Its concentration in NAM was similar to C1 and C2's due to having, all of them, a similar particle size. C4 and C5 are carbon blacks. Because of the high specific surface area of C4, its load in NAM was reduced to 0.8 wt.%. In order to get an increase on the electrochemical active area, C5 was added at 0.15 wt.%.

In order to understand how carbon materials and lignosulfonates interact with the active material during mixing and curing processes, BET SSA of unformed negative plates was measured, see Table 2. This data helps to understand the effect of these additives on NAM morphology, considering that after cell formation, where Pb^{2+} is reduced to lead, BET SSA will change [3]. BET SSA of mixture 1 was lower than 2's, despite of containing the same carbon material (C1) at the same concentration. In the case of LS1 or LS2, experiments performed in our laboratory have confirmed that both of them increase similarly the surface area of the negative unformed plates. Consequently, in the case of mixtures 1 and 2, an increase on lignosulfonate's concentration could be responsible for improving BET SSA of the negative unformed plates.

In Table 2, differences on BET SSA of mixtures 2 and 3 are shown. Mixture 3 was expected to have higher specific surface than mixture 2, since this mixture contained a carbon material (C2) with a larger surface. This contradiction could be explaining by a not proper dispersion of C2 in mixture 3. Internal resistance after cell formation was also measured, see Table 2. No significant differences were found among all mixtures.

In an effort to link the carbon content to the BET SSA of the unformed negative plates, a carbon factor was calculated for those mixtures that include LS2 (0.30 wt.%). Carbon factor was calculated as: (carbon material BET SSA)*(carbon material load in NAM). It can be seen in Fig. 1 a linear distribution between this factor and NAM specific surface for mixtures 1, 5 and 6. Mixture 4 did not follow the linear distribution. D. Pavlov et al. describe that the specific surface area of formed negative plates increases with a rising in carbon black content. However, for those carbon materials with a graphitic component this increase is less appreciated [3]. For mixture 4, we can assume that C3 at concentrations higher than 0.5 wt.% did not follow the linear distribution due to its graphitic component.

3.2. Initial tests: capacity and cold cranking

The capacity test consisted in a discharge at a low rate until the cells reach the voltage of 1.75 V. The results of this test can be linked to the utilization of the NAM, and to the lignosulfonate efficiency. Lignosulfonates cause a delay of the passivation phenomena caused by the $PbSO_4$ layer, increasing the capacity [20]. Table 3 shows results of first and second capacity, where an increase in the second capacity was associated with a better recharge ability behavior of the cell after first capacity. There were not significant differences between the mixtures, suggesting that all of them had a similar NAM skeleton surface, which mainly depends on the lignosulfonate's nature and stability, determining the surface area of this energetic structure [21]. At this discharge rate, significant differences between the amount and type of lignosulfonate were not found.
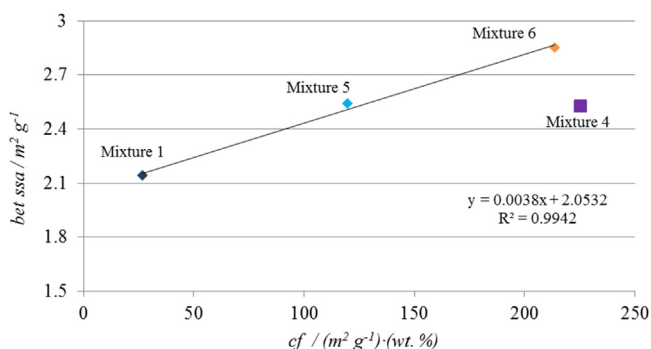
Table 3
Results on first and second capacity test performed at (27 ± 2) °C.

Mixture	First capacity/Ah	Second capacity/Ah
1	0.79 ± 0.05	0.83 ± 0.06
2	0.79 ± 0.07	0.85 ± 0.04
3	0.81 ± 0.02	0.89 ± 0.02
4	0.75 ± 0.02	0.84 ± 0.02
5	0.79 ± 0.01	0.87 ± 0.01
6	0.78 ± 0.00	0.80 ± 0.02

The cold cranking test consisted in a high rate discharge (5A = 5C) of the cell at extreme low temperature conditions (−18 °C), in order to know if the battery would be able to give enough output power to start the cold engine. The cell was discharged very quickly, increasing internal resistance due to the formation of a $PbSO_4$ superficial layer on the negative plates. Time spent by the cells until they reached the cut off voltage (1 V) is represented in Fig. 2.

Apparently, mixtures 2 and 3, which contain a lignosulfonate with a higher sulfonation degree (LS1), were expected to respond better to this test [19]. On the contrary, they showed worse results, which could be associated with an increase in the internal resistance due to a higher content of lignosulfonate. The unexpected result of mixture 3 is attributed to a novel carbon material (C2) in this field that must be further investigated in order to explain this behavior. Mixtures 1, 4 and 5, showed similar results as a consequence of containing the same lignosulfonates (LS2) at 0.30 wt.%. Mixture 6, in spite of having LS2 at 0.30 wt.% showed lower time to 1 V. This result could be linked to the interaction between C5 and LS2: this carbon material was supplied as a mix that contained 17 wt.% of LS2, although the final LS2 concentration in the mixture was 0.30 wt.%. That amount of LS2 inside the carbon mix did not take part in the discharge reaction. Consequently, effective amount of LS2 was lower for mixture 6 and thus, its cold cranking ability was impaired.

3.3. Initial charge acceptance test

In order to simulate the battery behavior while regenerative braking is performed, cells were discharged to 90% SoC. During a period of three days, a passive layer of lead sulfate was formed on negative plate's surface which implied an increase in the ohmic resistance of the cell. After this rest period, they were charged at a constant voltage of 2.42 V and the current was recorded. In order to know what mixtures had a better charge acceptance, current value after 5 s of charge was measured; data are shown in Fig. 3.

Charge processes are determined by the electron transfer to the Pb^{2+} ions, which can be adsorbed on the carbon phase or on the polymeric layer of the expander (LS1 and LS2). This process is less resistive when it occurs on the carbon phase [22]. Consequently, mixtures 2 and 3 showed lower charge acceptance than the rest,

Fig. 1. Graphical representation of cf (carbon factor) and bet ssa (BET SSA of unformed negative plates) of the mixtures 1, 4, 5 and 6. Linear regression equation for mixtures 1, 5 and 6.
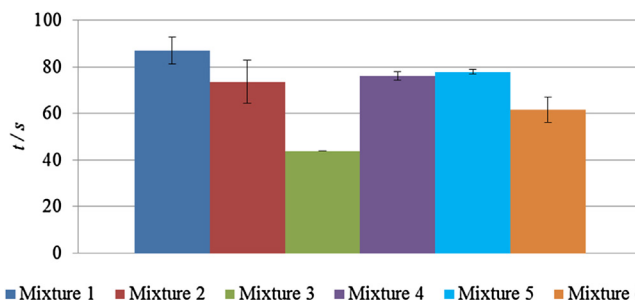

Fig. 2. Cold cranking test at extreme low temperature conditions (−18 ± 1) °C. Time spent by the cells until 1 V was reach. Error bars are related to standard deviation.
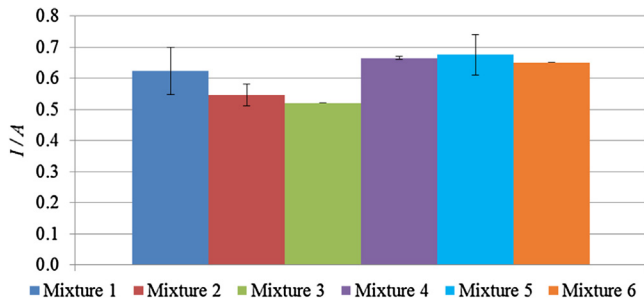
Fig. 3. Results on initial charge acceptance test $(27 \pm 2)\,°C$. Current reached by cells after 5 s of being charged at 2.42 V. Error bars are related to the standard deviation.

Fig. 5. Overpotentials for the negative electrode of mixtures 1 to 6 at the end of charging the cells at $0.98 \times 10^{-3}\,A\,cm^{-2}$.

due to their higher LS1 content. The rest of the mixtures contained less amount of lignosulfonate, therefore the polymeric layer of the expander would induce less resistance than in the other mixtures.

As it was mentioned before, C1, C2, C3 and C4 would form a lead-carbon electrode with high specific surface and conductivity, if the carbon material used has enough affinity for lead [8]. C5 at 0.15 wt.% would be pushed to the lead skeleton branches and increase NAM's electrochemical active area where the electrochemical reaction of Pb^{2+} reduction takes place [18].

Carbon particles contained in lead-carbon electrodes from mixtures 1, 4 and 5, could act as super-capacitors during charging processes: electrical charges were concentrated inside their porous structure, with the subsequent decrease of the ohmic resistance throughout the negative plate, and the increase of its charge acceptance ability [8]. In the case of mixture 6, C5 increased electrochemical active area where Pb^{2+} reduction takes place, improving charge acceptance. For these reasons, mixtures 1, 4, 5 and 6 showed the best results in this test (Fig. 3).

3.4. Negative polarization study

Fig. 4 shows the cathodic polarization curves in H_2SO_4 solution $(1.28\,g\,cm^{-3})$ for the mixtures 1 to 6. These curves were obtained by a galvanostatic method: different fixed current densities $(10^{-3}-0.05\,10^{-3}\,A\,cm^{-2})$ were applied to the cells until reaching a steady state. The negative plate potentials were measured (vs Ag/AgCl reference electrode) and the overpotentialas of the negative plates were calculated. At low current densities the reduction of the remaining $PbSO_4$ could take place (Eq. (1)) and compete with hydrogen evolution (HER) see (Eq. (2)).
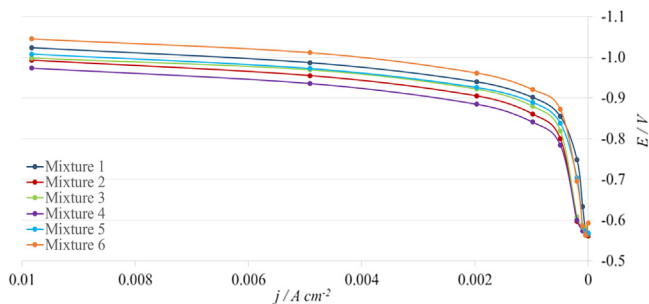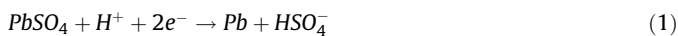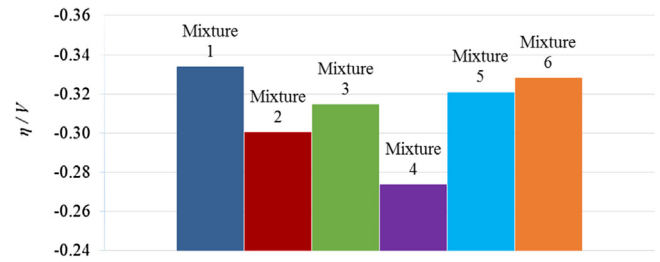
$$PbSO_4 + H^+ + 2e^- \rightarrow Pb + HSO_4^- \qquad (1)$$

$$2H^+ + 2e^- \rightarrow H_2 \uparrow \qquad (2)$$

However, when the cell was over-charged, the relation between potential and current density showed a linear distribution, which indicated the continuous hydrogen evolution. This behavior disappears when current density had reached $0.98\,10^{-3}\,A\,cm^{-3}$. Carbon materials could increase the specific surface area of the NAM, contributing to improving charge acceptance, but also to accelerating the hydrogen evolution due to the creation of the more active sites where hydrogen can be reduced.

Lower overpotentials when hydrogen evolution was taking place were an indication of high water consumption of the mixture. Overpotentials (calculated as $\eta = E - E_{eq}$; being E_{eq} steady state electrode potential) at $0.98\,10^{-3}\,A\,cm^{-2}$ are shown in Fig. 5; mixture 1 and 6 showed the highest overpotential followed by mixture 5, 3, 2, and 4 respectively. Mixtures 3 and 2, which contained LS1 (0.35 wt.%), have shown lower overpotentials than those mixtures that incorporated LS2 (0.30 wt.%). LS1 improved hydrogen evolution, which could be attributed to the higher sulfonation degree of this lignosulfonate, reporting that acidic groups promote hydrogen evolution [23].

Mixture 2 (C1) showed lower overpotential than mixture 3 (C2), although both mixtures incorporated the same amount of carbon material. Despite being more conductive C2 than C1, the bad dispersion of C2 in the NAM could hinder the accessibility of the water to the activate sites of this carbon material, lowering the hydrogen evolution.

Among the other mixtures, their behavior could be related to the amount of carbon material in NAM. In this way, mixture 4 (C3 at

Fig. 4. Polarization curves for mixtures 1 to 6. The negative plate potential was measured vs Ag/AgCl reference electrode.
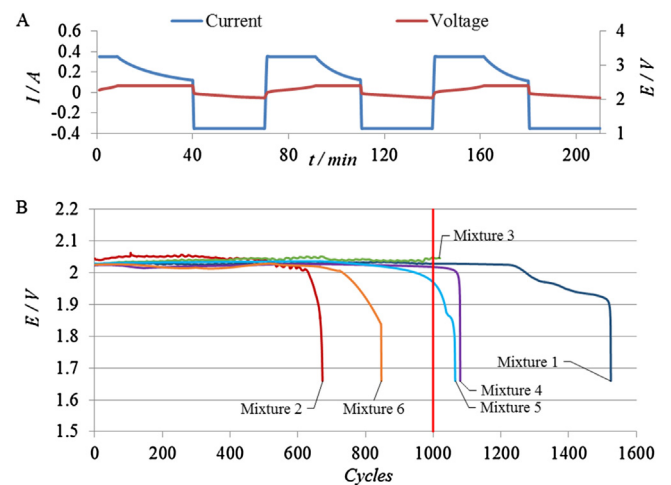
Fig. 6. A. Schematic procedure of cycles at PSoC at $(27 \pm 2)\,°C$. B. Results on this test: 1- 1525 cycles. 2- 673 cycles. 3- 1020 cycles. 4- 1080 cycles. 5- 1065 cycles. 6- 847 cycles. Red line: 1000 cycles. (For interpretation of the references to colour in this figure legend, the reader is referred to the web version of this article.)
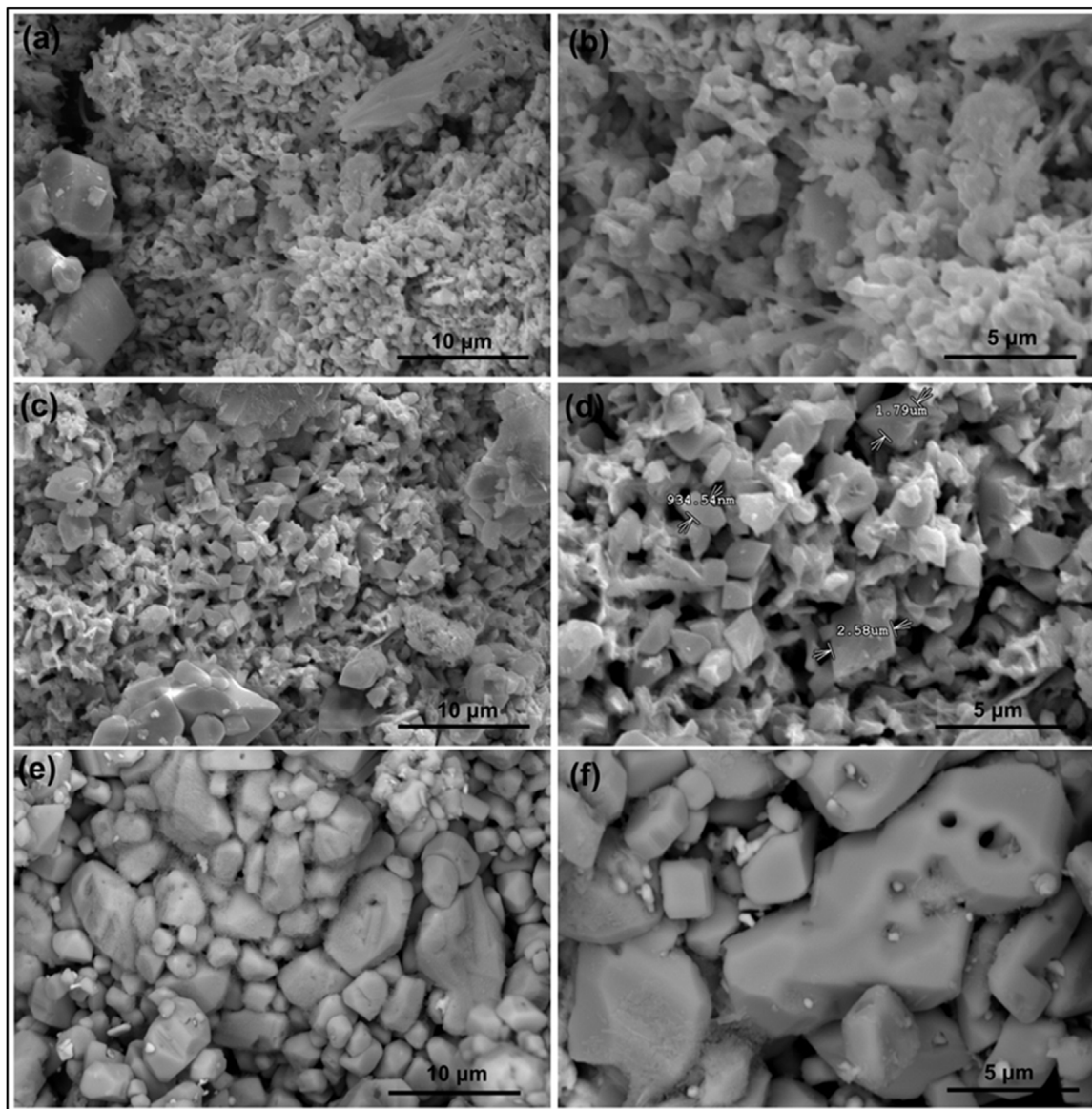
Fig. 7. SEM Images of formed negative plates for mixture 6 (a) (b), cycled negative plates for mixture 4 (1080 cycles) (c) (d), and 6 (847 cycles) (e) (f). Magnification: 3000× and 6000×.

1.80 wt.%) showed the lowest overpotential because of having more activated sites where hydrogen was able to be reduced, followed by mixture 5 (C4 at 0.80 wt.%) and 6 (C5 at 0.15 wt.%). Finally, in the case of mixture 1, the low surface area of C1 was not able to display enough activated sites for hydrogen evolution, resulting in a high overpotential for the HER reaction.

3.5. Effect of different additives on PSoC cycle life

Cycle life test at PSoC is represented in Fig. 6A. This test was performed in order to simulate the effect of the additives on Micro-Hybrid automotive battery usage. During these cycles a $PbSO_4$ passive layer was formed on the lead structure which increases internal resistance and hampers the Pb^{2+} reduction. Carbon materials are known to increase NAM specific surface area and conductivity, due to the promotion of the Pb^{2+} reduction on their surface. In this way they can create isolated $PbSO_4$ crystals

Table 4
Cycles at PSoC conditions completed by each mixture. Carbon and $PbSO_4$ content for cycled negative plates of mixtures 1, 4, 5 and 6.

Mixture	Completed cycles	Carbon content/wt.%[a]	$PbSO_4$ content/wt.%[a]
1	1525	1.58	26.0
2	673	[b]	[b]
3	1020	[b]	[b]
4	1080	1.80	30.2
5	1065	0.95	32.7
6	847	0.41	66.8

[a] Weighted percentage related to NAM mass.
[b] Data not available.

while preventing the formation of $PbSO_4$ continuous layer, increasing cycle life at PSoC.

Mixture 2 has only reached 673 cycles (see Fig. 6B); its higher content of LS1 (0.35 wt.%) has resulted in an increase of the
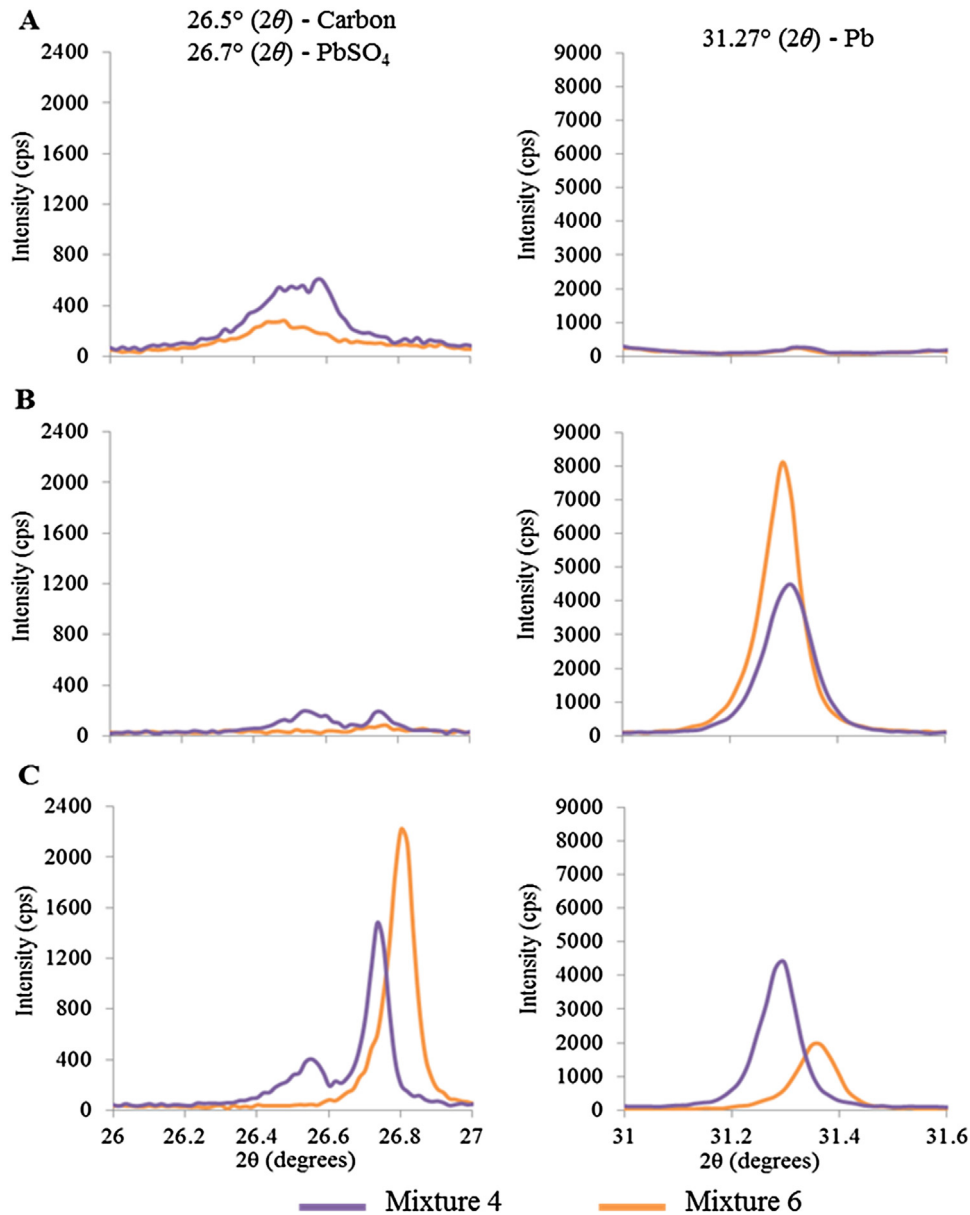
Fig. 8. XRD pattern for negative plate of mixtures 4 and 6 in different states: A. Unformed (after curing). B. Formed (after cell formation process). C. Cycled (after being cycled at PSoC). Left: Diffraction peak for Carbon (002): $2\theta = 26.5°$, and for $PbSO_4$ (021): $2\theta = 26.7°$. Right: Diffraction peak for Pb (111): $2\theta = 31.27°$.

polymeric layer of expander, which provided a greater resistance to the Pb^{2+} reduction. In this way, this process might be hampered while $PbSO_4$ concentration increased and a passive layer of this compound was formed on the lead structure. C1 formed a lead-carbon electrode in mixture 2 which could be deteriorated during these cycles. However, mixture 3 easily fulfilled more than 1000 cycles despite of its high LS1 content. Conductivity throughout negative plate was maintained by C2, which has higher conductivity than C1. Pb^{2+} reduction was performed on the lead-carbon electrode surface, preventing a $PbSO_4$ passive layer, and fulfilling more than 1000 cycles, before its skeleton was deteriorated. Test for mixture 3 was stopped at 1020 cycles.

Most of the mixtures containing LS2 (0.30 wt.%) performed more than 1000 cycles, except mixture 6 (see Fig. 6B). Differences between mixture 6 and the rest were related to the lower carbon concentration of this mixture, and how C5 was incorporated into

the NAM material; it has increased the electrochemical active area of the negative plate. This could lead to a saturation of the electrochemical surface by $PbSO_4$ crystals, and then the failure of the cell working in PSoC conditions. These results conclude that the formation of a lead-carbon electrode would increase cycle life of the cells in PSoC performance.

3.6. Teardown analysis of PSoC cells

In an effort to see the lead skeleton structure for mixture 6, the cross section of formed negative plate was studied by SEM; (see Fig. 7(a) (b)). These two images show an inner structure covered by very small particles interconnected, forming a heavy folder structure. Carbon black particles would be pushed to the lead skeleton surface during the formation process, and be covered by

Pb/PbSO$_4$ due to their involvement in the charge discharge processes.

During cycling, lead skeleton was deteriorated by the deposition of lead sulfate crystals on its surface, which impeded H$_2$SO$_4$ flow, electron transfer and charge acceptance, increasing the ohmic resistance. Mixtures with higher porosity should need more amount of lead sulfate to fail in these conditions, as the H$_2$SO$_4$ flow throughout these plates should be further facilitated. After the cycle life test at PSoC, negative plates were removed from the cycled cells, washed with water and dried in a vacuum chamber for their subsequent analysis.

The SEM images of cycled negative plates of mixtures 4 and 6 are presented in Fig. 7 (c) that mixture 4, even after fulfilling 1080 cycles, has maintained a uniform lead structure with some PbSO$_4$ crystals on the surface. In the case of mixture 6, differences between formed and cycled negative plates can be easily noticed in Fig. 7 (a) (b) and (e) (f) respectively. Fig. 7 (e) shows PbSO$_4$ crystal that can be easily differentiated due to their big size. Fig. 7 (d) and (f) PbSO$_4$ crystal sizes can be compared between mixtures 4 and 6, respectively. Crystal's size of mixture 6 multiplies by almost six the size of crystals of mixture 4.

On the one hand, the incorporation of carbon materials into the bulk of the lead skeleton's branch would create a more dynamic electric system as a lead-carbon electrode which could allow a delay on the irreversible lead sulfate formation working in PSoC conditions. Such was the case of mixtures 1, 3, 4 and 5. On the other hand, carbon materials with very high surface area at low content, as C5 in mixture 6, increased the NAM's electrochemical active area, but, involved more suitable seats for irreversible lead sulfate accommodation, triggering a good distribution of big crystals that would finally lead to the failure of the cell.

Focusing on mixtures 1, 5 and 6, which followed the linear distribution shown in Fig. 1, the last one has performed the lowest amount of cycles. Despite of having the highest BET SSA (Table 2), mixture 6 showed the highest lead sulfate content (and largest PbSO$_4$ crystals) on failure, with the lowest cycling duration. However, mixtures 1 and 5 have performed more than 1000 cycles and their PbSO$_4$ concentration on failure was around 30 wt.% (Table 4). In this way, sulfation of the negative plate has been the failure mode; however the limiting lead sulfate amount depends on NAM active surface area.

3.7. Changes induced in the NAM structure

In order to know the effects of carbon materials on NAM composition, XRD analysis of unformed, formed and cycled negative plates of mixtures 4 and 6 were performed. Lead was identified in Fig. 8. (Right) (31.27° (2θ) (111) [24]). At first sight, the lead concentration in formed plates (Fig. 8.B right) was higher for mixture 6, indicating that C5 improved the cell formation process by the promotion of the Pb^{2+} reduction. However, after cycling at PSoC, all lead was practically converted into lead sulfate, and its diffraction peak has been drastically reduced (see Fig. 8C right). This has not happened to mixture 4, which maintained similar lead concentration after cycling.

Fig. 8 (Left) shows the diffraction peak related to PbSO$_4$ (021) at 26.7° (2θ) [24]. Lead sulfate concentration of formed plates (see Fig. 8B left) was higher in the case of mixture 4, corroborating that C5 in mixture 6 was able to improve the cell formation process. As it was mentioned in section 3.6, failure mode at cycling in PSoC was related to the negative plates sulfation. For cycled plates (see Fig. 8C left), lead sulfate concentration was higher for mixture 6, as it was also shown in Table 4.

Fig. 8(left) also shows a diffraction peak related to the family of planes of Carbon (002) at 26.5° (2θ) [24,25]. This peak is an indication of the graphitization degree, which remained after the

formation process and PSoC cycles for mixture 4 (see Fig. 8 left), but disappeared for mixture 6 which could be related to a lower carbon concentration in this mixture. Furthermore, peak height showed by mixture 4 could be related to the graphitic component of C3. Results indicate that carbon materials were resistant enough to any chemical attack inside the negative active material.

4. Conclusions

Those carbon materials with high particle size (C1, C2, C3, and C4) have shown improvements in charge acceptance and cycle life at PSoC. The failure mode was related to the passivation of the NAM skeleton by a PbSO$_4$ layer.

However C5, which was a carbon black material with low particle size, at concentrations lower than 0.50 wt.%, were pushed towards the NAM skeleton surface and has shown improvements in the electrochemical surface area of the NAM (2.85 m^2 g^{-1} for unformed negative plates of the mixture 6). In this way, it was able to improve the charge acceptance, but also to increase water consumption, but it failed to enhance the cycle life at PSoC, performing just 847 cycles.

Those carbon materials, able to form a lead-carbon electrode, were more suitable to be added to the negative plate in order to improve charge acceptance by acting as super-capacitors during charging process, and also improved cycle life at PSoC by reducing the formation of irreversible lead sulfate (PbSO$_4$ concentration in cycled negative plates was around 30 wt.%) reaching up to 1525 cycles.

LS2 had a beneficial effect on cycle life if the mixture was combined with a high conductive carbon material, although, results on charge acceptance and cold cranking were impeded.

The negative polarization study revealed that is necessary to find an optimal amount of carbon material to not excessively promoting in excess the hydrogen reduction in activated sites supplied by these materials. Furthermore, acidic groups contained in lignosulfonates may improve this reaction.

References

[1] S. Schaeck, A.O. Stoermer, F. Kaiser, L. Koehler, J. Albers, H. Kabza, J. Power Sources 196 (2011) 1541–1554.
[2] P. Tong, R. Zhao, R. Zhang, F. Yi, G. Shi, A. Li, H. Chen, J. Power Sources 286 (2015) 91–102.
[3] D. Pavlov, Lead-acid batteries, Sci. Technol. (2011).
[4] K.R. Bullock, J. Power Sources 195 (2010) 4513–4519.
[5] P.T. Moseley, R.F. Nelson, A.F. Hollenkamp, J. Power Sources 157 (2006) 3–10.
[6] M. Fernández, J. Valenciano, F. Trinidad, N. Muñoz, J. Power Sources 195 (2010) 4458–4469.
[7] J. Valenciano, A. Sánchez, F. Trinidad, A.F. Hollenkamp, J. Power Sources 158 (2006) 851–863.
[8] D. Pavlov, P. Nikolov, T. Rogachev, J. Power Sources 196 (2011) 5155–5167.
[9] X. Zou, Z. Kang, D. Shu, Y. Liao, Y. Gong, C. He, J. Hao, Y. Zhong, Electrochim. Acta 151 (2015) 89–98.
[10] P.T. Moseley, D.A.J. Rand, J. Power Sources 133 (2004) 104–109.
[11] A.F. Hollenkamp, W.G.A. Baldsing, S. Lau, O.V. Lim, R.H. Newnham, D.A.J. Rand, J.M. Rosalie, D.G. Vella, L.H. Vu. ALABC Project N1.2 Overcoming negative-plate capacity loss in VRLA batteries cycled under partial state-of-charge duty Final Report: July 2000–June 2002.
[12] P. Bača, K. Micka, P. Křivík, K. Tonar, P. Tošer, J. Power Sources 196 (2011) 3988–3992.
[13] D.P. Boden, D.V. Loosemore, M.A. Spence, T.D. Wojcinski, J. Power Sources 195 (2010) 4470–4493.
[14] P.T. Moseley, J. Power Sources 127 (2004) 27–32.
[15] M.L. Soria, J.C. Hernández, J. Valenciano, A. Sánchez, F. Trinidad, J. Power Sources 144 (2005) 473–485.
[16] S.W. Swogger, P. Everill, D.P. Dubey, N. Sugumaran, J. Power Sources 261 (2014) 55–63.

[17] R. Marom, B. Ziv, A. Banerjee, B. Cahana, S. Luski, D. Aurbach, J. Power Sources 296 (2015) 78–85.
[18] D. Pavlov, T. Rogachev, P. Nikolov, G. Petkova, J. Power Sources 191 (2009) 58–75.
[19] A.C. Zachlin, J. Electrochem. Soc. 98 (1951) 325–333.
[20] Power Sources for electric vehicles, (1984) .
[21] V. Iliev, D. Pavlov, J. Appl. Electrochem. 15 (1985) 39–52.
[22] D. Pavlov, P. Nikolov, T. Rogachev, J. Power Sources 195 (2010) 4444–4457.
[23] L. Wang, H. Zhang, G. Cao, W. Zhang, H. Zhao, Y. Yang, Electrochim. Acta 186 (2015) 654–663.
[24] R.J. Hill, J. Power Sources 9 (1983) 55–71.
[25] N. Iwashita, C.R. Park, H. Fujimoto, M. Shiraishi, M. Inagaki, Carbon 42 (2004) 701–714.
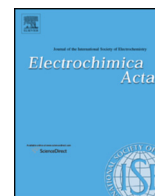
Research Paper

Graphitized Carbon Nanofibers: new additive for the Negative Active Material of Lead Acid Batteries

M. Blecua[a], E. Fatas[a], P. Ocon[a,*], B. Gonzalo[b], C. Merino[c], F. de la Fuente[d], J. Valenciano[d], F. Trinidad[d]

[a] Universidad Autónoma de Madrid, Departamento de Química Física Aplicada, C/Francisco Tomás y Valiente 7, 28049, Madrid, Spain
[b] GAIKER Centro Tecnológico, Parque Tecnológico de Bizkaia, Ed. 202, 48170 Zamudio, Vizcaya, Spain
[c] Grupo Antolin Ingenieria S.A., Carretera Madrid-Irun km. 244.8, E-09007 Burgos, Spain
[d] Exide Technologies, R&D Centre, 19200 Azuqueca de Henares, Spain

ABSTRACT

Graphitized Carbon Nanofibers (GANFg) were dispersed with a certain amount of organic expander and used as additive for the negative plates of the Lead Acid Batteries (LABs). Due to the high aspect ratio of these fibers, they are thought to reach the percolation threshold inside the Negative Active Material (NAM) and create a conductive network which would improve the cycle life of the LABs working in Partial State of Charge (PSoC) conditions. These fibers were added at three concentrations (0.50, 0.20 and 0.10 wt. %) and dispersed in a sodium lignosulfonate aqueous solution. Unformed negative plates of three mixtures were prepared, together with a NAM Control sample, and 2 V/1 Ah small lead acid cells were assembled for testing the electrical performance of the different mixtures (capacity, cold cranking ability, charge acceptance, negative polarization study, PSoC cycles and Cyclic Voltammetry (CV)). Continuous physicochemical analysis was carried out for the negative plates. As a result, Carbon Nanofibers were able to increase cell cycle life working in PSoC conditions and slightly improve the charge acceptance, but also raised the water loss. However, this gassing increase was lower for Carbon Nanofibers in comparison with other carbon materials used in flooded LABs.

© 2017 Elsevier Ltd. All rights reserved.

1. Introduction

Lead Acid Batteries (LABs) are in continuous upgrade in order to supply the necessities of the current automotive industry. One of their main objectives is to work in the Micro Hybrid vehicle as power supply source, where LABs must be able to accept the charge of the regenerative braking and to work in High Rate Partial State of Charge (HRPSoC) conditions. When LABs are working in these conditions, lead sulfate ($PbSO_4$) crystals are progressively accumulated on the lead surface, which increases the internal resistance of the negative plate and leads to the battery failure.

In order to avoid this sulfation, many carbon materials have been used as additives for the negative plate, such as activated carbon, carbon black, graphite, lamp black and expanded graphite [1–12]. Carbon materials, among other features, are able to improve the overall electrical conductivity of NAM [10], and to improve the $PbSO_4$ recrystallization, but their effects are different depending on their particle size and concentration in NAM [11]. Former studies corroborated that micrometers particle size carbon materials at concentrations higher than 0.50 wt. % are introduced into the bulk of the lead skeleton branches and act as supercapacitors. In this way they are able to improve the charge acceptance and the cycle life in Partial State of Charge (PSoC) conditions [13]. During prolonged PSoC cycling the lead skeleton can afford more stability if the carbon material is mixed in wet conditions with the leady oxide, building up a conductive network inside NAM [14].

The reduction of $PbSO_4$ can take place in two different phases: the lead or the carbon material surface; this is known as "parallel mechanism of charge" [12]. Consequently, carbon materials have a catalytic effect on the charge reactions, including the Hydrogen Evolution Reaction (HER) due to the fact that the overpotential of the different reactions is lower on the carbon material/H_2SO_4 interface [5,15]; the knowledge of the optimum carbon amount is a key factor for preventing an excessive water consumption [13].

* Corresponding author.
E-mail address: pilar.ocon@uam.es (P. Ocon).

New carbon nanomaterials [16–19] are being considered in the LABs latest developments, improving their performance even when they are added at a very low concentration. In the case of discrete Carbon Nano Tubes (dCNT), when they are added at a final concentration of 0.16 wt. % (related to the leady oxide mass), they are able to enhance the charge acceptance, reserve capacity and cold cracking performance [17]. dCNT have been also added in both, Positive Active Material (PAM) and NAM; these experiments resulted in an increase in cycle life by 60% (HRPSoC), and water consumption of the battery [18]. In Flooded Lead Acid Start Light Ignition (SLI) batteries, Multi Wall Carbon Nano Tubes (MWCNT) can double the cycle life of real batteries when they are added in positives and negative plates [19]. However, sulfation of the negative plate prevails as the failure mode of these batteries [17–19]. Three-dimensional reduced graphene oxide (3DRGO) has been employed as NAM additive. Results show a high porosity of those 3DRGO's NAM, which implies a decrease on the size of the $PbSO_4$ crystals, and a prolonged cycle life of the LABs working in HRPSoC conditions [20]. Nanostructured materials, such as MWCNT or graphene, have been also tested by S. Logeshkumar and R. Manoharan [16]; these materials are incorporated into the lead skeleton and undergo the creation of bead shape $PbSO_4$ crystals with small size, making easier their conversion into lead and prolonged PSoC cycle life.

All these carbon materials, due to containing several impurities and increasing the negative plate's conductivity, raise HER rate, and thus the water consumption, leading to the battery death. In the case of nanomaterials, as they are normally added at low concentrations, this water consumption increase is lower [16–19].

Lignosulfonates have been also used for many years in the manufacturing of the LABs, where they work as organic expanders. These compounds prevent the deposition of a $PbSO_4$ passive layer on the negative plate surface, making possible the accommodation of small $PbSO_4$ crystals and increasing the capacity [21]. Another authors [22] have indicated that lignosulfonates delay the charge/discharge reactions, and in this way, they hamper the charge acceptance of the negative plates, which leads to the failure of LABs in HRPSoC cycles. D. Pavlov, P. Nikolov and T. Rogachev [21] have demonstrated the influence of lignosulfonate concentration on NAM structure, concluding that high amounts of this compound change the inner structure of NAM and impair the cycle life in HRPSoC conditions. R. Khayat Ghavami, F. Kameli, A. Shirojan and A. Azizi [23] have tested different surfactants as NAM additives, concluding that the hydrophobicity and the charged head groups of surfactants are important key factors for their performance as organic expanders.

In this study graphitized Carbon Nanofibers from Grupo Antolin (GANFg) have been used as additives for the negative plates in three concentrations: 0.50, 0.20 and 0.10 wt. %. Due to GANFg high aspect ratio and conductivity, low GANFg dosages were selected with the aim of keeping the minimum water consumption. These fibers have been properly dispersed in water together with a certain amount of a sodium lignosulfonate acting as surfactants, in order to facilitate their uniform distribution in NAM. In this way, GANFg can reach the percolation threshold and improve the electrical conductivity throughout the negative plate. The final concentration of the sodium lignosulfonate (LS) was 0.30 wt. %. A reference mixture, called NAM Control, was also prepared with LS (0.30 wt. %.) and without any carbon material. Finally, four different NAMs mixtures were prepared to be tested in 2 V/1 Ah small lead acid cells. Their electrical characterization was accomplished by the capacity test, cold cranking ability test, charge acceptance test, deep HER study, performance at PSoC cycles and Cyclic Voltammetry (CV). In order to study NAM physicochemical properties during the whole process, determination of sulfate and carbon content, BET Specific Surface Area (BET SSA) calculation, porosity measurements, X Ray Diffraction (XRD) and Scanning Electron Microscopy (SEM) were also carried out.

2. Experimental

2.1. Preparation of GANFg dispersions and unformed negative plates

GANFg, with nearly 100% graphitization degree, as carbon materials and LS as organic expander were both incorporated as additives in the NAM. GANFg were dispersed in water and a certain amount of organic expander (see Table 1). The dispersion was performed in three consecutives stages: soaking, milling, and high shear, using dispersion equipment called as DISPERMAT® CN10 (VMA-GETZMANN GmbH).

NAM was prepared using leady oxide powder (1 kg, oxidation degree = 72%), Polyacrylonitrile fiber (PAC) (0.22 wt. %), $BaSO_4$ (1.00 wt. %), H_2SO_4 (5.40 wt. %, 1.40 g cm^{-3}), H_2O (11.20–11.50 wt. %), LS (0.30 wt. %) and GANFg (0, 0.10, 0.20 or 0.50 wt. %). All wt. % related to the leady oxide mass. According to Table 1, in the case of mixtures S5, S6 and S7, part of LS and water were used to disperse the GANFg; the rest was added during the mixing process, in order to reach the final concentrations of each compound in NAM. Pastes were prepared according to this procedure: (1) Dry materials (leady oxide, PAC and part of the organic expander) were mixed for 3 min. (2) GANFg dispersion, and the rest of the water (1.20 − 1.5 wt. %) were added and the mix was stirred for 5 min. (3) H_2SO_4 (1.40 g cm^{-3}) was added dropwise to the mixture during 10 min. At the end, the paste's density was measured. In the case of NAM Control, no dispersion was prepared; LS (0.30 wt. %) was added together with the dry materials. Table 1 summarizes the final composition of each mixture, and their pastes density.

A certain amount of paste (8 g) was coated on a Pb-Sn grid with an area of around 10 cm^2 (4.83 cm · 2.11 cm) in order to prepare the 1 Ah negative plates. Then the curing process was carried out by two stages. First one: 24 hours at 55 °C and 85% of relative humidity. Second one: 24 hours at 30 °C and 100% of relative humidity. After that, the plates were dried at room temperature. Table 2 summarizes the physicochemical properties of these cured negative plates. Positive plates of the same dimensions and capacity were prepared following a standard procedure.

Table 1
GANFg dispersions composition (D5, D6 and D7). Mixtures final composition and NAM pastes density after the mixing process (NAM Control, S5, S6 and S7).

Dispersions	Composition			Mixtures	Composition		NAM density/g cm^{-3}
	H_2O/g[a]	GANFg/g[a]	LS/g[a]		GANFg/wt. %[b]	LS/wt. %[b]	
–	–	–	–	NAM Control	0.00	0.30	4.63
D5	100	5	3.0	S5	0.50	0.30	4.62
D6	100	2	1.2	S6	0.20	0.30	4.64
D7	100	1	0.6	S7	0.10	0.30	4.63

[a] Compounds contained in the GANFg dispersion. Each dispersion was used for preparing 1 kg of leady oxide paste.
[b] Final composition of the mixtures; wt. % related to the leady oxide mass.

Table 2
Physicochemical properties of the unformed (after the curing process) and formed (after the formation process) negative plates: carbon and lead sulfate concentrations, median pore diameter and BET specific surface area.

Status	Unformed plates		Formed plates		
Mixture	Carbon/wt. %[a]	Median pore diameter/μm	Carbon/wt. %[a]	PbSO$_4$/wt. %[a]	BET SSA/m^2 g^{-1}
NAM Control	0.60	0.18	0.36	4.80	0.66
S5	1.60	0.13	0.90	1.70	0.96
S6	1.40	0.15	0.48	4.00	0.80
S7	0.80	0.18	0.35	4.90	0.73

[a] wt. % related to the total mass of the sample.

2.2. Assembly and formation of test cells

2 V/1 Ah small lead acid cells were prepared with one negative/two positive plate's assembly using a glass mat separator. This assembly was compressed between two methacrylate sheets, and introduced in a 500 mL beaker, where it was submerged in H$_2$SO$_4$ (1.28 g cm^{-3}) until 250 mL.

The formation process at 40 °C comprised: an initial charge at constant current (0.35 A) for 13 hours followed by several charges and discharges (-0.12 A/4.7 h, 0.24 A/3.0 h, 0.16 A/6.3 h, −0.24 A/2.5 h, 0.24 A/3.2 h, 0.12 A/4.2 h). After the formation process, physicochemical properties of the formed negative plates were analyzed; results are summarized in Table 2.

2.3. Electrical tests

ARBIN BT2543 potentiostat/galvanostat and Metrohm Autolab PGSTAT204 potentiostat/galvanostat combined with a 10 Amp Current Booster, were used for testing the performance of the 2 V/1 Ah small lead acid cells.

2.3.1. Capacity and Cold-cranking ability test

Cells were discharged at 0.05 A, with a cutoff of 1.75 V; time was measured in order to know the low discharge rate performance (C$_{20}$ capacity). After this test, cells were recharged for 24 hours at 2.67 V with a current limit of 0.25 A. Float currents were measured during the whole recharge. Cold cranking ability test comprised a high rate discharge at 5 A (5C) at low temperature (−18 ± 1) °C with a cutoff cell potential of 1.00 V. Time spent by the cells until reaching the cutoff was measured in order to compare their performance. Cells were recharged for 16 hours at 2.67 V with a current limit of 0.25 A, after this test. Both tests were performed twice.

2.3.2. Initial charge acceptance

Cells were discharged for 2 hours at 0.05 A, in order to reach the 90% of their State of Charge (SoC). They were resting for 72 hours, and then charging at constant cell potential of 2.42 V for 1 min. During this charge, the current was measured every 0.01 s; the current at 5 s was used as comparative parameter of the charge acceptance of the mixtures. Finally, cells were recharged until reaching their 100% SoC.

2.3.3. Negative polarization study

The fully charged cells were subjected to a total amount of eight different charges for a certain time: 0.200A/50 min, 0.100A/20 min, 0.040A/20 min, 0.020A/20 min, 0.010A/20 min, 0.004A/15 min, 0.002A/10 min and 0.001A/10 min. Negative plate potential was measured vs Ag/AgCl reference electrode: at the beginning, when current density was cero, j = 0, open circuit potential (E$_{OCP}$) and at the end of every charge (E$_j$). Apparent overpotential in every charge was calculated as: $\eta_{app,H2} = E_{j=1mA \cdot cm^{-2}} - E_{OCP}$.

2.3.4. Cyclic Voltammetry (CV)

CV experiments were performed in three-electrode cell consisting of a negative plate-working electrode, two positive plates as counter electrode and an Ag/AgCl electrode as reference electrode used with Luggin capillary. The scan rate was 5.00 mV s^{-1} between −1.50 V to 0.50 V for 300 cycles.

2.3.5. Partial State of Charge (PSoC) cycles

At the beginning of the test the cell was fully charge. Cycles were comprised by two steps: (a) charge at 0.35 A until reaching 2.42 V for 40 min. (b) discharge at 0.35 A for 30 min. The test stopped when a cell potential of 1.66 V was reached.

2.4. Physicochemical characterization

SEM (SEM, S-3000N; magnifications: 3000× and 6000×) and XRD (polycrystalline between 10−90° θ using Cu-K α radiation on a Siemens D-5000 X-ray generator) techniques were used for studying the morphology and phase composition of the negative plates. A micromeritics FlowSorb II 2300 Surface Area Analyzer was used to compute the BET SSA, at liquid nitrogen temperature (77 K), with previous dry of the samples, and degasification at room temperature. Median pore diameter of the cured negative plates was analyzed with a Micromeritics 9405 CE Auto Pore III Intrusion Mercury Porosimeter. This method consisted in the automatic measurement of the mercury volume absorbed by unformed NAM at different applied pressures. Carbon and PbSO$_4$ content in negative plates was determined by an ELTRA CS-800 analyzer.

3. Results and discussion

3.1. Effect of GANFg on paste rheology and consistency

GANFg were selected as carbon materials additives for the negative plates due to their high aspect ratio (diameter: mainly 20–80 nm and length: up to 30 μm) and low electrical resistivity (1·10^{-4} Ohm m). GANFg are Ni-catalyzed helical ribbon carbon nanofibers whose manufacturing process is explained somewhere else [24]. In order to reduce the Ni content and functionalities from the GANFg surface, these fibers were graphitized at 2500 °C [25]. The carbon atoms inside GANFg are organized by planar graphene layers with 3-dimensional graphitic structure (AB stacking). These planar graphene layers comprise several planes that are made by at least, 15 graphene layers. Therefore, the cross-section of the GANFg become clearly polygonal [25].

Non graphitized GANF have been used as additives for unsaturated polyester resins, where they have reached the percolation threshold at concentrations between 0.10 and 0.30 wt. %. In this way they create an adequate conductive network in that matrix [26]. For this reason, low GANFg concentrations of 0.50, 0.30 and 0.10 wt. %, were studied during this work in order to explore the GANFg percolation threshold in NAM. In this way, they

would create a conductive network in NAM; increase the overall conductivity and, thereby reduce the negative plate sulfation. Furthermore, both, the graphitization process and low GANFg dosages wouldn't considerably affect to the water consumption. GANFg dispersion was accomplished in three stages (section 2.1). In order to improve the dispersion, part of the organic expander, which acts as a dispersant in NAM, was added together with the GANFg. After the mixing process the paste density was measured (Table 1) which verified that GANFg concentration did not affect the paste density.

3.2. Unformed negative plates properties

After the curing process, unformed negative plates were analyzed. Results are shown in Table 2. To verify GANFg inclusion in NAM, carbon content was determined. It is understood from the data, that GANFg together with the organic expanders was well incorporated in NAM. However, the carbon content of all the mixtures was higher than expected. Hydrocerussite ($2PbCO_3 \cdot 1Pb(OH)_2$) as part of the lead hydrocarbonate ($PbO \cdot 6PbCO_3 \cdot 3Pb(OH)_2$), could cause this effect. This compound becomes from the reaction between carbon dioxide and lead hydroxide ($Pb(OH)_2$) during the mixing process [27]. In an attempt to prove this theory, an XRD analysis was performed on unformed negative plates (Fig. 1). The Carbon diffraction peak (002), located at $26.5°$ (2θ) (Fig. 1a), follows the same tendency as hydrocerussite diffraction peak (110) at $34.2°$ (2θ) (Fig. 1b), which also has a diffraction peak related to the family planes (015) at $27°$ (2θ), that exerts an influence on the carbon peak ($2\theta = 26.5°$). Thus, the higher carbon content of unformed negative plates (Table 2) was linked to the negative paste carbon evolution during the mixing process. Presence of the tribasic lead sulfates (3BS: $3PbO \cdot PbSO_4 \cdot H_2O$), tetragonal PbO, $PbSO_4$ and Pb, was also appreciated in the diffractograms. Furthermore, GANFg content reduced the median pore diameter, although, this reduction was not appreciated when GANFg were added at 0.1 wt. %.

3.3. Formed negative plates properties

Small lead acid cells were assembled and filled with H_2SO_4 (1.28 g cm^{-3}). After a soaking period at 40 °C, formation process started (section 2.2). After this process, formed negative plates were washed and dried in a vacuum chamber. During the

formation process, GANFg took part in the charging reaction acting as current collector (for being more conductive than the rest of the materials; mainly 3BS and PbO). Small lead crystals would deposit around these Nano compounds, increasing the specific surface area of the formed negative plates. Table 2 shows the physicochemical properties of these formed plates. The hydro-cerussite found in the unformed negative plates was converted into CO_2, which escaped from the cell during the electrolyte filling process [28]. As a result, carbon content considerably decreased, being at that point, consistent with the GANFg amount of each mixture. No differences were found between carbon content of NAM Control and S7. GANFg content, and thus a higher carbon concentration, improved the formation process efficiency, as $PbSO_4$ concentration was lower for S5. Formed negative plates BET SSA was consistent with GANFg contained in each mixture; an increase in GANFg content involved more activated sites for Pb^{2+} reduction, and thus, decreased the Pb crystals size. In both, lead sulfate content and BET SSA, no differences between NAM Control and S7 were found due to the low GANFg content of S7. At this point, addition of GANFg at 0.1 wt. % did not make any effect.

3.4. Capacity and cold cranking ability

Cells were discharged at 0.05 A (cutoff = 1.75 V) in order to measure low rate capacity (C_{20}); results are shown in Fig. 2a. During the discharge, Pb is oxidized in the negative plate; $PbSO_4$ crystals obtained are deposited on the lead skeleton, increasing the internal resistance and decreasing the cell potential, until reaching the cutoff. Lignosulfonates cause a delay of the charge/discharge reactions that occur inside the cell. Furthermore, their sulfonic groups exert a delay of the passivation phenomena caused by the $PbSO_4$ layer [29]. Higher concentrations of this organic expander increases the capacity, but decrease the HRPSoC cycle life [21]. In this case, there were not significant differences among mixtures, due to all mixtures comprised the same amount and chemical structure of lignosulfonate, including NAM Control. An increase in the second capacity was related to the NAM activation.

During the cold cranking ability test, a high rate discharge (5 A) was applied to the cells at low temperature conditions (-18 ± 2 °C) until reaching the cutoff = 1.00 V. This test was performed in order to simulate the engines cold-start. Cells were aggressively and rapidly discharged; this caused a lead sulfate passivating layer, which could be avoided by the presence of lignosulfonates [21]. This test was performed twice, and corresponding results are shown in Fig. 2b. Because of using the same amount and type of lignosulfonate (0.30 wt. %), no significant differences were expected. However, NAM Control showed worse results in contrast to GANFg mixtures, probably in this case, there was not good dispersion of LS and its performance declined.

3.5. Initial charge acceptance evaluation

LABs of Micro Hybrid vehicles must be able to absorb the kinetic energy from the braking, namely to have a high charge acceptance at high SoC. In order to test this charge acceptance ability, cells were discharged to 90% of their SoC (at 0.05 A for 2 hours). During this discharge, a $PbSO_4$ passivating layer was formed, which remained on the lead skeleton for 72 hours of rest. After this, cells were recharged at constant cell potential (2.42 V); current at 5 s was studied as an indication of the charge acceptance of the negative plates (Fig. 2c). At the beginning of the charge, the negative plate was partially sulfated; at that point, GANFg should be able to conduct part of the current throughout the negative plates due to their low electrical resistivity ($1 \cdot 10^{-4}$ Ohm m). If they have reached the percolation threshold this conduction would be well distributed in the negative plate. Results show a very slight
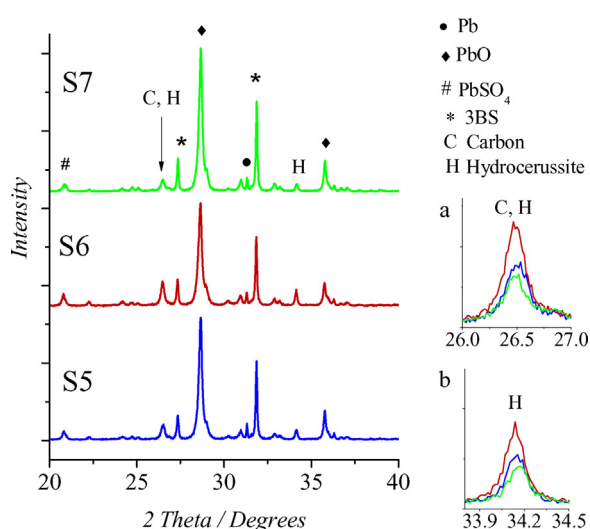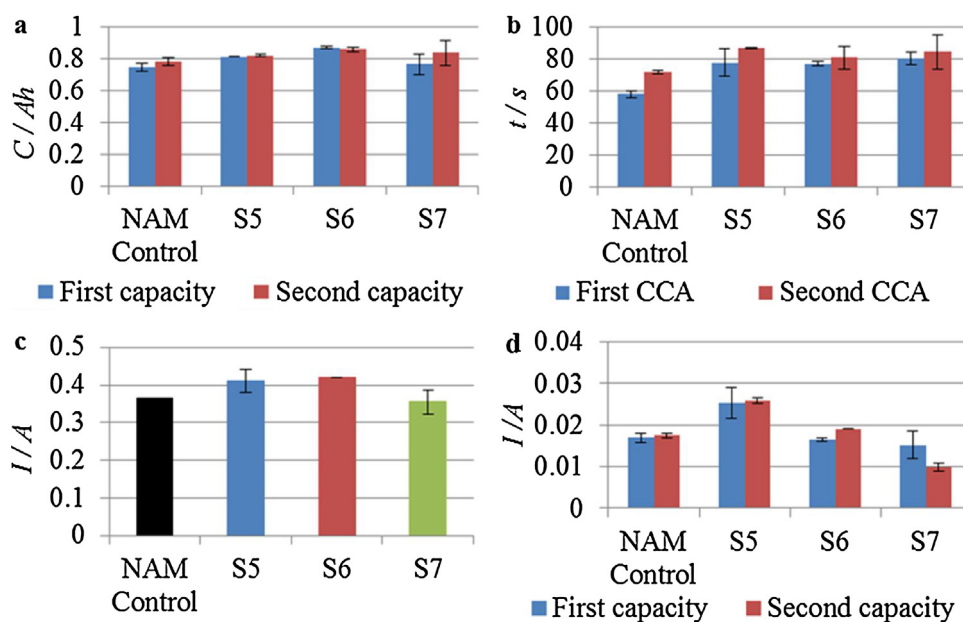

Fig. 1. XRD patterns for unformed negative plates of mixtures S5, S6 and S7. **a.** Hydrocerussite and Carbon peaks around $26.5°$ (2θ). **b.** Hydrocerussite peak at $34.2°$ (2θ).
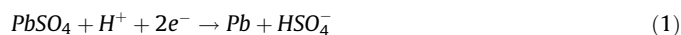
Fig. 2. a. Results on first and second capacity test performed at $(27 \pm 2)\,°C$. **b.** Results on first and second cold cranking ability test performed at extreme low temperature $(-18 \pm 2)\,°C$. **c.** Results on initial charge acceptance test performed at $(27 \pm 2)\,°C$. Current at 5th second of charge at 2.42 V. **d.** Float currents during the recharge of the cells after the first and the second capacity.

increase in the charge acceptance when GANFg content was increased and almost same results for NAM Control. Carbon materials with high BET SSA improve the charge acceptance of the negative plates due to increasing NAM electrochemical active area. In this way these carbon materials are able to storage charges inside them, and could promote the $PbSO_4$ reduction on them [10]. However, these GANFg, with a BET SSA of $105–115\,m^2\,g^{-1}$, can be integrated into the lead skeleton. In this way they do not make a great effect on NAM electrochemical surface area and thus, nor the charge acceptance of the negative plates.

3.6. Water consumption evaluation

Under cell operation, at least three reactions can take place in the negative plate:

$$PbSO_4 + H^+ + 2e^- \rightarrow Pb + HSO_4^- \tag{1}$$

$$Pb + HSO_4^- \rightarrow PbSO_4 + H^+ + 2e^- \tag{2}$$

$$2H^+ + 2e^- \rightarrow H_2 \uparrow \tag{3}$$

In the negative plate, lead sulfate is reduced to lead during the charge reaction (1), and lead is oxidized to lead sulfate during the discharge reaction (2). The third possible reaction in the negative plate (3) is related to HER, and occurs in overcharge conditions or during self-discharge processes. If HER rate is not under control, hydrogen gassing inside the battery increases, leading to high water consumption. Water loss is computed as the global hydrogen and oxygen gassing output, which provokes the electrolyte saturation and leads to the final battery failure. In order to study this parameter in the different mixtures, two experiments were performed: measurement of the float currents (Fig. 2d) and the negative polarization study (Fig. 3).

After each capacity test, cells were recharged at 0.25 A/2.67 V for 24 hours, until reaching the 100% SoC. At the end of this recharge, the float currents were measured. At that point, reaction (1) was not taking place, as all reversible $PbSO_4$ had already been converted to lead. Therefore HER (3) was the only reaction that took place, and measured float currents were an indication of HER rate. Float currents are shown in Fig. 2d, where can be appreciated higher float currents when GANFg concentration increased. NAM Control, without comprising any carbon material, showed unexpectedly, similar results to mixtures S6 and S7. LS performance plays also a key role in HER; good distribution of LS in NAM hampers the HER, as this is a nonconductive material and no reaction can take place on its surface, lowering water loss. Good LS distribution was expected for mixtures S5, S6 and S7, as LS was previously dispersed in water, as well as low HER rates. In the case of NAM Control, LS distribution was expected to be worse, because of using no dispersion, leading to higher HER rates. S5 showed higher float currents than NAM Control: the high GANFg
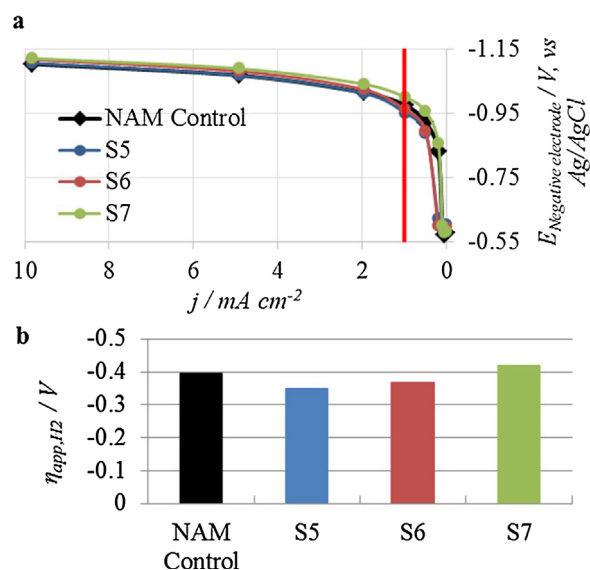
Fig. 3. a. Negative electrode potential vs current density. Polarization curves for mixtures NAM Control, S5, S6 and S7. Red line at $j= 1\,mA\,cm^{-2}$. **b.** HER apparent overpotential: $\eta_{app,H2}$, of mixtures NAM Control, S5, S6 and S7.

concentration of S5 will be more relevant than a good distribution of LS, improving HER on the carbon surface.

In order to corroborate these results, negative polarization study was performed. The E_{OCP} of negative plates was measured and then, cells were subjected to a set of fixed currents for a certain time (section 2.3.3). At the end of each charge, the potential electrode of the negative plate was measured (E_j) and polarization curves were drawn, see Fig. 3a.

Two behaviors were well appreciated in Fig. 3a:

– **A.** $j > 1$ mA cm^{-2}: where there was a linear distribution between potential and current density. In these conditions, HER process was better developed and protons were easily reduced to hydrogen.
– **B.** $j < 1$ mA cm^{-2}: there was no linear relation between potential and current density. In this range, two reactions could occur together: reduction of some reversible PbSO$_4$ according to reaction (1), and proton reduction to hydrogen, reaction (3), so both reactions were competing.

In order to explore which mixtures showed higher HER rate, H$_2$ apparent overpotential ($\eta_{app,H2}$), was calculated as: $\eta_{app,H2} = E_{j = 1 mA \cdot cm^{-2}} - E_{OCP}$. At this point, the relation between current density and electrode potential became linear; it can be assumed better development of HER in comparison with reaction (1). $\eta_{app,H2}$, for all mixtures, is shown in Fig. 3b.

Lower HER overpotentials are related to higher HER rates and H$_2$ gassing, which causes an increase in water loss and a charge efficiency reduction. In our study, an increase in GANFg content was related to higher water loss by lowering the HER overpotential. As preliminary conclusions, GANFg at loads higher than 0.30 wt. % increased the water loss.

The negative polarization study has already been performed to mixtures containing different carbon materials that are currently used in LABs industry (carbon black, graphite and hybrid carbons) [13]. In already said study, Mixture 1 (LS (0.30 wt. %) and graphite

(1.50 wt. %)), showed the lowest $\eta_{app,H2}$ (-0.33 V) following the same experimental set-up study. However, in this case, GANFg $\eta_{app,H2}$ was higher than −0.33 V for all mixtures. Any mixture that contains carbon black, graphite or hybrid carbon studied in [13], would show higher water consumption than GANFg mixtures.

GANFg improved electrical conductivity throughout NAM and also the number of activated sites where protons were reduced, increasing HER rate. Furthermore, GANFg were obtained by a Ni catalyst [24] [26], which was not completely eliminated after the manufacturing process of this Nano-material (Ni final concentration in GANFg was < 20 ppm). This element is related to exert a detrimental synergistic effect on hydrogen evolution [30], which gives further information about the effect of GANFg on HER.

3.7. Cyclic voltammetry (CV)

In order to study in more depth the electrochemical reactions that take place in the negative plate ((1), (2) and (3)), 300 cycles of CV at a constant scan rate of 5 mV s^{-1}, in the range of 0.60 V to −1.50 V were performed for S7 (see Fig. 4a). During one cycle, reaction (2) occurs in the anodic part of the cycle, and reactions (1) and (3) occur in the cathodic part. As was mentioned in section 3.6, these two last reactions compete at low negative potentials, but at more negative potentials, just reaction (3) takes place. After cycling process (300 cycles), voltammograms show a decrease on discharge peak (Fig. 4a). However, the shape of cathodic peak was not very affected. Differences between peak potentials for reactions (1) and (2) were more pronounced after cycling, indicating a loss of reversibility associated with these cycles. In the case of HER study (see Fig. 4b), the current associate with this process was higher for the 1st scan, indicating more hydrogen production. However, for the 300th scan, the curve went down at less negative overpotentials but became flatter than in the 1st scan. The amount of charge stored during discharge (Q$_d$) and charge (Q$_c$) reactions is shown in Fig. 4c. During the whole experiment, Q$_d$ was higher than Q$_c$; this explained the reversibility loss: the discharge
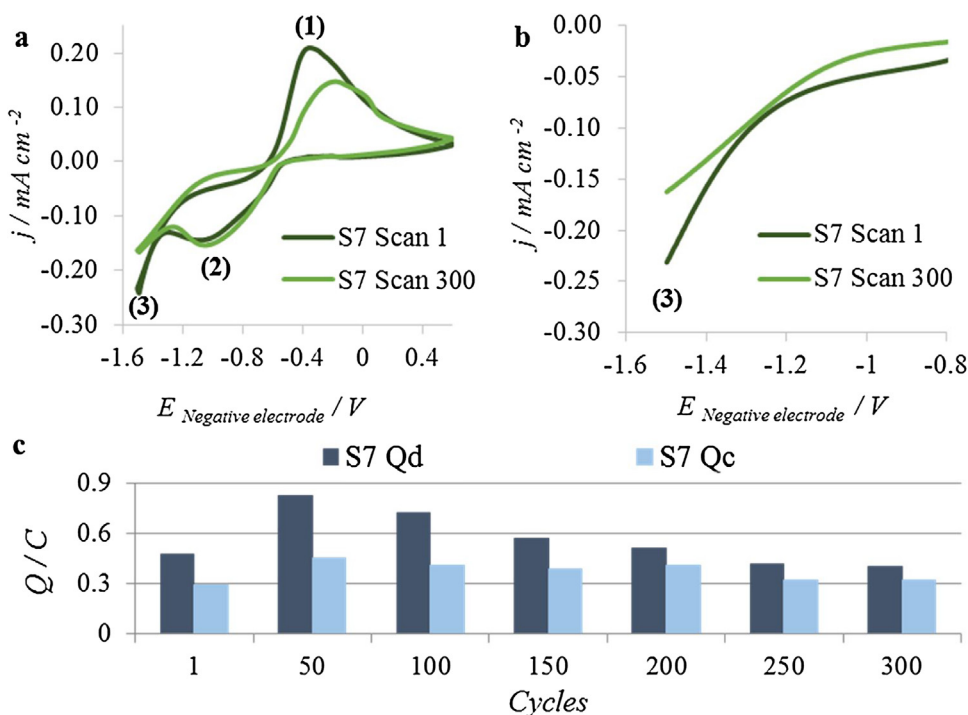
Fig. 4. E: Negative electrode potential vs Ag/AgCl reference electrode. CV at 5.00 mV s^{-1} from 0.60 V to −1.50 V. 300 cycles. S7. **a.** 1st and 300th. Discharge **(1)**, charge **(2)** and Hydrogen Evolution **(3)** peaks. **b.** HER (3); From −0.80 V to −1.50 V. **c.** Stored charge during discharge (Q$_d$) and charge (Q$_c$) reactions. Data were represented every 50 cycles.

reaction rate was higher and more irreversible $PbSO_4$ was produced in the negative plate. Q_d showed an increase at the beginning of the experiment (50 cycles), but later it became to its initial value. This could be associated with the material activation during cycling process; however, this effect was less noticeable for Q_c. As main conclusion, discharge reaction (1) was more favored than charge reaction (2), leading to a $PbSO_4$ deposition which decreased both, HER rate and system reversibility.

3.8. Cycle life in PSoC conditions

Schematic procedure of PSoC cycle test is shown in Fig. 5a. During these cycles, irreversible lead sulfate was deposited on the lead surface, developing a $PbSO_4$ passivating layer which leads to the cell failure. In this "$PbSO_4$ rich" environment, the electrical conductivity of the negative plates was drastically reduced, and an important part of the current should be carried out by GANFg, due to they were the second most conductive compound in NAM, after lead. The NAM electrical conductivity improvement by carbon materials was clarified by P.T. Moseley and D. Rand [31]. In this manner, addition and concentration of GANFg should increase the cycle life working in PSoC conditions, which was confirmed in Fig. 5b. All GANFg mixtures fulfilled more than 1000 cycles. For this reason, all of them are expected to work properly as NAM additives improving EFB performance in Micro Hybrid vehicles. In addition, GANFg increased the number of cycles accordingly to NAM Control results (893 cycles). There were no significant differences on the cycles performed by S6 and S7, meaning that a GANFg increase of 0.10 wt. % did not affect in the cycle life.

3.9. NAM properties after cell operation

After cell operation (Initial Charge Acceptance test and Negative Polarization Study; T: Tested negative plates) and PSoC cycles (C: Cycled negative plates), cells were disassembled and NAM properties were studied. Diffractograms of tested plates are shown in Fig. 6. As expected, lead was present in all the mixtures. In addition, hydrocerussite (27° and 34.2° (2θ)) was not detected in these plates; this compound was converted to CO_2 and abandoned the cell during the soaking process [28]. $PbSO_4$ peak was lower for S5, which could be associated with a better charge acceptance of this mixture. PbO appeared in all the mixtures, as a consequence of the partial oxidation of lead on air.

Table 3 shows carbon and $PbSO_4$ content of cycled negative plates. Carbon content in formed and cycled negative plates (see Tables 2 and 3), was very similar, concluding that GANFg and LS remained in NAM during PSoC cycles. As has been said before, negative plate sulfation was the failure mode of this test. The low
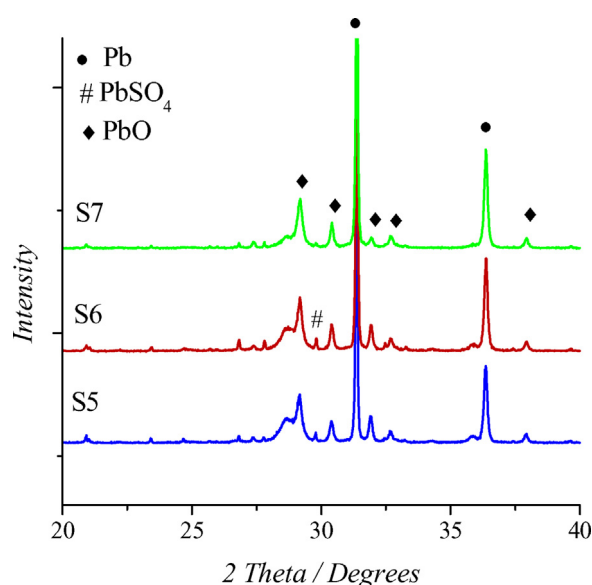
Fig. 6. XRD patterns for tested negative plates of mixtures S5, S6 and S7.

Table 3
Carbon and lead sulfate concentration of the negative plates after PSoC cycles.

Mixture	Cycles	Carbon/wt. %[a]	$PbSO_4$/wt. %[a]
NAM Control	893	0.33	11.4
S5	1670	0.84	26.35
S6	1095	0.54	16.40
S7	1139	0.36	36.20

[a] wt. % related to the total mass of the sample.

amount of lead sulfate found in all plates was consistent with the initial SoC of the cells: 100%. $PbSO_4$ content was higher for those mixtures that fulfilled more cycles, as exception of S7. According to negative plate conductivity, S5, due to containing the highest GANFg amount, performed the maximum number of cycles. This mixture was followed by mixtures S7, S6 and NAM Control, respectively. In the case of mixtures S7 and S6, both fulfilled similar number of cycles, meaning that a GANFg increase of 0.1 wt. % did not make a great effect on this test, did not considerably increase NAM conductivity. However, NAM Control, as expected, completed the lowest number of cycles. This mixture failed at a very low lead sulfate concentration (11.4 wt. %), thereby a great loss on conductivity was reached at that point.

SEM micrographs of tested and cycled negative plates are shown in Fig. 7. Among the tested plates, all mixtures showed a compact structure built by small lead particles. It seems that GANFg content increased the NAM compactness (see big agglomerates of S5T.1). Higher GANFg content could increase dispersion viscosity, and promote the agglomerates formation.

For the cycled plates, the size of the crystal was consistent with the number of cycles fulfilled by each mixture. S5, S6 and S7 were not much damaged; GANFg was able to maintain a good particle distribution through PSoC cycles. However, in reference to carbon materials utilized in former study [13], S5, S6 and S7 fulfilled more cycles than the majority of those mixtures. Indeed, addition of GANFg at 0.10 wt. % improved the PSoC cycle life in comparison to NAM comprised by carbon blacks, graphite or hybrid carbon materials. Mixture 1 (graphite (1.5 wt. %) and LS (0.3 wt. %)), performed 1525 PSoC cycles in that study [13]. In the current study,
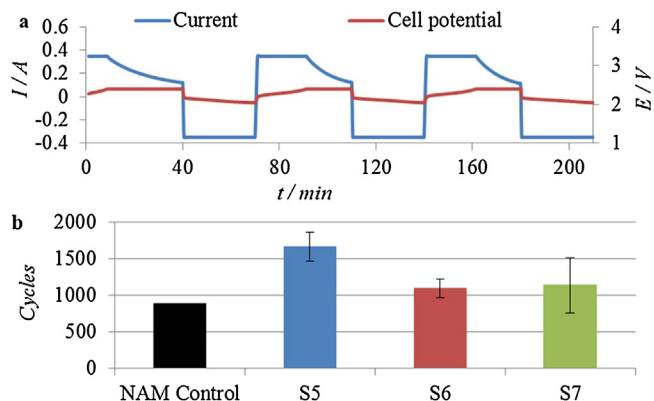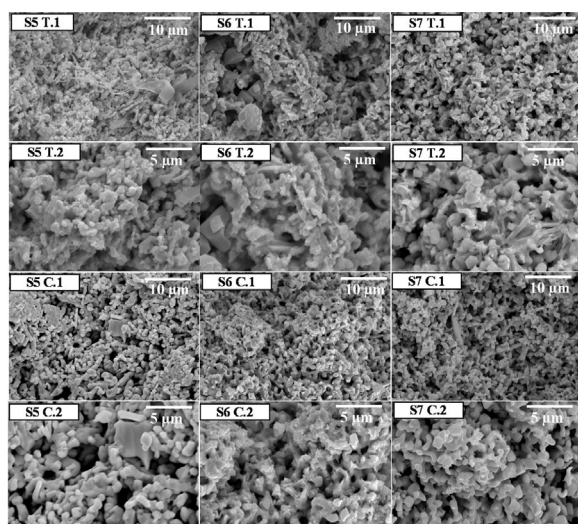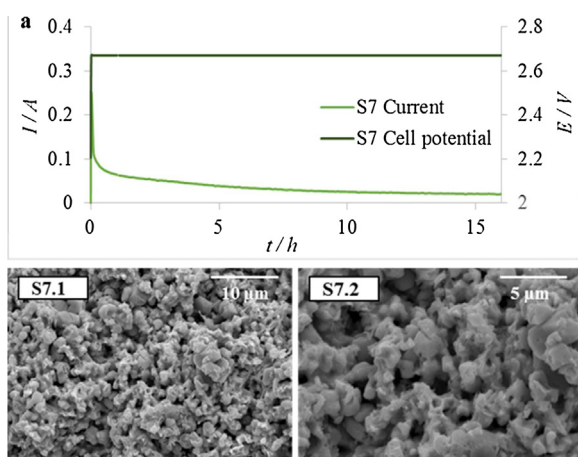
Fig. 5. a. Schematic procedure of cycles at PSoC at (27 ± 2) °C. **b.** Results on this test: NAM Control − 893. S5 − 1670 cycles. S6 − 1095 cycles. S7 − 1139 cycles.

Fig. 7. SEM micrographs. T: NAM after initial charge acceptance test and negative polarization study. **C:** NAM after cycling at PSoC. Magnifications: **1**. x3000. **2**. x6000.

Fig. 8. a. Recharge after PSoC cycles for mixtures S7. SEM micrographs. NAM after PSoC cycles followed by a 16 hours recharge. **S7** (1139 cycles): **1**. x3000. **2**. x6000.

more cycles have been achieved adding only 0.50 wt. % of carbon material.

One S7 cell was recharged (0.25 A/2.67 V/16 hours) after failing at PSoC cycles, in an attempt to have information from the irreversible $PbSO_4$ concentration in NAM. Recharge of the cell is shown in Fig. 8a. S7 float current was around 0.02 A, doubling initial float current showed in Fig. 2d. $PbSO_4$ content was 17.1 wt. %, higher than in formed negative plates (Table 2), but lower than in cycled negative plates (Table 3). Fig. 8b shows the SEM micrographs of this cycled and recharged plate. Most of the particles in these micrographs were related to lead, as it came from the $PbSO_4$ reduction during the recharge. These particles were highly interconnected with bigger lead sulfate particles, forming a less porous structure. High sulfation of the negative plates after PSoC cycles increased irreversible $PbSO_4$ content, the HER rate and lowered the NAM porosity.

4. Conclusions

Graphitized Carbon Nanofibers (GANFg) manufactured by floating catalyst process at 0.50, 0.30, and 0.10 wt. % were well dispersed together with water and an organic expander: LS (sodium lignosulfonate). These dispersions were added to NAM,

and the final LS concentration was adjusted to 0.30 wt. %. Main electrical test results were compare with NAM Control (LS: 0.30 wt. %) performance. GANFg facilitated the formation process of the 2 V/ 1 Ah small lead acid cells, increasing the formed negative plates BET SSA.

Due to their high aspect ratio, GANFg were suitable to integrate the lead skeleton and slightly improved the charge acceptance of the negative plates. Water consumption studies revealed that GANFg increased HER rate by lowering its overpotential, and LS dispersion played a key role in this reaction.

GANFg increased NAM conductivity during PSoC cycles, leading always to the performance of more than 1000 cycles. In comparison with other carbon materials, GANFg at very low concentration (0.50 wt. % vs 1.5 wt. % of graphite) showed a higher increase in cycle life. In addition, this new additive, due to being added at low concentrations, shows less water consumption than other carbon materials that are currently used in the battery industry.

As a summary, GANFg, added at very low dosages (0.10–0.50 wt. %), were able to create a conductive network inside the NAM, increasing the PSoC cycled life of the formed negative plates. GANFg concentration raised the water loss, but less than other carbon materials.

References

[1] L. Wang, W. Zhang, L. Gu, Y. Gong, G. Cao, H. Zhao, Y. Yang, H. Zhang, Tracking the morphology evolution of nano-lead electrodeposits on the internal surface of porous carbon and its influence on lead-carbon batteries, Electrochim. Acta 222 (2016) 376–384, doi:http://dx.doi.org/10.1016/j.electacta.2016.10.189.

[2] L. Wang, H. Zhang, G. Cao, W. Zhang, H. Zhao, Y. Yang, Effect of activated carbon surface functional groups on nano-lead electrodeposition and hydrogen evolution and its applications in lead-carbon batteries, Electrochim. Acta. 186 (2015) 654–663, doi:http://dx.doi.org/10.1016/j.electacta.2015.11.007.

[3] X. Zou, Z. Kang, D. Shu, Y. Liao, Y. Gong, C. He, J. Hao, Y. Zhong, Effects of carbon additives on the performance of negative electrode of lead-carbon battery, Electrochim. Acta. 151 (2015) 89–98, doi:http://dx.doi.org/10.1016/j.electacta.2014.11.027.

[4] J. Valenciano, A. Sánchez, F. Trinidad, A.F. Hollenkamp, Graphite and fiberglass additives for improving high-rate partial-state-of-charge cycle life of valve-regulated lead-acid batteries, J. Power Sources. 158 (2006) 851–863, doi: http://dx.doi.org/10.1016/j.jpowsour.2005.11.058.

[5] P. Tong, R. Zhao, R. Zhang, F. Yi, G. Shi, A. Li, H. Chen, Characterization of lead (II)-containing activated carbon and its excellent performance of extending lead-acid battery cycle life for high-rate partial-state-of-charge operation, J. Power Sources. 286 (2015) 91–102, doi:http://dx.doi.org/10.1016/j.jpowsour.2015.03.150.

[6] M. Calábek, K. Micka, P. Křivák, P. Bača, Significance of carbon additive in negative lead-acid battery electrodes, (2006), doi:http://dx.doi.org/10.1016/j.jpowsour.2005.11.022.

[7] E. Ebner, D. Burow, J. Panke, A. Börger, A. Feldhoff, P. Atanassova, J. Valenciano, M. Wark, E. Rühl, Carbon blacks for lead-acid batteries in micro-hybrid applications −Studied by transmission electron microscopy and Raman spectroscopy, J. Power Sources. 222 (2013) 554–560, doi:http://dx.doi.org/10.1016/j.jpowsour.2012.08.089.

[8] M. Fernández, J. Valenciano, F. Trinidad, N. Muñoz, The use of activated carbon and graphite for the development of lead-acid batteries for hybrid vehicle applications, J. Power Sources. 195 (2010), doi:http://dx.doi.org/10.1016/j.jpowsour.2009.12.131.

[9] L.T. Lam, R.H. Newnham, H. Ozgun, F.A. Fleming, Advanced design of valve-regulated lead-acid battery for hybrid electric vehicles, J. Power Sources. 88 (2000), doi:http://dx.doi.org/10.1016/S0378-7753(99)00515-7.

[10] P.T. Moseley, R.F. Nelson, A.F. Hollenkamp, The role of carbon in valve-regulated lead–acid battery technology, J. Power Sources 157 (2006) 3–10, doi: http://dx.doi.org/10.1016/j.jpowsour.2006.02.031.

[11] D. Pavlov, P. Nikolov, T. Rogachev, Influence of carbons on the structure of the negative active material of lead-acid batteries and on battery performance, J. Power Sources. 196 (2011) 5155–5167, doi:http://dx.doi.org/10.1016/j.jpowsour.2011.02.014.

[12] T. Rogachev, P. Nikolov, G. Petkova, Mechanism of action of electrochemically active carbons on the processes that take place at the negative plates of lead-acid batteries, J. Power Sources. 191 (2009) 58–75, doi:http://dx.doi.org/10.1016/j.jpowsour.2008.11.056.

[13] M. Blecua, E. Fatas, P. Ocon, J. Valenciano, F. de la Fuente, F. Trinidad, Influences of carbon materials and lignosulfonates in the negative active material of lead-acid batteries for microhybrid vehicles, J. Energy Storage. 11 (2017) 55–63, doi: http://dx.doi.org/10.1016/j.est.2017.01.005.

[14] M. Saravanan, M. Ganesan, S. Ambalavanan, An in situ generated carbon as integrated conductive additive for hierarchical negative plate of lead-acid battery, J. Power Sources. 251 (2014) 20–29, doi:http://dx.doi.org/10.1016/j.jpowsour.2013.10.143.

[15] D. Pavlov, T. Rogachev, P. Nikolov, G. Petkova, Mechanism of action of electrochemically active carbons on the processes that take place at the negative plates of lead-acid batteries, J. Power Sources. 191 (2009) 58–75, doi: http://dx.doi.org/10.1016/j.jpowsour.2008.11.056.

[16] S. Logeshkumar, R. Manoharan, Influence of some nanostructured materials additives on the performance of lead acid battery negative electrodes, Electrochim. Acta. 144 (2014) 147–153, doi:http://dx.doi.org/10.1016/j.electacta.2014.08.080.

[17] S.W. Swogger, P. Everill, D.P. Dubey, N. Sugumaran, Discrete carbon nanotubes increase lead acid battery charge acceptance and performance, J. Power Sources. 261 (2014) 55–63, doi:http://dx.doi.org/10.1016/j.jpowsour.2014.03.049.

[18] N. Sugumaran, P. Everill, S.W. Swogger, D.P. Dubey, Lead acid battery performance and cycle life increased through addition of discrete carbon nanotubes to both electrodes, J. Power Sources. 279 (2015) 281–293, doi: http://dx.doi.org/10.1016/j.jpowsour.2014.12.117.

[19] R. Marom, B. Ziv, A. Banerjee, B. Cahana, S. Luski, D. Aurbach, Enhanced performance of starter lighting ignition type lead-acid batteries with carbon nanotubes as an additive to the active mass, J. Power Sources. 296 (2015) 78–85, doi:http://dx.doi.org/10.1016/j.jpowsour.2015.07.007.

[20] Q. Long, G. Ma, Q. Xu, C. Ma, J. Nan, A. Li, H. Chen, Improving the cycle life of lead-acid batteries using three-dimensional reduced graphene oxide under the high-rate partial-state-of-charge condition, J. Power Sources. 343 (2017) 188–196, doi:http://dx.doi.org/10.1016/j.jpowsour.2017.01.056.

[21] D. Pavlov, P. Nikolov, T. Rogachev, Influence of expander components on the processes at the negative plates of lead-acid cells on high-rate partial-state-of-charge cycling. Part I: Effect of lignosulfonates and BaSO4 on the processes of charge and discharge of negative plates, J. Power Sources 195 (2010) 4435–4443, doi:http://dx.doi.org/10.1016/j.jpowsour.2009.11.060.

[22] N. Hirai, S. Kubo, K. Magara, Combined cyclic voltammetry and in situ electrochemical atomic force microscopy on lead electrode in sulfuric acid solution with or without lignosulfonate, J. Power Sources. 191 (2009) 97–102, doi:http://dx.doi.org/10.1016/j.jpowsour.2008.10.090.

[23] R. Khayat Ghavami, F. Kameli, A. Shirojan, A. Azizi, Effects of surfactants on sulfation of negative active material in lead acid battery under PSOC condition, J. Energy Storage. 7 (2016) 121–130, doi:http://dx.doi.org/10.1016/j.est.2016.06.002.

[24] J. Vera-Agullo, H. Varela-Rizo, J.A. Conesa, C. Almansa, C. Merino, I. Martin-Gullon, Evidence for growth mechanism and helix-spiral cone structure of stacked-cup carbon nanofibers, Carbon N. Y. 45 (2007) 2751–2758, doi:http://dx.doi.org/10.1016/j.carbon.2007.09.040.

[25] M. Weisenberger, I. Martin-Gullon, J. Vera-Agullo, H. Varela-Rizo, C. Merino, R. Andrews, D. Qian, T. Rantell, The effect of graphitization temperature on the structure of helical-ribbon carbon nanofibers, Carbon N. Y. 47 (2009) 2211–2218, doi:http://dx.doi.org/10.1016/j.carbon.2009.03.070.

[26] I. Martin-Gullon, J. Vera, J.A. Conesa, J.L. González, C. Merino, Differences between carbon nanofibers produced using Fe and Ni catalysts in a floating catalyst reactor, Carbon N. Y. 44 (2006) 1572–1580, doi:http://dx.doi.org/10.1016/j.carbon.2005.12.027.

[27] M. Matrakova, D. Pavlov, Thermal analysis of lead-acid battery pastes and active materials, J. Power Sources. 158 (2006) 1004–1011, doi:http://dx.doi.org/10.1016/j.jpowsour.2005.11.007.

[28] D. Pavlov, Lead-Acid Batteries: Science and Technology, (2011) .

[29] A.C. Zachlin, Functions and Behavior of the Components of Expanders for the Negative Plates of Lead-Acid Storage Batteries, J. Electrochem. Soc. 98 (1951) 325–333, doi:http://dx.doi.org/10.1149/1.2778215.

[30] L.T. Lam, H. Ceylan, N.P. Haigh, T. Lwin, Influence of residual elements in lead on oxygen- and hydrogen-gassing rates of lead-acid batteries, J. Power Sources. 195 (2010) 4494–4512, doi:http://dx.doi.org/10.1016/j.jpowsour.2009.12.020.

[31] P. Moseley, D.A. Rand, Changes in the demands on automotive batteries require changes in battery design, J. Power Sources. 133 (2004) 104–109, doi:http://dx.doi.org/10.1016/j.jpowsour.2003.12.034.
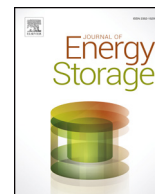
Improvement of the lead acid battery performance by the addition of graphitized carbon nanofibers together with a mix of organic expanders in the negative active material

M. Blecua[a], A.F. Romero[a], P. Ocon[a,*], E. Fatas[a], J. Valenciano[b], F. Trinidad[b]

[a] Universidad Autónoma de Madrid, Departamento de Química Física Aplicada, C/Francisco Tomás y Valiente 7, 28049, Madrid, Spain
[b] Exide Technologies, R&D Centre, 19200, Azuqueca de Henares, Spain

ABSTRACT

Lead Acid Batteries (LABs) in the Micro Hybrid vehicle have to work in Partial State of Charge (PSoC) conditions, where the negative plates may develop high sulfation leading to the battery death. In order to reduce this sulfation, Graphitized Carbon Nanofibers (GANFg) at 0.10% and two types of Organic Expanders (OEs) were used as additives for the negative plates. These fibers were previously dispersed with a certain amount of OEs. Five mixtures were selected, and the corresponding negative plates were prepared. 2 V / 1 Ah cells were assembled and tested, together with the physicochemical properties of the plates. During the formation of the cells, GANFg are thought to be integrated into the NAM skeleton where would improve the NAM energetic structure. As a result, the use of GANFg slightly enhanced the capacity and the cold cranking ability, although this last one was essentially dominated by the OEs concentration. A lower OEs concentration led to higher charge acceptance, and the use of GANFg involved a higher water loss. However, the water loss rate was considered low in comparison with other carbon materials. GANFg addition increased the cycle life of the cells during the 17.5% DoD cycling test (at PSoC).

1. Introduction

Lead Acid Batteries (LABs) have been in continuous development for more than 150 years. These secondary batteries are based on the reversible electrochemical reactions of the $Pb/PbSO_4$ and $PbSO_4/PbO_2$ electrode systems, and are used in our everyday life (transport vehicles, telecommunications, information technologies, etc.). Due to the development of the automotive industry, LABs are supposed to supply power for a wide range of accessories for the modern vehicles. In addition, the battery performance has to be also upgraded to work in the Micro Hybrid vehicles that implement Start & Stop system. This system reduces fuel consumption and emissions. It is based on the engine switch off when the vehicle is stopped. In addition, it can also implement the regenerative braking; therefore, the kinetic energy can be used for recharging the battery. For working in these conditions a good cycle life of the battery at Partial State of Charge (PSoC) is needed, as well as, a high charge acceptance. It is well known that these two parameters can be impeded by the negative plate, due to the formation of irreversible $PbSO_4$ crystals, which leads to the battery failure. In order to avoid these problems, three-component expander are added to the

Negative Active Material (NAM): Organic Expanders (OEs), barium sulfate and carbon [1]. Lignosulfonates, which act inside the NAM as a OE, is a surface active polymer that prevents the negative plate to be completely covered by $PbSO_4$ crystals [2]. The barium sulfate is isomorphic to $PbSO_4$ and that's why it behaves as a nucleating agent during the discharge of the negative plate, increasing the porosity of the $PbSO_4$ layer [3].

The carbon materials are the third component, whose influence on the NAM has been under study for more than 20 years. Two stages can be defined for the use of carbon materials in LABs: (1) the use of carbon black [Nakamura] and (2) the use of more specialized carbon materials, as activated carbons, expanded graphite… [4]. The addition of carbon materials increases the NAM electrochemical surface area. In this way, the creation of isolated $PbSO_4$ crystals is promoted during the discharge of the battery. These crystals prevent the formation of a $PbSO_4$ passivated layer, increasing the charge acceptance and the cycle life. Carbon materials also increase the overall conductivity of the NAM, leading to an improvement in the charge acceptance of the negative plates. This effect is more pronounced when high surface area carbon materials are added to the NAM, as they increase in a higher rate the sites where the

---

$PbSO_4$ can be reduced [5–8]. However, carbon material must show a high affinity for the lead in order to improve all of these parameters [9]. The influence of many carbon materials (graphite, expanded graphite activated carbon, carbon black etc.) in NAM have been studied [6–13]. However, all studies lead to the same conclusions: carbon materials are able to improve the charge acceptance and the cycle life of LABs, but they also increase the Hydrogen Evolution Reaction (HER) in the negative plate, which could lead to the H_2SO_4 concentration increase and the final battery failure. For this reason, it is important to select the right type and dosage of carbon materials.

Nowadays, several nanostructured carbon materials [14–17], such as discrete Carbon Nano Tubes (dCNT) [18,19], Multi Wall Carbon Nano Tubes (MWCNT) [20], Carbon nanofibers [21], or three-dimensional reduced graphene oxide (3DRGO) [22], have been also used as additives for the NAM in laboratory trials. The advantage of using this type of materials is the low concentration needed for reaching a high cycle life (maximum concentration of 0.50%). However caution must be taken, as these materials can contain impurities that raise the HER rate and thus, water loss [23].

Following the conclusions from the former study [21], graphitized Carbon Nanofibers from Grupo Antolin (GANFg) at 0.10% have been used as additives for the NAM in this work. Grupo Antolin is one of the largest players in the car interiors market internationally and number 1 worldwide supplier of headliner substrates, and also a supplier of advanced carbon materials, such as GANFg [24].

In addition, two types of OEs have been selected, and added to the NAM at different concentrations. The use of the GANFg involved their pre-dispersion using a certain amount of OEs. Finally, five NAM mixtures, and their corresponding negative plates, were prepared at the laboratory. 2 V / 1 Ah small Lead-Acid cells were assembled and formed, and different features of the cells were evaluated: capacity and cold-cranking ability, initial charge acceptance, negative polarization and cycle life test with 17.5% Depth of Discharge (DoD). Corresponding physicochemical analyses were done through the whole study.

2. Experimental

2.1. Preparation of GANFg dispersions and unformed negative plates

GANFg, with nearly 100% graphitization degree, as carbon materials and two different OEs (1 and 2) were incorporated as additives in the NAM. GANFg and a certain amount of OEs were dispersed in water (see Table 1). OE 1 was a highly modified lignin-based additive, and OE 2 was a highly polymerized naphthalene sulfonate. The dispersion was made in three consecutive stages: soaking, milling, and high shear. A dispersion equipment called as DISPERMAT® CN10 (VMA-GETZMANN GmbH) was used.

Table 1 shows the composition of all NAM mixtures. These mixtures

were prepared following the following procedure: First, the addition of all dry components was carried out: lead oxide powder (1 kg, oxidation degree = 72%), Polyacrylonitrile fiber (PAC) (0.22 wt. %), and $BaSO_4$ (1.00 wt. %). OEs were also added at this step, except for the blank mixture which did not contain these compounds. In the case of the GANFg mixtures (S25 and S26), the remaining amount of OEs was added, because part of these compounds was added during the dispersion step of the GANFg. OEs concentration was different for each mixture (see Table 1). All these materials were mixed for 3 min. After that, the water and / or GANFg were included in the dispersion. The final concentration of water was 12.70–14.70 wt. %. This mixture was stirred for 5 min. Dropwise addition of H_2SO_4 (1.40 g cm^{-3}) to the mixture for 10 min was carried out. The concentration of the acid in the mixture was 4.60 wt. %. Once the mixture temperature was steady, the density of the paste was measured. This parameter is also shown in Table 1. All wt. % are related to the lead oxide mass.

A certain amount of paste (8 g) was coated on a Pb-Sn (0.80%) grid of 0.90 mm thickness, with an area of around 10 cm^2 (4.83 cm · 2.11 cm) in order to prepare the 1 Ah negative plates. The final thickness of the plates was 1.70 mm for both plates, positive and negative. Then curing process was carried out by two stages: curing for 22 h at 55 °C and 85% of relative humidity and drying for 2 h at 70 °C and a relative humidity lower than 30%.

Table 2 summarizes the physicochemical properties of the cured negative plates. Positive plates of the same dimensions and capacity were prepared following a standard procedure.

2.2. Assembly and formation of test cells

2 V / 1 Ah small Lead-Acid cells were prepared with one negative / two positive plate's assembly using a glass mat separator of a thickness of 0.37 mm (at 10 kPa). This glass mass separator is made of glass fiber (86%) and polyester fiber (14%). The assembly was compressed between two methacrylate sheets. This assembly was introduced into a 500 mL beaker which was filled with 250 mL of H_2SO_4 (1.28 g cm^{-3}).

The formation process at 40 °C comprised: an initial charge at constant current (0.35 A) for 13 h followed by several charges and discharges (−0.12 A/ 4.7 h, 0.24 A/ 3.0 h, 0.16 A/ 6.3 h, −0.24 A/ 2.5 h, 0.24 A/ 3.2 h, 0.12 A/ 4.2 h). After the formation process, physicochemical properties of the formed negative plates were analyzed; results are summarized in Table 2.

2.3. Electrical tests

ARBIN BT2543 potentiostat/galvanostat was used for testing the performance of the 2 V / 1 Ah small Lead-Acid cells.

2.3.1. Capacity and cold-cranking ability test
The cells were discharged at 0.05 A until they reached the cutoff of 1.75 V. The time was measured in order to know the low discharge rate

Table 1
Final composition of the mixtures and density of the NAM pastes after the mixing process (Blank, S25B, S25, S26B, and S26).

Components	Mixtures				
	Blank	S25B	S25	S26B	S26
PbO (kg)	1.00	1.00	1.00	1.00	1.00
H_2SO_4 (1.4 g cc^{-1}) (%)	4.60	4.60	4.60	4.60	4.60
H_2O (%)	14.70	13.50	13.50	13.70	12.70
PAC fiber (%)	0.22	0.22	0.22	0.22	0.22
$BaSO_4$ (%)	1.00	1.00	1.00	1.00	1.00
OE1 (%)	0.00	0.15	0.15	0.10	0.10
OE2 (%)	0.00	0.15	0.15	0.10	0.10
GANFg (%)	0.00	0.00	0.10	0.00	0.10
NAM density (g cc^{-1})	4.54	4.63	4.40	4.64	4.29

The final composition of the mixtures; wt. % related to the lead oxide mass (1 kg). OE: Organic Expanders.

Table 2
Physicochemical properties of the unformed (after the curing process) and formed (after the formation process) negative plates: carbon and lead sulfate concentrations, and BET SSA.

Sample	Unformed plates			Formed plates		
Mixture	Carbon (wt. %)*	$PbSO_4$ (wt. %)*	BET SSA (m^2 g^{-1})	Carbon (wt. %)*	$PbSO_4$ (wt. %)*	BET SSA (m^2 g^{-1})
Blank	0.40	6.30	1.42	0.10	4.50	0.25
S25B	0.90	6.10	1.92	0.30	2.80	0.50
S25	0.45	5.80	2.33	0.41	4.25	0.72
S26B	0.80	6.30	1.88	0.30	2.40	0.54
S26	0.43	6.25	2.18	0.39	4.45	0.66

*wt. % related to the total mass of the sample.

performance (C_{20} capacity). After this test, the cells were recharged for 24 h at 2.67 V with a current limit of 0.25 A. Float currents were measured during the whole recharge. The entire test was carried out in a water bath at 25 ± 2 °C. Cold cranking ability test comprised a high rate discharge at 5 A (5C) at an extreme low temperature (-18 ± 1) °C until they reached the cutoff of 1.00 V. Time spent by the cells until reaching the cutoff was measured. After this test, the cells were recharged for 16 h at 2.67 V with a current limit of 0.25 A. Both tests were performed twice. The discharge step was carried out in a climate chamber at -18 ± 2 °C and the charge step in a water bath at 25 ± 2 °C.

2.3.2. Initial charge acceptance test

Fully charged cells were used to perform this test. The initial State of Charge (SoC) was 100%. These cells were discharged for 2 h at 0.05 A, in order to reach the 90% of their SoC. They were left to stand for 24 h and then charged at a constant cell potential of 2.42 V for 1 min. During this charge, the current was measured every 0.01 s; the current at 5 s was used as a comparative parameter of the charge acceptance of the negative plates. Finally, the cells were recharged for 24 h at 2.67 V with a current limit of 0.25 A, until reaching their 100% SoC. The entire test was carried out in a water bath at 25 ± 2 °C.

2.3.3. Negative polarization test

During the negative polarization test the cells were charged at different steps: (1) 0.200A/50 min, (2) 0.100A/20 min, (3) 0.040A/20 min, (4) 0.020A/20 min, (5) 0.010A/20 min, (6) 0.004A/15 min, (7) 0.002A/10 min and (8) 0.001A/10 min. A reference electrode (Ag/AgCl) was used for measuring the negative plate potential. The Open Circuit Potential E_{OCP} (OCP), and during the test, at the end of every charge: Ej (j from 1 to 8) were determined. The apparent overpotential reached in every step was calculated as $\eta_{app, H2} = E_{j = 1 \ mA\cdot cm^{-2}} - E_{OCP}$. The entire test was carried out in a water bath at 25 ± 2 °C.

2.3.4. Cycle life test with 17.5% DoD

This test is based on the Endurance in cycle test with 17.5% DoD from the European Standard EN 50342-1 [25]. The fully charged cells (100% SoC) were discharged at 0.20 A (4 × I_{20}) during 2.5 h until they reached 50% of SoC. Cycles were comprised of two steps:

a) Charge at 0.35 A (7 × I_{20}) until reaching 2.42 V for 40 min.
b) Discharge at 0.35 A (7 × I_{20}) for 30 min. The test stopped when a cell potential of 1.66 V was reached.

The entire test was carried out in a water bath at 25 ± 2 °C.

2.4. Physicochemical characterization

SEM (SEM, S-3000 N; magnifications: 3000x) and XRD (polycrystalline between 10-90° θ using Cu-K α radiation on a Siemens D-5000 X-ray generator) techniques were used for studying morphology and phase composition of the negative plates. A Micromeritics Flow Sorb II 2300 Surface Area Analyzer was used to compute the BET SSA, at liquid nitrogen temperature (77 K), with previous drying of the samples, and degasification at room temperature. Carbon and $PbSO_4$ content in the negative and positive plates was determined using an ELTRA CS-800 analyzer. Carbon content represents the amount of carbon atoms that were part of any kind of chemical compound, form or structure, inside the active material.

3. Results and discussion

3.1. NAM composition and physicochemical properties of the pastes

For this study, GANFg were selected as carbon materials additives on the negative plates. The effect of this carbon material on the

performance of the negative plate of LABs was previously studied in [21]. As it is explained in that study, GANFg were selected due to their high aspect ratio (diameter: mainly 20–80 nm and length: up to 30 μm) and low electrical resistivity ($1\cdot10^{-4}$ Ohm m). When the negative plate is sulfated, the GANFg, because of showing lower electrical resistivity than the lead sulfate will be able to improve the current distribution throughout the negative plate. More data about the properties and the manufacturing process of these fibers can be found somewhere else [26,27]. It was also found out that the optimum concentration of GANFg in the negative plate was 0.10% (mixture S7 in [21]), as this concentration implied the lower water consumption together with the fulfillment of more than 1000 cycles working on PSoC conditions. GANFg must be previously dispersed in water before being added to the pastes. This dispersion was made through the use of the organic expanders (OE1 and OE2) and using dispersion equipment DISPERMAT® CN10 (VMA-GETZMANN GmbH). OE1 is a highly modified lignin-based additive, also called lignosulfonate, and OE2 a highly polymerized naphthalene sulfonate; their dispersant capabilities have been proved in many different mixtures such as concrete and coal water mixtures [5,6,10,12]. In addition, OE1 is well known for improving the performance of the negative plate in LABs [7,30,29]. Using these OEs, the nanofibers were separated and the homogeneity of GANFg throughout the negative plate was ensured. The dispersion composition for D25 and D26 was the same: 100 g H_2O, 1 g GANFg, 0.3 g OE1 and 0.3 g OE2. The only difference between mixtures S25 and S26 was the final concentration of organic expanders (see Table 1).

Five different mixtures were selected which can be organized into three groups: (1) Blank: reference mixture without organic expanders or GANFg. (2) S25B and S26B: mixtures that only contained organic expanders at a different concentration. (3) S25 and S26: mixtures that contained organic expanders at two different concentrations and GANFg at the same concentration.

Table 1 also shows the final density of the mixtures. The results show that the addition of the dispersions to the Blank composition reduced the density of the pastes (S25 and S26). This could be an effect of the previous dispersion of the organic expanders, which would improve the mixing process. In the case of the Blank mixture, more water (10 mL extra in comparison to the rest of the mixtures) was needed in order to prepare an easy to handle paste. Despite adding more water, the specific gravity was relatively high (4.54 g cm^{-3}) and the penetration lower than the others. This fact clearly confirmed the positive dispersant effect of the organic expanders on the mixing process.

3.2. Unformed negative plates properties

After the mixing and the pasting process, the plates were subjected to a curing process to obtain unformed negative plates. The physicochemical properties of these plates were studied and they are included in Table 2. No significant differences were found in the lead sulfate concentration of the unformed negative plates, as the same amount of sulfuric acid was used for all the mixtures. Regarding the BET SSA, Blank mixture showed the lowest value, which could be related to the absence of any OEs or carbon material. BET SSA of the mixtures S25B and S26B were higher (around 0.50 $m^2 g^{-1}$) but not significantly different from each other, i.e. the amount of OEs did not modify the final BET SSA value. However, when the GANFg were added to the dispersion, BET SSA values were higher. In addition, these values can be linked to the fact that mixtures S25 and S26 showed lower density values than the others mixtures (see Table 1). A lower density evolves a higher water content. This water comes out from the paste during the curing process, creating a more porous active material, which was the case of the mixtures S25 and S26, that showed a higher BET SSA. S25 showed slightly higher BET SSA than S26, probably due to the higher amount of OEs (0.30 vs 0.20%, respectively).

In order to verify the presence of GANFg and the OEs in the negative plates, the carbon content was determined. As can be seen in Table 2,
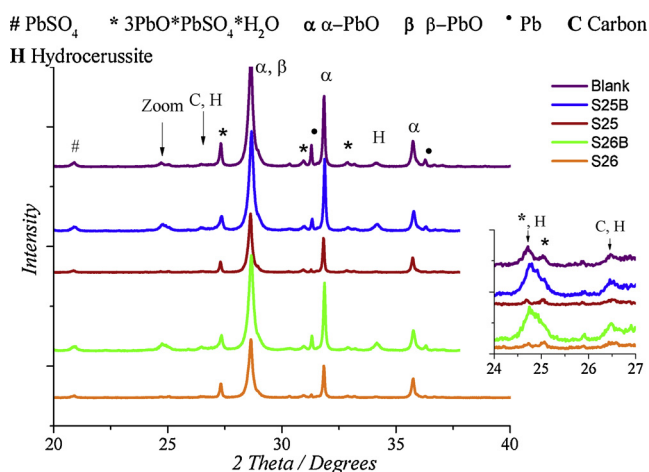
PbSO₄ * 3PbO*PbSO₄*H₂O α α–PbO β β–PbO • Pb C Carbon

H Hydrocerussite

Fig. 1. XRD patterns for the unformed negative plates. Zoom from 24° to 27° (2θ).

Fig. 2. XRD patterns for the formed negative plates.

the mixtures S25 and S26 showed a carbon content as expected, according to their GANFg (0.10%) and OEs (0.20 & 0.30% concentrations, respectively). In the case of the mixtures Blank, S25B and S26B the carbon concentrations were higher than expected. As was shown in the former study [21] this high carbon concentration could be due to the formation of Hydrocerussite (2PbCO₃·1Pb(OH)₂), a lead hydrocarbonate that was formed during the mixing process [34]. In order to confirm the presence of this compound, an XRD analysis was performed (see Fig. 1). It can be seen how mixtures Blank, S25B, and S26B showed higher intensity for the peaks related to Hydrocerussite: diffraction peaks at 24.7° (2θ; family planes (104)), at 34.2° (2θ; family planes (110)), and at 27.0° (2θ; family planes (015)). The diffraction peak at 24.7° was also related to the tribasic lead sulfate (3BS: 3PbO·PbSO₄·H₂O), but in the case of the mixtures Blank, S25B, and S26B this peak was masked by the Hydrocerussite peak. Hydrocerussite also exerted an influence over the Carbon diffraction peak at 26.5° (2θ; family planes (002)), as this peak was only appreciated for the mixtures Blank, S25B, and S26B. It can be concluded that the addition of the dispersion may reduce the formation of Hydrocerussite during the mixing process. More diffraction peaks can be observed in Fig. 1: tetragonal PbO (α-PbO), orthorhombic PbO (β-PbO), PbSO₄ and Pb. α-PbO was the main component of the pastes, due to the ball mill process used for obtaining the Lead Oxide [1]. The diffraction peak related to the metallic lead (Pb) is located at 31.3° (2θ; family planes (111)). The Pb concentration was taken as criteria for assessing the efficiency of the curing process [31]. As can be seen in Fig. 1, the presence of Pb was only appreciated in mixtures Blank, S25B and S26B, which again confirmed the benefits of these additives: the use of GANFg dispersions in mixtures S25 and S26 conferred to the pastes better rheological properties that also improved the curing process, facilitating the oxidation of the metallic lead.

3.3. Formed negative plates properties

After preparing the unformed negative plates for every mixture, the small lead acid cells were assembled according to Section 2.2. of this manuscript. This assembly was submerged in H₂SO₄ (1.28 g cm⁻³) and the final cell was placed in a water bath at 40 °C for soaking. During this soaking period, the Hydrocerussite found in the unformed negative plates reacts with the H₂SO₄, whereby CO₂ was released [1]. On account of this process, the carbon content decreased from the unformed to the formed negative plates, as can be seen in Table 2. The carbon content of the formed negative plates was according to the GANFg and OEs content of each mixture. Blank mixture showed a carbon content of 0.10% due to the PAC fibers added to the pastes. In addition, Fig. 2
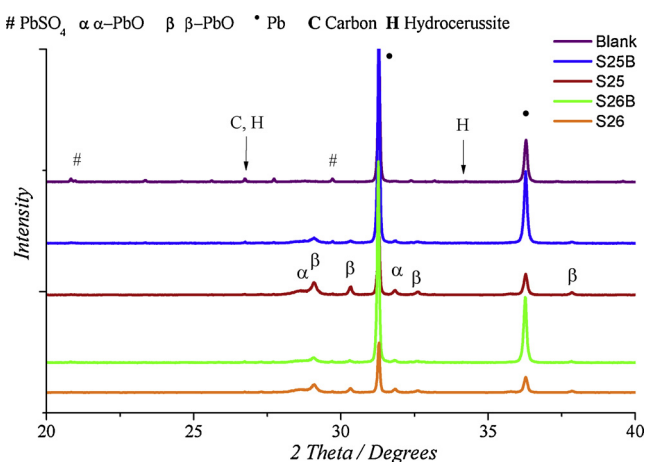
shows the diffractograms of the formed negative plates, and proved the absence of Hydrocerussite in this plate, related to the conversion of this compound into CO₂ gas.

After the soaking time, the cells were subjected to the formation process. This process is carried out in two steps [32]: (1) Reduction of 3BS and PbO to Pb and formation of the NAM skeleton. (2) Reduction of the PbSO₄ to large surface Pb crystal and formation of the energetic structure of NAM [10,33]. After this formation process, one cell of each type of mixture was disassembled, and the corresponding negative plates were washed and dried in a vacuum chamber in order to study their physicochemical properties.

As was mentioned in the previous study [21] GANFg can be considered the most conductive compound in the unformed plates, as they have a low electrical resistivity (1·10⁻⁴ Ohm m). In this way, GANFg that were properly dispersed and located throughout the negative plate, where they would improve the formation process. Starting with the formation of a more conductive and homogeneous NAM skeleton, which would lead to a more porous energetic structure. As a result, we found that the formed negative plates of mixtures S25 and S26 due to containing GANFg showed higher BET SSA (see Table 2). It is important to notice in Table 2 that the use of organic expanders enhanced the porosity of the formed negative plates, as there was a significant difference among mixtures Blank and mixtures S25B and S26B, where Blank BET SSA was significantly higher.

The efficiency of the formation process can be also evaluated by the concentration of PbSO₄ of the formed negative plates. In this case, mixtures S25B and S26B showed lower PbSO₄ concentrations (see Table 2). However, it can be seen in the diffractograms (see Fig. 2) that there were significant differences regarding the Pb peaks: S25B and S26B showed the most intense peaks. However, there was not such a difference between the PbSO₄ concentration of GANFg mixtures (S25 and S26) and reference mixtures (S25B and S25B and 26B). Probably, mixtures S25 and S26 could contain more amorphous lead particles that were not detected by XRD analysis, but there is not a clear reason behind this behavior.

3.4. Capacity and cold cranking ability

In order to know the utilization of the active material, the cells were subjected to a capacity test. During this test, the cells were discharged at a constant current of 0.05 A until they reached the cutoff 1.75 V. The energetic structure of the NAM is the one that determines the capacity of the cells [1]. During the discharge the small Pb crystals that form this structure are oxidized to PbSO₄ crystals. The formation of a PbSO₄ layer impedes the contact between the Pb crystals and the electrolyte, increasing the ohmic resistance and leading to the cutoff of the cell. This effect is called passivation phenomenon. It is known that the sulfonic
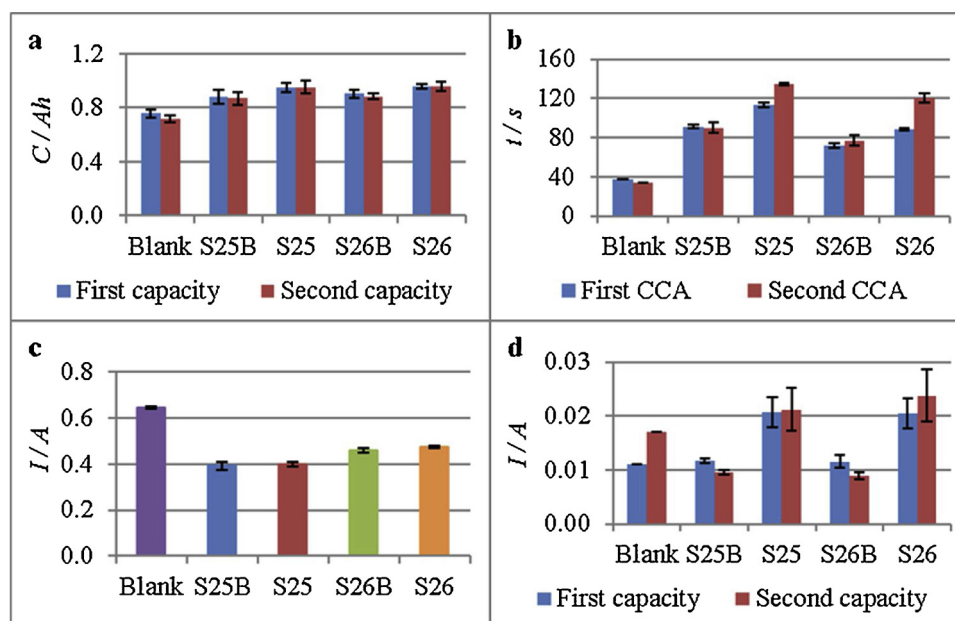
Fig. 3. a. Results on the first and the second capacity test performed at (27 ± 2) °C. **b.** Results on first and second Cold Cranking Ability (CCA) test performed at an extreme low temperature (-18 ± 2) °C. **c.** Results on initial charge acceptance test performed at (27 ± 2) °C. Current at the 5th second of charge at 2.42 V. **d.** Float currents at the end of the re-charge of the cells after the first and the second capacity.

groups in OEs exert a delay in this passivation phenomena [28,34]. The two OEs used for these experiments contained sulfonic groups, so they were expected to improve the capacity of the cells. As can be seen in Fig. 3.**a**, Blank mixture showed the lowest capacity results, which confirmed that the addition of OEs improve the capacity and thus, the utilization of the active material.

Regarding the differences between the two OEs concentration, no significant differences were found between mixtures S25B and S25 (0.30% OEs concentration) and mixtures S26B and S26 (0.20% OEs concentration), respectively, so it can be concluded that the utilization of the active mass was not significantly affected by the OEs concentration. However, a slight increase of the capacity was observed when GANFg (mixtures S25 and S26) were used. This effect can be linked to the improvement of the energetic structure of the NAM due to the GANFg addition. This test was repeated twice in order to confirm the results.

In order to check the behavior of the negative plates during the engine start, a cold cranking ability test was performed. For this test, the cells were placed in a climatic chamber at -18 ± 2 °C for 24 h. After that time, the cells were discharged at a constant current of 5 A until they reached the cutoff of 1.00 V. During this kind of discharge, the negative plate could be limited by the fast formation of PbSO$_4$ crystals at its surface, which will lead again to the passivation phenomena and the resulting failure of the cell. As was explained for the capacity test, and due to the same reason, OEs improve the cold cranking ability of the negative plates, delaying the passivation phenomena [28]. As can be seen in Fig. 3.**b**, Blank mixture showed clearly the lowest results, indicating the importance of the OEs during this test. In this case, the use of higher OEs amounts (0.30% for mixtures S25B and S25) increased the cold cranking ability of the negative plates. As the third comparison, the use of GANFg (mixtures S25 and S26) also enhanced the cold cranking ability, due to increasing the BET SSA of the formed plates, and thus the energetic structure of the NAM. This test was repeated twice in order to confirm the results.

3.5. Initial charge acceptance evaluation

Charge acceptance is a key parameter of the LAB as it determines its cycle life under partial state of charge (PSoC). Regarding the negative plate, this parameter plays an important role, as the negative plate easily undergoes the sulfation of its surface, leading to a low charge acceptance, and thus, a reduced cycle life. In addition, when the

regenerative braking is implemented in the vehicle, the charge acceptance is even a more important parameter: these batteries are supposed to absorb the kinetic energy from the brakes for being recharged.

The initial charge acceptance test was performed on fully charged cells and consisted in (1) discharge of the cell until reaching the 90% of their SoC (at 0.05 A for 2 h); (2) resting period of 24 h; (3) recharge of the cells at constant cell potential (2.42 V) for 60 s. Step (2) forces the passivation of the negative plate, whereby the charge acceptance was more impeded. In order to evaluate the charge acceptance of each mixture, the current at the 5th second of the recharge (step (3)) was taken as charge acceptance indicator value. The Pb^{2+} reduction can take place on two surfaces: the metal or the carbon material surface, as carbon is located at the energetic structure of the NAM, where it improves the electrochemically active surface, and enhances the charge processes [28]. The Pb^{2+} reduction is determined by the migration of Pb^{2+} ions through the porous PbSO$_4$ layer and the adsorbed OE layer. This diffusion is lower through the adsorbed OE layer, i.e. a higher OEs concentration will decrease the charge acceptance [1]. Results are shown in Fig. 3.**c**. It is clear from this figure that the charge processes were highly dominated by the OEs concentration in NAM, as expected. Blank mixture because of not containing OEs showed the best results. Mixtures S25B and S25 showed lower charge acceptance than mixtures S26B and S26, as S25B and S25 contained higher OEs concentration (0.30% versus 0.20%). With regards to the effect of GANFg in this test as they form a more dynamic electric system inside the NAM skeleton, which will be charged and discharged easier, improving the charge acceptance of the negative plates [9]. However, mixtures S25B and S26B showed the same performance as mixtures S25 and S26 respectively, so they did not cause any effect on the charge acceptance parameter. This could be related to the low GANFg concentration in the mixtures, as in the former study an increase in the GANFg concentration led to an improvement in the charge acceptance [21].

3.6. Water loss evaluation

During operation conditions, LABs can undergo electrolyte losses mainly due to the water electrolysis during charge, overcharge and self-discharge of the battery [1]. In order to achieve an adequate performance of free maintenance LABs, the water loss must be minimized. For this reason, a water consumption evaluation of the different mixtures under study was carried out. The reactions that could take place on the negative plate are the following:

$$PbSO_4 + H^+ + 2e^- \rightarrow Pb + HSO_4^- \tag{1}$$

$$Pb + HSO_4^- \rightarrow PbSO_4 + H^+ + 2e^- \tag{2}$$

$$2H^+ + 2e^- \rightarrow H_2 \uparrow \tag{3}$$

Reduction of $PbSO_4$ to Pb (1) and oxidation of Pb to $PbSO_4$ (2) are the reactions that mainly occur during the charge and discharge processes respectively. Reaction (3) is related to Hydrogen Evolution Reaction (HER). This reaction takes place on the negative plates when certain conditions are given: charging or during self-discharge processes. When HER occurs the charge processes are not efficient, as part of the energy is spent in reducing the protons to hydrogen. In addition, this reaction increases the water loss, which is computed as the sum of released hydrogen and oxygen gasses from the negative and the positive plates, respectively. The water loss leads to the consequent increase of the H_2SO_4 concentration and, thus the increase of the positive plates passivation [1].

In this study, a water loss evaluation was carried out performing two tests: negative polarization test, for studying the HER rate (see Fig. 4), and the measurement of the float currents at the end of the recharge of the cells (see Fig. 3.**d**), for exploring the overall amount of water lost by the cells.

In the case of the negative polarization test, fully charged cells were subjected to 8 different constant current charging steps for a certain time (see Section 2.2.3). The potential of negative plates was measured at the beginning of the test (E_{OCP}) and at the end of each charging step (E_i). The negative polarization curves are shown in Fig. 4**a** where two behaviors can be easily differentiated according to the relation between the current density (j) and the negative plate potential (E):

- **A.** $j > 1 \, mA \, cm^{-2}$: the linear relationship between the electrode potential and the current density indicated that only one reaction was taking place. In this overcharge conditions, the dominating reaction was the HER reaction (**3**).
- **B.** $j < 1 \, mA \, cm^{-2}$: as there was not a linear relationship between the current density and the electrode potential, it was clear that two reactions were taking place at the same time: the reduction of the remaining $PbSO_4$ (reaction (**1**)) and the HER (reaction (**3**)).
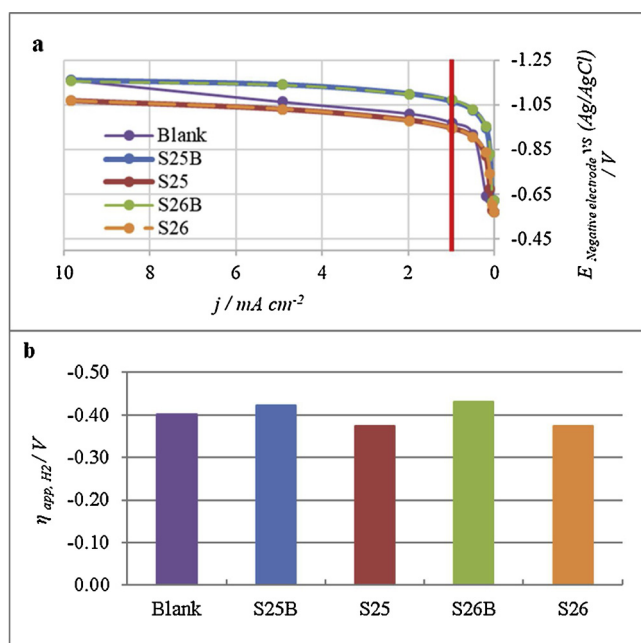

Fig. 4. Hydrogen Evolution Reaction (HER) study for the different mixtures. **a.** Negative electrode potential vs current density. Negative polarization curves. **b.** HER apparent overpotential: $\eta_{app, H2}$.

In order to find out the HER rate for each mixture, H_2 apparent overpotential ($\eta_{app, \, H2}$), was calculated at $1 \, mA \, cm^{-2}$ (or $1.2 \, mA \, g^{-1}$ and $10 \, mA \, Ah^{-1}$; NAM mass $= 8 \, g$, plate surface $= 10 \, cm^2$, capacity $= 1 \, Ah$) as $\eta_{app, \, H2} = E_{j \, = \, 1 \, mA \cdot cm^{-2}} - E_{OCP}$. At this point, the relation between current density and electrode potential became linear. In this way, $\eta_{app, \, H2}$ can be taken as an indicator of the HER rate. The $\eta_{app, \, H2}$ values for each mixture can be seen in Fig. 4.**b**. Lower $\eta_{app, \, H2}$ will indicate higher HER rates, as HER will be more facilitated. It is known that OEs increase the hydrogen over-voltage [1], and this is confirmed in this study: as can be seen in Fig. 4.**b**, mixtures S25B and S26B showed the highest $\eta_{app, \, H2}$. The mixtures containing GANFg, S25 and S26, showed the lowest $\eta_{app, \, H2}$. This effect was also observed in the former study [21], and it was linked to the GANFg composition: GANFg were obtained by a Ni catalyst [26,35], which is not completely eliminated after the manufacturing process of this Nano-material (Ni final concentration in GANFg was < 20 ppm). In addition, this element is related to exert a detrimental synergistic effect on hydrogen evolution [23]. It is also important to notice that there was no difference in the $\eta_{app, \, H2}$ when different concentrations of OEs were used; mixtures S25B and S26B showed the same $\eta_{app, \, H2}$, as well as mixtures S25 and S26. Blank mixture showed lower $\eta_{app, \, H2}$ than mixtures S25B and S26B due to not containing any OEs, and higher $\eta_{app, \, H2}$ than mixtures S25 and S26 due to not incorporating any impurity (as Ni for the GANFg).

In order to confirm the negative polarization test results, and to try to have a predictive tool for the overall amount of water lost by the cells, the float currents at the end of the recharge of the cells (after the first and the second capacity) were measured. Results are shown in Fig. 3.**d**. These float currents are directly linked to the water loss: they are measured at the end of the recharge of the cell when all $PbSO_4$ has already been reduced to Pb, and the only reaction that can take place is the HER. The results confirmed the negative polarization test conclusions, as the ascending order of the float currents, and thus of the water loss was the same observed in the negative polarization test: S25B $\approx$ S26B $<$ Blank $<$ S25 $\approx$ S26.

3.7. 17.5% DoD cycling test

In order to know the behavior of the different mixtures during PSoC operation conditions, the 17.5% DoD cycling test that has been performed. This test is based on the norm EN 50342-6, and it is considered an accelerated life-test, whereby the behavior of the battery in the field after multi-year usage can be known. Fig. 5.**a** shows the schematic procedure of this test. Fully charged cells (100% SoC) were selected for this test; after a pre-discharge to 50% SoC of the cells, they were charged and discharged at a DoD of 17.5% (cycles from 50 to 67.5% SoC). It is known that when the cells are working in these PSoC conditions, the negative plates are not charged efficiently [11,28], due to the presence of a higher $PbSO_4$ concentration. This is confirmed by the results showed by mixtures Blank, S25B, and S26B (see Fig. 5.**b**). The Blank mixture, in spite of not containing any additive, showed better results than mixtures S25B and S26B. This was explained by the higher charge acceptance of this mixture, because of not containing any OE covering the surface of its negative plates. However, although mixtures S25 and S26 did not improve the charge acceptance of the cell, these mixtures showed the best results. This was linked to the effect of GANFg on the negative plate performance. It was explained in another study [9] that carbon materials with a particle size in the range of micrometers are able to confer to the NAM skeleton the properties of a more dynamic electric system, which improves the charge and discharge processes. This effect was not noticed during the charge acceptance test, but when the cells were subjected to more stressful conditions, as happens during the 17.5% DoD cycling test, the GANFg were able to improve the charge acceptance of the negative plates through this mechanism. A common failure mode during the 17.5% DoD cycling test is the acid stratification, which is impaired by the addition of carbon materials [36]. In these laboratory trials that effect was not
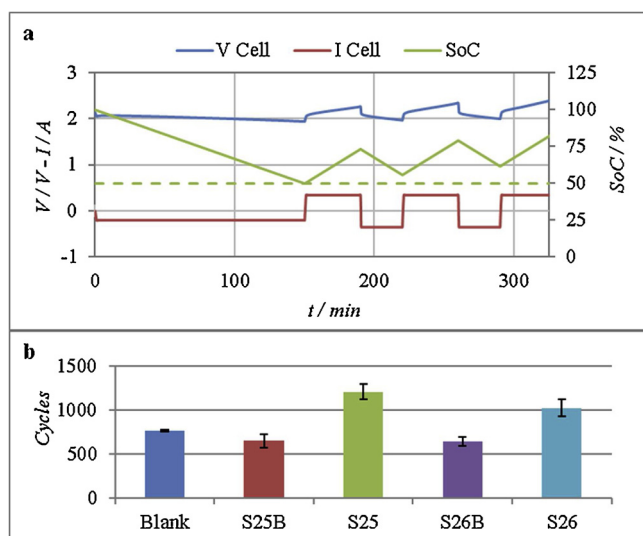
Fig. 5. a. Schematic procedure of cycles at 17.5% DoD at (27 ± 2) °C. **b.** Results on this test: **Blank** – 762. **S25B** – 649 cycles. **S25** - 1209 cycles. **S26B** - 645 cycles. **S26** - 1025 cycles.

appreciated, as the cell did not have any acid limitation, but in an industrial LAB GANFg could potentially reduce the acid stratification by distributing the current homogeneously throughout the negative plate. Regarding the amount of OEs, the mixture S25 showed slightly better results than the mixture S26, concluding that higher amounts of OEs can benefit the cycle life in these conditions, by the improvement of the discharge performance of the negative plates.

3.8. Negative and positive plates physicochemical properties after 17.5% DoD cycling test

After completion of the 17.5% DoD cycling test, the cells were torn down to determine the mode of failure. Before being analyzed, the negative and positive plates were washed and dried (in a vacuum chamber in the case of the negative plates). Fig. 6 shows the diffractograms of the negative plates. These diffractograms confirmed that the only substances presented in the negative plates were $PbSO_4$, Pb and lead oxides (α-PbO and β-PbO). The presence of the lead oxides was linked to the partial oxidation of the lead on air. Table 3 shows the physicochemical properties of the negative and positive cycled plates. Regarding the carbon content of the negative plates, it has remained practically equal after the cycling test, concluding that the carbon materials are resistant to the cycling conditions of the negative plates.
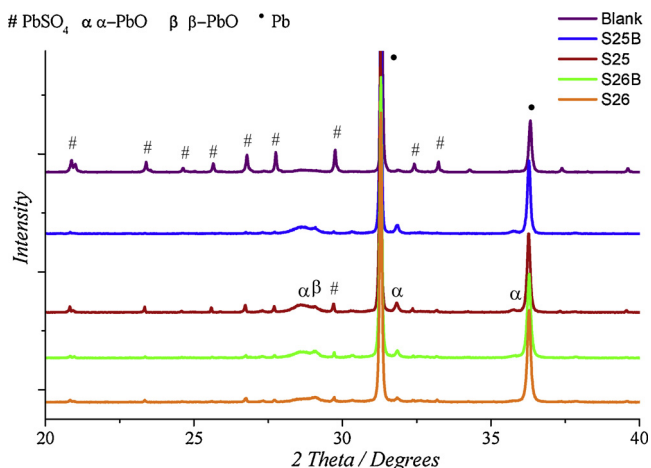

Fig. 6. XRD patterns for the cycled negative plates.

Table 3

Physicochemical properties of the cycled plates: after PSoC cycles at 17.5% DoD. The number of cycles performed by every mixture. Negative plates: carbon and lead sulfate concentrations, and BET SSA. Positive plates: lead sulfate concentration.

Mixture	Cycles	Negative plates			Positive plates
		Carbon (wt. %)*	$PbSO_4$ (wt. %)*	BET SSA (m^2 g^{-1})	$PbSO_4$ (wt. %)*
Blank	762	0.20	10.60	0.22	15.60
S25B	649	0.28	2.45	0.44	23.00
S25	1209	0.34	4.40	0.41	6.60
S26B	644	0.30	2.45	0.45	27.80
S26	1025	0.38	3.30	0.38	14.10

*wt. % related to the total mass of the sample.

The mixture Blank showed double carbon content after the cycles. However, differences in concentration ranges lower than 0.20% were not considered significant, due to the limitations regarding the analyzer. In the case of the BET SSA, only the mixtures S25 and S26 underwent a decrease of this parameter, comparing to the BET SSA of the formed plates (see Table 2). As these mixtures performed more cycles than the others, the negative plates were more utilized and therefore aged, and then the BET SSA was lower.

It is clear from the Table 3 data that the failure mode during this test was the amount of irreversible lead sulfate that was found in the positive plate. This failure mode is according to the one described by J. Albers [37], in AGM and Flooded LABs that fulfilled the 17.5% DoD cycling test. In that publication he explained that the failure mode is based on the softening of the positive active-mass and sulfation of the plates.

In former experiments [7,21] we performed similar cycle life test, except that the initial SoC of that test was 100%, instead of 50%. This could be the reason why the number of cycles reached by the cells was higher (around 1600 cycles were performed by some mixtures) and the failure mode was related to the sulfation of the negative plates, as the lead sulfate concentration was higher in the negative plates than in the positive ones.

The above results also indicate that the negative plates can be successfully recharged after the cycle life test, which means that these plates were not under much stressed conditions. However, there is still a correlation between the number of cycles and the addition of GANFg, as we can see that the mixtures containing GANFg (S25 and S26) were able to perform more cycles. As was explained before, during this test, GANFg could improve the recharge ability of the negative plates when they are integrated in the NAM skeleton. In this way, the negative plate can reduce the sulfation of the positive plates and extend the cycle life.

In order to confirm the good state of the negative plates after the 17.5% DoD cycling test, SEM micrographs were taken for the cross section of the formed and the cycled negative plates. They are shown in Fig. 7. It can be appreciated that, in the case of the mixtures S25B (**b, c**), S25 (**d, e**), S26B (**f, g**), and S26 (**h, i**), the formed plates structure (left side) was very similar to the cycled plates structure (right side), as, as expected, no big lead sulfate crystals were found in the latter. All these mixtures showed similar structures, indicating the important effect of the OEs on the energetic structure of NAM, which was also elucidated by D. Pavlov, who explained the structural differences when different OEs concentrations were used [30]. However, mixtures S25 and S26, showed a higher compactness; this compactness can be linked to the utilization of GANFg dispersions. As was shown in the former study [21], an increase in the GANFg concentration increased the dispersion viscosity, which leads to a higher compactness of the negative plates. Regarding the Blank mixtures (Fig. 7. **a, b**), more differences are appreciated between the structure of the formed and cycled negative plates, as the cycled negative plates, in this case, contained a higher
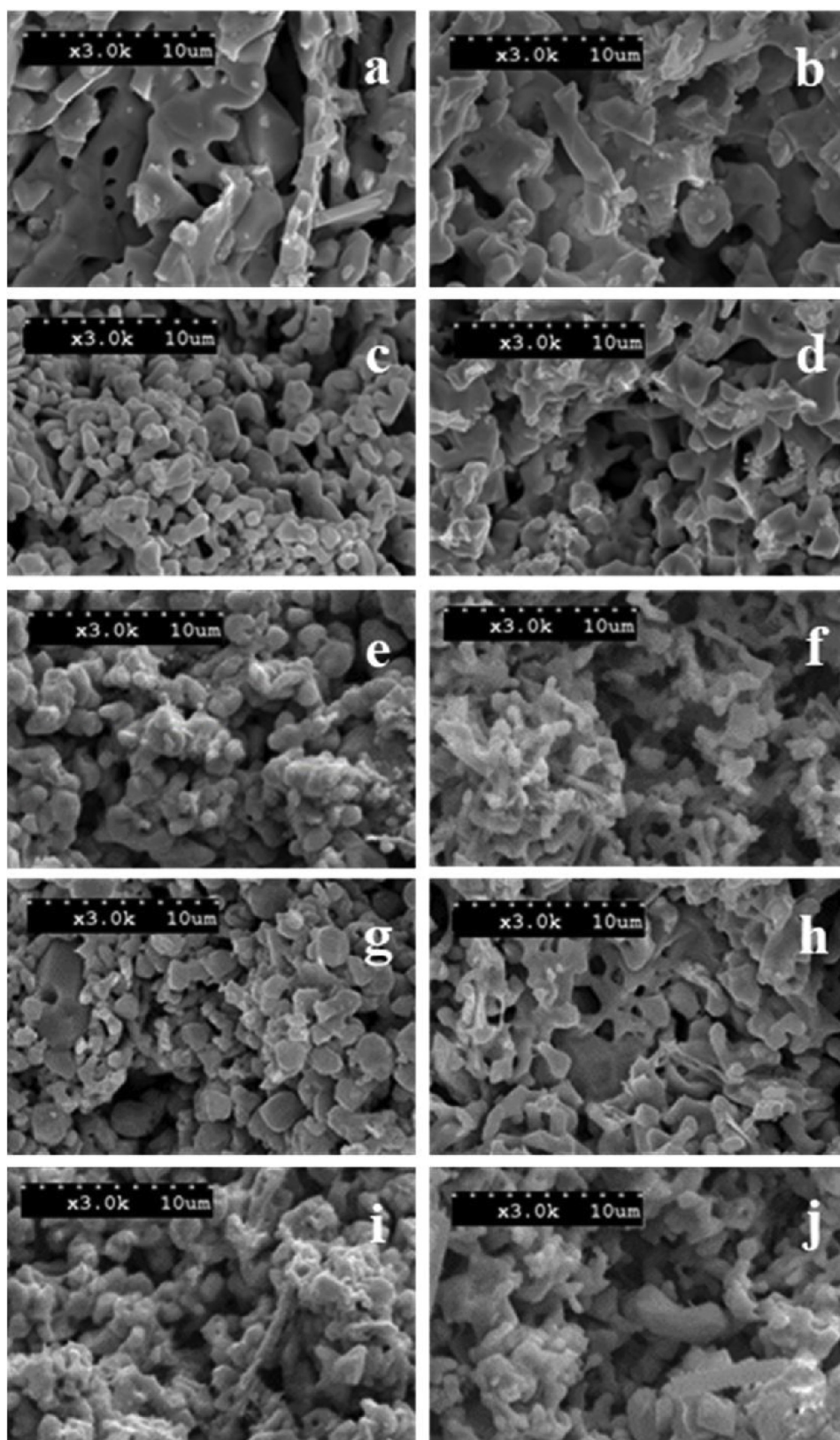
Fig. 7. SEM micrographs. **Left side**: formed NAM (NAM after the formation process). **Right side**: Cycled NAM (NAM after the 17.5% DoD cycle life test). **a, b**: Blank. **c, d**: S25B. **e, f**: S25. **g, h**: S26B. **i, j**: S26. Magnifications: x3000.

amount of PbSO$_4$. However, the main difference between this mixture and the other was the absence of the energetic structure of NAM, due to the lack of small crystals at the surface of the NAM skeleton. This kind of structure also reaffirmed the bad results obtained for this mixture in

the capacity and cold cranking ability tests.

4. Conclusions

Based on former experiments, GANFg at 0.10% were well dispersed together in water with two different OEs, a lignosulfonate (1) and a highly polymerized naphthalene sulfonate (2). This dispersion was used to prepared unformed negative plates with 0.10% of GANFg and 0.30 and 0.20% of OEs (mixtures S25 and S26 respectively). Their corresponding reference mixtures without GANFg were also prepared (S25B and S26B), together with a Blank mixture without GANFg or OEs. Physicochemical properties of the unformed plates revealed that the used of OEs and GANFg increased the BET SSA of the plates.

2 V/1 Ah small lead acid cells were assembled with the unformed negative plates. During the formation process, GANFg are supposed to be integrated into the NAM skeleton where would improve the NAM energetic structure. For this reason, a slightly higher BET SSA of the formed plates was observed in the GANFg mixtures.

The capacity test revealed the importance of the OEs for avoiding the passivation phenomenon. This effect was more pronounced during the cold cranking ability test than in the capacity test, because of the extreme conditions of this test.

As expected, GANFg at 0.10% did not improve the charge acceptance of the cells. The same happened in the former study [21], where the charge acceptance was not significantly increase even when the GANFg concentration was 0.5%. Moreover, the addition of OEs reduced this parameter. The adsorbed OE layer impaired the diffusion of the Pb^{2+} ions, leading to a lower charge acceptance.

GANFg increased the water loss by lowering the H_2 apparent overpotential. This effect was linked to the high level of Nickel in GANFg. This Nickel comes from the manufacturing process of the GANFg and cannot be completely eliminated. Addition of OEs reduced the water loss.

Finally, GANFg were able to increase the cycle life of the cells working in PSoC conditions, by improving the performance of the negative plates and enhancing the reversibility of the electrochemical reaction of the $Pb/PbSO_4$ electrode system, and thus the cycle life of the cell.

In this way, we can confirm that GANFg at a concentration of 0.10% improved the performance of the LABs: a higher cycle life is possible, maintaining at a safe degree the water loss. However, this effect is just possible if the GANFg are properly dispersed with the OEs.

References

[1] D. Pavlov, Lead-Acid Batteries: Science and Technology, (2011).
[2] E.J. Ritchie, Addition agents for negative plates of lead-acid storage batteries: II. Pure organic compounds, J. Electrochem. Soc. 100 (1953) 53–59, https://doi.org/10.1149/1.2781082.
[3] D. Pavlov, T. Rogachev, P. Nikolov, G. Petkova, Mechanism of action of electrochemically active carbons on the processes that take place at the negative plates of lead-acid batteries, J. Power Sources 191 (2009) 58–75, https://doi.org/10.1016/j.jpowsour.2008.11.056.
[4] L.H.V. A.F. Hollenkamp, W.G.A. Baldsing, S. Lau, O.V. Lim, R.H. Newnham, D.A.J. Rand, J.M. Rosalie, D.G. Vella, Overcoming Negative-Plate Capacity Loss in VRLA Batteries Cycled Under Partial State-of-Charge Duty, ALABC Project N1.2 Final Report, July 2000–June 2002, n.d.
[5] M. Fernández, J. Valenciano, F. Trinidad, N. Muñoz, The use of activated carbon and graphite for the development of lead-acid batteries for hybrid vehicle applications, J. Power Sources 195 (2010), https://doi.org/10.1016/j.jpowsour.2009.12.131.
[6] J. Valenciano, A. Sánchez, F. Trinidad, A.F. Hollenkamp, Graphite and fiberglass additives for improving high-rate partial-state-of-charge cycle life of valve-regulated lead-acid batteries, J. Power Sources 158 (2006) 851–863, https://doi.org/10.1016/j.jpowsour.2005.11.058.
[7] M. Blecua, E. Fatas, P. Ocon, J. Valenciano, F. de la Fuente, F. Trinidad, Influences of carbon materials and lignosulfonates in the negative active material of lead-acid batteries for microhybrid vehicles, J. Energy Storage. 11 (2017) 55–63, https://doi.org/10.1016/j.est.2017.01.005.
[8] P.T. Moseley, R.F. Nelson, A.F. Hollenkamp, The role of carbon in valve-regulated lead–acid battery technology, J. Power Sources 157 (2006) 3–10, https://doi.org/10.1016/j.jpowsour.2006.02.031.
[9] D. Pavlov, P. Nikolov, T. Rogachev, Influence of carbons on the structure of the negative active material of lead-acid batteries and on battery performance, J. Power Sources 196 (2011) 5155–5167, https://doi.org/10.1016/j.jpowsour.2011.02.014.
[10] V. Iliev, D. Pavlov, The effect of the expander upon the two types of negative active mass structure in lead-acid batteries, J. Appl. Electrochem. 15 (1985) 39–52, https://doi.org/10.1007/BF00617739.
[11] T. Rogachev, P. Nikolov, G. Petkova, Mechanism of action of electrochemically active carbons on the processes that take place at the negative plates of lead-acid batteries, J. Power Sources 191 (2009) 58–75, https://doi.org/10.1016/j.jpowsour.2008.11.056.
[12] K.R. Bullock, Carbon reactions and effects on valve-regulated lead-acid (VRLA) battery cycle life in high-rate, partial state-of-charge cycling, J. Power Sources 195 (2010) 4513–4519, https://doi.org/10.1016/j.jpowsour.2009.10.027.
[13] M. Calábek, K. Micka, P. Křivák, P. Bača, Significance of Carbon Additive in Negative Lead-acid Battery Electrodes, (2006), https://doi.org/10.1016/j.jpowsour.2005.11.022.
[14] S. Logeshkumar, R. Manoharan, Influence of some nanostructured materials additives on the performance of lead acid battery negative electrodes, Electrochim. Acta 144 (2014) 147–153, https://doi.org/10.1016/j.electacta.2014.08.080.
[15] L. Wang, W. Zhang, L. Gu, Y. Gong, G. Cao, H. Zhao, Y. Yang, H. Zhang, Tracking the morphology evolution of nano-lead electrodeposits on the internal surface of porous carbon and its influence on lead-carbon batteries, Electrochim. Acta 222 (2016) 376–384, https://doi.org/10.1016/j.electacta.2016.10.189.
[16] L. Wang, H. Zhang, W. Zhang, H. Guo, G. Cao, H. Zhao, Y. Yang, A new nano lead-doped mesoporous carbon composite as negative electrode additives for ultralong-cyclability lead-carbon batteries, Chem. Eng. J. 337 (2018) 201–209, https://doi.org/10.1016/J.CEJ.2017.12.089.
[17] S. Zhang, H. Zhang, J. Cheng, W. Zhang, G. Cao, H. Zhao, Y. Yang, Novel polymer-graphite composite grid as a negative current collector for lead-acid batteries, J. Power Sources 334 (2016) 31–38, https://doi.org/10.1016/J.JPOWSOUR.2016.09.097.
[18] S.W. Swogger, P. Everill, D.P. Dubey, N. Sugumaran, Discrete carbon nanotubes increase lead acid battery charge acceptance and performance, J. Power Sources 261 (2014) 55–63, https://doi.org/10.1016/j.jpowsour.2014.03.049.
[19] N. Sugumaran, P. Everill, S.W. Swogger, D.P. Dubey, Lead acid battery performance and cycle life increased through addition of discrete carbon nanotubes to both electrodes, J. Power Sources 279 (2015) 281–293, https://doi.org/10.1016/j.jpowsour.2014.12.117.
[20] R. Marom, B. Ziv, A. Banerjee, B. Cahana, S. Luski, D. Aurbach, Enhanced performance of starter lighting ignition type lead-acid batteries with carbon nanotubes as an additive to the active mass, J. Power Sources 296 (2015) 78–85, https://doi.org/10.1016/j.jpowsour.2015.07.007.
[21] M. Blecua, E. Fatas, P. Ocon, B. Gonzalo, C. Merino, F. de la Fuente, J. Valenciano, F. Trinidad, Graphitized carbon nanofibers: new additive for the negative active material of lead acid batteries, Electrochim. Acta 257 (2017) 109–117, https://doi.org/10.1016/J.ELECTACTA.2017.10.067.
[22] Q. Long, G. Ma, Q. Xu, C. Ma, J. Nan, A. Li, H. Chen, Improving the cycle life of lead-acid batteries using three-dimensional reduced graphene oxide under the high-rate partial-state-of-charge condition, J. Power Sources 343 (2017) 188–196, https://doi.org/10.1016/j.jpowsour.2017.01.056.
[23] L.T. Lam, H. Ceylan, N.P. Haigh, T. Lwin, Influence of residual elements in lead on oxygen- and hydrogen-gassing rates of lead-acid batteries, J. Power Sources 195 (2010) 4494–4512, https://doi.org/10.1016/j.jpowsour.2009.12.020.
[24] Grupo Antolin, (n.d.). http://www.grupoantolin.com.
[25] CENELEC, EN 50342-6 Lead-acid starter batteries - Part 6: Batteries for Micro-Cycle Applications, (n.d.).
[26] J. Vera-Agullo, H. Varela-Rizo, J.A. Conesa, C. Almansa, C. Merino, I. Martin-Gullon, Evidence for growth mechanism and helix-spiral cone structure of stacked-cup carbon nanofibers, Carbon 45 (2007) 2751–2758, https://doi.org/10.1016/j.carbon.2007.09.040.
[27] M. Weisenberger, I. Martin-Gullon, J. Vera-Agullo, H. Varela-Rizo, C. Merino, R. Andrews, D. Qian, T. Rantell, The effect of graphitization temperature on the structure of helical-ribbon carbon nanofibers, Carbon 47 (2009) 2211–2218, https://doi.org/10.1016/j.carbon.2009.03.070.
[28] D. Pavlov, P. Nikolov, T. Rogachev, Influence of expander components on the processes at the negative plates of lead-acid cells on high-rate partial-state-of-charge cycling. Part I: effect of lignosulfonates and BaSO4 on the processes of charge and discharge of negative plates, J. Power Sources 195 (2010) 4435–4443, https://doi.org/10.1016/j.jpowsour.2009.11.060.
[29] N. Hirai, S. Kubo, K. Magara, Combined cyclic voltammetry and in situ electro-chemical atomic force microscopy on lead electrode in sulfuric acid solution with or without lignosulfonate, J. Power Sources 191 (2009) 97–102, https://doi.org/10.1016/j.jpowsour.2008.10.090.
[30] M. Matrakova, D. Pavlov, Thermal analysis of lead-acid battery pastes and active materials, J. Power Sources 158 (2006) 1004–1011, https://doi.org/10.1016/j.jpowsour.2005.11.007.
[31] S. Ruevski, D. Pavlov, Accelerated curing of negative plates for lead/acid batteries, J. Power Sources 31 (1990) 217–223, https://doi.org/10.1016/0378-7753(90)80073-M.
[32] D. Pavlov, V. Iliev, G. Papazov, E. Bashtavelova, Formation processes of the lea-d-acid battery negative plates, J. Electrochem. Soc. 121 (1974) 854–860, https://

doi.org/10.1149/1.2401936.

[33] D. Pavlov, V. Iliev, An investigation of the structure of the active mass of the negative plate of lead—acid batteries, J. Power Sources 7 (1981) 153–164, https://doi.org/10.1016/0378-7753(81)80052-3.

[34] A.C. Zachlin, Functions and behavior of the components of expanders for the negative plates of lead-acid storage batteries, J. Electrochem. Soc. 98 (1951) 325–333, https://doi.org/10.1149/1.2778215.

[35] I. Martin-Gullon, J. Vera, J.A. Conesa, J.L. González, C. Merino, Differences between carbon nanofibers produced using Fe and Ni catalysts in a floating catalyst reactor, Carbon 44 (2006) 1572–1580, https://doi.org/10.1016/j.carbon.2005.12.

027.

[36] E. Ebner, D. Burow, J. Panke, A. Börger, A. Feldhoff, P. Atanassova, J. Valenciano, M. Wark, E. Rühl, Carbon blacks for lead-acid batteries in micro-hybrid applications – studied by transmission electron microscopy and Raman spectroscopy, J. Power Sources 222 (2013) 554–560, https://doi.org/10.1016/j.jpowsour.2012.08.089.

[37] J. Albers, E. Meissner, 6 - automotive absorptive glass-mat lead–acid batteries: State of the art, in: J. Garche, E. Karden, P.T. Moseley, D.A.J. Rand (Eds.), Lead-Acid Batter, Futur. Automob., Elsevier, Amsterdam, 2017, pp. 185–211, , https://doi.org/10.1016/B978-0-444-63700-0.00006-4.

- R&D project/test report -		
Loss on Ignition – Laboratory method		
ECN2 #:	**EFB+ new Product**	Date: 23/03/2018
Author:	María Blecua	Project leader: Holger FRICKE
Product segment: *(cross main segment, highlight sub segment in bold)* ⊠ **Basic Research**		
Key words: EFB, Carbon, Additives, NAM, Charge acceptance, Cycling, Micro-cycling, Water consumption		

Summary:

• *Carbon materials for Lead Acid Batteries*
Enhanced Flooded Battery (EFB) must be prepared to work at a High Rate Partial State of Charge (HRPSoC). However, this condition provokes the formation of big lead sulfate ($PbSO_4$) crystals, in the negative plates, which can't be converted efficiently to lead (Pb) leading to the battery failure [1]. This sulfation is partially avoided by carbon materials, among other additives. Due to the addition of carbon materials, Negative Active Material (NAM) electrochemical surface area is increased and the creation of isolated $PbSO_4$ crystals is facilitated, preventing the formation of a $PbSO_4$ continuous layer and increasing cycle life at HRPSoC. Carbon materials also increases the overall conductivity of NAM, which involves an improvement of charge acceptance due to proper current flow through the plate [3, 4]. However, the addition of carbon materials can lower Hydrogen Evolution Reaction (HER) overpotential in the negative plate [1], leading to an increase in water loss, which finally accelerates the battery failure. For this reason, adequate type and dosage of the carbon materials are an important factor for water consumption prevention.

After more than 13 years of investigations (ALABC R&D Program), many battery companies have started the commercialization of Lead-Carbon batteries. Lead Carbon electrodes can be produced in different ways:

- Carbon superficial impregnation, leading to a carbon Supercapacitor attached to the negative plate. Ultrabattery from East Penn or Furukawa.
- Addition of carbon materials during the mixing process. EFB or AGM from Exide, Varta, GS-Yuasa, Moll…

These carbon materials are most of the time related to activated carbon, carbon black, expanded graphite and hybrid carbons (a mix of graphite and carbon black). Graphitic materials normally come from natural sources, while carbon black is a synthetic material.

It is known that carbon materials with high Specific Surface Area (SSA; higher than 100 m^2/g) are prompted to highly increase water consumption by lowering HER overpotential. However, this effect is less noticed for expanded graphite materials, as they have lower SSA (around 10-30 m^2/g). Furthermore, the impurities content of these carbon materials must be taken in account, as they can also increase the water consumption, especially the transition elements and noble metals.

• *Carbon materials used at Exide Technologies*
Exide has selected a special type of Purified Expanded Graphite – Conductive Carbon manufactured by **COMPANY 1** with a low surface area (<30 m^2/g) and, a priori, minimal harmful impurities. Depending on the particle size, this material has different grades (CX, C1…) but the same structure and chemical composition.

The use of CX and C1 in EFB, which are manufactured in Exide automotive plants. Different problems related to the impurities content of C1 can appear during production:

1. C1 batches with high contents of Tungsten and Molybdenum which are thought to form a carbide compound during the battery formation. This compound increases in a higher way the water consumption [4].
2. C1 batches with a very high content of Iron, which is generally accepted but at low concentrations.

These problems can affect to the Chemical Labs which have optimized the method for analyzing the impurities content inside carbon materials. This method is currently based on a hydrochloride acid microwave digestion followed by Inductively Coupled Plasma Atomic Emission Spectroscopy (ICP-OES) analyses.

- *Loss on Ignition (LOI)*
LOI is defined as the change in mass as a result of heating a sample under specified conditions. LOI is expressed as a weight percentage of the dry mass [5].

In the case of carbon materials, this parameter indicates the percentage of organic carbon. Carbon materials with low LOI are related to high impurities level inside them, and vice versa. In this way, LOI is also related to the water consumption. In order to prove this theory, some electrical data from C1 EFB prototypes have been analyzed. These prototypes have been electrically tested following the standards EN 50342-1:2006.

The relation between LOI and water consumption is shown in Figure 1, as well as Figure 2 shows the relation between LOI and the rechargeability during the second capacity recharge. Lower LOI clearly leads to higher water consumption and rechargeability. There is a slightly linear correlation between LOI and recharge ability. In this case, an increase in the rechargeability of these batteries means that part of the input energy is used to produce Hydrogen (negative plates) and Oxygen (positive plates), instead of being used to convert $PbSO_4$ to Pb (negative plates) /PbO_2 (positive plates). This effect is promoted by the impurities inside the carbon materials, which are also related to a low carbon materials LOI.
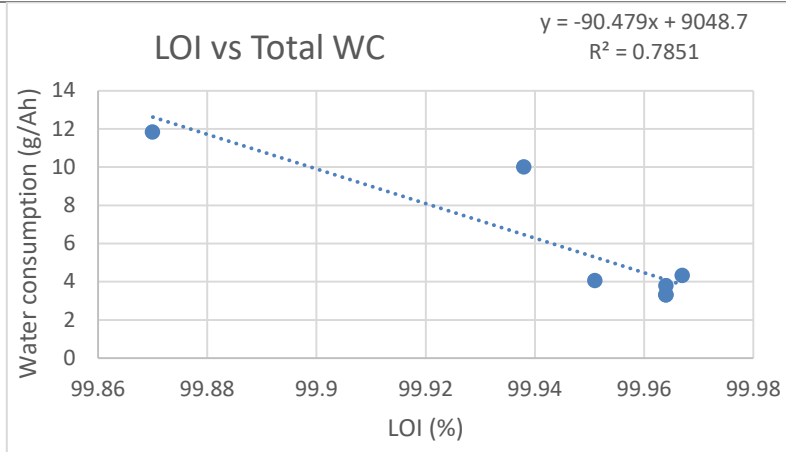
Figure 1. *C1 EFB prototypes. Electrical tests. LOI values of the C1 batches and corresponding total water consumption values.*
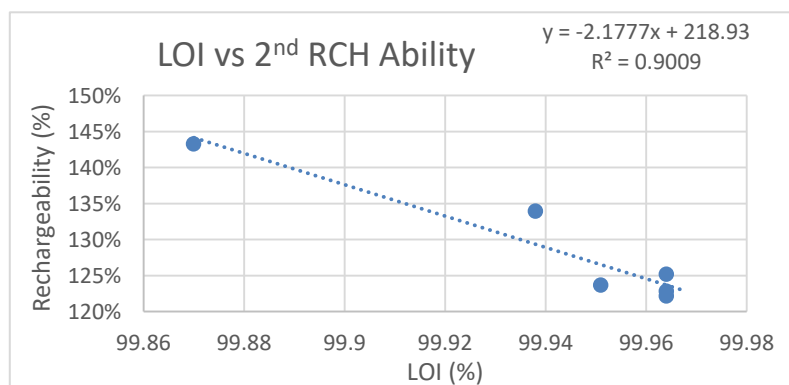
Figure 2. *C1 EFB prototypes. Electrical tests. LOI values of the C1 batches and corresponding rechargeability after second capacity test values.*

- *Aim of the study*

  To sum up, LOI is an indication of the impurities content of a carbon material. In this way, this parameter can be used to accept or discard different carbon batches that will be used to produce batteries, as it will take part in the carbon material specification. Exide specification establishes that all carbon batches used for production must have a LOI higher than 99.95%. Otherwise, they will be rejected. After that, carbon materials must fulfill Exide impurities specification (**¡Error! No se encuentra el origen de la referencia.**).

  As LOI has become a crucial parameter for rejecting/accepting carbon batches, both, preparation and optimization of the LOI method, are explained along this report.

Execution: *(fielded in plan, sample built, results of sample built, electrical tests, chemical tests - > RESULT)*

- Carbon batch:
  - The same sample was used for all the experiments. It was a sample of an expanded graphite named **CY**, from **COMPANY 2**. Batch name: GFG 20 HP - 10kg - LJ442/1 - 68/02/16. This sample was received in July 2017 (sack 12; 300kg).
  - This sample is located in Büdingen laboratory and its data sheet is attached here (Figure 3).
  - A sample of this batch was also analyzed by Azuqueca chemical laboratory (analysis request: M17-127b). Results are shown in Table 1.

*Figure 3. **CY** - GFG 20 HP - 10kg - LJ442/1 - 68/02/16. Data sheet from **COMPANY 2**.*

Table 1. *Results on trace elements analyses by ICP-OES. Three different methods were used to attack the carbon samples.*

CY	Concentration (ppm)									
Method	**Cr**	**Cu**	**Cd**	**Fe**	**Mn**	**Ni**	**Mo**	**W**	**Ti**	**Co**
1	2.1	0.5	0.5	75.4	0.5	3.0	0.5	0.5	2.5	0.5
2	2.0	0.5	0.5	65.1	0.5	1.6	0.5	0.5	2.4	0.5
HCl + Microwave Digester	1.8	1.1	0.5	91.0	0.5	1.7	0.5	0.5	5.5	0.5

- LOI Procedure:

1. Materials
- Electric muffle furnace capable of maintaining temperatures of 927ºC +/- 25°C.
- Porcelain crucibles (Wide-Form Crucible, Porcelain; 80mL, 60mm top OD, 48mm H. According to DIN 12 904).
- Electric balance with the resolution of 0.0001g.
- Pure lab water.
- Proper extraction system.
- Supra HNO_3 (69%) solution.

2. Execution
2.1. Preheating of the crucibles
Launching LOI program to the empty crucibles: 12h in the muffle oven at 927°C (15min for reaching this temperature).

2.2. Carbon material: humidity
Weighing the empty crucible (W1) and 3.0000 to 3.1000g of carbon material (W2) in each crucible (see **¡Error! No se encuentra el origen de la referencia.**. a, b). Placing the crucibles in the oven at 110°C overnight (see **¡Error! No se encuentra el origen de la referencia.**. c).
Weighing the crucibles containing the *dry carbon materials* (W3).

2.3. Carbon material: LOI
Placing these crucibles in the muffle oven and launching LOI program: 12h in the muffle oven at 927°C (15min for reaching this temperature) (see **¡Error! No se encuentra el origen de la referencia.**. d).
When the temperature of the muffle oven is steady (for minimum 2h) and lower than 30°C, taking out the crucibles and weighing them (W4) (see **¡Error! No se encuentra el origen de la referencia.**.

e).
Cleaning the crucibles with warm HNO_3 (69%) solution.

2.4. Calculations

$$\text{LOI (\%)} = [\text{ash weight (g)} / \text{dry carbon material weight (g)}] * 100$$
$$\text{ash weight (g)} = W4 - W1$$
$$\text{dry carbon material weight (g)} = W3 - W1$$

The complete procedure has been prepared as a non-official document: PV05-18-01 LOI Procedure (draft 1).

- Results

Above procedure was followed to determine the LOI of our **CY** sample. In total, 36 samples were analyzed in four different batches. One of the batches was discarded due to finding different anomalies among the results. After this, the interquartile range (IQR) was calculated for the rest of the samples, as well as the internal and external limits. As one of the results was out of the external limit, only 26 results were selected as valid values. Results (see Table 2) were higher than method 1 results (LOI = 99.07%), which can be related to a lower efficiency of the method 1 due to using different parameters (for 1 to 5g, T = 800°C, t = 5 to 10h).

In addition, Figure 4 shows the statistical dispersion of the results, as well as the external (Average ± 0.0014%) and internal (Average ± 0.0024%) limits.

*Table 2. **CY** - LOI (%) Results.*

CY - LOI (%)				
N	Average	STD Dev	Internal limits	External limits
26	99.8106%	0.0049%	99.7964% - 99.8241%	99.7861% - 99.8345%
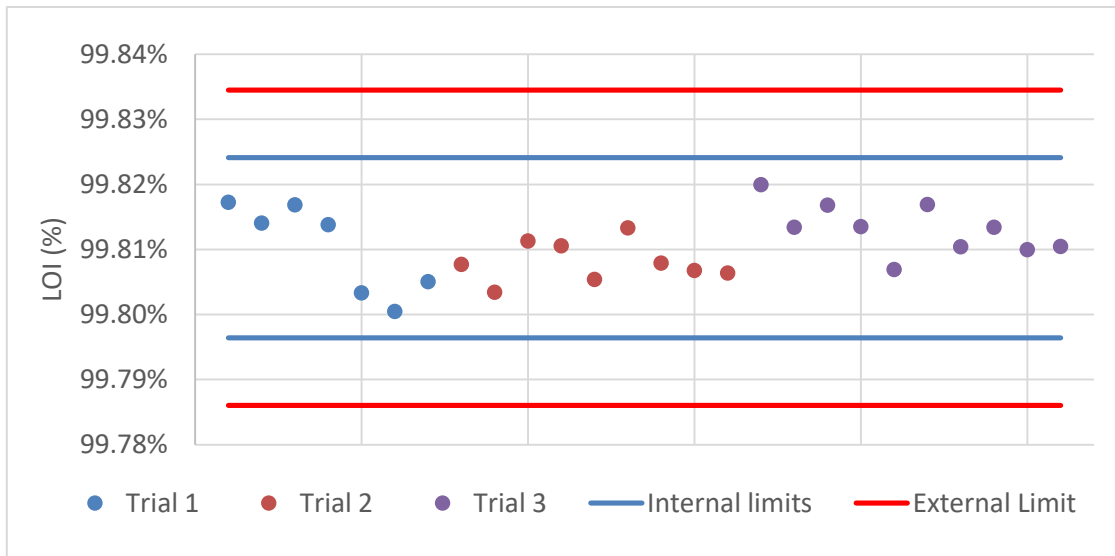
Figure 4. *CY - LOI (%) Results.*

- Trace elements analysis for **CY** ashes

  In order to know the ashes' composition, the ashes of 5 **CY** samples were digested with HCl in a Microwave Digester and analyzed by ICP-OES. The procedure is described below:

1. The digestion of the ashes was accomplished according to "*HCl + Microwave digester*" method. The ashes were removed from the crucibles using a brush, and placed in Teflon tubes, together with 5mL of HCl (37%) (see **¡Error! No se encuentra el origen de la referencia.**. f, g). After this, the crucibles were weighed (W5).
2. The Teflon tubes were placed in the MLS Microwave Digester. Program "Carbon ashes" (see Table 3) was launched (see **¡Error! No se encuentra el origen de la referencia.**. h).

Table 3. *MLS Microwave digester - Carbon ashes program parameters.*

Step	Time (min)	T1 (°C)	T2 (°C)	E (W)
1	5	100	60	1000
2	10	180	90	1000
3	20	240	130	1000

3. Once the program was finished, and the tubes were cold enough, the final solution was filtered and placed directly in a 10mL flask, using Pure lab water to sweep along and level up (see **¡Error! No se encuentra el origen de la referencia.**. i, j, k).
4. The weight of the ashes was calculated as the difference between W4 and W5.
5. Trace elements analyses by ICP-OES was performed following PV-04-31.

Table 4 shows the trace element analysis results of the **CY** ashes. The concentration of the different elements in **CY** ashes was lower than in **CY** samples (see Table 1). In order to compare these results, the weighted percentages of each element were calculated. The results confirmed that the most predominant element in the ashes was iron, as well as in the **CY** samples.

Table 4. Results on trace elements analysis by ICP-OES for CY ashes. Weighted percentages related to the total weight of these impurities.

Sample	Test method	Unit	Impurities									
			Cd	Co	Cr	Cu	Fe	Mn	Mo	Ni	Ti	W
CY ashes (n = 5)	HCl + MW Digester	ppm	0.00	0.00	0.18	0.04	3.24	0.05	0.00	0.16	0.15	0.01
		%*	**0.0%**	**0.0%**	**4.6%**	**1.1%**	**84.4%**	**1.4%**	**0.0%**	**4.2%**	**4.0%**	**0.3%**
CY	Method 1	%*	0.6%	0.6%	2.4%	0.6%	87.7%	0.6%	0.6%	3.5%	2.9%	0.6%
	Method 2	%*	0.7%	0.7%	2.7%	0.7%	87.9%	0.7%	0.7%	2.2%	3.2%	0.7%
	HCl + MW Digester	%*	0.5%	0.5%	1.7%	1.1%	87.8%	0.5%	0.5%	1.6%	5.3%	0.5%

*% = [Impurity (ppm) / ∑ Impurities (ppm)] *100

Method 1 is used by **COMPANY 2.**
Method 2 is used by **COMPANY 1.**

- Trials with C1 batches
  In order to prove this method, the LOI of 6 different C1 batches was determined. Table 5 shows the impurities content of these batches as well as the LOI values, provided by **COMPANY 1** and by Exide. It is important to notice here that **COMPANY 1** uses the LOI as a Key Performance Indicator (KPI). This parameter is measured after the purification of their principal source, the natural flake graphite. According to this fact, Exide LOI values should be as minimum, equal or higher than **COMPANY 1** LOI values. However, this did not happen for three of the analyzed batches (450-5/1, 450-5/5 and 526-1/5), which could be related to the differences in the same batch.

Table 5. Tested C1 batches. The total amount of impurities (Cr, Cu, Cd, Fe, Mn, Ni, Mo, and W) measured by ICP-OES using method 2. LOI values provided by COMPANY 1 and by Exide.

C1 batch	Total impurities (ppm)	LOI (%)		
	Method 2	COMPANY 1 VALUES	Exide	
450-5/1	50.7	99.9510	99.9101	± 0.0001
450-5/5	48.8	99.9376	99.9157	± 0.0016
450-6/5	29.9	99.8700	99.9286	± 0.0050
526-1/5	*	99.9870	99.9717	± 0.0042
526-12/5	*	99.8410	99.8512	± 0.0026
2847-4/5	33.0	99.9900	99.9867	± 0.0083

*These batches were not analyzed.

In order to deeply study these batches, Figure 5 relates the total amount of impurities with the different LOI values. As a rule, a higher LOI indicates a low level of impurities. This rule is not followed by LOI values provided by **COMPANY 1**, due to the LOI was not measured at the end of the manufacturing process as the trace elements. However, in the case of Exide LOI values, these ones follow the rule: higher LOI leads to a lower amount of impurities; which makes much more reliable our LOI results.
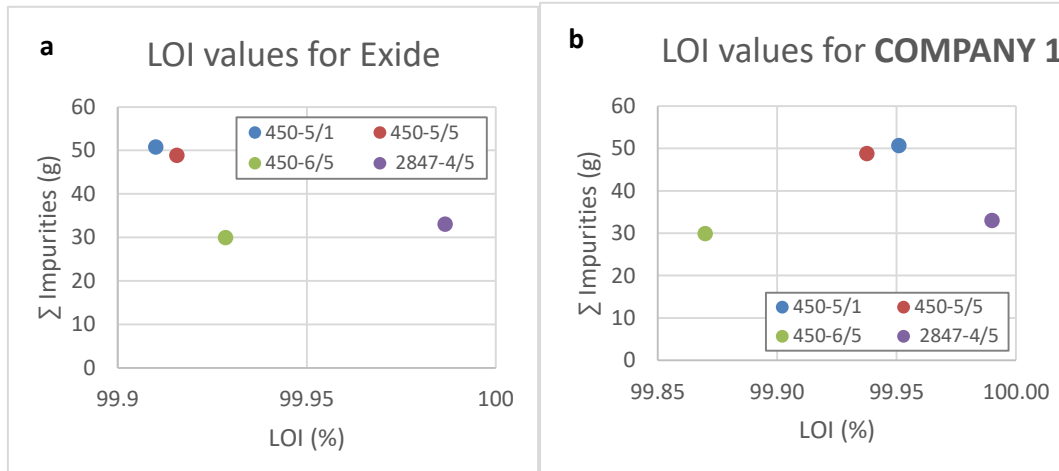
Figure 5. a. *Impurities level vs. Exide LOI values.* **b**. *Impurities level vs. COMPANY 1 LOI values.*

- Conclusions
  - Carbon materials with low LOI are related to high impurities level inside them, and vice versa.
  - Lower LOI leads to higher water consumption and rechargeability. However, this rechargeability is based on the energy expenditure due to the water consumption.
  - Exide method for determining the LOI is based on removing the humidity of the carbon sample (T = 110°C, t = overnight), and burning the sample (T = 927°C, t = 12h). After that, LOI is determined as the weighted percentage of the ashes inside the dry carbon sample.
  - Exide method seems to be more efficient than method 2, due to reaching higher temperature as well as higher burning time.
  - Determination of LOI for different C1 batches:
    - **COMPANY 1** uses the LOI as a KPI. This parameter is measured after the purification of the natural flake graphite.
    - LOI values from Exide are supposed to be higher than for **COMPANY 1**. If this rule is not followed, differences in the same batch could be the main reason.
    - It can be assumed that LOI values from Exide were reliable, as the relation between these values and the total amount of impurities was coherent: lower LOIs values were related to higher level of impurities.

Outlook/Next steps: *(how to proceed next)*

- Approval of PV05-18-01 LOI Procedure.
- Establishing the determination of LOI as a routine analysis for carbon materials.

References:

1. P. Tong, R. Zhao, R. Zhang, F. Yi, G. Shi, A. Li, H. Chen, J. Power Sources 286 (2015) 91–102.
2. M. Fernández, J. Valenciano, F. Trinidad, N. Muñoz, J. Power Sources 195 (2010) 4458–4469.
3. J. Valenciano, A. Sánchez, F. Trinidad, A.F. Hollenkamp, J. Power Sources 158 (2006) 851–863.
4. Catalytic effects on Conductive Carbon. F. Trinidad, J. Valenciano (Azuqueca, November 2015).
5. Chemical Analyses – Determination of loss on ignition in sediment, sludge, soil, and waste. 2003-08. European Standard. TC WI :2003 (E).

Lead Acid Batteries for Micro Hybrid Electrical Vehicles – influence of different carbon materials and organic expanders on the performance of the negative plates.

RESUMEN - ABSTRACT

Tesis Doctoral / Doctoral Thesis
María Blecua de Pedro

Dirigida por / Directed by
Pilar Ocón Esteban
Jesús Valenciano Martínez

Abstract

As we all know, climate change is one of the world's most pressing challenges. The emission of greenhouse gasses, which includes the emission of carbon dioxide, has increased the global temperatures by around 1°C since pre-industrial times. For the purpose of reducing CO_2 emissions, the European Commission has established CO_2 emissions targets for the European passengers' cars since 1995. Nowadays the CO_2 emissions average for a European passenger car is 119.4g/km, and the target for 2021 is 95g/km. The unfulfillment of this restriction can lead to the payment of fines 5€ to 95€ per gram of CO_2 exceed per car sold.

In order to achieve this target, the automotive industry is continuously developing new ways to reduce the fuel consumption of the car. One of the recent approaches is the implementation of the Start and Stop system as well as the regenerative braking in Internal Combustion Engine cars named Micro Hybrid Electrical Vehicles (HEVs). These two features are carried out by the Lead Acid Battery (LAB) from the car.

For working in a micro HEV the LAB must be able to fulfill several cycles for the good performance of the Start & Stop system. In addition, the battery is recharged by the regenerative braking, which means that the cycles will be performed when the battery is working at 60% – 70% State of Charge (SoC). Conventional LABs are not able to work in these conditions. Therefore, the industry has developed a new fleet of batteries called Enhanced Flooded Batteries (EFBs), which incorporate carbon materials, such as expanded graphite, graphite, carbons blacks, nanocarbon materials, in their negative plates for improving their Specific Surface Area (SSA).

The NAM of the LABs is made of metallic lead mixed with a group of additives called expanders. These expanders increase the porosity of the NAM. When they are not added, the porosity is quite low, and the electrolyte is not able to reach the inner part of the plate. The lead sulfate crystals created during the discharge of the battery cannot be reconverted to lead, and LAB fails. This fact is known as sulfation of the negative plate. The addition of carbon materials lead to the increase of the SSA of the negative plate. This effect depends on the size and concentration of the carbon materials. Nanometer carbon materials with high SSA at concentrations lower than 0.5% in the negative plate, are pushed to the surface of the Negative Active Material (NAM) during the formation process, also known as energetic structure, improving its SSA. When these types of carbon materials are added at concentrations higher than 0.5% they are

incorporated into the bulk of the lead skeleton during the formation process. The same happens for the micrometer carbon materials no matter their concentration; they are always incorporated into the lead skeleton. From the lead skeleton, the carbon materials are able to create a more porous structure which results in a more dynamic electric system, as the electrolyte can reach the inner parts of the negative plate. In addition, when these materials are electrically conductive they improve in a further way the current distribution throughout the negative plate, especially when it is partly sulfated.

The worst disadvantage of using carbon materials in the negative plate of the LAB is that they increase the Hydrogen Evolution Reaction (HER) rate during the overcharge of the battery. This water consumption increase leads to the dry out of the battery, and the resulting failure, as EFB are Valve Regulated Lead Acid (VRLA) batteries that cannot be refilled with water. For this reason, the type of carbon additive, as well as the dosage, must be wisely selected.

Another important additive for the negative plate is the Organic Expanders (OEs) which are active polymers that are able to delay the passivation phenomena, i.e. accumulation of lead sulfate crystals on the surface of the negative plate which leads to the collapse of the pores and the failure of the LAB. Most usual OEs are the sodium lignosulfonates (LS).

During this doctoral thesis, we have worked on the addition of different carbon materials and OEs in the negative plates of LABs on the purpose of achieving longer cycle life, as well as charge acceptance. In addition, the effect of the concentration and type of carbon material was studied in order to find the best LAB performance while maintaining the lowest water consumption. All the experiments were done on 2 V / 1 Ah LAB cells where the negative plate was the limiting component. In this way, the successful additives could be used in the negative plates of EFBs.

The first part of the study was focused on performing all the LABs manufacturing processes in the laboratory: mixing, pasting and curing processes for getting the unformed negative and positive plates. Once all these processes were optimized, 2 V / 1 Ah LAB cells were assembled and formed. The most relevant electrical tests for EFBs, according to the standards *VW75073 2012-07 and RNDS SS 36 11 003 2014-05,* were selected and adapted to the cells. This procedure included the capacity test, Cold Cranking Ability (CCA) test, Initial Charge Acceptance (ICA) test, the negative polarization study and the cycle life at Partial State of Charge (PSoC) test. Furthermore, the negative plates were analyzed during the whole process with the following techniques: lead sulfate

and carbon determination, porosity analyses, Brunauer, Emmett and Teller (BET) SSA, X-Ray diffraction, Scanning Electron Microscopy (SEM) study. The results of this thesis were divided into 4 different batches.

The first carbon materials understudies in batch 1 were 5 carbon materials (C1, C2, C3, C4 and C5) and 2 LS (LS1 and LS2). 6 mixtures were chosen and the negative plates were prepared, as well as the 2 V / 1 Ah cells. Carbon materials from C1 to C4 were micrometer carbon materials, so they were expected to be allocated in the bulk of the lead skeleton. C5 was a nanometer carbon material that was pushed to the surface of the NAM. All these carbon materials were able to improve the charge acceptance of the negative plate; however, C5, which was located at the surface of the NAM, showed the lowest cycle life. In the case of C5 it was also appreciated how this carbon material interacted with the LS impairing its performance. Higher HER rates were found for those carbon materials whose dosage was not well chosen. LS2 showed good performance when it was accompanied by micrometer carbon materials. In the case of LS1, its performance was better when it was accompanied by high conductive carbon materials.

The second type of carbon material understudy in **batch 2** was the graphitized carbon nanofibers produced by the company Grupo Antolin (GANFg). These fibers were chosen because of their high aspect ratio: high aspect ratio, as well as their low electrical resistivity ($1 \cdot 10^{-4}$ Ohm m). They had a diameter between 20 – 80 nm, and a maximum length of 30 μm. In this way, these fibers were thought to be integrated into the lead skeleton, and due to their high aspect ratio, they could for a conductive network inside the lead skeleton if the percolation threshold was reached. The selected LS was LS2 from batch 1, which was called OE1 for this batch and the following. The first step of this batch was the dispersion of the GANFg together with a part of OE1. This process was carried out by GAIKER, a technological center that provided the GANFg dispersions. The dispersions were used to prepare the different mixtures with different GANFg concentrations: S5 – 0.50%, S6 – 0.20% and S7 – 0.10%, all of them accompanied with an OE1 final concentration equal to 0.30 %. As a result, the GANFg did not improve the charge acceptance, as they neither improved the BET SSA of the formed negative plates, but they improved the cycle life of the 2 V / 1 Ah cells. This improvement was noticeable even when GANFg were added at 0.10%, so this concentration was established as the optimum one. Furthermore, the HER rate, and thus the water consumption, did not increase by the addition of GANFg at 0.10%.

For the **batch 3,** we used the optimum GANFg dosage (0.10%) together with a mix of OEs = OE1 + OE2. In this way, we wanted to see if it was possible to improve the charge acceptance of the negative plate by changing the OEs types and concentration. The mix of OEs was also used for dispersing the GANFg. Finally, 5 mixtures were prepared with or without 0.10% of GANFg, and including 0.20% or 0.30% of the OEs mix. The results confirmed the effect of the OEs on the performance of the negative plate: impaired the passivation phenomena while restrainting the charge acceptance processes. The charge acceptance of the plates was not improved by the addition of the OEs mix. However, the cycle life of the 2 V / 1 Ah cells was improved again by the addition of GANFg, and was higher for the mixture that contained 0.30% of OEs mix.

As we failed to improve the charge acceptance of the negative plates by adding the mix of OEs, for **batch 4**, we selected C1 (expanded graphite) and C4 (conductive carbon black) to be added together with GANFg (at 0.10%) to the negative plate. The concentration of the carbon materials was adapted according to the batch 1 results. Therefore, we expected an increase of the charge acceptance and the cycle life while maintaining the water consumption of the cells. The GANFg dispersions were prepared with part of the carbon material, and the rest was added during the mixing process. OE1 at 0.30% was used for all the mixtures. The charge acceptance of the negative plates was not significantly improved by the addition of carbon materials together with GANFg. In the case of the cycle life, a little increase was seen when the carbon materials were added, especially in the addition of C1. The water consumption was increased by the addition of carbon materials. After the results of this batch, we can conclude that the carbon materials must be added in their optimum dosage in order to improve the charge acceptance of the negative plates.

The results of this doctoral thesis led to the conclusion that the most suitable additives for the negative plates of the EFB are carbon materials such as expanded graphite or conductive carbons blacks, although they lead to higher water consumption. The addition of GANFg or combination of them with different carbon materials led to higher cycle life but failed to improve the charge acceptance of the cells which would lead to a bad performance of the LAB during the regenerative braking. Therefore, the future approaches in the EFB research should be focused on finding new additives that restrain the water consumption and add them together with carbons blacks or expanded graphites.

Resumen

Como todos sabemos, el cambio climático es uno de los retos más importantes de nuestra época. La emisión de gases de efecto invernadero, que incluye la emisión de dióxido de carbono, ha provocado la subida de 1°C de la temperatura global antes de la edad industrial. Con el propósito de reducir las emisiones de CO_2 la comisión europea ha marcado objetivos referentes al nivel de emisiones de los coches de pasajeros europeos desde 1995. Hoy en día las emisiones de CO_2 de un coche de pasajeros europeo son 119.4g/km, cuando el objetivo para 2021 es de 95g/km. El incumplimiento de este objetivo puede dar lugar a multas entre 5€ y 95€ por gramo de CO_2 extra emitido por coche vendido.

Para conseguir este objetivo, la industria de la automoción está continuamente desarrollando nuevos formas de reducir el consumo de combustible del vehículo. Una de las recientes iniciativas es la implementación del sistema Start & Stop junto con la parada regenerativa para coches de Ingeniería de Combustión Interna, también llamados Micro Vehículos Híbridos Eléctricos (VHE). Estas dos nuevas implementaciones son alimentadas por la batería de Plomo Ácido del coche.

En el caso de un micro VHE, la batería tiene que ser capaz de realizar los suficientes ciclos de vida para el buen funcionamiento del sistema Start & Stop. Además, la batería es recargada por medio de la parada regenerativa, por lo que los ciclos se realizan cuando el estado de carga de la batería es del 60% – 70%. Las baterías convencionales no están preparadas para trabajar en estas condiciones. Por ello, una nueva flota de baterías llamadas Enhanced Flooded Batteries (EFBs) han entrado en el mercado. Estas baterías incorporan materiales de carbón, como grafitos expandidos, grafito, carbones black, materiales de carbón nanométricos, en la placa negativa para así aumentar el Área de la Superficie Específica (ASE) de la Materia Activa Negativa (MAN).

La placa negativa de la batería está compuesta por plomo metálico mezclado con un grupo de aditivos denominados "expanders". Estos expanders son responsables del incremento de la porosidad de la MAN. Cuando no son adicionados, la porosidad de la MAN es baja, y por ello el electrolito no puede alcanzar la parte interna de la placa. De este modo, los cristales de sulfato de plomo creados durante la descarga de la batería no pueden ser reconvertidos a plomo, y la batería deja de funcionar. Este hecho es conocido como sulfatación de la placa negativa. La adición de materiales de carbono incrementa la ASE de la placa negativa. Este efecto depende del tipo y de la concentración utilizada del

material de carbón. Carbonos nanométricos, con alta ASE, añadidos a concentraciones menores de 0.5% en la placa negativa, son empujados a la superficie de la MAN, o estructura energética, durante el proceso de formación, desde donde aumentan la ASE de dicha estructura. Cuando este tipo de materiales de carbono se añaden en concentraciones más altas del 0.5%, se incorporan en el interior del esqueleto de plomo durante el proceso de formación. Lo mismo ocurre en el caso de los materiales de carbono de tamaño micrométrico, sin tener importancia aquí la concentración a la que se añadan. Desde el esqueleto de plomo los materiales de carbono son capaces de generar una estructura más porosa que acaba siendo un sistema eléctrico más dinámico, ya que el electrolito puede alcanzar las partes más internas de la placa negativa. Además, en el caso de que estos materiales sean conductores, mejoran la distribución de la corriente a lo largo de la placa negativa, especialmente cuando ésta está parcialmente sulfatada.

La peor desventaja de utilizar estos materiales es que aumentan el rendimiento de la Reacción de Evolución de Hidrógeno (REH) durante la carga de batería. Este consumo de agua puede conducir al secado del electrolito, y al correspondiente fallo de la batería, ya que las EFBs son baterías plomo ácido reguladas por válvula que no pueden ser rellenadas con agua. Por esta razón, el tipo y dosis de material de carbón tienen que ser minuciosamente seleccionados.

Otro importante aditivo para la placa negativa son los Expanders Orgánicos (EOs); polímeros activos capaces de retrasar el fenómeno de pasivación, es decir, la acumulación de cristales de sulfato de plomo en la superficie de la placa negativa, lo que conduce a colapso de los poros y al fallo de la batería. Los EOs más utilizados son los lignosulfonatos de sodio (LS).

Durante esta tesis doctoral hemos trabajado en la adición de diferentes materiales de carbono y EOs en la placa negativa de baterías plomo ácido con el objetivo de alcanzar una mayor durabilidad, así como un incremento de la aceptación de carga. El efecto de la concentración y del tipo de carbón ha sido estudiado para encontrar una dosis óptima que mejore las características de la batería sin aumentar el consumo de agua. Todos los experimentos se llevaron a cabo sobre celdas plomo ácido de 2 V / 1 Ah donde la placa negativa era el componente limitante. De esta manera, los mejores aditivos podrían ser utilizados en las placas negativas de las EFBs.

La primera parte del estudio estuvo centrada en la adaptación de todos los procesos de fabricación de baterías plomo ácido en el laboratorio: procesos de mezclado, empastado y curado para conseguir las placas positivas y negativas

curadas y sin formar. Una vez que todos estos procesos fueron optimizados, las celdas de 2 V / 1 Ah fueron montadas y ensayadas. Los test eléctricos más relevantes realizados para EFBs, de acuerdo a los estándares *VW75073 2012-07 y RNDS SS 36 11 003 2014-05,* fueron seleccionados y adaptados a nuestras celdas. Este procedimiento incluyó el test de capacidad, el arranque en frío, la aceptación de carga, el estudio de polarización negativa y el test de ciclos de vida trabajando en un estado parcial de carga. Las placas negativas también fueron analizadas a lo largo de todo el estudio utilizando las siguientes técnicas: determinación de sulfato de plomo y carbón, análisis de porosidad, determinación de la ASE de Brunauer, Emmett y Teller (BET), difracción de rayos X, y Microscopía Electrónica de Barrido. Todos los resultados derivados de esta tesis se dividieron en 4 lotes.

En el **lote 1** se estudiaron 5 tipos de materiales de carbono (C1, C2, C3, C4 y C5) y dos LS (LS1 y LS2). 6 formulaciones fueron seleccionadas y las placas negativas fueron preparadas, junto con las celdas de 2 V / 1 Ah. Los materiales de carbono de C1 a C4 eran carbonos de tamaño micrométrico, por lo que se esperaba que se localizaran en el esqueleto de plomo de la placa negativa. En el caso del carbón C5, éste era un carbón de tamaño nanométrico, el cual se encontraría localizado en la estructura energética de la MAN, al haber sido expulsado hacia la superficie del esqueleto de plomo durante el proceso de carga. Todos estos materiales de carbono mejoraron la aceptación de carga de la placa negativa. Sin embargo, C5, que fue el único carbón localizado en la estructura energética de la MAN, fue el que menos ciclos de vida completó. En el caso del material de carbón C5 se pudo apreciar la interacción entre este material y el LS, lo que resultó en el empeoramiento del funcionamiento de dicho EO. En el caso de los materiales de carbono cuya dosis no fue bien escogida, un incremento del rendimiento de la REH fue apreciado. LS2 mostró un buen comportamiento cuando iba acompañado de materiales de carbono micrométricos. En el caso del LS1, éste mostró un mejor comportamiento cuando fue acompañado de material de carbono micrométrico y altamente conductor.

El segundo tipo de materiales de carbono que estudiamos durante el **lote 2** fueron las nanofibras de carbono grafitizadas comercializadas por el Grupo Antolin (GANFg). Estas fibras fueron elegidas debido a su alta relación de aspecto, y a su baja resistividad eléctrica ($1 \cdot 10^{-4}$ Ohm m). Estas fibras tienen un diámetro entre 20 y 80 nm, y una longitud máxima de 30 μm. De este modo, se encontrarían integradas en el esqueleto de plomo, y debido a su alta relación de aspecto podrían ser capaces de crear una red conductora dentro de dicho esqueleto si el umbral de percolación es alcanzado. El LS seleccionado fue el

LS2 del lote 1, que durante este lote y en adelante se ha denominado OE1. El primer paso fue la dispersión de las GANFg utilizando parte del OE1. Este proceso fue realizado por GAIKER, un centro tecnológico que nos proporcionó las dispersiones de GANFg. Estas dispersiones fueron utilizadas para preparar las siguientes formulaciones con diferente contenido en GANFg: S5 – 0.50%, S6 – 0.20% y S7 – 0.10%, todas ellas acompañadas de OE1 con una concentración final de 0.30%. Las placas negativas sin formar fueron preparadas, al igual que las celdas de 2 V / 1 Ah. Como resultado, GANFg no mejoraron la aceptación de carga, ya que tampoco mejoraron la superficie específica de las placas negativas formadas. Sí mejoraron la durabilidad de las celdas durante los ciclos de vida. Esta mejora fue representativa cuando las GANFg fueron adicionadas al 0.10%, y por ello esta concentración fue elegida como la concentración óptima de GANFg. Además, el rendimiento de la REH, y con ello el consumo de agua, no sé incrementó cuando las GANFg fueron añadidas al 0.10%.

En el caso del **lote 3,** utilizamos la concentración óptima de GANFg (0.10%) junto con una mezcla de EOs = OE1 + OE2. De este modo, nuestro objetivo fue ver si era posible mejorar la aceptación de carga de la placa negativa cambiando el tipo y concentración de EOs. La mezcla de EOs también se utilizó para la dispersión de las GANFg. Finalmente, se prepararon 5 formulaciones con y sin GANFg al 0.10%, e incluyendo la mezcla de EOs al 0.20% y 0.30%. Los resultados confirmaron el efecto de la adición de EOs en la placa negativa: evitan el fenómeno de pasivación mientras que empeoran los procesos de aceptación de carga. La aceptación de carga de las placas negativas no mejoró debido a la adición de la mezcla de EOs. Sin embargo, la durabilidad de las celdas en el test de ciclos de vida mejoró con la adición de las GANFg, y fue mejor para la formulación que contenía la mezcla de EOs al 0.30%.

Debido a que no conseguimos mejorar la aceptación de carga de las placas negativas con la adición de la mezcla de EOs, en el **lote 4** decidimos utilizar como aditivos las GANFg al 0.10% junto con materiales de carbono del lote 1: C1 (grafito expandido) y C4 (carbón black conductivo). La concentración de los materiales de carbono fue elegida acorde a los resultados obtenidos en el lote 1. De este modo los resultados esperados eran un aumento de la aceptación de carga y de los ciclos de vida, mientras se mantenía el consumo de agua. Las dispersiones de GANFg fueron preparadas con parte del material de carbono, y el resto fue adicionado durante el proceso de mezclado. La concentración final de OE1 fue 0.30% para todas las formulaciones. La aceptación de carga de las placas negativas no se incrementó significativamente por la adición de materiales de carbono junto con las nanofibras. En el caso de los ciclos de vida, pudimos

ver un pequeño aumento en el número de ciclos cuando los materiales de carbono fueron añadidos, especialmente en el caso del material de carbón C1. El consumo de agua se incrementó debido a la adición de materiales de carbono. Después de los ensayos correspondientes a este lote, podemos concluir que los materiales de carbono deben ser añadidos en su dosis óptima para mejorar la aceptación de carga de las placas negativas.

Los resultados de esta tesis doctoral nos llevaron a la conclusión de que los aditivos más adecuados para la placa negativa de las EFBs son los materiales de carbono como grafitos expandidos y cabón blacks conductores, aunque éstos conllevan un alto consumo de agua. La adición de GANFg o su combinación con otros materiales de carbono conllevó a un aumento de los ciclos de vda, pero no mejoró la aceptación de carga de las celdas, lo cual conduciría a un comportamiento no apropiado de la batería durante la parada regenerativa. Por todos estos motivos, los siguientes pasos para mejorar las prestaciones de las EFBs deberían estar centrados en la búsqueda de aditivos que disminuyan el consumo de agua, para así poder utilizar al mismo tiempo grafitos expandidos o carbon blacks como aditivos.